Mechanisms of non-centrosomal MTOC formation at the nucleus in muscle cells

Petra Gimpel

Mechanisms of non-centrosomal MTOC formation at the nucleus in muscle cells

Dissertation

In fulfillment of the requirements for the Joint Degree (Cotutelle)
"Doctor rerum naturalium" (Dr. rer. nat.)

integrated in the International Graduate School for Myology
"MyoGrad"
in the Department of Biology, Chemistry and Pharmacology
at the Freie Universität Berlin

and in Cotutelle Agreement
with the Ecole Doctorale "Complexité du Vivant"
at the Université Pierre et Marie Curie Paris 6

Submitted by

Petra Gimpel

from Berlin

June 2017

The doctorate studies were performed from October 2013 to September 2017 under supervision of Dr. Edgar R. Gomes (Instituto de Medicina Molecular, Lisbon, Portugal and Center for Research in Myology, UMRS 974, Paris, France) and Prof. Dr. Simone Spuler (Experimental and Clinical Research Center, Berlin, Germany). The experiments were conducted at the Center for Research in Myology, UMRS 974, Paris, France and at the Charité Berlin, Campus Mitte, CharitéCrossOver, Berlin, Germany.

Thesis jury:

Prof. Dr. Simone Spuler, thesis supervisor in Berlin (1st reviewer for FU Berlin)
Prof. Dr. Sigmar Stricker (2nd reviewer for FU Berlin)
Dr. Christian Kähler, postdoctoral research fellow at FU Berlin

Dr. Edgar R. Gomes, thesis supervisor in Paris
Dr. Michel Bornens, examiner from UPMC
Dr. Mónica Bettencourt-Dias, external examiner (1st reviewer for UPMC)
Dr. Antoine Guichet, external examiner (2nd reviewer for UPMC)

Date of Defense: 4th September, 2017

Hereby I declare that I have completed the doctoral thesis 'Mechanisms of non-centrosomal MTOC formation at the nucleus in muscle cells' on my own and with no other aid and sources than noted.

This work was done in collaboration with the laboratory of Prof. Dr. Brian Burke (Institute of Medical Biology, Agency for Science, Technology and Research (A*STAR), Singapore) and the laboratory of Dr. Jan Schmoranzer (Charité Universitätsmedizin Berlin, Campus Mitte, CharitéCrossOver, Berlin, Germany). All experiments that were performed by our collaborators are clearly indicated within each figure legend.

Berlin, June 12th 2017

Acknowledgements

"Are microtubules growing from nuclear pore complexes in muscle cells?" With this seemingly simple question my supervisor **Dr. Edgar R. Gomes** had fired the starting gun for an exciting and fascinating PhD project, which turned out to be much more complex than initially thought. I would like to thank **Dr. Edgar R. Gomes** for the opportunity and all his support to explore this starting question in every possible direction that I aimed at.

I am deeply grateful for the excellent supervision that I received from **Dr. Bruno Cadot**, for all of the efforts he put into this project, for his never-ending enthusiasm and motivation and for his support inside and outside the lab. This project would not have been possible without him.

I would like to thank **Prof. Dr. Simone Spuler**, **Prof. Dr. Sigmar Stricker**, **Dr. Mónica Bettencourt-Dias** and **Dr. Antoine Guichet** for reading and evaluating my PhD thesis and being part of my thesis jury. In addition, I thank **Dr. Michel Bornens** and **Dr. Christian Kähler** for accepting to be members of my thesis jury.
Dr. Michel Bornens and his group laid the foundation for my PhD project back in 1985 with their discoveries that microtubules and microtubule-organizing centers are reorganized to the nucleus in skeletal muscle cells. I am thus especially honored that he takes part in my thesis defense to discuss the recent progress in this field.

I want to thank **Prof. Dr. Simone Spuler** for giving me the opportunity to be part of the MyoGrad PhD program through which I was able to perform my PhD in Paris and Berlin and to attend international conferences. The MyoGrad summer schools helped me a lot to gain substantial knowledge within the muscle field outside my personal project and allowed me to get in contact with international scientists. I want to thank **Susanne Wissler** for all her support and advice regarding administrative work at both universities, for arranging flights between Berlin and Paris and

her contributions to the MyoGrad summer schools.

I would like to thank **la Fondation pour la Recherche Médicale (FRM)** for supporting my work with a fourth-year scholarship (FDT20160435051) and the **Université Franco-Allemande (UFA)** for providing me a mobility aid stipend within the cotutelle de thèse program (CT-46-14-II).

I would like to thank **Dr. Renata Basto**, **Dr. Vanessa Ribes**, **Dr. Fanny Pilot-Storck**, **Prof. Dr. Simone Spuler** and **Dr. Jan Schmoranzer** for being part of my thesis committee and their guidance in finding the right direction for my project.

I am grateful for the excellent training that I received from **Dr. Jan Schmoranzer** in order to perform 3D-SIM and SD-*d*STORM microscopy. I thank him for accepting me to be part of his laboratory and for his support during my lab relocation. I would like to thank **Dr. Robyn Brackin** for showing me the fascinating possibilities and advantages of Nikon spinning disk confocal microscopy.

I want to acknowledge **Prof. Dr. Brian Burke** and **Dr. Yin Loon Lee** for the fruitful collaboration which was ultimately important for the success of this project. I especially want to thank **Dr. Yin Loon Lee** for all the scientific discussions and for teaching me how to perform BioID experiments. Moreover, I want to thank him for making my stay in Singapore such a memorable experience.

I thank **Prof. Dr. Markus Schülke** for hosting and supporting me in his laboratory during my stay in Berlin. Thanks to all members of the **AG Schülke/ AG Seelow**, especially to **Ioanna Polydorou**, **Franziska Seifert** and **Esther Gill**, for welcoming me in the laboratory and their technical and organizational support. I especially want to thank Ioanna for her motivation, the discussions and for continuing to improve my Greek.

Thanks to all other members of the **Gomes/Cadot group** and all other teams of the **105 building** for creating such an enjoyable work atmosphere during my three years in Paris and for the very inspiring discussions during work seminars and in between: **Dr. William Roman**, **Dr. David Ollitrault**, **Dr. Rosamaria Correra**, **Dr. Vanessa Ribes**, **Bernadette Drayton**, **Dr. Philippos Mourikis**,

Frederic Aurade, **Dr. Amalia Stantzou**, **Mafalda Pimentel**, **Cátia Janota**, **Dr. Yue Jiao**, **Dr. Jheimmy Diaz**, **Marine Guilbaud**.

I want to thank **Dr. Judite Costa**, **Sara Ferreira** and **Telma Carrilho** for their organizational support and for sending packages with lab material back and forth between Lisbon, Paris and Berlin.

I would like to thank **Dr. Sestina Falcone**, **Aurore Besse**, **Dr. Sonia Alonso-Martin**, **Dr. Maria Grazia Biferi**, and **Mathilde Cohen-Tannoudji** for introducing me to the world of Gym Suédoise, for all the sportive activities and funny moments.

I would like to thank **Dr. Valérie Vilmont**, **Dr. Despoina Mademtzoglou**, **Dr. Audrey Der Vartanian** and **Jean-François Darrigrand** for being both - great colleagues and wonderful friends -, for all the shared moments inside and outside the lab, for all the favors and help, the intercultural exchange and for making me feel home in Paris.

I thank **Dr. Xenia Naj** for her immense friendship, for our shared adventure exploring Paris and San Francisco, her contagious happiness and her talent to discover the best restaurants.

Finally, I want to express my gratitude to my wonderful family and friends outside the scientific world for their optimism and understanding, no matter how time consuming my work turned out to be. Most importantly I wish to thank my **parents** and my **husband Tobias** for their never-ending support every single day, for their believe in me and for encouraging me to always move on.

Contents

List of Figures

List of Tables

List of Abbreviations

Ab	antibody
AchRs	acetylcholine receptors
AKAP450	A-kinase anchoring protein 450
AMP	adenosine monophosphate
ATP	adenosine triphosphate
A.U.	arbitrary units
Cdk5Rap2	CDK5 Regulatory Subunit Associated Protein 2
Cep152	centrosomal protein of 152 kDa
Cep192	centrosomal protein of 192 kDa
CG-NAP	centrosome and Golgi localized PKN-associated protein
CH domain	calponin homology domain
CMD	congenital muscular dystrophy
CNM	centronuclear myopathy
DNA	deoxyribonucleic acid
DOX	doxycycline
D-PLP	*Drosophila* Pericentrin-like protein
DTT	dithiothreitol
EB	end-binding protein
EDMD	Emery-Dreifuss muscular dystrophy
EM	electron microscopy
ER	endoplasmic reticulum
GAPDH	glyceraldehyde-3-phosphate dehydrogenase
GCP	γ-tubulin complex protein
GFP	green fluorescent protein
HCl	hydrochloric acid
hrs	hours
IF	Immunofluorescence
INM	inner nuclear membrane

KASH	Klarsicht/ANC-1/SYNE homology
KHC	kinesin heavy chain
KLC	kinesin light chain
LINC	linker of nucleoskeleton and cytoskeleton
LIS1	lissencephaly 1
NaOH	sodium hydroxide
NUDE	nuclear distribution E
MAPs	microtubule-associated proteins
MHC	myosin heavy chain
min	minutes
ms	milliseconds
MOZART	mitotic-spindle organizing protein associated with a ring of γ-tubulin
MT	microtubule
MTOC	microtubule-organizing center
MuSK	muscle-specific tyrosine kinase
N1α	Nesprin-1α
NE	nuclear envelope
NMJ	neuromuscular junction
NPC	nuclear pore complex
ONM	outer nuclear membrane
PACT	Pericentrin-Akap450 centrosomal targeting
PBS	phosphate buffered saline
PCM	pericentriolar material
Pcm1	pericentriolar material 1
PCR	polymerase chain reaction
PFA	paraformaldehyde
Plk1	polo-like kinase 1
Plp	Pericentrin-like protein
PNS	perinuclear space
RNA	ribonucleic acid
SUN	Sad1/UNC-84
rpm	revolutions per minute
s	seconds
SF	spreading factor
sgRNA	single guide ribonucleic acid

siRNA	small interfering ribonucleic acid
S. pombe	Schizosaccharomyces pombe
SR	sarcoplasmic reticulum
+TIPs	microtubule plus-end-tracking proteins
TBS	Tris buffered saline
γ-TuNA	γ-tubulin ring complex-mediated nucleation activator
γ-TuSC	γ-tubulin small complex
γ-TuRC	γ-tubulin ring complex
WB	Western Blot

Abstract

The accurate position of the nucleus within a cell is important for many biological processes such as cell migration or differentiation and relies on the connections between the nuclear envelope (NE) and the cytoskeleton. Nuclear positioning is particularly controlled during skeletal muscle formation, when post-mitotic myoblasts fuse to form multinucleated myotubes and when myotubes further differentiate into mature myofibers. Defects in nuclear positioning were shown to affect muscle function and are linked to many muscle diseases, such as Centronuclear Myopathies (CNM) and Emery-Dreifuss Muscular Dystrophy (EDMD). Nuclear movement during myogenic differentiation is highly dependent on microtubules (MTs) which adopt a unique organization during the muscle differentiation process. In comparison to proliferating myoblasts, where MTs are radially nucleated from the centrosome, MTs are nucleated from the NE in dense bundles parallel to the cell axis in differentiated myotubes. This dramatic reorganization of the MT network during muscle development is accompanied by a redistribution of the Golgi complex and proteins from the centrosome (e.g. Pericentrin, Pcm1, Akap450) to the NE. Thus, the nucleus takes over the function as a non-centrosomal microtubule-organizing center (MTOC) during myogenic differentiation. However, the molecular mechanisms underlying centrosomal protein recruitment and anchoring to the NE as well as their capacity to organize MTs are still unknown.

Here, we performed a siRNA screen against 299 genes encoding NE-transmembrane or NE-associated proteins and identified Nesprin-1, a KASH (Klarsicht/ANC-1/SYNE homology) domain protein located at the outer nuclear membrane (ONM), involved in the recruitment of Pericentrin to the NE during myogenic differentiation. In C2C12 myotubes depleted for Nesprin-1 or in myotubes from a congenital muscular dystrophy patient carrying a nonsense mutation within the *Nesprin-1/SYNE1 (23560 G>T)* gene, several centrosomal proteins, including Pericentrin, Akap450, Pcm1, and Cdk5Rap2, are mislocalized in the cytoplasm in close proximity to mislocalized Golgi fragments. During skeletal muscle formation, a muscle-specific isoform of Nesprin-1,

namely Nesprin-1α, is increasingly expressed. Using the proximity-dependent biotin identification method, BioID, we could show that Nesprin-1α is highly associated with Akap450, Pericentrin and Pcm1 in C2C12 myotubes. Moreover, re-expression of Nesprin-1α in Nesprin-1-depleted cells is sufficient to rescue the observed recruitment defects, thus confirming Nesprin-1α as the major receptor at the NE to anchor centrosomal proteins. However, Nesprin-1α together with Sun1/Sun2 are not only important for recruiting centrosomal proteins but also for MTOC activity. MTs are nucleated from the NE in differentiated muscle cells, whereas MTs grow from cytoplasmic foci containing mislocalized Golgi fragments and centrosomal proteins in Nesprin-1- or Sun1/Sun2-depleted cells. Among the recruited centrosomal proteins, solely Akap450 seems to be required for MT nucleation from the NE. Using computer simulations and knockdown experiments, we demonstrate that Akap450-Nesprin-1-mediated MT nucleation from the nucleus has a biological relevance for nuclear positioning during myotube formation.

Taken together, our data suggest a model where Nesprin-1α, when upregulated during myogenic differentiation, forms a complex with Sun1/Sun2 and thereby anchors centrosomal proteins at the nucleus. In turn, Akap450 plays a key role in inducing MT nucleation, thereby assuring proper nuclear positioning during skeletal muscle formation. These findings strengthen our understanding on how non-centrosomal MTOCs form in muscle and how defects within the underlying mechanism can potentially contribute to nuclear positioning defects in muscular dystrophies.

Zusammenfassung

Die korrekte Position des Zellkerns ist für viele biologische Prozesse, z.B. während der Zellmigration oder der Differenzierung, wichtig und erfordert Verbindungen zwischen der Kernmembran und dem Zytoskelett. Die Positionierung des Zellkerns ist vor allem während der Bildung des Skelettmuskels streng kontrolliert, wenn postmitotische Myoblasten miteinander fusionieren, um multinukleäre Myotuben zu bilden, und wenn Myotuben weiter in reife Muskelfasern differenzieren. Fehlpositionierte Zellkerne stehen im Verdacht, die Muskelfunktion zu beeinträchtigen und hängen somit oft mit verschiedenen Muskelerkrankungen, wie z.B. der zentronukleären Myopathie und der Emery-Dreifuss-Muskeldystrophie, zusammen. Die Bewegung von Zellkernen ist während der myogenen Differenzierung von Mikrotubuli abhängig, die während des Differenzierungsprozesses umfangreich umorganisiert werden. Während Mikrotubuli in proliferierenden Myoblasten radial vom Zentrosom nukleiert werden, werden sie in differenzierten Myotuben von der Kernmembran in dichten, parallel zur Zellachse verlaufenden, Bündeln nukleiert. Diese drastische Umstrukturierung des Mikrotubuli-Netzwerkes geht während der Muskelentwicklung mit einer Umordnung des Golgi-Komplexes und von zentrosomalen Proteinen (z.B. Pericentrin, Pcm1, Akap450) zur Kernmembran einher. Der Zellkern übernimmt somit während der myogenen Differenzierung die Funktion eines nicht-zentrosomalen Mikrotubulus-Organisationszentrums. Der molekulare Mechanismus, wie zentrosomale Proteine rekrutiert und an der Kernmembran verankert werden, und wie Zellkerne die Fähigkeit erlangen Mikrotubuli zu organisieren, ist jedoch bisher ungeklärt.

In der vorliegenden Arbeit haben wir mit Hilfe einer funktionalen siRNA-Analyse 299 verschiedene Gene untersucht, die transmembranäre Kernmembranproteine oder Kernmembran-assoziierte Proteine kodieren. Dabei haben wir Nesprin-1, ein KASH-(Klarsicht/ANC-1/SYNE Homologie) Domänen-Protein der äußeren Kernmembran, als potenziellen Rezeptor für die Rekrutierung von Pericentrin zur Kernmembran während der myogenen Differenzierung identifiziert. In Nesprin-1-defizienten C2C12

Myotuben sowie in Myotuben von einem Patienten mit kongenitaler Muskeldystrophie (Mutation innerhalb des *Nesprin-1/SYNE1 (23560 G>T)* Gens), waren einige zentrosomale Proteine, Pericentrin, Akap450, Pcm1 und Cdk5Rap2, im Zytoplasma in der Nähe von mislokalisierten Golgi-Fragmenten fehllokalisiert. Während der Bildung des Skelettmuskels, wird Nesprin-1α, eine muskelspezifische Isoform von Nesprin-1, verstärkt exprimiert. Mit Hilfe der BioID-Methode konnte gezeigt werden, dass Nesprin-1α stark mit Akap450, Pericentrin und Pcm1 in C2C12 Myotuben assoziiert ist. Weiterhin konnte gezeigt werden, dass die Reexprimierung von Nesprin-1α in Nesprin-1-defizienten Zellen ausreichend ist, um die beobachteten Rekrutierungsdefekte zentrosomaler Proteine zu beheben. Nesprin-1α konnte somit als wesentlicher Rezeptor für die Verankerung zentrosomaler Proteine an der Kernmembran bestätigt werden. Nesprin-1α wurde jedoch im Zusammenhang mit Sun1/Sun2 nicht nur für die Rekrutierung zentrosomaler Proteine als wichtig erwiesen, sondern auch für die Aktivität des Mikrotubulus-Organisationszentrums. Während Mikrotubuli in differenzierten Zellen von der Kernmembran nukleiert wurden, wurden sie in Nesprin-1- oder Sun1/Sun2-defizienten Zellen von zytoplasmatischen Stellen, die mislokalisierte Golgi-Fragmente und zentrosomale Proteine enthielten, gebildet. Von den zentrosomalen Proteinen, die bekannt sind, während der myogenen Differenzierung zur Kernmembran zu lokalisieren, war lediglich Akap450 benötigt, um die Mikrotubuli-Nukleation an der Kernmembran zu induzieren. Mit Hilfe von Computersimulationen und Knockdown-Experimenten konnten wir zeigen, dass die durch Akap450 und Nesprin-1 vermittelte Mikrotubuli-Nukleation von der Kernmembran eine wichtige Rolle bei der Positionierung der Zellkerne innerhalb von Myotuben spielt.

Zusammengefasst können wir anhand unserer Daten ein Modell vorschlagen, in dem Nesprin-1α, wenn es während der myogenen Differenzierung hochreguliert wird, einen Komplex mit Sun1/Sun2 bildet und dabei zentrosomale Proteine am Zellkern verankert. Anschließend induziert Akap450 die Nukleation von Mikrotubuli an der Kernmembran und gewährleistet somit die korrekte Positionierung von Zellkernen während der Bildung des Skelettmuskels. Insgesamt verstärken unsere Ergebnisse unser allgemeines Verständnis, wie nicht-zentrosomale Mikrotubulus-Organisationszentren im Muskel gebildet werden und wie Defekte in den zugrundeliegenden Mechanismen zu potenziellen Fehlern bei der Zellkernpositionierung in Muskeldystrophien beitragen können.

Résumé

Le juste positionnement du noyau au sein des cellules est important pour de nombreux processus cellulaires tel que la migration ou la différenciation cellulaire. Ce positionnement s'opère grâce à la connexion entre l'enveloppe nucléaire (NE) et le cytosquelette. La régulation du positionnement du noyau est particulièrement importante durant la formation musculaire lorsque les myoblastes post-mitotique fusionnent afin de former des myotubes multinucléés et lorsque ces myotubes se différencient en myofibres matures. Il a été démontré qu'un défaut du positionnement nucléaire affectait la fonction musculaire et ce défaut du positionnement nucléaire est une caractéristique de certaines myopathies telles que les myopathies centronucléaires (CNM) et la dystrophie d'Emery-Dreifuss (EDMD). Le mouvement nucléaire lors de la différenciation myogénique dépend des microtubules (MTs), qui adoptent une organisation unique lors de la maturation musculaire. Contrairement aux myoblastes où les MTs irradient du centrosome, dans les myotubes différenciés la nucléation des MTs commence au niveau de l'enveloppe nucléaire pour former des faisceaux parallèles à l'axe de la cellule. Cette réorganisation du réseau microtubulaire lors du développement musculaire s'accompagne de la redistribution de l'appareil de Golgi et des protéines centrosomales (ex. Pericentrin, Pcm1 et Akap450) vers l'enveloppe nucléaire. Ainsi, le noyau adopte le rôle de centre organisateur des microtubules (MTOC) aux dépens du centrosome. Néanmoins, les mécanismes moléculaires régissant le recrutement et l'ancrage de protéines centrosomales à l'enveloppe nucléaire ainsi que leur capacité à réorganiser le réseau microtubulaire demeurent inconnus.

Dans cette étude, nous avons réalisé un criblage par ARN interférence ciblant 299 gènes codant des protéines contenant un domaine transmembranaire inséré au niveau de l'enveloppe nucléaire ou associé à cette dernière. Nous avons identifié la protéine Nesprin-1 qui contient un domaine KASH (Klarsicht/ANC-1/SYNE homology) et qui est localisée à la membrane nucléaire externe. Nesprin-1 recrute la protéine Pericentrin à l'enveloppe nucléaire lors de la différenciation myogénique. Dans des myotubes C2C12 appauvris en Nesprin-1 ainsi que dans des myotubes

provenant d'un patient affecté d'une dystrophie musculaire congénitale due à une mutation non-sens du gène *Nesprin1/SYNE1 (23560 G>T)*, plusieurs protéines centrosomales incluant Pericentrin, Akap450, Pcm1 et Cdk5Rap2, sont mal localisées dans le cytoplasme à proximité de fragments de l'appareil de Golgi, qui sont également mal localisés. Nous avons remarqué que lors de la formation musculaire, l'expression d'une isoforme spécifique de Nesprin-1, Nesprin-1α, augmentait. Grace à l'utilisation de la méthode d'identification BioID, nous démontrons que Nesprin-1α est associé à Akap450, Pericentrin et Pcm1 dans les myotubes C2C12. De plus, la réexpression de Nesprin-1α dans des cellules déplétées en Nesprin-1 est suffisante pour corriger les défauts de recrutement de ces protéines à l'enveloppe nucléaire. Ceci confirme l'importance de Nesprin-1α comme récepteur clé au niveau de l'enveloppe nucléaire pour l'ancrage des protéines centrosomales. En parallèle à leur activité de recrutement des protéines centrosomales à l'enveloppe nucléaire, Nesprin-1α et Sun1/Sun2 sont également nécessaires à l'activité du MTOC. En effet, la diminution de Nesprin-1 ou de Sun1/Sun2 dans les myotubes engendre des altérations dans la localisation des fragments de l'appareil de Golgi ainsi que des protéines centrosomales. Parmi les protéines centrosomales recrutées par Nesprin-1, seul Akap450 semble nécessaire à la nucléation des MTs à l'enveloppe nucléaire. Grâce à la modélisation informatique et des expériences d'ARN interférence, nous avons démontré que la nucléation des microtubules par Akap450 et Nesprin-1 a une fonction biologique pour positionner de manière précise le noyau lors du développement des myotubes.

Ainsi, nos données permettent d'établir un modèle où l'accroissement de Nesprin-1α durant la différenciation myogénique permettrait son association avec Sun1/Sun2, engendrant l'ancrage de protéines centrosomales à l'enveloppe nucléaire. Ceci permettrait à Akap450 d'induire la nucléation des MTs assurant ainsi le juste positionnement du noyau lors de la formation musculaire. Cette étude renforce notre compréhension du fonctionnement du centre organisateur des microtubules non-centrosomal et nous éclaire sur les conséquences d'une défaillance de ce système dans les dystrophies musculaires.

1 Introduction

1.1 Skeletal muscle

Coordinated movement is one of the major characteristics of all animals that is afforded by muscles. Generally, muscles can be divided into three main types, cardiac muscle that is found in the heart, smooth muscles that are present in the walls of some internal organs (e.g. blood vessels, stomach) and skeletal muscle. Skeletal muscle is one of the most specialized and fascinating tissue of the human body that accounts for about 40% of the total body mass. Skeletal muscles are connected to bones through tendons and are controlled by the somatic nervous system to initiate voluntary movements. In contrast to most of the skeletal muscles, movements accomplished by cardiac and smooth muscles are not under conscious control and are thus involuntary. The architecture of skeletal muscle is unique and specially constructed to allow for quick and repetitive contractions.

1.1.1 Structure of skeletal muscle

Skeletal muscles contain multinucleated muscle fibers, also termed myofibers or muscle cells, that are well-arranged into bundles (fascicules) and encircled by a layer of connective tissue, termed the perimysium (Figure 1.1). A large number of fascicules is further grouped and surrounded by another connective tissue layer, known as the epimysium, to finally form a distinct muscle (Frontera and Ochala, 2015).

Individual muscle fibers are cylindrical cells that are surrounded by a cell membrane, known as the sarcolemma. The cytoplasm of each muscle fiber, termed sarcoplasma, contains parallel arranged myofibrils, which in turn are composed of small regularly repeating units, termed sarcomeres. In resting muscle, sarcomeres are approximately 2 μm long but they can reduce their length by approximately 70% when the muscle contracts (Au, 2004). From an ultrastructural perspective, sarcomeres are made up of two different filament types - thick filaments, containing myosin II molecules, and thin filaments, comprising predominantly actin and tropomyosin-troponin complexes.

Thin filaments are attached by dimeric α-actinin molecules at one site to the Z-disc, which forms the boundary between adjacent sarcomeres and appears in electron micrographs of longitudinal sections as a densely stained band (Luther, 2009). On both sites of the Z-disk are the I-bands, which appear as lightly stained regions in electron micrographs and solely consist of actin thin filaments. Thin filaments extend from the Z-disc and interdigitate with thick filaments, the latter forming the so-called A-band. Thick filaments are crosslinked within the M-band at the middle of the sarcomere (Agarkova and Perriard, 2005). During muscle contraction, thick and thin filaments basically slide past each other, resulting in a shortening of the sarcomere (Herzog et al., 2015; Holmes and Geeves, 2000).

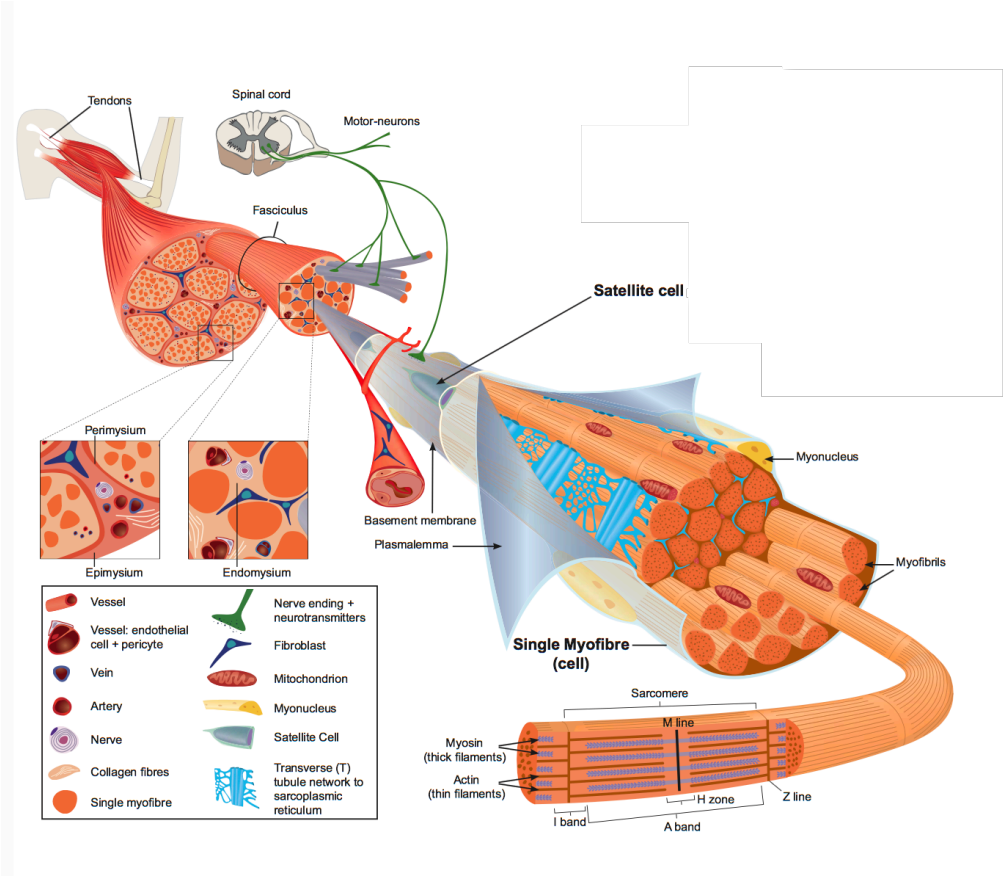

Figure 1.1: Structure of skeletal muscle. Skeletal muscles are connected to the skeleton by tendons. Tendons are contiguous with the epimysium, a layer of connective tissue that surrounds the entire muscle. The perimysium surrounds individual muscle fibers and groups them into bundles (fascicules). Muscle fibers are connected to the central nervous system through motor neurons. Individual muscle fibers contain multiple myofibrils which themselves are composed of repeating contractile units, the sarcomeres. Nuclei are located at the periphery, under the sarcolemma of the muscle fiber. Modified from (Tajbakhsh, 2009). Reprinted by permission (License #4120890420701) from Wiley Company: J Intern Med. 266(4):372-89, copyright (2009).

Common to all eukaryotic cells, muscle fibers contain several organelles, including nuclei for gene regulation, the Golgi complex for protein sorting, a three-dimensional network of mitochondria for energy production (Dahl et al., 2015), and a specialized form of the endoplasmic reticulum, termed the sarcoplasmic reticulum (SR), which stores and releases calcium (Mazzarello et al., 2003; Rossi and Dirksen, 2006). However, in contrast to other eukaryotic cells, nuclei do not localize within the middle of the muscle fiber but at the periphery under the sarcolemma.

1.1.2 Myogenesis

Multinucleated muscle fibers are formed during embryonic development in a tightly regulated multi-step process, known as myogenesis. Embryonic myogenesis begins with a process known as determination, when embryonic precursor cells commit to the myogenic lineage. Subsequently, the committed myoblasts proliferate, withdraw from the cell cycle and differentiate into postmitotic myocytes which fuse to form multinucleated myotubes (Figure 1.2). Maturation of myotubes finally leads to the formation of muscle fibers (Bentzinger et al., 2012; Buckingham et al., 2003; Tajbakhsh, 2009). These processes are spatiotemporally controlled by the combined action of multiple transcription factors, growth factor-induced signaling pathways [Wnt, Bone Morphogenetic Proteins (BMPs), Notch, Sonic hedgehog (Shh), p38] and epigenetic regulatory factors (Bentzinger et al., 2012; Cisternas et al., 2014; Jin et al., 2016; Knight and Kothary, 2011). During embryonic skeletal muscle formation, determination and differentiation of muscle cells is strongly dependent on four members of the myogenic regulatory factor (MRF) family: Myf5 (myogenic factor 5), MRF4 (muscle-specific regulatory factor 4), MyoD (myoblast determination protein) and Myogenin (Sabourin and Rudnicki, 2000). MRFs are basic helix-loop-helix (bHLH) transcription factors that activate the expression of muscle-specific genes during myogenesis. Myf5 and MyoD are important for the commitment of precursor cells to the myogenic lineage, whereas Myogenin and MRF4 regulate the differentiation of committed myoblasts into elongated myocytes and their subsequent fusion into myotubes (Bentzinger et al., 2012; Berkes and Tapscott, 2005). Terminal differentiation of muscle cells triggers the expression of genes encoding for proteins that are important for muscle fiber architecture and function, including myosin heavy (MHC) and light chains (MLC), and muscle creatine kinase (Berkes and Tapscott, 2005). Other important transcription factors during myogenesis include the paired-box transcriptional factors Pax3 and Pax7, which act upstream of MRFs (Buckingham and Relaix, 2015), the myocyte enhancer factor 2 (MEF2) protein

family (Pon and Marra, 2015), and the six family of homeo-box proteins (Relaix and Buckingham, 1999; Wu et al., 2014).
It is important to note that some muscle precursor cells escape the differentiation program and reside as quiescent muscle stem cells, so-called satellite cells, under the basal lamina. Quiescent satellite cells can be activated upon muscle injury and transit into the proliferating myoblast state. Activated satellite cells give thus rise to a population of myoblasts which can differentiate and fuse with the damaged muscle fiber (Le Grand and Rudnicki, 2007; Relaix and Zammit, 2012; Yin et al., 2013).

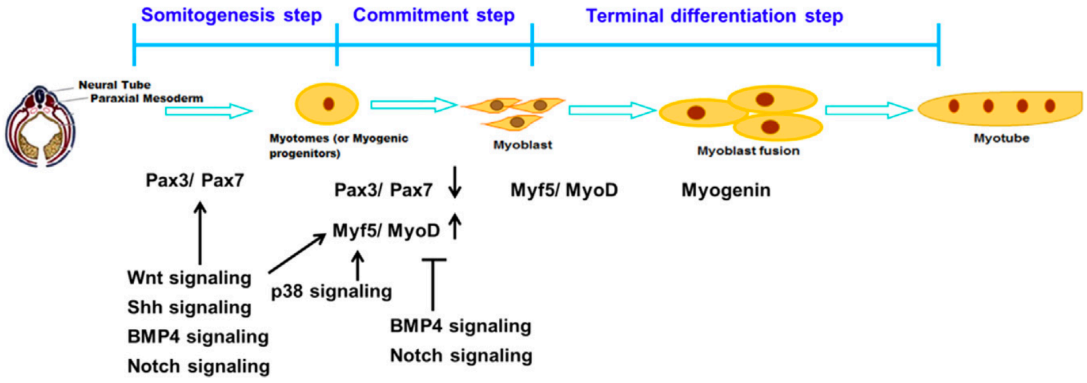

Figure 1.2: Simplified scheme of embryonic myogenesis. During embryonic development, muscle progenitor cells that arise from the somites express Pax3/Pax7. Certain embryonic progenitors commit to the myogenic lineage and the committed myoblasts differentiate into myocytes, which further fuse with each other to form myotubes. These processes are tightly regulated by a plethora of transcription factors and signaling cascades. Taken from (Jin et al., 2016), https://doi.org/10.1016/j.bbrep.2016.04.009, reprinted under the terms of the Creative Commons user license, https://creativecommons.org/licenses/by-nc-nd/4.0/ [02.06.2017].

1.2 Nuclear positioning and the nuclear envelope

In skeletal muscle, nuclei are positioned at the periphery under the sarcolemma of the muscle fiber. However, not only during skeletal muscle formation but in a diversity of cellular processes, such as cell migration, cell division and zygote formation, is the positioning of the nucleus strictly controlled (Gundersen and Worman, 2013). The nuclear envelope (NE) plays a major role in the regulation of nuclear positioning processes.

The NE is a double membrane that forms a boundary between the nucleus and the cytoplasm and thereby functions to shelter the genome but also to couple the

nucleus to the cytoskeleton. It comprises two lipid bilayers, the inner nuclear membrane (INM) and the outer nuclear membrane (ONM) which is continuous with the endoplasmic reticulum (ER) (Franke et al., 1981). The INM and ONM are separated by a 40-50 nm luminal gap, the perinuclear space (PNS). Together, INM and ONM are believed to contain more than 100 potential transmembrane proteins, yet their composition may vary depending on the cell type or differentiation status (Chen et al., 2006; Datta et al., 2009; Korfali et al., 2010; Liu et al., 2009; Malik et al., 2010; Schirmer et al., 2003; Wilkie et al., 2011). Underlying the INM is a 10-20 nm thin protein network, the nuclear lamina that is mainly composed of A- and B-type lamins (Burke and Stewart, 2013). The nuclear lamina provides structural support for the NE but moreover regulates chromatin organization and gene expression (Guelen et al., 2008; Kind and van Steensel, 2010; Shimi et al., 2008; Towbin et al., 2013).

Two key structures of the NE that span INM and ONM include the nuclear pore complexes (NPCs) and the linker of nucleoskeleton and cytoskeleton (LINC) complexes. NPCs are multi-protein channels that comprise more than 30 different nucleoporins (Nups) and regulate nucleocytoplasmic transport (Beck and Hurt, 2017). LINC complex are built of transmembrane SUN (Sad1/UNC-84) domain proteins at the INM that bind within the PNS to KASH (Klarsicht/ANC-1/SYNE homology) domain proteins of the ONM (Starr and Fridolfsson, 2010). On the nucleoplasmic site, SUN domain proteins interact with the nuclear lamina, chromatin and other INM proteins. On the cytoplasmic site, KASH domain proteins interact with cytoskeletal components, including actin filaments, microtubules, and intermediate filaments. SUN and KASH domain proteins span together as the LINC complex the entire NE and can thus transmit forces from the cytoskeleton to the nuclear lamina (Figure 1.4 B).

Several components of the NE have been linked with a diversity of diseases, including laminopathies, bone disorders, and accelerated aging syndromes (Stewart et al., 2007; Wilkie et al., 2011; Worman, 2012). However, most diseases resulting from mutations in nuclear transmembrane or NE-associated proteins affect muscle.

1.2.1 SUN domain proteins

Sun proteins were firstly discovered by genetic characterization of *C. elegans* mutants showing nuclear positioning defects (Horvitz and Sulston, 1980; Malone et al., 1999). These studies firstly identified Unc-84 with a characteristic C-terminal domain that displayed high homology to the C-terminus of Sad1 in *Schizosaccharomyces pombe*

and to two human proteins, named Sun1 and Sun2 (Figure 1.3). This conserved C-terminal domain (∼ 175 amino acids) was thus termed the SUN (Sad1/UNC-84) domain (Malone et al., 1999).

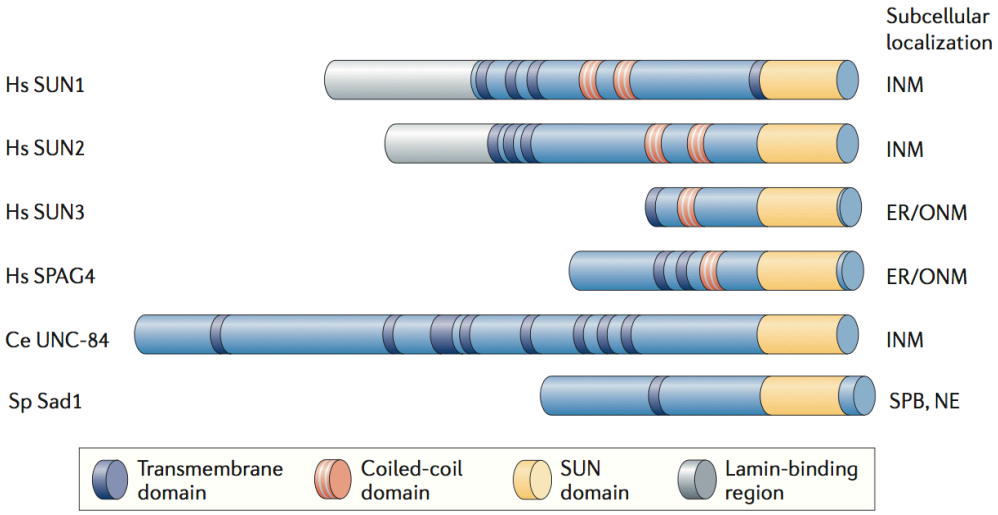

Figure 1.3: Schematic structure of SUN domain proteins. Different domains of SUN domain proteins from different species are drawn to scale. Ce, *Caenorhabditis elegans*; Dm, *Drosophila melanogaster*; Hs, *human*; Sp, *Schizosaccharomyces pombe*; SPB, *spindle pole body*. Modified from (Tzur et al., 2006). Reprinted by permission (Licence #4121560829884) from Macmillan Publishers Ltd: Nat Rev Mol Cell Biol. 7(10):782-8., copyright (2006).

Sun proteins are evolutionarily conserved and can be found in various species ranging from *Drosphila melanogaster* (Klaroid) and *Saccharomyces cerevisiae* (Mps3) to plants (Graumann et al., 2010; Jaspersen et al., 2006; Kracklauer et al., 2007).
In mammalian cells, Sun proteins are encoded by at least five genes, *Sun1-5*. However, only Sun1 and Sun2 are ubiquitously expressed, whereas the expression of Sun3, Sun4 (also termed SPAG4) and Sun5 (also termed SPAG4L) is largely restricted to testis (Crisp et al., 2006; Frohnert et al., 2011; Göb et al., 2010; Pasch et al., 2015; Shao et al., 1999). Besides their prominent SUN domain, Sun proteins contain at least one transmembrane and a more variable N-terminal region that is orientated towards the nucleoplasm and mediates binding to various nuclear components, including lamins and chromatin (Figure 1.3) (Chi et al., 2007; Crisp et al., 2006; Haque et al., 2006; Hodzic et al., 2004; Oza et al., 2009; Wang et al., 2006). Whereas Sun1 localizes to the INM independently of A- or B-type lamins, Sun2 seems to require A-type lamins for its retention at the NE, as Sun2 mislocalizes to cytoplasmic membranes (e.g. ER) in laminA/C-deficient fibroblasts (Crisp et al., 2006; Haque et al., 2006; Hasan et al., 2006). The C-terminal domain of Sun proteins extends into the PNS and

comprises the SUN domain as well as a preceding coiled-coil region that likely forms a triple coiled-coil to induce trimerization of SUN domains (Nie et al., 2016; Sosa et al., 2013; Wang et al., 2012; Zhou et al., 2012). These trimeric SUN domains form a platform for the interaction with three KASH domain proteins which together form higher-order LINC complexes (Chang et al., 2015).

1.2.2 KASH domain proteins and their connections to the cytoskeleton

The family of KASH domain proteins were described based on a conserved C-terminal region in *Drosophila* Klarsicht, *C. elegans* ANC-1 and in mammalian Syne-1/Nesprin-1, which was thus termed the Klarsicht/ANC-1/SYNE homology (KASH) domain (Starr and Han, 2003). The KASH domain comprises the transmembrane domain and a region of $\sim$ 40 amino acids that reaches into the PNS and interacts with SUN domains (Starr and Fridolfsson, 2010). The KASH domain is sufficient to localize these proteins to the ONM (Fischer et al., 2004; McGee et al., 2006; Starr and Han, 2002). Upon targeting to the ONM, the large but more variable N-terminus of KASH domain proteins can bind to different cytoskeletal components and thus functions, for example, to position the nucleus within the cell or to tether the centrosome to the nucleus.
In mammalian cells, KASH domain proteins are broadly known as Nuclear Envelope SPectRIN repeat proteins (Nesprins or *Syne* according to the gene name), of which there are at least five known up to now: Nesprin-1, -2, -3, -4 and KASH5, the latter being specific to germ cells (Morimoto et al., 2012; Roux et al., 2009; Wilhelmsen et al., 2005; Zhang et al., 2001).

Binding to actin filaments

The giant isoforms of Nesprin-1 ($\sim$ 1 MDa) and Nesprin-2 ($\sim$ 800 kDa) contain besides their C-terminal KASH domains, multiple spectrin repeats (74 in the case of Nesprin-1 and 56 in the case of Nesprin-2) and N-terminal paired calponin homology (CH) domains that bind directly to actin (Figure 1.4 A, B) (Zhang et al., 2002; Zhen et al., 2002). Connections between Nesprin-2 and actin were shown to regulate nuclear shape of fibroblasts and keratinocytes, as these cells displayed severe nuclear morphological changes (e.g. NE blebbing, giant nuclei) in Nesprin-2 knockout mice lacking the CH domains (Lüke et al., 2008). Interactions of Nesprins with actin are moreover important to mediate nuclear anchorage and positioning in various

cell types (Luxton et al., 2010; Starr and Han, 2002). In polarizing fibroblasts, the nucleus moves to the rear of the cell prior to migration to reposition the centrosome towards the leading edge (Gomes et al., 2005). This nuclear movement depends on a retrograde flow of actin cables that are linked to the nucleus by Nesprin-2 giant and Sun2. Nesprin-2 giant and Sun2 congregate actin into linear arrays on the dorsal site of the nucleus and form so-called transmembrane actin-associated nuclear (TAN) lines (Luxton et al., 2010, 2011). Additional interaction of Nesprin-2 giant with the formin FHOD1 is required for TAN line formation and rearward nuclear movement (Kutscheidt et al., 2014).

Binding to microtubules (MTs)

Nesprin-1, Nesprin-2, Nesprin-4 in secretory epithelial cells, and KASH5 in spermatocytes bind to MTs through direct or indirect association with motor proteins, including kinesins and dynein/dynactin (see section 1.3.4 for a description of kinesin and dynein motor proteins) (Roux et al., 2009; Schneider et al., 2011; Wilson and Holzbaur, 2015; Yu et al., 2011; Zhang et al., 2009). However, only the KASH-less isoform $p50^{Nesp1}$, which is composed of the spectrin repeats 48-51 of Nesprin-1 and localized to processing bodies (P-bodies), was shown by cosedimentation assays to directly interact with MTs so far (Rajgor et al., 2014). The interaction between KASH domain proteins and MT-dependent motor proteins is often direct, although not all binding sites have been mapped so far. Nesprin-2 associates with dynein/dynactin and kinesin-1 motors at the NE to regulate centrosome-coupling to the nucleus during neuronal migration of the developing mouse brain and during nuclear migration in the mouse retina (Yu et al., 2011; Zhang et al., 2009). In contrast, Nesprin-4 binds directly to the light chain of kinesin-1 and, when ectopiclly expressed, disengages the centrosome and the Golgi complex from the nucleus (Roux et al., 2009). KASH5 interacts with dynein/dynactin and recruits these motor proteins together with Sun1 to telomere ends. Through the recruitment of dynein/dynactin to the NE, KASH5 and Sun1 mediate chromosome movement during meiosis (Horn et al., 2013; Morimoto et al., 2012).

Binding to intermediate filaments

Two different isoforms for Nesprin-3 have been described: Nesprin-3α and Nesprin-3β. Nesprin-3α comprises an unique N-terminal region that can bind to the actin-binding domain of plectin, which in turn interacts with intermediate filaments (Wilhelmsen et al., 2005). Additonally, Nesprin-3α can interact with the CH domains of Nesprin-1

and Nesprin-2, thus forming diverse Nesprin networks at the NE that are able to connect to different cytoskeletal components at the same time (Lu et al., 2012).

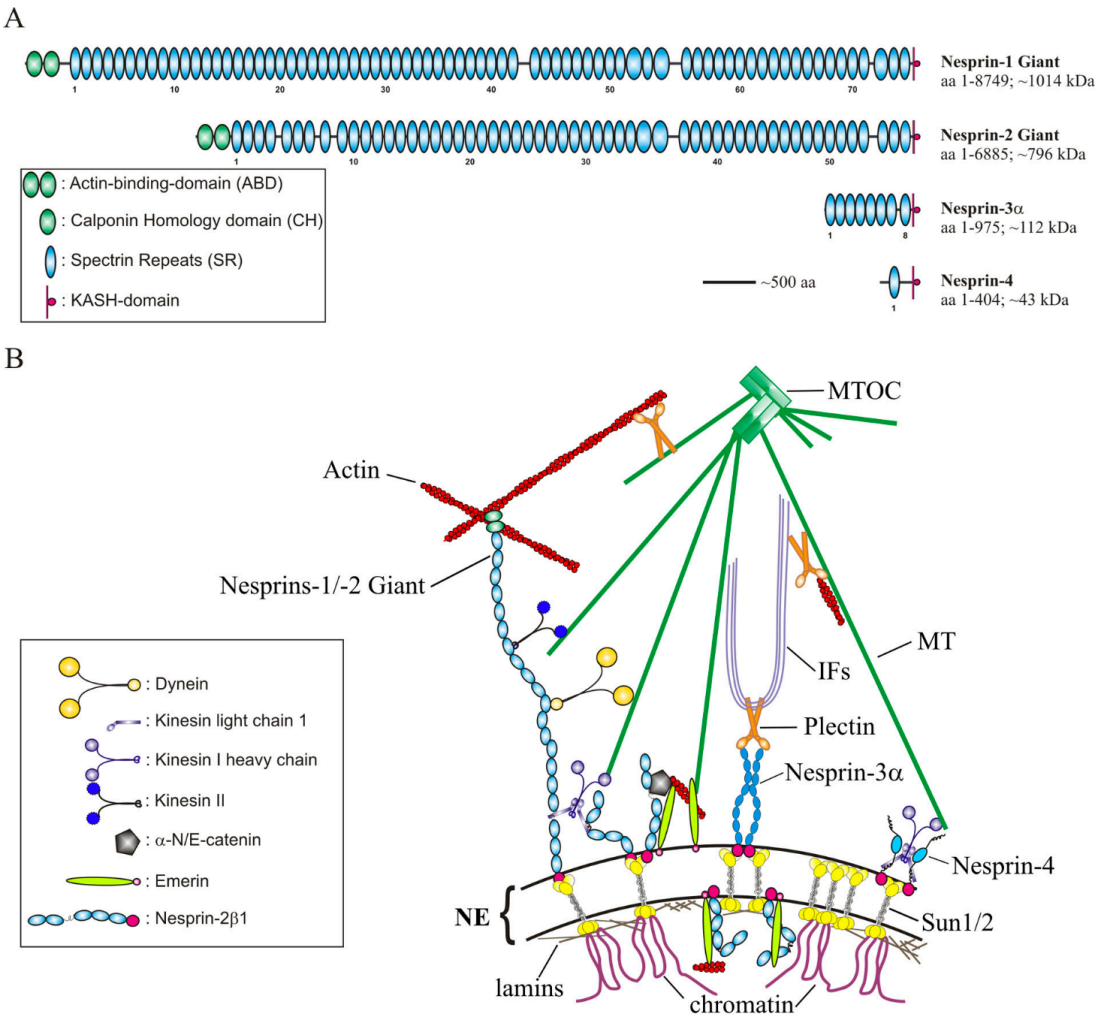

Figure 1.4: Nesprins connect the NE to different cytoskeletal components. (A) Schematic domain structure of the Nesprin family. Nesprins contain a C-terminal Klarsicht/ANC-1/SYNE homology (KASH) domain, several spectrin repeats and variable N-terminal regions. The giant isoforms of Nesprin-1 and Nesprin-2 possess actin-binding calponin homology (CH) domains at their N-termini. KASH5 is a meiosis-specific KASH protein and is not depicted here. **(B)** Nesprins localize to the outer nuclear membrane by binding to SUN domain proteins of the inner nuclear membrane (INM). Nesprin-1 and Nesprin-2 interact directly with actin filaments through their N-terminal CH domains and indirectly with microtubules (MTs) through kinesin-1 and dynein motor proteins. Nesprin-3α binds to intermediate filaments through plectin. Nesprin-4 binds to MTs through kinesin-1. Some smaller Nesprin isoforms may also localize to the INM. Within the nucleoplasm, Sun proteins interact with the nuclear lamina (lamins), chromatin and other proteins of the INM. Reprinted from (Cartwright and Karakesisoglou, 2014), 29:169-79, Nesprins in Health and Disease, copyright (2014), with permission from Elsevier (Licence #4118400155065).

1.2.3 Tissue-specific KASH splice variants

The giant isoforms of Nesprin-1 and Nesprin-2 are in general ubiquitously expressed and predominant in the majority of tissues but they additionally produce tissue-specific isoforms through alternative initiation of transcription and mRNA splicing (Duong et al., 2014; Rajgor et al., 2012; Zhang et al., 2001). Tissue-specific expression of certain Nesprin isoforms is believed to contribute to specific nucleus-cytoskeleton connections which account for the individual biomechanical properties of highly specialized cell types, e.g. muscle cells (Mellad et al., 2011). Many of these alternative-spliced isoforms contain the C-terminal KASH domain and subsequently localize to the ONM or in a few cases to the INM (smaller isoforms), respectively. However, also KASH-less isoforms that are unable to contribute to LINC complex formation were described to localize throughout the cell but their exact function *in vivo* remains elusive so far (Duong et al., 2014; Razafsky and Hodzic, 2015).
The expression of smaller Nesprin-1 and Nesprin-2 isoforms is in some tissues dominant (Duong et al., 2014; Rajgor et al., 2012; Zhang et al., 2001). In spleen, for example, expression of Nesprin-1β-1 is highly increased and in cardiac and skeletal muscle two smaller isoforms, Nesprin-1α-2 (hereafter referred to as Nesprin-1α) and Nesprin-2α-1, are exclusively expressed (Duong et al., 2014). During skeletal muscle differentiation, expression of Nesprin-1α was shown to be highly upregulated, both on mRNA and protein levels (Holt et al., 2016; Randles et al., 2010; Zhang et al., 2001). Nesprin-1α is structurally an N-terminally truncated version of Nesprin-1 giant: It contains the C-terminal KASH domain, seven spectrin repeats but lacks the N-terminal CH domains (Apel et al., 2000; Mislow et al., 2002b). Nesprin-1α contains additionally a short and unique N-terminal segment but apart from that is identical to the C-terminal region of Nesprin-1 giant (Simpson and Roberts, 2008). From a functional perspective, Nesprin-1α was suggested to homodimerize through its N-terminal spectrin repeat domains and to recruit the scaffolding protein muscle A-kinase anchoring protein (mAKAP) to the NE in cardiac myocytes (Mislow et al., 2002a; Pare et al., 2005). Additionally, Nesprin-1α was demonstrated to bind lamin A and emerin (Mislow et al., 2002a,b). Although Nesprin-1α was proposed to localize to the INM in these studies, this seems due to its size of $\sim$ 112 kDa rather unlikely. Together these three studies concluded that Nesprin-1α might function as a scaffold protein and molecular link for signaling molecules at the NE. However, a clear biological function for Nesprin-1α in skeletal muscle remains to be determined.

1.2.4 The LINC complex in muscle disorders

Various components of the LINC complex, including Nesprin-1/-2 and Sun1/2, as well as lamin A/C, are mutated in muscular dystrophies as exemplified by Emery-Dreifuss muscular dystrophy (EDMD) (Bonne et al., 1999; Mamchaoui et al., 2011; Meinke et al., 2014; Zhang et al., 2007b). EDMD is a neuromuscular disorder characterized by joint contractures that appear early in childhood as well as progressive skeletal muscle weakness and wasting and cardiomyopathy (Pillers and Von Bergen, 2016). Mutations within the *LMNA* or *EMD* gene, encoding lamin A/C or the INM protein emerin, respectively, were initially identified to cause autosomal-dominant and X-linked forms of EDMD (Bione et al., 1994; Bonne et al., 1999). Heterozygous mutations within the *SYNE1* and *SYNE2* gene, encoding for Nesprin-1 and Nesprin-2, respectively, were additionally associated with EDMD (Zhang et al., 2007b). Fibroblasts and muscle cells from these patients displayed marked alterations of nuclear shape and mislocalization of Nesprins, emerin and Sun2. Moreover, the interactions between Nesprins-1/-2, emerin and lamin A/C were either decreased or completely abolished, suggesting that any changes in LINC complex composition, stability or functionality can cause severe muscle disorders (Wheeler et al., 2007; Zhang et al., 2005). Mutations within the *SUN1* and *SUN2* gene have been further identified in patients with EDMD-like phenotypes (Meinke et al., 2014). Fibroblasts overexpressing one of the five disease-causing Sun1/2 variants (SUN1 G68D, SUN1 G338S, SUN1 W377C, SUN2 A56P, SUN2 R620C) failed to move their nuclei towards the rear of the cell and to reposition their centrosomes prior to migration. Primary myoblasts from a patient with compound heterozygous *SUN1* p.G68D/p.G338S variants showed increased levels of SUN1 and Nesprin-2 at the NE but a decreased capability to interact with emerin. Interestingly, *in vitro* differentiated myotubes from this patient showed disorganized myonuclei which failed to recruit the centrosomal protein Pericentrin to the NE and to nucleate MTs (Meinke et al., 2014).

A homozygous nonsense mutation within the *SYNE1 (23560 G>T)* gene (Protein: E7854X) was furthermore identified in patients suffering from congenital muscular dystrophy (CMD), a heterogenous group of inherited myopathies characterized by early onset of progressive muscle weakness (Mamchaoui et al., 2011; Voit et al., 2007, 2002). Quantitative PCR studies of these *SYNE1 (23560 G>T)* CMD patient cells showed that the mRNA levels of both Nesprin-1 giant and Nesprin-1α were highly reduced by 78% and 85%, respectively (Holt et al., 2016).

Why mutations within components of the LINC complex lead to tissue-specific

muscle diseases, is still a puzzling question. It is likely that changes within LINC complex components affect the nucleoskeleton-cytoskeleton coupling and thus render particularly muscle cells incapable to withstand mechanical forces during muscle contraction. However, muscle cells also undergo an extensive isoform switch from giant to smaller muscle-specific isoforms during myogenic differentiation (Randles et al., 2010). This suggests that also defects in gene expression of these tissue-specific isoforms could contribute to cause muscle diseases. Finally, the LINC complex is crucial for correct nuclear positioning during skeletal muscle formation and any defects in the underlying mechanisms were suggested to affect muscle function (see also section 1.2.5 and 1.2.6) (Elhanany-Tamir et al., 2012; Metzger et al., 2012).

1.2.5 Nesprin-1/2 and Sun1/2 knockout mouse models

Several knockout mouse models for components of the LINC complex were created to understand cellular functions of Nesprins and Sun proteins *in vivo* and in human muscle disorders. However, existing Nesprin-1 and Nesprin-2 knockout strains display a high variability in the severeness of the observed phenotypes.
Mice overexpressing either the KASH-domain of Nesprin-1 or Nesprin-2 under a muscle-specific promoter, displace endogenous Nesprin-1 and Nesprin-2 from the nucleus in muscle fibers due to the dominant-negative effect of the artificial KASH-construct. These mice display nuclear positioning defects with decreased numbers of extrasynaptic nuclei and increased numbers of non-synaptic nuclei (Grady et al., 2005; Zhang et al., 2007c). Studies with single Nesprin-1 or Nesprin-2 KASH-domain knockout mice, respectively, further clarified that Nesprin-1 but not Nesprin-2 is important for the anchorage of synaptic and non-synaptic nuclei in myofibers (Zhang et al., 2007c). Although single KASH-domain knockout mice are viable, double-homozygous KASH-domain knockout mice of Nesprin-1 and Nesprin-2 die within 20 min after birth from respiratory failure, suggesting that Nesprin-1 and Nesprin-2 fulfill partially redundant but essential functions (Zhang et al., 2007c). Another study, however, showed that homozygous mice lacking the KASH domain die around birth, while surviving mice develop typical features of EDMD, including muscle weakness, kyphoscoliosis, cardiac conduction defects, as well as centralized and misaligned nuclei (Puckelwartz et al., 2009). Both Nesprin-1 KASH-knockout mouse models show an important role for Nesprin-1 in nuclear positioning but they differ greatly regarding the viability of the mice and the observed EDMD-like phenotypes (Puckelwartz et al., 2009; Zhang et al., 2007c). These discrepancies might result from the different genetic mouse backgrounds used in the two studies

for generating the knockout lines as well as from the different strategies used to disrupt the KASH domain, resulting in slightly different C-terminal regions of the truncated Nesprin-1 protein. To make the picture even more complicated, two more recent knockout mouse models were generated by Ju Chen's laboratory. They first created knockout mice lacking all Nesprin-1 isoforms harboring the C-terminal spectrin repeats (KASH-containing and KASH-less Nesprin-1 isoforms are depleted) (Zhang et al., 2010). These knockout mice die postnatally between day 2 and 11 (60%), whereas surviving mice show decreased body weights, a decreased exercise capability, a large proportion of centralized nuclei and a lack of nuclei clusters under the NMJ. Secondly, Nesprin-1 knockout mice specifically lacking the N-terminal actin-binding CH domains were viable and displayed no obvious effects regarding nuclear shape, nuclear positioning or localization of other LINC complex components (Stroud et al., 2017). Moreover, in the same study they described Nesprin-1α-specific homozygous knockout mice which mostly die within 5 min after birth. Surviving mice showed growth retardation, kyphosis and nuclear positioning defects. Interestingly, in Nesprin-1α-knockout myofibers, Kif5b was absent at the NE, thus supporting a role for Nesprin-1α/Nesprin-1 in recruiting Kif5b/Kinesin-1 to the nucleus to support Kinesin-mediated nuclear movement in skeletal muscle cells (Stroud et al., 2017; Wilson and Holzbaur, 2015).
As Nesprin-1 is anchored to the ONM by Sun proteins, it is not surprising that also Sun1 and Sun2 double-knockout mice show displacement of Nesprin-1 from the NE and thus severe synaptic and non-synaptic nuclear positioning defects (Lei et al., 2009). However, Sun1 seems to have a more pronounced role in nuclear anchorage as the number of synaptic nuclei is partially decreased in Sun1 but not Sun2 knockout mice (Lei et al., 2009).

1.2.6 Nuclear positioning in skeletal muscle cells

Skeletal muscle fibers are multinucleated cells that arise from the fusion of hundreds of differentiated myoblasts (myocytes) (Abmayr and Pavlath, 2012). As a result, mature myofibers can contain more than 100 nuclei which are predominantly positioned at the periphery of the cell, while some nuclei are found in clusters under the neuromuscular junction (NMJ) (Bruusgaard et al., 2003; Grady et al., 2005; Kummer et al., 2004). Peripheral nuclei are equally spaced, resulting in a maximum distance between adjacent nuclei (Bruusgaard et al., 2003). This positioning is believed to create 'myodomains', where each nucleus is responsible for the transcriptional activity within its surrounding area, thus leading to decreased requirements

to transport mRNAs over long distances throughout the myofiber (Pavlath et al., 1989).
Mispositioning of myonuclei is often a hallmark of muscle diseases, such as Emery-Dreifuss muscular dystrophy (EDMD) or Centronuclear myopathy (CNM), suggesting that correct nuclear positioning is important for muscle function (Cohn and Campbell, 2000; Jungbluth et al., 2008; Metzger et al., 2012). However, a direct relation between nuclear positioning and muscle function still needs confirmation.
At least four distinct nuclear movements or positioning processes - (1) nuclear centration, (2) nuclear spreading, (3) nuclear dispersion and (4) nuclear clustering - can be observed during skeletal muscle formation (Cadot et al., 2015). The underlying mechanisms that drive and regulate these nuclear movements are only recently beginning to emerge.

Nuclear centration

After fusion of a differentiated myoblast with a pre-existing myotube, the myoblast nucleus moves rapidly towards the myotube center with an approximate speed of 0.88 μm/min (Cadot et al., 2012; Englander and Rubin, 1987) (Figure 1.5 A, centering). This nuclear movement, termed centration, requires an intact and dynamic MT network, the small GTPase Cdc42 and the dynein/dynactin complex. In fact, altering MT dynamics with the help of the MT-stabilizing drug taxol or low concentrations of nocodazole prevents nuclear centration movements after myoblast fusion (Cadot et al., 2012). The dynein/dynactin complex is in the presence of Par6 and Par3 proteins recruited to the nucleus in differentiated myoblasts and myotubes. There, it acts to transport the myoblast nucleus towards the minus-end of MTs emanating from myotube nuclei (Figure 1.5 B). Reciprocally, dynein/dynactin molecules located at myotube nuclei can move towards the minus-end of MTs emanating from the myoblast nucleus, thereby pulling the myoblast nucleus towards the center of the myotube (Cadot et al., 2012).

Nuclear spreading

Once nuclei are aligned in the middle of the myotube, they start to spread in parallel to the long axis of the myotube with an average speed of 0.2 μm/min (Cadot et al., 2015) (Figure 1.5 A, spreading). During these nuclear spreading movements, nuclei were observed to rotate and to undergo pausing events before they continue to translocate (Capers, 1960; Cooper and Konigsberg, 1961; Wilson and Holzbaur, 2012). Similar to nuclear centration movements, nuclear spreading depends on

an intact MT network (Englander and Rubin, 1987). Up to know three different models were proposed to explain these nuclear spreading movements. First, nuclear spreading was suggested to require an anti-parallel network of MTs, with each MT minus-end being anchored at one nucleus, as well as cytoplasmic complexes of Kif5b/kinesin-1 and Map7. Through the MT plus-end-directed motor activity of Kif5b, these Kif5b/Map7 complexes would act in concert to push nuclei apart from each other (Metzger et al., 2012) (Figure 1.5 C [1]). Secondly, nuclear spreading was proposed to depend on NE-localized Kif5b and to a lesser extent on NE-localized dynein molecules that transport myotube nuclei as cargo towards the plus-end or minus-end of MTs, respectively (Wilson and Holzbaur, 2012) (Figure 1.5 C [2]). In this model, Kif5b/kinesin-1 is recruited to the NE by Nesprin-1 or Nesprin-2 which share a common kinesin light chain-binding sequence ('LEWD' motif); interfering with the expression of either Nesprin1/2 or Kif5b/kinesin-1 affects nuclear spreading and nuclear rotation (Wilson and Holzbaur, 2012, 2015). How dynein molecules are linked to the NE is less understood but might involve Nesprins or unknown binding partners at the nucleus (Zhang et al., 2009). The third model was suggested based on muscle morphogenesis studies in *Drosophila melanogaster* (Figure 1.5 C [3]). Dynein is transported to the cell cortex of the myofiber pole by kinesin-mediated movement towards the MT plus-end (Folker et al., 2014). This transport requires Sunday Driver (Syd), a family member of the JNK-interacting proteins (JIP), which mediates complex formation of kinesin and dynein (Schulman et al., 2014). At the cell cortex, dynein is anchored by the protein Pins/Raps (partner of inscuteable; also termed rapsynoid) and is thus able to pull on MTs to move nuclei in the direction of the myofiber pole. Thereby, interactions between MTs and the cell cortex are stabilized by CLIP-190 and are important for correct myonuclear positioning (Folker et al., 2012). However, if this model is also important for nuclear spreading movements in mammalian muscle cells remains to be determined.

Nuclear dispersion

After nuclei are equally spread throughout the myotube, they move towards the periphery of the cell and finally get anchored below the sarcolemma (Figure 1.5 A, dispersion). In contrast to nuclear centration and spreading movements, nuclear dispersion seems to be dependent on the actin cytoskeleton but independent of the MT network (Falcone et al., 2014). Additionally, nuclear movement to the periphery involves Nesprins that couple myonuclei to actin, as well as the actin polymerization factor N-WASP, which activates the actin-nucleation capacity of the Arp2/3

complex (Falcone et al., 2014; Takenawa and Suetsugu, 2007). N-WASP itself is activated through interaction with Amphyphysin-2, a protein that is encoded by the *AMPH2/BIN1* gene and often found mutated in centronuclear myophathy (Falcone et al., 2014; Nicot et al., 2007). Other factors that contribute to nuclear positioning at the periphery include desmin intermediate filaments and blood vessels (Chapman et al., 2014; Ralston et al., 2006; Shah et al., 2004; Tokuyasu et al., 1983). Myonuclei were demonstrated to localize in close proximity to blood vessels, suggesting that blood vessels could locally stimulate nuclear movement to the periphery (Ralston et al., 2006). In contrast, desmin was shown to regulate nuclear spacing by acting as a repellent between nuclei (Ralston et al., 2006). Finally, nuclear anchorage at the periphery requires LINC complexes, including Nesprin-1 and Sun1/2, and at least in part desmin intermediate filaments (Chapman et al., 2014; Elhanany-Tamir et al., 2012; Lei et al., 2009; Zhang et al., 2010, 2007c).

Nuclear clustering

Typically 3-8 nuclei cluster and get anchored under the neuromuscular junction (NMJ) (Bruusgaard et al., 2003; Sanes and Lichtman, 2001) (Figure 1.5 A, clustering). These so-called synaptic nuclei are highly specialized as they express NMJ-specific genes (Nazarian et al., 2005). The mechanisms underlying nuclear movements to the NMJ as well as nuclear clustering at synaptic contact sites is still poorly understood. However, studies with chick muscle cultures suggested that nuclear clustering might be linked to the clustering of acetylcholine receptors (AchRs) at post-synaptic membranes (Englander and Rubin, 1987). Recruitment of AchRs to the post-synaptic membrane requires a complex signaling pathway involving the neuron-derived ligand Agrin, the co-receptor low-density lipoprotein receptor-related protein 4 (LRP4) and the muscle-specific tyrosine kinase (MuSK) (Kim et al., 2008; Zong and Jin, 2013). MuSK was demonstrated to interact with Nesprin-1, which is increased at synaptic nuclei in comparison to non-synaptic nuclei, suggesting that connections between Nesprin-1 and MuSK might be important for synaptic nuclei anchorage beneath the NMJ (Apel et al., 2000). In line with this hypothesis, transgenic mice overexpressing the dominant-negative KASH domain of Nesprin-1 displayed anchorage defects of synaptic nuclei due to displacement of endogenous Nesprin-1 from the NE (Grady et al., 2005).

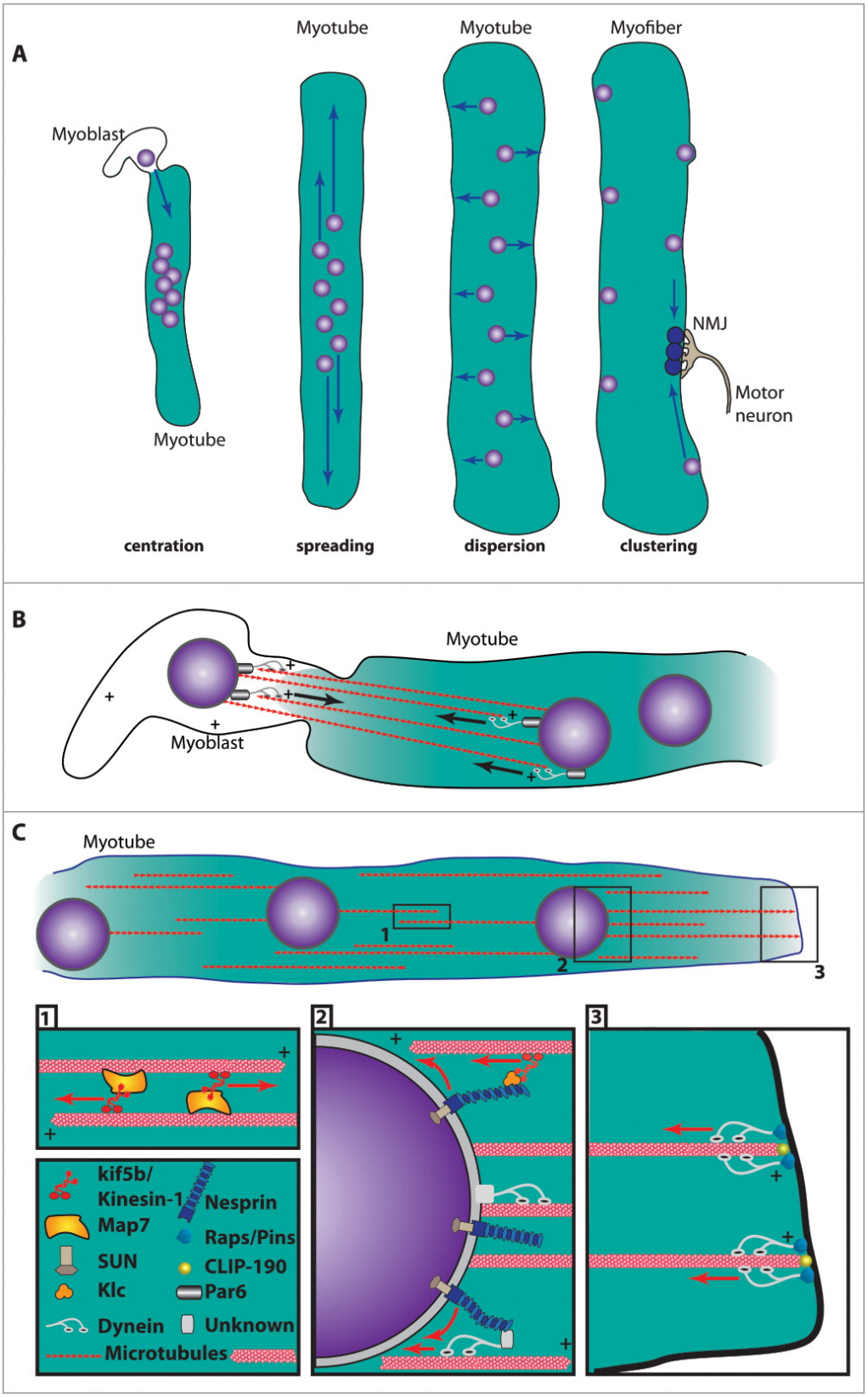
A
Myoblast
Myotube
Myotube
Myotube
Myofiber
NMJ
Motor neuron
centration
spreading
dispersion
clustering
B
Myotube
Myoblast
C
Myotube
1
2
3
kif5b/ Kinesin-1
Map7
SUN
Klc
Dynein
Microtubules
Nesprin
Raps/Pins
CLIP-190
Par6
Unknown

Figure 1.5: Different nuclear movements occur during skeletal muscle formation. (A) The nucleus of a differentiated myoblast moves towards the center of the myotube shortly after fusion (nuclear centration). Subsequently, nuclei spread along the long axis of the myotube (nuclear spreading) until they get evenly dispersed and move to the periphery of the myofiber (nuclear dispersion). Non-synaptic nuclei are evenly distributed at the periphery and anchored below the sarcolemma, whereas some synaptic nuclei cluster and are anchored beneath the neuromuscular junction (NMJ) (nuclear clustering). **(B)** Nuclear centration movements require MTs emanating from both myoblast and myotube nuclei, thereby forming an anti-parallel MT network. Dynein localizes through Par6 to the nucleus and moves towards the MT minus-end, thereby bringing myoblast and myotube nuclei together. **(C)** Three different models may explain MT-dependent nuclear spreading movements inside myotubes: [1] cytoplasmic complexes of Kif5b/kinesin-1 and MAP7 slide anti-parallel MTs. [2] Kif5b/kinesin-1 localizes to the nucleus by binding to Nesprins through the kinesin light chain (Klc). NE-localized Kif5b/kinesin-1 move towards the MT plus-end, thereby inducing nuclear rotation and translocation. Also dynein molecules bound to the NE through Nesprins or unkown binding partners contribute to nuclear translocation by moving towards the MT minus-end. [3] In *Drosophila*, dynein is bound at the cell cortex by Raps/Pins, where it can pull on MTs that are stabilized at the cell cortex by CLIP-190. Modified from Cadot et al. (2015). Reprinted by permission (Licence #P060617-03) from Taylor & Francis LLC: Nucleus. 6(5):373-81, copyright (2015), (http://www.tandfonline.com).

1.3 Microtubules

MTs are not only important for nuclear centration and nuclear spreading movements during skeletal muscle formation but also for a broad range of cellular processes. They build the structural component to separate chromosomes during mitosis and form due to their ability to bundle and to slide against each other the basis for cilia and flagella. Moreover, MTs regulate cell polarity and function as tracks for intracellular transport and MT-dependent motor proteins to position membrane-bound organelles within the cell. The involvement in these diverse cellular functions require MTs to form a dynamic and sophisticated network that extends long distances within the cell and adapts rapidly according to the cell context.

1.3.1 Microtubule structure and dynamics

MTs are polar hollow tubes with an outer diameter of approximately 25 nm that are made up of 13 protofilaments *in vivo*. Protofilaments are linear polymers of repeating $\alpha\beta$-tubulin heterodimers, two related subunits of 55 kDa that exist in all eukaryotes. Through lateral interactions, protofilaments form a helical structure, where adjacent α subunits or β subunits homotypically interact between two protofilaments (α-α and β-β) (Figure 1.6). This so-called B-type lattice is not totally consistent and features a longitudinal 'seam', where α and β subunits of two adjacent protofilaments heterotypically interact with each other (McIntosh et al., 2009; Metoz et al., 1997). Due to the head-to-tail arrangement of $\alpha\beta$-tubulin heterodimers and the parallel

association of protofilaments with the same directionality, MTs possess an intrinsic polarity: While β-tubulin subunits are exposed at the fast-growing MT plus (+) end, α-tubulin subunits are exposed at the slowly-growing MT minus (-) end (Figure 1.6). MTs grow or shrink through association or dissociation of $\alpha\beta$-tubulin heterodimers at the ends, respectively, a process that highly depends on the concentration of free $\alpha\beta$-tubulin heterodimers. MTs assemble spontaneously *in vitro* above a *critical concentration* (C_c) of $\alpha\beta$-tubulin heterodimers in a temperature-sensitive manner. When the surrounding tubulin concentration is higher than C_c, tubulin addition at steady state occurs preferentially at the plus-end, while tubulin dimers are lost at the minus-end. This concept of *treadmilling* was initially postulated by Margolis and Wilson (Margolis and Wilson, 1978, 1981) and describes the equilibrium between MT polymerization and depolymerization occurring simultaneously at opposite MT ends at steady state.

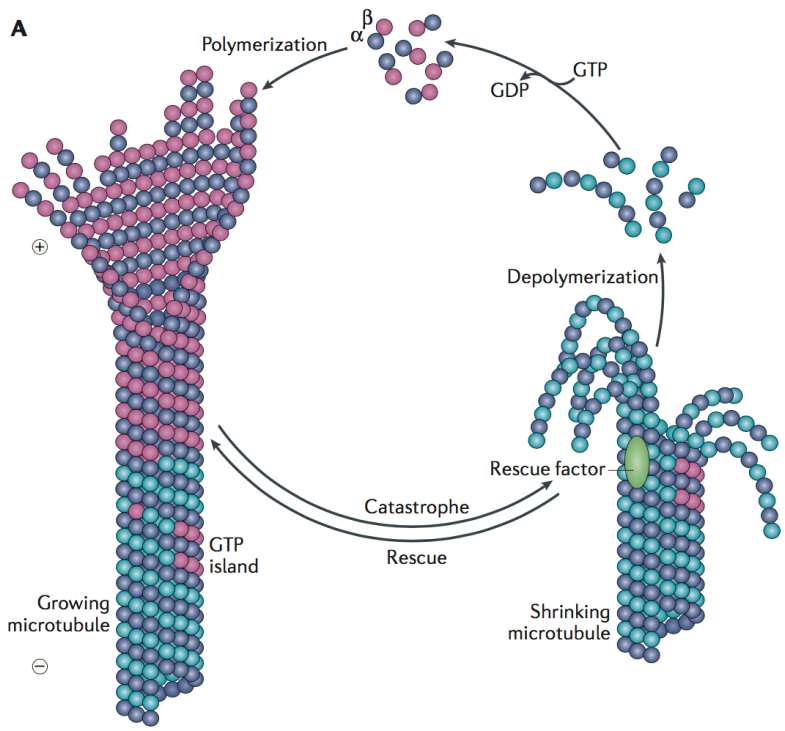

Figure 1.6: Microtubule assembly and disassembly. MT polymerization requires the addition of $\alpha\beta$-tubulin heterodimers and subsequent GTP hydrolysis within the β subunit. Growing MTs possess rather straight, sheet-like plus ends and a stabilizing GFP cap. Upon loss of the GFP cap, depolymerizing MTs display curved plus ends. Sudden alterations between growing and shrinking phases of MTs are termed catastrophe and rescue, respectively. Rescue events might occur in the presence of 'GTP islands' or certain 'rescue factors'. Taken from Akhmanova and Steinmetz (2015). Reprinted by permission (Licence #4102510375449) from Macmillan Publishers Ltd: Nat Rev Mol Cell Biol., 16(12):711-26, copyright (2015).

Another concept to describe MT dynamics, termed dynamic instability, was introduced by Mitchison and Kirschner (1984a) based on the observation that growing and shrinking MTs co-exist in one bulk population *in vitro* (Mitchison and Kirschner, 1984a,b). MTs can suddenly alternate from growing to shrinking phases by a phenomenon termed *catastrophe*. Conversely, shrinking MTs can undergo *rescue* events to switch back into polymerization modus. At the molecular level, dynamic instability depends on the ability of α- and β-tubulin to bind one molecule of GFP. While the GFP bound to α-tubulin is non-exchangeable and only seems to be structurally important, the one bound to β-tubulin can be hydrolyzed to GDP. When a new $\alpha\beta$-tubulin heterodimer is incorporated at the MT end, GTP hydrolysis is stimulated by interaction of the catalytic domain of the newly added α-subunit with the β-subunit of the previous tubulin heterodimer. As a result, the MT plus-end generally contains a cap of GTP-bound β-subunits, while the MT lattice harbours GDP-β-tubulin subunits down its length (GTP-cap model) (Caplow and Shanks, 1996; Drechsel and Kirschner, 1994). As long as the stabilizing GTP cap is present, MTs are found in a 'straight' conformation and continue growing, whereas upon loss of the GTP cap, MTs display an outwardly curved conformation and depolymerize (Figure 1.6) (Alushin et al., 2014; Hyman et al., 1995; Mandelkow et al., 1991; Yajima et al., 2012). The mechanisms and cellular factors leading to MT catastrophe or rescue events are generally poorly comprehended. Catastrophes were claimed to occur in an age-dependent manner due to structural changes at the MT tip and the higher probability of destabilizing events (Coombes et al., 2013; Gardner et al., 2011; Odde et al., 1995). Catastrophes were also shown to be more likely when forces are exerted on growing MTs (Janson et al., 2003). Rescue events of shrinking MTs were suggested to require GTP-bound β-tubulin subunits that escaped GTP hydrolysis and remained within the MT lattice (so-called GTP-islands) (Dimitrov et al., 2008). Collectively, MT dynamics are characterized by four parameters: the MT growth and shortening rate and the frequencies of catastrophe and rescue events.

1.3.2 Regulation of MT dynamics

MT dynamics are spatiotemporally controlled by intrinsic properties of MTs (e.g. the GTP-cap, tubulin modifications) but also by extrinsic regulators such as microtubule-associated proteins (MAPs) and motor proteins that either promote MT assembly/disassembly or the transition between growing and shrinking phases (catastrophe, rescue).

The best studied MAPs include members of the MAP2/Tau family of proteins, the

neuron-specific MAP2 and Tau proteins as well as MAP4 (Dehmelt and Halpain, 2005; Drechsel et al., 1992; Kowalski and Williams, 1993). These so-called 'structural MAPs' contain a N-terminal projection of varying sizes and a C-terminal MT-binding domain. Upon binding along the MT lattice, these MAPs can stabilize MTs to increase the net MT growth or crosslink MTs to induce bundling (Lewis et al., 1989). Phosphorylation of the KXGS motifs within the C-terminal domain by multiple kinases, such as cAMP-dependent protein kinase (PKA) or microtubule-affinity-regulating kinase (MARK), strongly regulate the activity of MAPs (Drewes et al., 1995; Ozer and Halpain, 2000). A MAP4 isoform, termed oMAP4, regulates MT organization into a paraxial array during muscle formation (Mogessie et al., 2015).
Another important group of MAPs, the microtubule plus-end-tracking proteins (+TIPs), specifically localize to growing MT plus-ends (Akhmanova and Steinmetz, 2010). The +TIP end-binding (EB) family protein consist of a N-terminal calponin homology domain (CH domain), a linker region and a C-terminal coiled-coil domain for dimerization of EB monomers (De Groot et al., 2010; Hayashi and Ikura, 2003). The C-terminal domain features additionally the EB homology domain and an EEY/F motif, which together are important for interactions with other +TIPs to form complex networks at MT plus-ends. However, only the CH domain and the linker region are necessary to autonomously target the mammalian EBs, EB1 and EB3, to the MT plus-end. Thereby, MT plus-end-binding probably occurs through recognition of the GTP cap (Komarova et al., 2009; Maurer et al., 2011). Several hundred EB molecules dynamically bind MT plus-ends, where they form comet-like structures and undergo rapid turn over (Bieling et al., 2008; Mimori-Kiyosue et al., 2000; Seetapun et al., 2012). EBs were generally shown to promote MT growth in cultured cells, likely by preventing the binding of MT depolymerases to the plus-end (Busch and Brunner, 2004; Komarova et al., 2009; Tirnauer et al., 2002), although controversial results were obtained *in vitro* (Maurer et al., 2014; Vitre et al., 2008). In differentiated muscle cells, mammalian EB3 is highly expressed and important to regulate MT dynamics at the cell cortex (Straube and Merdes, 2007).
Other regulator proteins which promote MT assembly are MT polymerases, such as XMAP215 of the +TIP protein family. XMAP215 family members contain different numbers of tubulin-binding domains (TOG) that mediate MT plus-end binding at the outermost part. They catalyze the addition of tubulin dimers to MT plus-ends and thus contribute to MT growth (Al-Bassam et al., 2012; Brouhard et al., 2008). Factors that facilitate MT rescue events include the cytoplasmic linker protein (CLIP)-associated proteins (CLASPs) (Al-Bassam et al., 2010).

Other MAPs function to destabilize or disassemble MTs. Several proteins, including katanin, spastin and fidgetin exhibit MT severing activity and break MTs to regulate the number of MTs, e.g. during mitotic spindle assembly (Roll-Mecak and McNally, 2010; Zhang et al., 2007a). Other MAPs function as MT depolymerases or so-called 'catastrophe factors' (e.g. Op18/stathmin or kinesin-13 family members) by catalyzing conformational changes within the $\alpha\beta$-tubulin heterodimer (Desai et al., 1999; Gigant et al., 2000; Steinmetz et al., 2000). Kinesin-8 family members move ATP-dependently towards the MT plus-end and locally remove tubulin dimers (Varga et al., 2009).
The growing list of MAPs regulating MT dynamics is tremendous. Especially through the formation of complex networks and interactions between different MAPs, MT dynamics can be finetuned according to the cellular context or in response to certain stimuli (Akhmanova and Steinmetz, 2015).

1.3.3 Microtubule nucleation

De novo formation of MTs is a key process for the organization of MTs within cells. Even though MTs assemble spontaneously *in vitro*, the initial nucleation phase is slow and an energetically unfavorable process. To circumvent this problem, cells rely on nucleating complexes which are spatially restricted to specific sites within the cell, the so-called microtubule-organizing centers (see section 1.4 for a detailed description).

MT nucleation from MTOCs requires the nucleating protein γ-tubulin, a member of the tubulin family that was initially identified in *Aspergillus nidulans* (Oakley and Oakley, 1989). γ-tubulin assembles together with γ-tubulin-associated proteins (GCPs) into larger MT nucleating complexes: In yeast, two γ-tubulin molecules form together with one molecule of GCP2 and GCP3 the γ-tubulin small complex (γ-TuSC) which shows mild MT nucleation activity *in vitro* (Figure 1.7 a) (Oegema et al., 1999). In higher eukaryotes, multiple copies of the γ-TuSC build together with GCP4, GCP5 and GCP6 the γ-tubulin ring complex (γ-TuRC) (Figure 1.7 b). Human γ-TuRCs were additionally shown to consist of non-GCP family members, such as the mitotic-spindle organizing protein associated with a ring of γ-tubulin 1 (MOZART1) or MOZART2 (Figure 1.7 e). However, these proteins play a more regulatory role in targeting the γ-TuRC to specific MTOCs rather than in γ-TuRC assembly (Hutchins et al., 2010; Lin et al., 2016; Masuda et al., 2013; Teixidó-Travesa et al., 2010).

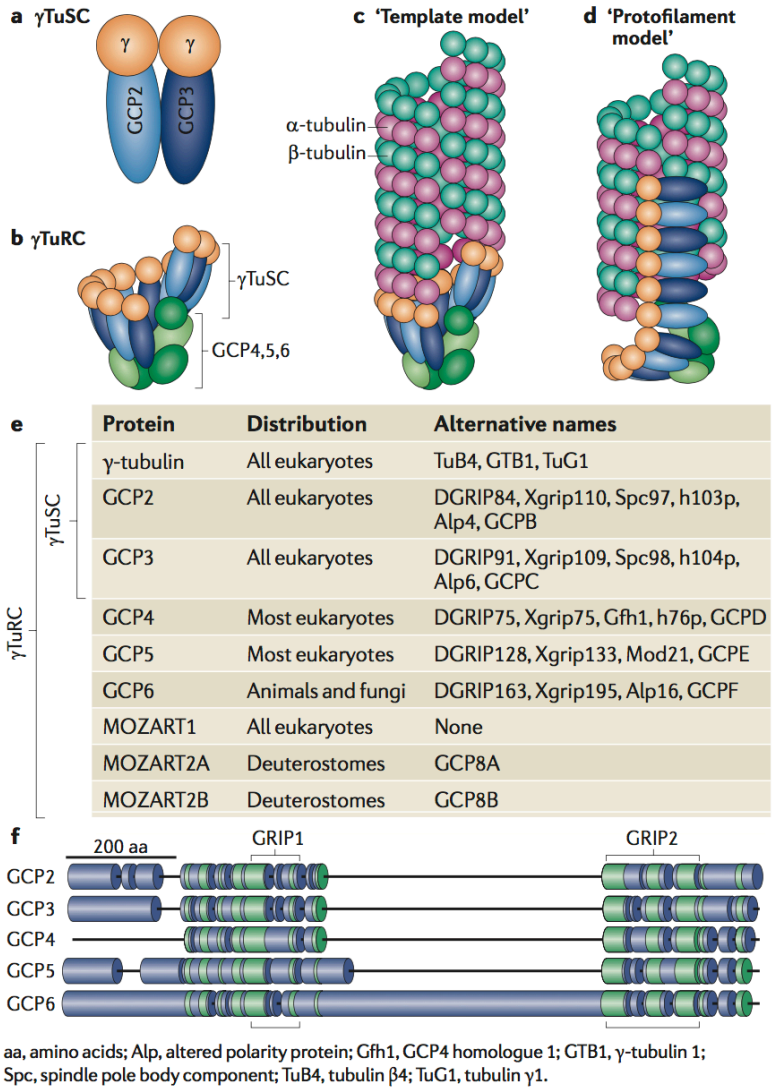

e

	Protein	Distribution	Alternative names
γTuSC	γ-tubulin	All eukaryotes	TuB4, GTB1, TuG1
γTuSC	GCP2	All eukaryotes	DGRIP84, Xgrip110, Spc97, h103p, Alp4, GCPB
γTuSC	GCP3	All eukaryotes	DGRIP91, Xgrip109, Spc98, h104p, Alp6, GCPC
γTuRC	GCP4	Most eukaryotes	DGRIP75, Xgrip75, Gfh1, h76p, GCPD
γTuRC	GCP5	Most eukaryotes	DGRIP128, Xgrip133, Mod21, GCPE
γTuRC	GCP6	Animals and fungi	DGRIP163, Xgrip195, Alp16, GCPF
γTuRC	MOZART1	All eukaryotes	None
γTuRC	MOZART2A	Deuterostomes	GCP8A
γTuRC	MOZART2B	Deuterostomes	GCP8B

aa, amino acids; Alp, altered polarity protein; Gfh1, GCP4 homologue 1; GTB1, γ-tubulin 1; Spc, spindle pole body component; TuB4, tubulin β4; TuG1, tubulin γ1.

Figure 1.7: γ-tubulin complexes and their proteins. **(a)** Scheme of the γ-tubulin small complex (γ-TuSC). **(b)** Several γ-TuSC subunits form together with γ-tubulin-associated protein (GCP) 4, 5 and 6 the γ-tubulin ring complex (γ-TuRC). **(c)** According to the 'template model', the γ-TuRC is assembled into a ring-like structure that matches the symmetry of MTs. Exposed γ-tubulins bind longitudinally to the α-tubulin subunits of MT minus-ends. **(d)** The 'protofilament model' proposes that MTs could be nucleated by γ-TuRCs with an extended protofilament-like structure, forming an elongated template for lateral interactions with $\alpha\beta$-tubulin heterodimers. **(e)** Protein members of the γ-TuSC or γ-TuRC and their alternative names in different organisms. **(f)** Schematic structure of all GCPs which share two unique domains, the GRIP1 and GRIP2 motif. Regions of distant homology are depicted in green. Taken from Kollman et al. (2011). Reprinted by permission (Licence #4105951351446) from Macmillan Publishers Ltd: Nat Rev Mol Cell Biol., 12: 709-721, copyright 2011.

The 2.2 MDa γ-TuRC protein complex exhibits a ring-shaped structure and features higher MT nucleation activity than the γ-TuSC (Oegema et al., 1999; Zheng et al., 1995). γ-TuSC and γ-TuRC are believed to assemble into oligomeric structures which function as templates for the assembly of αβ-tubulin heterodimers. Two different models for γ-tubulin-mediated MT nucleation have been proposed on the basis of two possible γ-TuRC configurations. In accordance with electron microscopy images of isolated γ-TuRCs, the 'template model' describes the assembly of γ-TuRC into ring-like structures resembling those of MTs (Moritz et al., 2000; Oegema et al., 1999; Zheng et al., 1995). Multiple radially arranged γ-TuSCs were suggested to build the backbone of a ring that positions γ-tubulin for its interaction with α-tubulin. GCP4, GCP5 and GCP6 were proposed to form an asymmetric cap at the bottom of the γ-TuRC (Figure 1.7 b, c). The alternative 'protofilament model' considered based on polymer studies of the bacterial tubulin homolog, FtsZ, that γ-TuRCs form a short protofilament which laterally interacts with αβ-tubulin to nucleate adjacent protofilaments (Figure 1.7 c) (Erickson, 2000; Erickson and Stoffler, 1996; Erickson et al., 1996). However, recent experimental advances in structural studies of γ-tubulin and the γ-TuSC are now strongly pointing towards the template model. Although the members of the GCP family differ largely in size (70-210 kDa), they share two unique structures, the N-terminal GRIP1 and the C-terminal GRIP2 motif (Figure 1.7 f). Negative-stain single-particle electron microscopy and cryoelectron microscopy of the *S. cerevisiae* γ-TuSC revealed that GCP2 and GCP3 dimerize through their N-termini into a V-shape structure (Choy et al., 2009; Kollman et al., 2008). At the tip of the V-shape, both GCP2 and GCP3 likely interact through their C-terminal GRIP2 motif with one γ-tubulin molecule (Guillet et al., 2011). The function of the GRIP1 motif, however, remains uncertain. GCP2- and GCP3-bound γ-tubulins interact laterally with other γ-tubulin molecules and longitudinally with αβ-tubulin heterodimers (Aldaz et al., 2005; Rice et al., 2008). Remarkably, *S. cerevisiae* γ-TuSCs were shown to form spontaneously spiral-shaped oligomers *in vitro*, which are highly stabilized in the presence of the spindle pole body component 110 (Spc110), a protein that targets γ-TuSC to the spindle pole body in budding yeast (Kollman et al., 2010; Lyon et al., 2016). These spiral-shaped oligomers contain seven γ-TuSC subunits, whereas the first and seventh γ-TuSC subunits overlap ('half γ-TuSC overlap') to expose 13 γ-tubulins per turn (Kollman et al., 2010; Lyon et al., 2016). Thereby, lateral γ-tubulin contacts were only observed between adjacent γ-TuSC subunits (inter γ-TuSC), whereas the two γ-tubulin molecules within one γ-TuSC (intra γ-TuSC) were more spaced ('open conformation') (Kollman et al.,

2010, 2008). This open conformation prevents the overall γ-TuSC structure to perfectly match the 13-fold protofilament arrangement of MTs and reduces its MT nucleation activity (Kollman et al., 2015). To reduce the intra γ-TuSC spacing and thus to reflect the precise MT geometry, γ-TuSCs must undergo conformational changes into a 'closed conformation' (Kollman et al., 2015). The transition between the open and closed state is likely mediated by a flexible hinge region within GCP3 (Kollman et al., 2010). Which factors drive conformational activation remain to be determined, however, post-translational modifications of γ-TuSC components or interaction with attachment factors could play a role.

In comparison to γ-TuSC oligomers, the structural arrangement of the γ-TuRC is still not resolved and generally less well understood. Nevertheless, all γ-TuRC-specific GCPs (GCP4, GCP5, and GCP6) were demonstrated to directly interact with γ-tubulin (Guillet et al., 2011; Gunawardane et al., 2003). This suggests that GCP4, GCP5 and GCP6 could form together with γ-tubulin so-called γ-TuSC-like assemblies rather than just a stabilizing cap at the bottom of the γ-TuRC (Figure 1.7 b) (Kollman et al., 2011). γ-TuSC-like structures could potentially consist of one classical GCP2 or GCP3 molecule and one γ-TuRC-specific GCP (hybrid γ-TuSC), two γ-TuRC-specific GCPs (novel γ-TuSC) or a single GCP4, GCP5 or GCP6 molecule bound to γ-tubulin (half γ-TuSC) (Figure 1.8 a). Through lateral interactions, classical γ-TuSC and γ-TuSC-like subunits could assemble into spiral-shaped oligomers to build a perfect template for a 13-protofilament MT (Figure 1.8 b).

Despite first attempts to determine the stoichiometry of the γ-TuRC, the precise number of GCP4/5/6 molecules and their position within the γ-TuRC is still unknown (Choi et al., 2010; Murphy et al., 2001). However, a recent study suggested that GCP4/5 and GCP6 might be incorporated at opposite ends of the γ-TuRC helix to stabilize the half γ-TuSC overlap or to control γ-TuRC assembly (Farache et al., 2016). Additional work is needed to understand how γ-TuRC-mediated MT nucleation is facilitated compared to γ-TuSC oligomers lacking GCP4, GCP5 and GCP6.

1.3.4 Microtubule-based motor proteins

MT-dependent motor proteins use MTs as tracks to transport membranous organelles, such as nuclei in skeletal muscle cells, or mRNAs and diverse protein complexes throughout the cell. Two prototypes of MT-based motor proteins exist: the MT plus-end directed motor protein kinesin and the MT minus-end directed motor

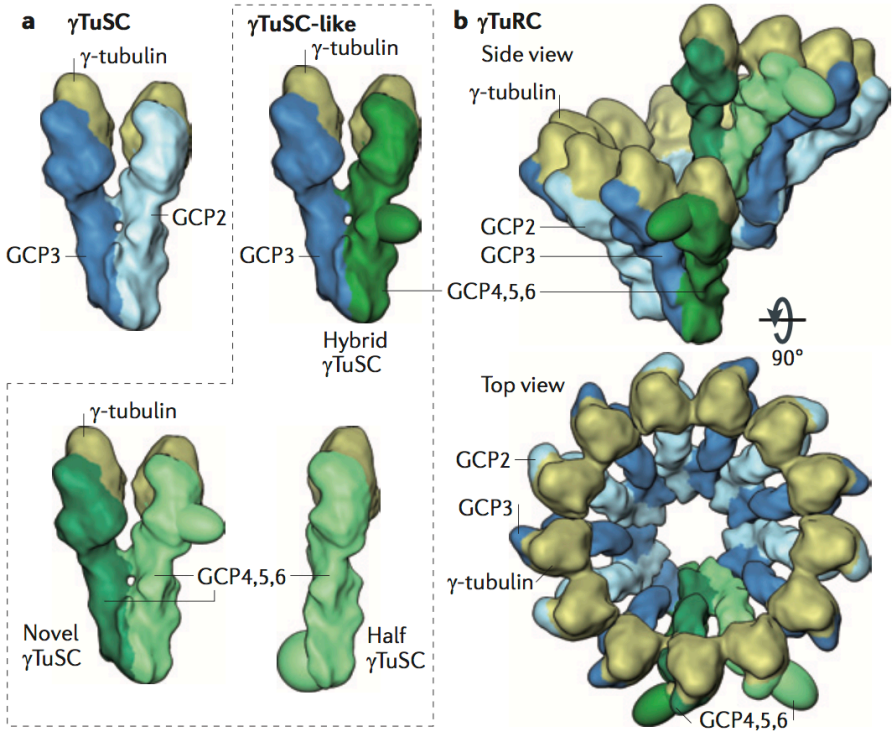

Figure 1.8: Current model of γ-TuRC arrangement. (a) V-shape structure of the classical γ-TuSC comprising GCP3 (blue) and GCP2 (light blue). γ-TuSC-like structures (hybrid γ-TuSC, novel γ-TuSC, half γ-TuSC) could be formed, when GCP4, GCP5 or GCP6 (depicted in green shapes) replace one or both molecules GCP2/GCP3 within the classical γ-TuSC. **(b)** γ-TuSC and γ-TuSC-like subunits laterally interact to form a spiral-shaped γ-TuRC, thereby exposing 13 γ-tubulins (yellow) for MT nucleation. GCP4, GCP5 or GCP6 are potentially incorporated at the end of the γ-TuRC ring. Taken from Kollman et al. (2011). Reprinted by permission (Licence #4105951351446) from Macmillan Publishers Ltd: Nat Rev Mol Cell Biol., 12, 709-721, copyright (2011).

protein dynein.

The kinesin superfamily of proteins (also known as KIFs) comprises at least 45 members, which are grouped into 15 distinct families (kinesin-1 to kinesin-14B family) according to the homology of their motor domains (Hirokawa et al., 2009). One of the first identified kinesins was the heterotetramer kinesin-1 (also known as KIF5), which is formed by the association of two kinesin heavy chains (KHCs) and two kinesin light chains (KLCs) (Figure 1.9). Both KIF5 heavy chains contain a N-terminal globular head domain that binds to MTs and ATP (motor domain), a flexible linker domain, a central α-helical stalk domain that mediates KHC dimerization and a C-terminal globular tail domain that binds to KLCs and the respective cargo or cargo adaptor proteins (Hirokawa and Noda, 2008). In mammals, three genes encode for different KIF5 motor isoforms, KIF5A, KIF5B, KIF5C. Whereas KIF5B is ubiquitously

expressed, KIF5A and KIF5C are solely expressed in neurons (Hirokawa et al., 2009; Kanai et al., 2000). The motor head domain of kinesin-1 attaches to MTs and hydrolyzes ATP to initiate movements along MTs. Members of the kinesin-1 family belong to the so-called N-kinesins as their motor domains are found within the N-terminal region. However, the structure of other kinesin family members can differ from the described domain structure of kinesin-1 (Hirokawa et al., 2009). The motor domains of M-kinesins, for example, is located within the middle region, whereas the motor domain of C-kinesins is located in the C-terminal region. The majority of kinesins, including the N-kinesins, transport cargos towards the MT plus-end but some kinesins, mainly C-kinesins (e.g. kinesin-14 family) can 'walk' towards the MT minus-end. In contrast, M-kinesins (e.g. kinesin-13 family) mainly function to drive MT depolymerization (Hirokawa and Tanaka, 2015).

In contrast to the kinesin superfamily of proteins, dynein motor proteins mediate the ATP-driven retrograde transport towards the MT minus-end. Dyneins are large multiprotein complexes with molecular weights ranging from 0.7 MDa to 1.8 MDa (Roberts et al., 2013). Two functional groups of dyneins can be distinguished: (1) *cytoplasmic* dynein and *intraflagellar transport* (IFT) dynein (also referred to as dynein 1B and dynein 2), which are responsible for the transport of cargos along MTs and (2) *axonemal* dynein, which is anchored in the axoneme and mediates beating of cilia and flagella.

However, as IFT dynein is solely responsible for transporting cargos along the axoneme (Lechtreck, 2015; Scholey, 2008), the major dynein isoform responsible for intracellular transport within the cytoplasm is cytoplasmic dynein (referred to as 'dynein' throughout the text). Dyneins belong to the AAA+ superfamily (ATPases associated with diverse activities) of ATPases and are generally composed of two heavy chains and multiple dynein intermediate chains, dynein light intermediate chains, and dynein light chains (Figure 1.9) (Schmidt and Carter, 2016). Each dynein heavy chain comprises a C-terminal globular head domain (motor domain) that contains the ATPase activity and a coiled-coil extension that contains the MT-binding region. The N-terminal tail domain of dynein is important for the homodimerization of heavy chains and for the binding of accessory dynein chains. Interactions with these accessory dynein chains are dispensable for dynein motility *in vitro* but are important for dynein binding to certain cargos or for the recruitment of adaptor/regulatory proteins (Farkasovsky and Küntzel, 2001; Karki and Holzbaur, 1995; Purohit et al., 1999; Tai et al., 1999; Vaughan and Vallee, 1995). One of the best studied adaptor proteins is dynactin, a large 11-subunit complex which

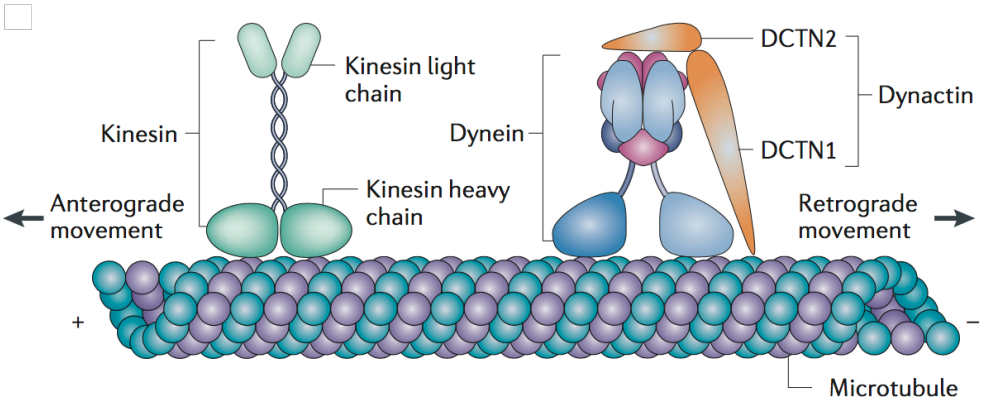

Figure 1.9: Kinesin and dynein motor proteins. Kinesin motor proteins are composed of two kinesin heavy chains and two kinesin light chains and move along MTs towards the plus-end (with a few exceptions, see text). Dynein motor proteins are composed of two dynein heavy chains, several accessory dynein chains and adaptor proteins, such as dynactin (depicted here are the dynactin subunits 1 [DCTN1] and 2 [DCNT2]). Dynein transports cargos towards the MT minus-end. Kinesins and dyneins have both globular motor domains that bind to MTs and through ATP hydrolysis drive motor protein movements along MT tracks. Taken from Millecamps and Julien (2013). Reprinted by permission (Licence #4121520561892) from Macmillan Publishers Ltd: Nat Rev Neurosci. 14(3):161-76, copyright (2013).

binds directly to dynein intermediate chains and to MTs through its $p150^{Glued}$ (also known as dynactin 1, DCTN1) component. Thereby, dynactin mediates interactions between dynein and its cargo and/or increases the processivity of dynein motor proteins (Gill et al., 1991; Karki and Holzbaur, 1999; Schroer, 2004). A multitude of other regulatory proteins, such a lissencephaly 1 (LIS1), nuclear distribution E (NUDE) and Bicaudal D are crucial to adopt the mechanical behaviour of dynein motor proteins according to the cellular context (Kardon and Vale, 2009).

1.4 Microtubule-organizing centers (MTOCs)

MT nucleation and organization is spatiotemporally controlled by the attachment of γ-TuRCs to specific microtubule-organizing centers (MTOCs). This term was initially introduced by Jeremy D. Pickett-Heaps and collectively refers to all cellular structures involved in MT organization (Pickett-Heaps, 1969). In animal cells, the probably best characterized and primary MTOC is the centrosome (section 1.4.1). However, in recent years it became evident that also other cellular organelles, so-called non-centrosomal MTOCs (section 1.4.2), can undertake or contribute to global MT arrangement, particularly in interphase cells.

1.4.1 The centrosome

Centrosomes, which were already described in the 19th century by Theodor Boveri due to their centered position within cells, are non-membranous organelles that consist of a few hundred proteins (Andersen et al., 2003; Jakobsen et al., 2011; Müller et al., 2010). In the majority of vertebrate cells, centrosomes organize and orientate the bipolar mitotic spindle during mitosis and arrange a radial MT array during interphase, where MT minus-ends are capped by γ-TuRCs and captured at centrosomes through anchoring proteins (Wiese and Zheng, 2000). Apart from their well established function in MT organization, centrosomes further play a role in cell cycle regulation, cilia formation and in orchestrating signaling cascades (Arquint et al., 2014; Rieder et al., 2001).

Centrosome structure and its MT organization capacity

Structurally, centrosomes are composed of two orthogonally orientated centrioles and a surrounding pericentriolar material (PCM) (Figure 1.10 a). Centrioles generally consist of nine radially arranged triplet MT arrays that build the basis for the cylindrical shape of centrioles (reviewed in Azimzadeh and Bornens (2007); Bettencourt-Dias and Glover (2007); Conduit et al. (2015)). The older, so-called 'mother centriole' of post-mitotic cells features subdistal and distal appendages which mediate MT anchorage at centrioles and centriole attachment to the cell cortex during ciliogenesis (Ishikawa et al., 2005; Paintrand et al., 1992). Although centrioles were initially believed to be essential for mitotic spindle assembly, cells that either naturally lack centrioles (e.g. higher plants) or artificially loose their centrioles (e.g. microsurgery or laser ablation) still form an acentrosomal but bipolar mitotic spindle (Hinchcliffe et al., 2001; Khodjakov et al., 2000; Murata et al., 2005). Therefore, it is not the centriole but the centriole surrounding PCM that harbors MT nucleation capacity by anchoring γ-TuRCs and where MTs can be seen to emanate from (Gould and Borisy, 1977; Moritz et al., 1995). In preparation for mitosis, the PCM largely increases in size by recruiting γ-tubulin as well as proteins involved in γ-TuRC attachment and recruitment (Khodjakov and Rieder, 1999). This process, termed 'centrosome maturation', is regulated by Polo-like kinase-1 and Aurora A (reviewed in Bettencourt-Dias and Glover (2007); Blagden and Glover (2003)) and generally highly enlarges the centrosome's capability to nucleate MTs.
For decades, the protein-rich PCM was recognized by electron microscopy as an amorphous cloud (Robbins et al., 1968) (Figure 1.10 a). However, recent advances

using super-resolution microscopy techniques reveal that the PCM during interphase is highly organized into concentric layers surrounding the mother centriole (Fu and Glover, 2012; Lawo et al., 2012; Mennella et al., 2012; Sonnen et al., 2012) (Figure 1.10 b). Some proteins, such as human Pericentrin or its *Drosophila* orthologue Pericentrin-like protein (Plp), acquire an elongated conformation with the C-terminus facing towards the centriole wall and the N-terminal domain towards the PCM periphery (Lawo et al., 2012; Mennella et al., 2012). Thereby, Pericentrin/Plp transverse inner and outer PCM layers and form a fibrillar network that functions as a matrix for the organization and assembly of PCM molecules (Mennella et al., 2012). Importantly, centrosomal proteins that are required for MT nucleation (γ-tubulin) or binding of γ-TuRCs, such as Nedd1 (also termed GCP-WD, reviewed in Manning and Kumar (2007)) generally localize to the outer PCM layer.
Newly nucleated MTs can either be released from the centrosome or anchored at the centrosome by attachment factors. One of these proteins promoting MT anchorage is ninein that localizes to the subdistal appendages and anchors γ-TuRCs to mother centrioles (Delgehyr et al., 2005; Mogensen et al., 2000). Also other molecules, such as the dynactin subunit $p150^{Glued}$ and EB1 play a role in MT anchorage to centrosomes (Askham et al., 2002; Bornens, 2002; Quintyne et al., 1999). Moreover, the capacity of centrosomes to anchor MTs additionally depends on so-called 'pericentrosomal satellites', cytoplasmic fibrous granules of approximately 70-100 nm that concentrate near the centrosome and can fuse with the PCM in a dynamic fashion (Bärenz et al., 2011; Baron et al., 1994). These granules contain the scaffolding protein **pericentriolar material-1 (Pcm1)** with a molecular weight of 228 kDa, and move dynein-dependently along MTs (Balczon et al., 1994; Dammermann and Merdes, 2002; Kubo et al., 1999). Thereby, Pcm1 seems to be required to target centrosomal proteins involved in MT anchorage (ninein) or MT nucleation (Pericentrin) from cytoplasmic granules to the centrosome (Dammermann and Merdes, 2002). In this way, loss of Pcm1 indirectly affects MT organization at the centrosome (Dammermann and Merdes, 2002).

Centrosomal proteins involved in γ-TuRC recruitment

The ability of the PCM to nucleate MTs is highly dependent on proteins that recruit γ-TuRCs to the centrosome. Among these proteins are Pericentrin, Akap450, Cdk5Rap2, and Cep192:

Pericentrin was discovered by screenings of mouse cDNA libraries using an au-

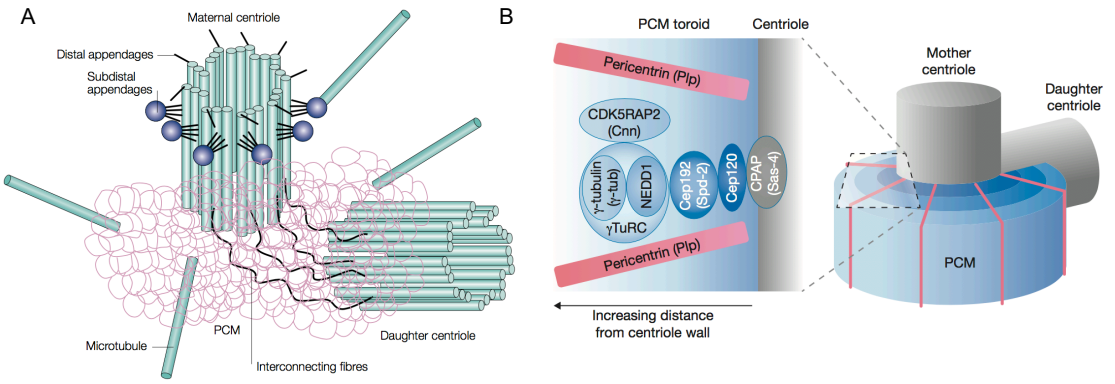

Figure 1.10: Models of the centrosome architecture. (A) Previous models of the centrosome structure suggested that a pair of centrioles is surrounded by an amorphous cloud, the pericentriolar material (PCM). Centrioles are composed of nine MT triplets. The mature mother centriole features additionally distal and subdistal appendages. Microtubules are nucleated from the PCM but a subset of MTs can be anchored at the subdistal appendages. Taken from Doxsey (2001). Reprinted by permission (Licence #4112650474520) from Macmillan Publishers Ltd: Nat Rev Mol Cell Biol. 9:688-98, copyright (2011). **(B)** New models of the centrosome structure reveal that the PCM is organized into toroidal layers around the mother centriole. Some scaffold proteins such as Pericentrin span all PCM layers: the C-terminus is near the centriole wall, whereas the N-terminus is facing towards the cell periphery. Proteins promoting MT nucleation localize to the outer PCM layers. Taken from Lüders (2012). Reprinted by permission (Licence #4112650765586) from Macmillan Publishers Ltd: Nat Cell Biol. 14(11):1126-8., copyright (2012).

toimmune serum from a patient with scleroderma and named after its prominent localization to the pericentriolar material (Doxsey et al., 1994). Through alternative splicing from orthologous genes in human and mice, up to three different isoforms, Pericentrin-B (also known as kendrin or Pericentrin-360; accession number (AN): NP_032813 or BAF36559), Pericentrin-A (AN: partial, AAO24322.1) and Pericentrin-S (also known as Pericentrin-250; BAF36560) are known until now (Figure 1.11) (Flory and Davis, 2003; Miyoshi et al., 2006a). Pericentrin-B is expressed in all adult tissues and is structurally composed of large coiled-coil regions and a C-terminal domain including a calmodulin-binding site and a region mediating centrosome-targeting, termed the PACT domain (Pericentrin-Akap450 centrosomal targeting) (Doxsey et al., 1994; Gillingham and Munro, 2000). Pericentrin-S which solely lacks a N-terminal part of Pericentrin-B, is developmentally expressed in cardiac and skeletal muscle (expression starting at E17) (Miyoshi et al., 2006a). Pericentrin was shown to form a lattice-like structure with γ-tubulin at the centrosome and to contribute to MT organization within the mitotic and meiotic spindle (Dictenberg et al., 1998; Doxsey et al., 1994; Ma and Viveiros, 2014).

Co-immunoprecipitation studies demonstrating that Pericentrin can interact with γ-tubulin through binding to GCP2 and GCP3, further prove a role for Pericentrin in γ-TuRC anchoring and MT nucleation (Takahashi et al., 2002; Zimmerman et al., 2004). Pericentrin localization to the centrosome is mediated at least in part by dynein-mediated transport along MTs (Purohit et al., 1999; Young et al., 2000) and requires Pcm1 (Dammermann and Merdes, 2002; Li et al., 2001). In turn, recruitment of other PCM components to the centrosome, such as Cdk5Rap2, Nedd1 and Cep192, depends on Pericentrin (Buchman et al., 2010; Chen et al., 2014; Haren et al., 2009; Lawo et al., 2012; Mennella et al., 2012). Apart from its direct function in PCM organization and MT nucleation, Pericentrin was further implicated in the DNA damage response pathway and cell cycle regulation (Antonczak et al., 2016; Griffith et al., 2008; Tibelius et al., 2009), as well as in the recruitment of regulatory proteins to the centrosome (Chen et al., 2004; Diviani et al., 2000) and in cilia formation (Jurczyk et al., 2004; Miyoshi et al., 2006b; Mühlhans et al., 2011). Mutations within the *PCNT* gene are linked to a rare autosomal recessive disease, Majewski/microcephalic osteodysplastic primordial dwarfism type II (MOPDII) (Piane et al., 2009; Rauch et al., 2008; Willems et al., 2010). Patients suffering from this disorder often manifest smaller body sizes already before birth, microcephaly and skeletal dysplasia (Delaval and Doxsey, 2010; Hall et al., 2004; Piane et al., 2009).

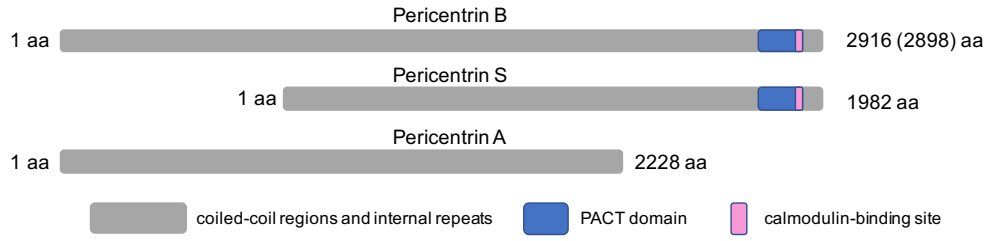

Figure 1.11: Scheme of Pericentrin isoforms. Scheme is not drawn to scale. aa, amino acids. Modified from Mühlhans et al. (2011).

A-kinase anchoring protein 450 (Akap450; also known as Akap9, Akap350 or CG-NAP for centrosome and Golgi localized PKN-associated protein) is a large coiled-coil protein of the PCM that localizes to the centrosome throughout the cell cycle and additionally to the Golgi complex during interphase (Keryer et al., 1993; Schmidt et al., 1999; Takahashi et al., 1999; Witczak et al., 1999) (see also section 1.4.2). Similar to Pericentrin, Akap450 localizes to the centrosome via its C-terminal PACT domain and binds to the γ-TuRC components GCP2 and GCP3

through its N-terminal domain (Gillingham and Munro, 2000; Takahashi et al., 2002). Pericentrin and Akap450 can interact with each other and partially fulfill redundant functions in MT nucleation and in anchoring regulatory proteins, such as protein kinase A (PKA), to the centrosome (Kawaguchi and Zheng, 2004; Keryer et al., 2003a; Takahashi et al., 2002). Moreover, Akap450 associates with diverse protein kinases (protein kinase N, protein kinase Cϵ, casein kinase 1δ/ϵ) and phosphatases (protein phosphatase 2A, protein phosphatase 1) and thus might regulate various signaling pathways (Sillibourne et al., 2002; Takahashi et al., 2000, 1999). Other studies further implicated Akap450 in the regulation of centrosome duplication, likely by anchoring cyclin E-cdk2 complexes to centrosomes (Keryer et al., 2003b; Nishimura et al., 2005).

CDK5 Regulatory Subunit Associated Protein 2 (Cdk5Rap2; also known as Cep215 or Centrosomin (Cnn) in *Drosophila*) is another large coiled-coil protein of the PCM with an elongated confirmation and was initially discovered as binding partner of CDK5 regulating kinase 1 (Ching et al., 2000; Mennella et al., 2012; Nagase et al., 2000). Cdk5Rap2 was shown to interact with γ-TuRC through its N-terminal 'Cnn motif ' (CM1), a short sequence that is highly conserved in *Drosophila* Centrosomin and *Schizosaccharomyces pombe* Mto1p and Pcp1p (Fong et al., 2008; Zhang and Megraw, 2007). This CM1 motif is not only required for binding to γ-TuRC but also to activate γ-TuRC-mediated MT nucleation at the centrosome and at non-centrosomal cytoplasmic nucleation sites (Choi et al., 2010; Fong et al., 2008). Strikingly, purified γ-TuRCs nucleated MTs *in vitro* but their nucleation capacity was greatly enhanced in the presence of the Cdk5Rap2 CM1 motif or also termed the γ-TuRC-mediated nucleation activator (γ-TuNA) from there on (Choi et al., 2010). Cdk5Rap2 localizes to the centrosome and to the Golgi complex (like Akap450) through a C-terminal 'Cnn motif 2' (CM2) (Wang et al., 2010) (see also section 1.4.2). Interestingly, Cdk5Rap2 localization to the centrosome depends on Pericentrin, whereas Ckd5Rap2 localization to the Golgi complex seems to require Pericentrin and Akap450 (Buchman et al., 2010; Wang et al., 2010). Other studies furthermore showed that Cdk5Rap2 localization to the centrosome might also depend on Cep152 or Cep192, respectively (Firat-Karalar et al., 2014; O'Rourke et al., 2014). Apart from the CM1 and CM2 motif, Cdk5Rap2 additionally contains two putative 'structural maintenance of chromosome' (SMC) domains and a basic Ser-rich domain that mediates binding to EB1 (Evans et al., 2006; Fong et al., 2009; Kraemer et al., 2011). This Cdk5Rap2-EB1 interaction is

important for targeting Cdk5Rap2 to MT plus-ends and thus for regulating MT dynamics (Fong et al., 2009). Mutation within the *Cdk5Rap2* gene are found in patients with autosomal recessive primary microcephaly (MCPH), a neurogenic disorder that is characterized by a decreased brain size (Bond et al., 2005).

Centrosomal protein of 192 kDa (Cep192; also known as spindle-defective 2 (SPD-2) in *Drosophila*) is an integral component of the PCM that lies at the interphase of the PCM and the centriole wall (Fu and Glover, 2012; Lawo et al., 2012). Cep192 localizes to centrosomes throughout the cell cycle but its presence is highly increased (> 10-fold) during mitosis (Gomez-Ferreria et al., 2007; Zhu et al., 2008). Cep192 regulates the mitotic spindle assembly mainly by recruiting components of the PCM to the centrosome, most importantly γ-tubulin as well as Pericentrin, Nedd1, Aurora A kinase and Plk1 (Gomez-Ferreria et al., 2007; Joukov et al., 2010, 2014; Pelletier et al., 2004; Zhu et al., 2008). Due to the recruitment of additional PCM components (centrosome maturation), the centrosome increases in size and enhances its potential to nucleate MTs for the separation of chromosomes during mitosis. Consistently, loss of Cep192 disturbs normal formation of bipolar mitotic spindles and rather promotes acentrosomal MT nucleation around chromosomes (Gomez-Ferreria et al., 2007). During mitosis, centrosome localization of Cep192 is at least in part dependent on Pericentrin, while during interphase Cep192 and Pericentrin seem to antagonize each other's localization to the centrosome (Gomez-Ferreria et al., 2007; O'Rourke et al., 2014). Although a role for Cep192 during mitosis is widely accepted, recent work shows that Cep192 additionally stimulates MT nucleation from interphase centrosomes and controls MT dynamics (O'Rourke et al., 2014). Thereby, Cep192 seems to regulate centrosomal versus non-centrosomal MT nucleation (O'Rourke et al., 2014; Yang and Feldman, 2015).

1.4.2 Non-centrosomal MTOCs

Although the centrosome is in many textbooks still considered as the main MTOC, it is becoming clear that also cellular locations other than the centrosome can nucleate and organize MTs in a γ-tubulin-dependent manner in various single-celled (e.g. *S. pombe*) and multi-cellular organisms (animals and plants).
During mitosis, for example, MTs can emanate from kinetochores or chromatin (Heald et al., 1996; Maiato et al., 2004; Prosser and Pelletier, 2017) and can be generated from pre-existing MTs of the mitotic/meiotic spindle through the γ-TuRC-recruiting complex augmin (Petry et al., 2013). During interphase, the plasma

membrane (e.g. polarized epithelial cells) and membrane-bound organelles such as the nucleus (e.g. skeletal muscle, see section 1.4.3) or the Golgi complex can function as non-centrosomal MTOCs (Chabin-Brion et al., 2001; Rios, 2014; Sanders and Kaverina, 2015; Zhu and Kaverina, 2013).
The Golgi complex is even generating approximately the half amount of the total MT cytoskeleton in some interphasic cells, such as human retinal pigment epithelium (RPE-1) cells (Efimov et al., 2007). MT nucleation from the Golgi complex is dependent on Akap450, which localizes to the *cis*-Golgi by interaction with GM130, and in turn recruits the γ-TuRC-binding proteins Cdk5Rap2 and myomegalin (Hurtado et al., 2011; Rivero et al., 2009; Roubin et al., 2013; Wang et al., 2010, 2014). Golgi-mediated MT nucleation requires additionally the MT-stabilizing proteins CLASPs that are recruited to the *trans*-Golgi network by the golgin GCC185 (Efimov et al., 2007; Miller et al., 2009). A more recent study furthermore suggests that the MT minus-end stabilizing protein CAMSAP2 bound to AKAP450 and myomegalin is important to attach MTs to the Golgi complex (Wu et al., 2016). However, how exactly MT formation at the Golgi complex is achieved, when several MT-nucleation or-stabilization factors localize to different Golgi compartments (*cis* versus *trans* Golgi) is currently uncertain.
Non-centrosomal MTOCs play especially an important role in a variety of differentiated cells, such as polarized epithelial cells, neurons or skeletal muscle cells. In these cells, MT organization is displaced from the centrosome to non-centrosomal sites, allowing the generation of non-radial MT arrays that are highly adapted according to the specialized function of each cell type.
Polarized epithelial cells exhibit linear MT arrays that are aligned according to the apical-basal cell axis. In these non-centrosomal MT arrays, MT minus-ends are anchored in close proximity to apical membranes, whereas MT plus-ends are facing towards the basal site of the cell (Figure 1.12) (Bacallao et al., 1989; Bré et al., 1987, 1990; Meads and Schroer, 1995). Centrosomes remain present in polarized epithelial cells, although some centrosomal proteins, such as the MT-anchoring protein ninein, are relocalized to non-centrosomal sites underlying the apical membrane (Mogensen et al., 2000; Tucker et al., 1992). MT formation in most epithelial cells seems to involve centrosome-mediated MT nucleation, subsequent MT release from the centrosome through MT-severing enzymes and MT anchorage at apical sites through proteins like ninein (Mogensen, 1999; Mogensen et al., 2000; Moss et al., 2007).

Also neurons possess a dense network of non-centrosomal but distinct MT arrays in

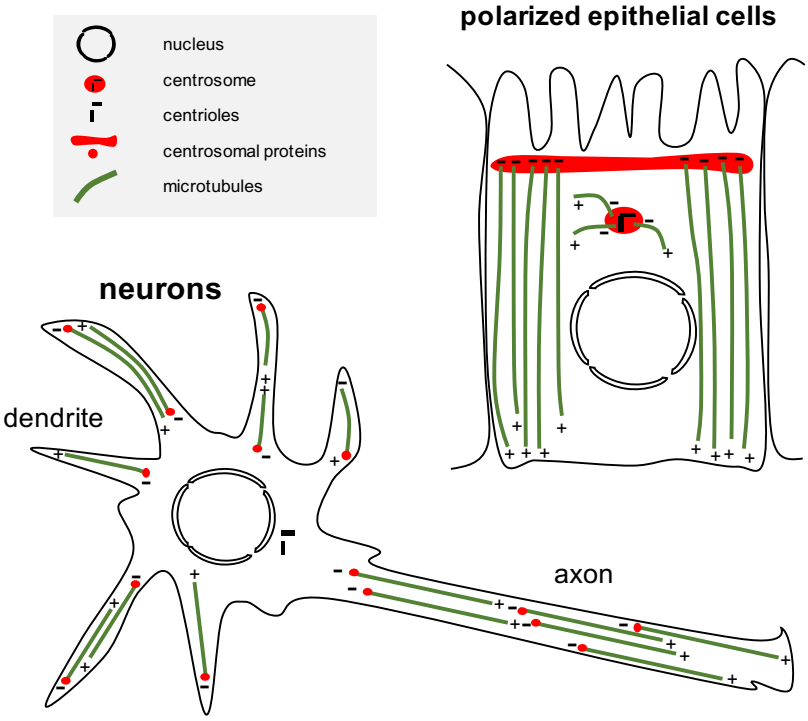

Figure 1.12: Non-centrosomal MT arrays in polarized epithelial cells and neurons. In polarized epithelial cells, the apical membrane serves as a non-centrosomal MTOC to organize MTs into linear arrays arranged according to the apical-basal axis. In differentiated neurons, non-centrosomal MTs are freely distributed in the cytoplasm and not tethered to any obvious cellular structure. Within dendrites, MTs display mixed polarity, whereas in axons MTs are uniformly orientated with their minus-ends facing towards the cell body. Centrioles remain present in the cell body after the centrosome loses its MT organization capacity. Scheme is not drawn to scale.

axons and dendrites. Whereas MTs are uniformly orientated in axons with their MT minus-ends facing towards the cell body (soma), MTs display mixed orientations within dendrites (Baas et al., 1988; Burton, 1988; Heidemann et al., 1981). In differentiated neurons, non-centrosomal MTs are free in the cytoplasm, meaning the MT minus-ends are allocated throughout the cell (Baas and Joshi, 1992; Baas and Lin, 2011; Bray and Bunge, 1981; Chalfie and Thomson, 1979). Although the centrosome is still present and nucleates MTs as a classical MTOC in newly polarized neurons, it loses its activity at later stages during neuronal development; centrioles remain in the soma and likely become basal bodies during ciliogenesis (Berbari et al., 2007; Stiess et al., 2010). Proteins, such as γ-tubulin, Pericentrin or Nedd1, that are important for MT nucleation or binding to γ-TuRCs are lost from the centrosome and partially localize to non-centrosomal sites within the cytoplasm (Nguyen et al., 2014; Ori-McKenney et al., 2012; Stiess et al., 2010; Yau et al.,

2014). Although Golgi outposts have been suggested to function as non-centrosomal MTOCs in dendrites (Ori-McKenney et al., 2012), it remains to be determined at which cellular structures *de novo* MT formation occurs during neuronal development (Kapitein and Hoogenraad, 2015).
In comparison to polarized epithelial cells and neurons, the MT network of skeletal muscle cells is remodeled several times during the differentiation process and requires distinct non-centrosomal MTOCs, the nuclear membrane and the Golgi complex as discussed in the next section.

1.4.3 Non-centrosomal MTOCs in skeletal muscle cells

During skeletal muscle formation, the MT network is dramatically rearranged from a radial centrosome-organized MT array into a non-centrosomal MT array organized parallel to the long axis of the cell (Figure 1.13) (Tassin et al., 1985a; Warren, 1974). This longitudinal MT network is organized by the nucleus, which functions as a non-centrosomal MTOC in differentiated muscle cells. In fact, MTs grow in a 'sun-like' fashion from the nuclear envelope (NE) and from small cytoplasmic foci in myotubes after treatment with the MT-depolymerizing drug nocodazole (Bugnard et al., 2005; Tassin et al., 1985a). Reorganization of the MT network is accompanied by a redistribution of centrosomal proteins from the centrosome to the outer surface of the nucleus (Srsen et al., 2009; Tassin et al., 1985a). Concomitantly, centrosomes seem to loose their direct proximity to one nucleus and rather tend to aggregate nearby nuclei groups in myotubes (Tassin et al., 1985a). These smaller 'centrosome-like' structures might account for some remaining MT asters observed within the cytoplasm of myotubes, although their MT nucleation capability seems to be decreased when compared to centrosomes in myoblasts (Bugnard et al., 2005; Fant et al., 2009). Moreover, centrioles appear to be gradually lost in the course of myogenic differentiation and as a result are likely completely absent or at least rarely present in mature muscle fibers (Connolly et al., 1986; Kano et al., 1991; Przybylski, 1971).
The underlying mechanisms how cells regulate MTOC displacement from the centrosome to the nucleus during differentiation is still obscure. However, it is known that centrosomal proteins assemble into a highly insoluble filamentous network at the NE of differentiated muscle cells and that the amount of redistributed centrosomal material at the nuclear membrane is relative to the amount of MTs growing from the nucleus (Fant et al., 2009; Srsen et al., 2009). Among the proteins known to relocalize are predominantly components of the PCM, including Pericentrin, Akap450,

Cdk5Rap2, and γ-tubulin as well as Pcm1, Cep135 and the MT-anchoring protein ninein (Bugnard et al., 2005; Fant et al., 2009; Oddoux et al., 2013; Srsen et al., 2009). However, detection of γ-tubulin at the nuclear membrane is difficult due to its high abundance within the cytoplasm and its relatively low concentration at the NE (5-fold decrease) when compared to the centrosome, and requires detergent extraction prior to fixation (Bugnard et al., 2005). Consistent with its role as the main MT-nucleator, γ-tubulin localization to the NE is absolutely required for cells to nucleate MTs from nuclear membranes, as myotubes microinjected with anti-γ-tubulin antibodies fail to do so (Bugnard et al., 2005).
The reorganization of centrosomal proteins and MT nucleation capacity is accompanied by a redistribution of endoplasmic reticulum (ER) exit sites and Golgi complex elements to nuclear membranes (Lu et al., 2001; Ralston, 1993; Ralston et al., 2001; Tassin et al., 1985b). In myotubes, Golgi complex elements seem to be tightly associated with the nucleus and orientated in such a way that the *cis*-Golgi is facing towards the NE and the *trans*-Golgi network towards the cell periphery (Ralston et al., 2001; Tassin et al., 1985b). All these subcellular changes (reorganization of centrosomal proteins, MTs, Golgi complex elements, and ER exit sites) already occur before differentiated myoblasts fuse into myotubes and persist during the myotube and myofiber stage (Ralston, 1993; Srsen et al., 2009). Interestingly, recruitment of centrosomal proteins to the NE seems to occur independently of the actin and MT cytoskeleton (Fant et al., 2009; Zaal et al., 2011). In fact, depolymerizing MTs by nocodazole treatment or altering MT dynamics in the presence of the MT-stabilizing drug taxol have no major effects on perinuclear localization of Pcm1 or Pericentrin in myotubes, respectively (Fant et al., 2009; Zaal et al., 2011).
Additional subcellular organelle arrangements occur when myotubes proceed the myogenic differentiation program. The longitudinal MT network observed in myotubes is further remodeled into an orthogonal grid with dynamic and bundled MTs running longitudinally and transversally throughout the myofiber (Figure 1.13). Strikingly, Golgi components localize together with γ-tubulin and Pericentrin to the intersections of the MT grid (Oddoux et al., 2013). Thus, the Golgi complex functions additionally to the nucleus as a non-centrosomal MTOC in myofibers, although the pattern of Golgi complex elements at the NE and the density of MTs slightly differ between muscle fiber types (Ralston et al., 1999): In slow-twitch muscle fibers, Golgi complex elements are distributed as a perinuclear belt around the nucleus and MTs are intertwined, forming dense bundles within the MT grid-like lattice with no obvious starting points. In comparison, in fast-twitch muscle fibers, Golgi

localization is often restricted to nuclei poles and to the myofiber core. Additionally, MTs are rather individually distributed with distinct starting points in the form of MT asters nearby nuclei or throughout the myofiber. Nuclei that cluster under the neuromuscular junction (NMJ), however, display a uniform Golgi perinuclear belt and a dense surrounding MT network regardless of the fiber type (Ralston et al., 1999).

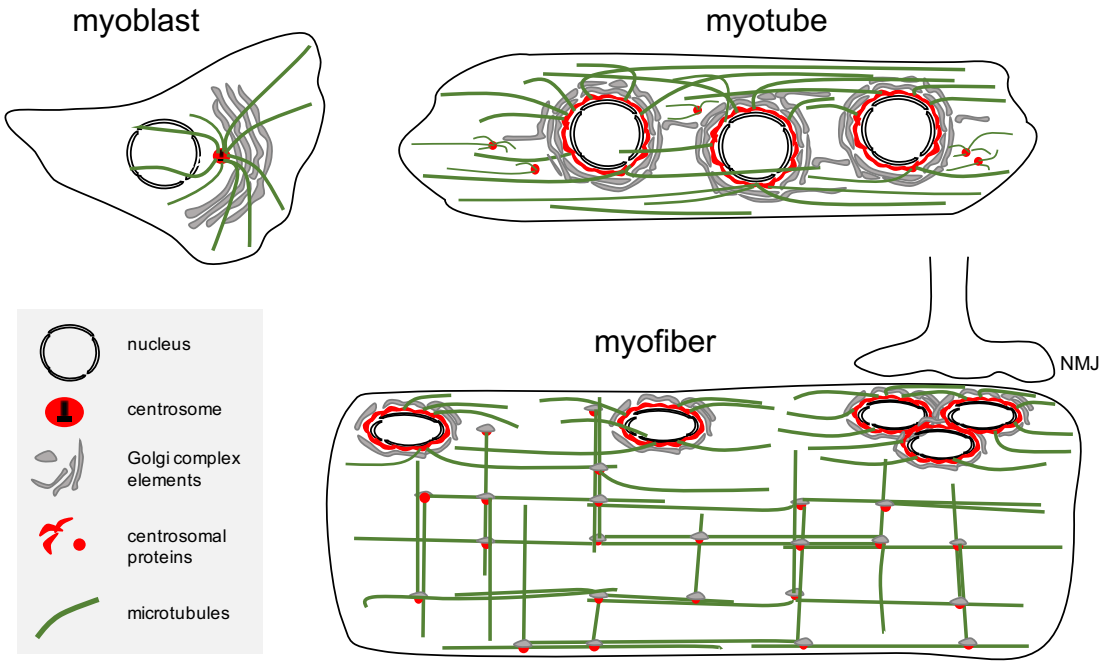

Figure 1.13: MTOC rearrangements during myogenic differentiation. In undifferentiated myoblasts, microtubules (MTs) are radially organized by the centrosome and the Golgi complex is juxtanuclearly positioned around the centrosome. In differentiated myoblasts and myotubes (shown here), centrosomal proteins and the Golgi complex relocalize to the nucleus which takes over the function as a non-centrosomal MTOC and organizes MTs into a longitudinal array. Some remaining centrosome-like structures within the cytoplasm can contribute to nucleate MTs. In myofibers, centrosomal proteins and Golgi complex elements act together to organize MTs into an orthogonal grid. Nuclei surrounded with centrosomal proteins and Golgi complex elements are positioned in the periphery or in clusters under the neuromuscular junction (NMJ) and continue to nucleate MTs. Note that also ER exits sites are rearranged during myogenic differentiation (not depicted here). Scheme is not drawn to scale.

Since the initial discovery by Tassin and colleagues in 1985 that the centrosome and MT network undergo profound changes during myogenic differentiation, little progress has been made on how these processes are time-wise regulated during skeletal muscle formation and why these processes are important and specific to muscle. It is known that the ability of differentiated muscle cells to form a functional

non-centrosomal MTOC at the nucleus is not simply resulting from the fusion of myoblasts into multinucleated myotubes. In fact, artificial polykaryons induced by the fusion of HeLa cells fail to assemble centrosomal proteins at their nuclei and to grow MTs from the NE (Tassin et al., 1985a). But nuclei from non-muscle U2OS cells are able to accumulate Pcm1 and Pericentrin at the nucleus, although to a lesser extent than muscle cells, when human U2OS cells are artificially fused with mouse differentiated myotubes (Fant et al., 2009). This suggests that also other non-muscle cells might have the potential to form a non-centrosomal MTOC at the nucleus but that additional muscle-specific factors are required to induce these remodeling processes.

Several ideas why the highly specialized MT network is important for muscle came from early studies of muscle cell cultures in the presence of different cytoskeleton-altering drugs. MTs were suggested to be important for myoblast fusion into myotubes and subsequent myotube elongation (Saitoh et al., 1988; Straube and Merdes, 2007). Also stabilized MTs (detyrosination and acetylation) which increase during myogenic differentiation were proposed to regulate myoblast cell shape and myotube elongation (Gundersen et al., 1989). Additionally, MTs were implicated in the orientation of myosin filaments (Antin et al., 1981; Holtzer et al., 1975), a finding that was later confirmed by live-cell experiments using fluorescently labeled tubulin and myosin molecules (Pizon et al., 2005). Together these studies indicated that MT rearrangements could be a prerequisite for the organization of skeletal actin and myosin during sarcomere formation. Moreover, MTs were shown to be important for nuclear positioning during skeletal muscle formation (see section 1.2.6 for further explanations). Overall, MTs seem to be required for diverse biological processes during differentiation - regulation of muscle cell morphology, sarcomere assembly, and nuclear positioning - suggesting that any disturbances of MT regulation, assembly or dynamics could affect muscle function.

1.5 Aim of the project

The cytoskeleton, MTOC and organelle rearrangements that occur during skeletal muscle formation are fascinating but the underlying mechanisms that drive these processes are still poorly investigated. Although a multitude of centrosomal proteins were described to relocalize to the NE, it is still unknown how centrosomal proteins are anchored at the nucleus and how they contribute to MT nucleation from the NE. In this study, we thus aimed to unravel the nuclear 'receptors' at the NE that bind centrosomal proteins and initiate MTOC formation at the nucleus during myogenic differentiation. We further considered to examine if all centrosomal proteins are recruited to the NE by the same receptor and if certain centrosomal proteins contribute to the recruitment of other centrosomal proteins through mutual interactions. Moreover, we set out to determine which of the relocalized centrosomal proteins that aid in γ-TuRC recruitment at the centrosome are actually important for MT nucleation from the NE in skeletal muscle cells. Finally, as MTs were demonstrated to play a crucial role in nuclear positioning during myogenic differentiation, we wanted to investigate how active MT nucleation from the nucleus is contributing to these processes. Therefore, we aimed to analyze the impact of centrosomal proteins and the identified receptor on nuclear spreading movements.

2 Materials and Methods

2.1 Materials

2.1.1 Chemicals and disposables

General chemicals were obtained from Sigma-Aldrich, Merck or Carl Roth GmbH + Co. KG if not otherwise stated. Common disposables were purchased from Corning and Merck Millipore.

2.1.2 Solutions and media

Ultrapure water (ddH_2O) with a resistivity of 18 MΩ.cm at 25°C was used from a Milli-Q® reference water purification system (Millipore, Merck) to prepare all buffers and solutions. The pH was adjusted using NaOH or HCl.

Table 2.1: Buffers and Media for Molecular Biological Methods

Buffer / Medium	Composition	Source / Cat.No
LB Medium (Lennox)	Dissolve 20 g in 1 L ddH_2O 10 g/L Tryptone 5 g/L Yeast extract 5 g/L NaCl pH 7.0 ±0.2	Carl Roth, #X964
LB Agar (Luria/Miller)	Dissolve 40 g in 1 L ddH_2O 10 g/L Tryptone 5 g/L Yeast extract 10 g/L NaCl 15 g/L Agar-Agar pH 7.0 ±0.2	Carl Roth, #X969
Antibiotics	Ampicillin 100 mg/ml in ddH_2O (1000x)	

(stock solutions)	Kanamycin 50 mg/ml in ddH_2O (1000x)	
S.O.C. medium	2% Tryptone	Invitrogen, #15544034
	0.5% Yeast Extract	
	10 mM NaCl	
	2.5 mM KCl	
	10 mM $MgCl_2$	
	10 mM $MgSO_4$	
	20 mM glucose	

Table 2.2: Buffers and Media for Cell Culture

Buffer / Medium	**Composition**	**Source / Cat.No**
Growth Medium	Dulbecco's modified Eagle's medium	Gibco, #41966
for C2C12 cells	(DMEM)	
	4.5 g/L D-glucose	
	4 mM L-glutamine	
	1 mM sodium pyruvate	
	10% fetal calf serum	Eurobio, #CVFSVF0001
	100 U/ml penicillin,	Gibco, #15140-122
	100 μg/ml streptomycin	
Differentiation Medium	DMEM	Gibco, #41966
for C2C12 cells	4.5 g/L D-glucose	
	4 mM L-glutamine	
	1 mM sodium pyruvate	
	100 U/ml penicillin,	Gibco, #15140-122
	100 μg/ml streptomycin	
	2% horse serum	Gibco, #26050088
Growth Medium for	320 ml DMEM with GlutaMAX	Gibco, #61965-026
human immortalized	80 ml DMEM 199 medium	Gibco, #41150
myoblasts	20% fetal bovine serum	Gibco, #10270
	25 μg/ml bovine fetuin	Life Technologies, #10344026

	5 ng/ml recombinant human EGF	Life Technologies, #PHG0311
	0.5 ng/ml recombinant human FGF-basic	Life Technologies, #PHG0026
	5 μg/ml recombinant human insulin	Sigma-Aldrich, #91077C
	0.2 μg/ml dexamethasone	Sigma-Aldrich, #D4902
	0.1% gentamicin	Gibco, #15750
Differentiation Medium for human immortalized myoblasts	Iscove's Modified Dulbecco's Medium (IMDM) with GlutaMAX	Gibco, #31980
	2% horse serum	Gibco, #26050088
	0.1% gentamicin	Gibco, #15750
1x DPBS no calcium no magnesium	2.67 mM KCl	Gibco, #14190250
	1.47 mM KH_2PO_4	
	137.93 mM NaCl	
	8.06 mM Na_2HPO_4-$7H_2O$	
0.05% Trypsin-EDTA	5.33 mM KCl	Gibco,#25300054
	0.44 mM KH_2PO_4	
	4.17 mM $NaHCO_3$	
	137.93 mM NaCl	
	0.34 mM Na_2HPO_4-$7H_2O$	
	5.56 mM D-Glucose (Dextrose)	
	0.48 mM EDTA 4Na $2H_2O$	
	0.025 mM Phenol Red	
	0.021 mM Trypsin	

Table 2.3: Buffers for Cell Biological Methods.

Buffer	Composition	Source/ Cat.No
1x PBS	PBS tablet dissolved in 500 ml ddH_2O	Gibco, # 18912014
	10 mM sodium phosphates	
	2.68 KCl	
	140 mM NaCl	
	pH 7.45	

4% PFA	10 ml formaldehyde solution, 16% 30 ml PBS	Electron Microscopy Sciences #15710-S
IF blocking buffer	10% goat serum diluted in PBS	Sigma-Aldrich, #G9023
PHEM buffer	60 mM PIPES 25 mM HEPES 10 mM EGTA 2 mM $MgCl_2$ pH 6.9	
Pre-extraction buffer	1% Triton X-100 diluted in PHEM buffer	
Imaging buffer	50 mM Tris/HCl pH 8.0 10 mM NaCl 10 mM β-mercaptoethylamine (MEA) 0.5 mg/mL glucose oxidase 40 μg/mL catalase 10% (w/v) glucose	 Sigma-Aldrich, #30070 Sigma-Aldrich, #G2133 Sigma-Aldrich, #C100

Table 2.4: Buffers for Biochemical Methods.

Buffer	**Composition**	**Source/ Cat.No**
Buffer A	50 mM Tris pH 7.4 0.5% sodium deoxycholate 150 mM NaCl 1% NP-40 0.1% SDS	
Buffer B	20 mM Tris pH 7.4	
IP Lysis Buffer	10 mM Tris pH 7.5 100 mM NaCl 1 mM EDTA pH 8.0 1% Triton X-100 0.5% NP-40 add freshly 1x protease inhibitors	 Roche, #4693132001
IP Wash Buffer	10 mM Tris pH 7.5 100 mM NaCl 1 mM EDTA pH 8.0 add freshly 1x protease inhibitors	 Roche, #4693132001

NuPage®MOPS SDS Running Buffer (20x)	To dilute to 1x with ddH_2O 50 mM MOPS 50 mM Tris Base 0.1% SDS 1 mM EDTA pH 7.7	Life Technologies, #NP0001
Kyle lysis buffer	50 mM Tris pH 7.4 500 mM NaCl 0.4% SDS 5 mM EDTA pH 7.4 add freshly 1x protease inhibitors 2% Triton X-100 1 mM DTT	 Roche, #4693132001
Ponceau S	0.1% (w/v) Ponceau S 5% acetic acid	Sigma-Aldrich #P7170-1L
10x TBS (Tris Buffered Saline)	To dilute to 1x with ddH_2O 0.25 M Tris base 1.37 M NaCl 26.8 mM KCl	Euromedex, #ET-220-B
TBS-Tween	1x TBS 0.05% Tween	
10x TG (Tris/Glycine)	To dilute to 1x with ddH_2O 25 mM Tris 192 mM Glycine pH 8.3	Bio-Rad, #3030-917
10x TGS (Tris/Glycine/SDS)	To dilute to 1x with ddH_2O 25 mM Tris 192 mM Glycine 0.1% SDS pH 8.3	Bio-Rad, #161-0772
WB Blocking solution	1x TBS-Tween 5% milk powder	
WB Transfer	1x TG buffer 10% ethanol 0.025% SDS	

2.1.3 Molecular weight standards

Table 2.5: Molecular weight standards.

Marker	Composition	Source/ Cat.No
Novex® Sharp Pre-stained Protein Standard	260, 160, 110, 80, 60, 50, 40, 30, 20, 15, 10, 3.5 kDa protein bands	Invitrogen, #LC5800
HiMark™ Pre-stained Protein Standard	460, 268, 238, 171, 117, 71, 55, 41, 31 kDa protein bands	Invitrogen, #LC5699

2.1.4 Plasmids

Table 2.6: Plasmids used for overexpression.

Constructs	Backbone	Source
dsRed-PACT (human Pericentrin)	pCMV-DsRed-Express (Clontech)	Gift from Sean Munro
myc-PACT (human Pericentrin)	homemade Gateway Destination vector based on pCS2	Gift from Brian Burke, Yin Loon Lee
GFP-Nesprin-1α	pcDNA3.1	Gift from Brian Burke
GFP	EGFP-C1	
EB1-GFP	EGFP-C1	

2.1.5 Small interfering RNAs (siRNAs)

The following siRNAs were directed against the mouse mRNA sequence and were either obtained from Life Technologies (Ambion, *Silencer*™Select) or synthesized by GeneCust (Luxembourg). Dried oligonucleotides were dissolved in nuclease-free water to a final stock concentration of 10 μM and stored at -20°C. RNA oligonucleotides used for the siRNA screen (Ambion, *Silencer*™siRNA costum-made library) were delivered in 96-well plates and were reconstituted as described before using multi-channel pipettes. For the siRNA screen, a mix of three different RNA oligonucleotides was directed against each mRNA as listed in Table 2.8.

Table 2.7: siRNAs

siRNA	Gene name	Gene description	Gene ID	Sense siRNA sequence 5'-3'
Akap450 #1	Akap9	A kinase (PRKA) anchor	100986	AUCACUGUGCAACUUGAAUAAAGAA
Akap450 #2		protein (yotiao) 9		UACCUUUCAUUGGACAGGUUUCUAUCG
Cdk5Rap2 #1	Cdk5rap2	CDK5 regulatory subunit	214444	GAGAUCACCUUGAUAGUAAtt
Cdk5Rap2 #2		associated protein 2		CAGUGAGGCUAUUAUCACAtt
Cdk5Rap2 #3				GCACAUGGAUUCCAAUAUUtt
Cep192 #1	Cep192	Centrosomal protein 192	70799	GAACUUGCUUAGUACAGCAtt
Cep192 #2				GGAUUUUCAGAUGCACGUUtt
Cep192 #3				GGUUAUCCAGAGUAAAUCUtt
control #1		non-targeting		UUCUCCGAAGCUGUCACGUtt
control #2				CGUUAAUCGCGUAUAAUACGCGUAT
control #3				CGUACGCGGAAUACUUCGATT
Nesprin-1 #1	Syne1	spectrin repeat containing,	64009	CCAUCGAGUCUCACAUCAAtt
Nesprin-1 #2		nuclear envelope 1		AGUAAGAGGAGAAGGAAUAtt
Sun1 #1	Sun1	Sad1 and UNC84 domain containing 1	77053	GGCUAUUGAUUCGCACAUUtt
Sun2 #1	Sun2	Sad1 and UNC84 domain containing 2	223697	CUCUCAGGAUGAUAACGAUtt
Pcm1 #1	Pcm1	pericentriolar material 1	18536	AGUCAGAUUCUGCAACAUGAUCUTG
Pcm1 #2				AAUAGUAUCCCGUAAAGCUUCAAACAU
Pcnt #1	Pcnt	pericentrin (kendrin)	18541	GCCGAUCAACAAUUGCUAAtt
Pcnt #2				GGGUUUAAUGAAUUGGUCAtt
γ-tubulin #1	Tubg1	tubulin, gamma 1	103733	ACGUGGUGGUCCAACCCUAtt
γ-tubulin #2				UCCUGGAACGGCUAAAUGAtt
γ-tubulin #3				AGGACAAUUUUGACGAGAUtt

Table 2.8: siRNAs used for the siRNA screen

Gene symbol/ Gene name	Gene description	Gene ID	Antisense siRNA sequence 5'-3'
0610007P14Rik	RIKEN cDNA 0610007P14 gene	58520	UGUAGAUAAAAGAGGAGCCtg
			AUGGUUUAAGGAUAGAGGGtg
			AGUCUAUGUGCUCAGGACCtt
Glmp	glycosylated lysosomal membrane protein	56700	AAUAACCUCCAUAGAUACCtg
0610031J06Rik	RIKEN cDNA 0610031J06 gene		GCAAGAUCCAAUGAGUUGGtg
			UCUAGAAAAGGCUUGGACCtt
Timm21	tranlocase of inner mitochondrial membrane 21	67105	GUUUUAAAGCAAGCUUUGGtg
1700034H14Rik	RIKEN cDNA 1700034H14 gene		GAAUUUCACACGGAUGCGCtt
			UUGCUUGGUACUAUCCUCCtt
Tmem120a	transmembrane protein 120A	215210	UUUGUAAGCGAACUUAGCCtg
2010310D06Rik	RIKEN cDNA 2010310D06 gene		CAGACUCAGGUACAACCCGtt
			GGAGUUUGUACAGUUGGCCtg
Ostc	oligosaccharyltransferase complex subunit	66357	GUUUGGUGCAUUGGAUCGGtc
2310008M10Rik	(non-catalytic)		GGAUUAUGAAACCUAAACCtc
	RIKEN cDNA 2310008M10 gene		AUGAACAGAAGAAGAAACCtg
Tmem209	transmembrane protein 209	72649	UUUCAUUCGUAACAUCUGGtt
2700094F01Rik	RIKEN cDNA 2700094F01 gene		AACUUAACACACUUUGACCtt
			UGUAGUCUGCACAACAGCCtg
Syne3	spectrin repeat containing, nuclear envelope	212073	CUUCAUACUUUGGUAUUCCtg
4831426I19Rik	family member 3		GGUGAUUUUUUUUUUCCCtc
	RIKEN cDNA 4831426I19 gene		CAGUUGAGUUUGUAACCGGtc
Timmdc1	translocase of inner mitochondrial membrane	76916	UUAUUCUGAAAAGACCUCCtg
4930455C21Rik	domain containing 1		AGUUUAUUCUGAAAAGACCtc
	RIKEN cDNA 4930455C21 gene		AAAUAAAAGCAGGUAUUCCtc
Scai	suppressor of cancer cell invasion	320271	UUUAACUUAUGGAUUGUCCtc
A930041I02Rik	RIKEN cDNA A930041I02 gene		UUAAGAGUAAAUUCAGUCCtg
			GGAUGUCAUCUUCAGCACCtc
Aadacl1	arylacetamide deacetylase-like 1	320024	UUCACUUUCGGAGAAGACCtt
			AUGUUUUUCAGAAAAACCCtg
			ACCUAAGGCUAUUUCUAGCtc
Abhd12	abhydrolase domain containing 12	76192	GCAGAAAGAACCAUUUUCCtg
			CCAAUAUAAGGGCAUCUGGtg
			UCUGAGUCCUCUUUCUAGGtg
Acbd5	acyl-Coenzyme A binding domain containing 5	74159	UUGUUAAAUGGUGUAUUCCtg
			UUCUUAUCAUCACUGCCGCtc
			AUGCAAAAUCGAUUUAACCtc
Ace	angiotensin I converting enzyme (peptidyl-	11421	ACGCACAUAGGCAUGCAGGtt
	dipeptidase A) 1		CCAUUAUAUCUCCAAUAGCtt
			AUCCGUGUAGCCAUUGAGCtt

Acsl1	acyl-CoA synthetase long-chain family member 1	14081	GUAUAAACAACAGCUUGGAta AAGUUAGGCUACCAAAUAGtg GCAAUUAAGAAUACGAGUAtg
Acsl5	acyl-CoA synthetase long-chain family member 5	433256	CAUAGAGGCUCUUGAUUUGtg GGGAUAUCAGCCCUGUUGAtg UUAAGCUACUACUCCUCGAtg
Actr1a	ARP1 actin-related protein 1 homolog A (yeast)	54130	UGAACAGGGUAGAACCUCCtg GGCCAAUGAAGAUGUCACCtt AGCUCUUUCCUUUAUGGCCtt
Afg3l2	AFG3(ATPase family gene 3)-like 2 (yeast)	69597	GGUCCAAUAAAAAUCUGCCtg UCCAGAAACUCAGAUCCGCtc ACUUCAUCGUCUAUCAUCCtc
Ager	advanced glycosylation end product-specific receptor	11596	ACAGCUUAGCACAAGUGGCtc UUCAGGCUCAACCAACAGCtg CCUUAUUAGGGACACUGGCtg
Syne4	spectrin repeat containing, nuclear envelope family member 4	233066	AAGAUGGUGUCUCGGUGGGtt ACAAAGAUGUAGACUGUCCtg
AI428936	expressed sequence AI428936		AUAGCUGAUCAACUGGGCCtg
AI464131	expressed sequence AI464131	329828	ACAUUACAGUGUCCUUAGGtc GACUUGCUCACCCUUCUGGtt AAAUGGCUGCGGUUCUUGCtg
Urb2	URB2 ribosome biogenesis 2 homolog (S. cerevisiae)	382038	GCAAUUCAGCUAGCUCUGCtg AUGAAUGACCUCAAACAGCtt
AK122209	cDNA sequence AK122209		UAGAAAUUGCAAUGCUGCCtg
Aldh3a2	aldehyde dehydrogenase family 3, subfamily A2	11671	AAUUUCUUCUUGCAUCACCtt UAACAAUGGCAGCAUUUCCtg UAUGAAAUUUAUGGCUUCGtc
Aldh6a1	aldehyde dehydrogenase family 6, subfamily A1	104776	UCAUAAUCAGUAUAGAAGCtc CUGAUAACGAAGCAGGACCtg UCUAAGAAACAAGAAACCCtt
Aoc3	amine oxidase, copper containing 3	11754	AGAUCUUCAAUCGAAUUGCtc GAUCAUCUCCUCGAUAUCCtg CUUAUGAUCUAUCAGAAGCtc
Aph1c	anterior pharynx defective 1c homolog (C. elegans)	68318	CACAGUUACAACGGUCACCtt AAUGAAAGUGAAAUUUGCCtg GGGUAAGAUUCUAGCCAGCtc
App	amyloid beta (A4) precursor protein	11820	UUGAACACAUGAUGAGGCCtt CAAUGCAGGUUUUGGUCCCtg ACAAACAUCCAUCCGCUCCtg
Aqp1	aquaporin 1	11826	CUGAGUUGAUAAAUCUUGGtc AAGCCUCCUCUAUUUGGGCtt GGGAGUGACUUUGGUCAGCtt
Arl6ip5	ADP-ribosylation factor-like 6 interacting protein 5	65106	UUUGUUGAUGUUAUCUUCCtg UUUCUUCAGGCCGAUUCCCtc AUUGUCCUAAACAGCUACCtt
Asph	aspartate-beta-hydroxylase	65973	ACCAUGUGAAAAAGGACCCtc UUCUCCCAUUCUUGUGUCCtc AUGUGAAAAAGGACCCUCCtg
Atp1a1	ATPase, Na+/K+ transporting, alpha 1 polypeptide	11928	CAUUUCGAAUCACAAGGGCtt AUCCCUUUCCUUCUUGGCCtt UAUCAAAAAUCAGACGACCtt
Atp1a2	ATPase, Na+/K+ transporting, alpha 2 polypeptide	98660	UGAUGUCACUCUCAGCUGCtt GAUUUCUGCCACCUUAGGGtt CUUAGUUCCCUCAGGUGCCtt
Atp1a3	ATPase, Na+/K+ transporting, alpha 3 polypeptide	232975	CUCUGUCAUAGCCACUUCCtt UCACCUGCAUCUUUUCACCtt GAGCUCUUGUCGAAAGAGGtc
Atp2a2	ATPase, Ca++ transporting, cardiac muscle, slow twitch 2	11938	UCUACAAAGGCUGUAAUCGtt AUUUUCAGCAUUUCUUUCCtg GUUCCAGCAAGGUUUUUCCtt
Atp2b1	ATPase, Ca++ transporting, plasma membrane 1	67972	CGGAACCUUUUUAUAAUGCtt AAGAAUACUAUCUUGUCCGtc UCACUCAAUGAUCCAGGGCtc
Atp2b2	ATPase, Ca++ transporting, plasma membrane 2	11941	UCCGAUUGAAUUCUUUGCCtt CUUGAUCUUGACCACAGCCtc GAGCAGUGCCUGGUAAACCtt
Atp4a	ATPase, H+/K+ exchanging, gastric, alpha polypeptide	11944	AUUUGUGCUCUUGAACUCCtg GUCGUUAAUCUCCAUCUCCtt GCUUCUCCUUCUUCUUGCCtc
Atp6v0a1	ATPase, H+ transporting, lysosomal V0 subunit A1	11975	CAAAGCCAAGUCGUAAGGGtg AAUAAUUUCAGCAUCCUCCtc GCGGGUUUUCGAUUUCAGCtt
Atp8a2	ATPase, aminophospholipid transporter-like, class I, type 8A, member 2	50769	GAUAAUUUCAUCUCCAUCCtt GUUAACUGCAUUGUCUGCCtt CUAUGAUCUCUUUGAUGCCtg

Aytl2	acyltransferase like 2	210992	GAUGUCUCUGCUCUCUGCCtt CAGGAAUGAACGCACCAGGtt UCCUAUUUGUACAAGUUCCtt
Nepro BC027231	nucleolus and neural progenitor protein cDNA sequence BC027231	212547	GAUUCUUUGCACAGUAUCGtt CUUUAAGCACUGUUCUACCtg UCAUAUAAGGAAAUGAGCCtt
Bcam	basal cell adhesion molecule	57278	ACGGAUGGUUAUGUAGCCCtt GUUUUAACUCUGGUGCUCCtt UGCAAGGGUCACAGAAUCCtt
Bcap31	B-cell receptor-associated protein 31	27061	UAAACAACAAUCAGGUCCCtt GAUAAAACAGUUGACCUGCtt AUUGUUCUGGAGGUUCACCtt
Bcl2l13	BCL2-like 13 (apoptosis facilitator)	94044	CCUAAUUGAACCCUAUCCCtt CCACAUCUAGUUGAACUCCtg UUAAGAGGUCAAAUAGACCtt
Bin1	bridging integrator 1	30948	CAGAUAGGUCCGAAGAUCCtt CUCUUUAUGGAAGUUUUCCtc UUAACAGAAGCCAGAUAGGtc
Bsg	basigin	12215	UGUCGUUUGGAGCAUUCCCtt ACAUUUACGUCAAGGUUGCtg UAUGUACUUCGUAUGCAGGtc
C3	complement component 3	12266	AGUUGAAUUCCUUACUGGCtg AAUCUUCUUAUCGCCAUCCtg CUUAUCUGAGUUGAAUUCCtt
Cadm4	cell adhesion molecule 4	260299	CCCAAAUCCUUAUUACCCGtc AAAGAAAUCUGUGUUUCCCtt GCUCACUCCUUUCAACUCCtt
Canx	calnexin	12330	AAUAUACUCAGGUUCGUCGtc UCCAUUCUGAAAAUUAACCtc AGAUUUUGAAUCUUCUACCtc
Cav1	caveolin, caveolae protein 1	12389	UUUGUAUGACAUCAUCACCtt GUUGACCAGGUCAAUCUCCtt AUAGUCUCCAAAUUGAUGGtg
Ccdc90b	coiled-coil domain containing 90B	66365	CUGUUAUUUCCUGCUGAGCtt ACUUUUGGUUUGUGUAUCCtt UCUGACUUAGUUGUGGUGGtc
Cd34	CD34 antigen	12490	AUCAUUUUCACUCAUCACGtt UUGAAUUAGAUCUUCUCCCtt UGAUAGAUCAAGUAGUGGCtg
Cd36	CD36 antigen	12491	UCUUCAAGGACAACUUCCCtt UUUUGAAAGCAGUGGUUCCtt AACACAGCGUAGAUAGACCtg
Cdc42bpa	Cdc42 binding protein kinase alpha	226751	AGCUUAUCGAGUUCACUCGtt GAUAUCUUUUCGACUUGCGtg AACAUUUGUUACUAGGUGCtg
Cdc42bpb	Cdc42 binding protein kinase beta	217866	GUAUCCUUCGCUCGUACGCtt GUAGCAAAGGAUUAGUCGCtt AUCUCGCCAAUGUAGAACCtc
Cdc42bpg	CDC42 binding protein kinase gamma (DMPK-like)	240505	GGUAACAGAGAACUUGGCGtt CAGGAAUUCUUCCUGCCGGtt GAGGGUAUCAUCAUCCACGtc
Cdh2	cadherin 2	12558	UAUCAGGAACUUUGCCUGCtc AUGUGGUUCCUUCAUAGGCtc CUGUCCUUCGUGCACAUCCtt
Cdh5	cadherin 5	12562	AGCAUUCUGGCGGUUCACGtt UUUAGAUUGGACUUGAUCCtt UGACAGAGGUCCCUAUAGCtg
Cdk5rap2	CDK5 regulatory subunit associated protein 2	214444	AUGAUGUCUCUCUGUAACCtt AUCAAAGAUGACUUUCUCCtg AACCUUUCAUUUUCUUCCCtt
Ckap4	cytoskeleton-associated protein 4	216197	UACUAUAAAUUUGACUGCCtg UGAAUUUGCAUAGUUACCGtt AAACAACCUAUCCAGGUCGtt
Clec14a	C-type lectin domain family 14, member a	66864	UCUCUUGAAGGUAGCGUGGtg UCCUUAAUUAUUUACCACCtg CCUUAAAGGCUCUUUCUCCtg
Colec12	collectin sub-family member 12	140792	GGUUUUUUCUGUGAUCUCCtg AAUAUCUGUCUCAAAGACCtg UUUGUUGUCAUAAGUCUGGtg
Cox4i1	cytochrome c oxidase subunit IV isoform 1	12857	AACUGAACUUUCUCAUCCCtg AUGUCCAGCAUUCGCUUGGtc UUUUUUCCACGUAAACUGGtc
Cox6a1	cytochrome c oxidase, subunit VI a, polypeptide 1	12861	UACUCAUCUUCAUAGCCGGtc AUUUAUUUAAGCCAUCUCCtc AAACCAGUGCUGUGGUCCCtt

Cox7a1	cytochrome c oxidase, subunit VIIa 1	12865	ACACGGUUUUCUAAGUGGCtt UUGAUGUUUGUCCAAGUCCtc UUUCAAGUGUACUGGGAGGtc
Cox7a2	cytochrome c oxidase, subunit VIIa 2	12866	UUGAUGAAACUGAACCACGtg CUUUUGUUUCUCUGGAACCtt ACCUUGUUUUCAAAAUGCCtt
Cspg4	chondroitin sulfate proteoglycan 4	121021	AGAAUUCUUCAGCACAACCtt UUCAUAUGGGCCAUAGACCtc AGAGAUGGUCAUCUUGGCCtg
Ctsd	cathepsin D	13033	AGGAAUCAUAUACUCACCCtg CACCUUGAUACCUCUUGCCtt GUAGUUCAUAGUUUUUGCCtc
Cttn	cortactin	13043	GUGAAUGUUGAUGUGUUCCtg CGUUUCCAGCUCCUUCUCCtt ACUUUUAUCCACCUUGUCCtt
Cyb5	cytochrome b-5	109672	CUUGGUCAGAUCGUACACCtt AGUCUUUUAGUUCUUCGGCtt AGGAUGCUCUUCGAGAAACtt
Cyb5b	cytochrome b5 type B	66427	UAAUGUUUUUUCAUGACCCtc UGGGAAAAGAUUCAUAACCtg AAGGAUCCUUGUCAUCGCCtt
Cyc1	cytochrome c-1	66445	AAUAGUCAGACAACUUCCCtg CAGGGAAAAUACGUAGUCCtc CUAGCUCGAACGAUGUAGCtg
Cyp2b13	cytochrome P450, family 2, subfamily b, polypeptide 13	13089	AAUGAAGUUGAGGAUUUCCtg UUGUUCACCAGAGCCUCCCtt CAGUCUAGUUUCCAGCAGCtc
Cyp2f2	cytochrome P450, family 2, subfamily f, polypeptide 2	13107	UACUCCUUGCUAAGCUUGGtg AUAAGACGGGUAUUUCACCtt GGGUGCAUCAUAGAAUAGGtt
Cyp3a16	cytochrome P450, family 3, subfamily a, polypeptide 16	13114	ACCAUUGAUUUCAACAUCCtt GCUAGAGAGAUGGAUUUACtc CCUCAAGGGAAAAUCACGCtc
Cyp4b1	cytochrome P450, family 4, subfamily b, polypeptide 1	13120	CUAACUGCCAGGUAGUAGCtg GCUGGAACCAUUUUGGCCCtt AGCUUUAGCAUAGUCAGGCtc
Cyp51	cytochrome P450, family 51	13121	UUUGUAACGGAUUACUGGGtt AGCUGUCAAAAUUAUGAGCtc UAUGUGGUGGACUUUUCGCtc
D4Ertd429e	DNA segment, Chr 4, ERATO Doi 429, expressed	230917	UGUGAAAGCAGCCAGCUGCtt UAGAUAAUGCUCUGCCAGGtg AUAGGGCACCAGUGUAUCGtg
Dag1	dystroglycan 1	13138	UGUAAGGACAGUCACUGGCtc AUUAAAUCCGUUGGAAUGCtc CUGUUCAACAGAUCGAUCCtt
Dctn1	dynactin 1	13191	CUGGGUGAACUUGAUGUGGtc UCACAUGUGAAAUACUUCCtt ACUACAUGAUGUUUCCAGGtc
Dctn2	dynactin 2	69654	AUGUGUUCCACGCUUGUGCtg GUACAACAGCAUUUAAUGGtc AAACUCUGCUUGAUCAUCCtc
Dctn3	dynactin 3	53598	UUGUAGAGAAUCUUCACCCtc AAUGUUCCCUAAAGCCACCtg UUGUAGUCUUGUUAUACCCtt
Ddost	dolichyl-di-phosphooligosaccharide-protein glycotransferase	13200	CUAUACUCCACCAAGUCGGtg AGUAAGAGGUUGAAGAGCCtg GAUGUAUCACUUAAAUACCtg
Disc1	disrupted in schizophrenia 1	244667	CUGUGCUUCUCAUGUAGCCtg GUUGCUCAGUAGGUAGUCCtg UAAAAUUAAGGAAGUGACCtc
Dlg1	discs, large homolog 1 (Drosophila)	13383	AAAUAUGUUAAUAAACCCGCtc UUUGGAUUAUCAAGUAAGGtc CGUUCUUUAGUGCAGCUGCtg
Dlg2	discs, large homolog 2 (Drosophila)	23859	GGAAUGAUCAUGUGGACCGtc UAUCUUCUAAGGUAUCUCCtt UCAUAUAAAAUAGUGGUGGGtt
Dlg4	discs, large homolog 4 (Drosophila)	13385	AGCCAAGUCCUUUAGGCCCtt UUAUACUGAGCGAUGAUCGtg GAUAAAGAUGGAUGGGUCGtc
Dnajb11	DnaJ (Hsp40) homolog, subfamily B, member 11	67838	AGUGAUUAUCAAAGAGCCCtt AAGCAUCGUACUGUUUUCGtt CUACGAUGAUAUCACUUCCtc
Dnm2	dynamin 2	13430	UCCCGAGCCUUCAAUUCGCtt UUAAUAUGGCCAAAGGAGCtc UCAAGUUCAACACGUGUGGtg

Dpp4	dipeptidylpeptidase 4	13482	ACUCAUUUCAACGUGCUGCtg AGCAGAACUAUUGGCACGGtg CUUUGCAUAUAUGAUUUCCtg
Dtnbp1	dystrobrevin binding protein 1	94245	ACAAGUCACUUAAAUGUCCtg CAGCAAAUGGUUCUCUACCtc GUGUGUAAAAUUGAAAACCtc
Dullard	Dullard homolog (Xenopus laevis)	67181	GUGUUUGUCUAUUACCACCtt CAGGAUCUUCCUCUUCACCtg ACAAGCUCAUACCACUGGCtt
Dync1h1	dynein cytoplasmic 1 heavy chain 1	13424	GGAAAUGAAUUCUUUCUCCtc CUGCAUCAAUCACAGGAGCtc AGUUUUAAACAUAACCUCCtc
Dync1i1	dynein cytoplasmic 1 intermediate chain 1	13426	CUUCUUCCUCUCCUCUUCCtt AAUCAUGACCAAUUUUGGGtt GAUCUGCUGUUUUUCUUCCtc
Dync1i2	dynein cytoplasmic 1 intermediate chain 2	13427	UACAAUUCUCGUAGAAUGGtc AAAGAAGAUGUUAAUCUGCtc UUCCUUUUUUUUCCUUUCCtc
Dync1li1	dynein cytoplasmic 1 light intermediate chain 1	235661	AAUUGUCUUUCUUAGCCGGtc UGCUAAAAGAGACUGUAGCtt AUCCAAAGCAGUCCAAGGCtt
Dync1li2	dynein, cytoplasmic 1 light intermediate chain 2	234663	UGUCAGCUACUUAACCUGCtt CAGGUUAUGAGUCAGCACGtt UAAGAGAAGAAGUGCUACGtt
Dynll1	dynein light chain LC8-type 1	56455	GUACUUCUUGUCAAACUCCtt GAACAGAAGAAUGGCCACCtg UGGAAUUUGGAUGCAGUCCtt
Dynll2	dynein light chain LC8-type 2	68097	GUUGUACUUCUCCAUGGCCtg GAUAUAGGCAGCAAUGUCCtt CAUUGCUAUACUUCAGACCtg
Dynlrb1	dynein light chain roadblock-type 1	67068	GAGCGAAUUCGAAGGAAGGtt AAGCUCUCAUUCCAAAGCCtg UGCUCUUGAUGGGAAUGCCtt
Dynlrb2	dynein light chain roadblock-type 2	75465	GACAAUCAGAAGAUAUUCCtt GUACAAUAUCAUGGAUUCGtg CCUAAGAAAAGUCAGGUCGtt
Dynlt1	dynein light chain Tctex-type 1	21648	GCUGAAGUCAUGUGGUUCCtg UAAGACAAGUGGUACUGCCtg GACUUGAGUUUUUAGCACCtt
Dynlt3	dynein light chain Tctex-type 3	67117	AUAGACUGUUCCACUAUGCtt CAAACUUAAGUUAAUGGCCtt GUGUGAAAUCCAUACGGGCtc
Ebp	phenylalkylamine Ca2+ antagonist (emopamil) binding protein	13595	GAUAUAUCGGCUAUCUCCCtt AGUAGCUCAACUUGUUCCCtt CCUUUUCUGACUCUGGCCCtt
Emd	emerin	13726	GGUGGUCAAAUAACUCUCCtc GAUUUUCUUUUCGUAGAGCtt UGCUCUAAAACCAAUACCCtt
Enpep	glutamyl aminopeptidase	13809	UACUCUAUUAGUAUCUUCCtg UAUAAUUCAGAAGUUGAGCtc AAGUUUUUCCAUUCUCCGCtt
Ergic1	endoplasmic reticulum-golgi intermediate compartment (ERGIC) 1	67458	AGAAUGAGUUGGCAUGUGCtc CAAACUGUGCCUUAUAUGGtc CUUAAAGAUUGUCAAAGCCtg
Erlin2	Erlin2 ER lipid raft associated 2	244373	CUUGUUGAAGAUGAGGGCCtt UUUCAGGAUAAGAAAUCCCtt UGAGCACAUUAAAAUGUCCtt
Erp29	endoplasmic reticulum protein 29	67397	CUUGCUUUUGGGAAUGACCtt AUUACACUCAUCAAGGACCtg UGGAAAGUCCUCACCUUGGtc
Esam1	endothelial cell-specific adhesion molecule	69524	UGAGCAGUAGGUUUACUCCtt AAGACAACACCUGGUUUGGtt AUUAAUGUAAGACAACACCtg
F11r	F11 receptor	16456	UGAGUUAAGAAUAUAGUCCtg AUUCACCACUAUCAAAGGCtg UAAAAAACAGCCGAGUUGGtt
Fads1	fatty acid desaturase 1	76267	AUGGUUGUAUGGCAUGUGCtt AUACUUUCUCACAAGACCCtt GUCGCUGAUGUUGUACACCtt
Fer1l3	fer-1-like 3, myoferlin (C. elegans)	226101	AUCUCCUUGAUCUUCUUCCtc UGUUUGUAGGGCAAAGACCtg UUCUUUCAAUCUCAAAACCtc
Fmo1	flavin containing monooxygenase 1	14261	AGAGUUUUCCUUUACCUCCtt UUUAAGUGAACAAAAGUGCtg CCUUAAAAGUUAGUAUACCtg

Fmo2	flavin containing monooxygenase 2	55990	UUCUUAUACUUUCACAUGGtg AUAAGAACAUCCUGUAACCtt AAUUUCUUGGCAAAGAUCCtg
Fmo3	flavin containing monooxygenase 3	14262	CUUUAAAACGGUUCAGUCCtg UAUUUAUACUGGUUACAGGtg CCUGGUUCCUUAUAGUCCCtg
Fmo5	flavin containing monooxygenase 5	14263	AAUUCUUUGGCAUACAUCCtg GUCAAUAGGAUAUCCAUGCtt ACUGAAACACAUCAUUUCCtt
Ganab	alpha glucosidase 2 alpha neutral subunit	14376	AUCUUGAUCCAUUUGUCCCtt CAUGUUCUUCUGAAGGCCCtg AAUGAUUUUGUAGGGUCCCtc
Gcs1	glucosidase 1	57377	GACCAGAAGACAUUGUAGCtg ACUUCAACUGUCCUUUGGCtc AAGGGAAGGAAGGUGUACCtg
Glg1	golgi apparatus protein 1	20340	GAUACUCAGUGAUGUUGCCtc GUAAGAGAAUCGAAAAUCCtt GGAUUCUUCAAACUUAUGGtt
Gpd2	glycerol phosphate dehydrogenase 2, mitochondrial	14571	UAGUAAGUUGGCACGUUCGtg AUCCAAGUUCAUGAUAGCCtt CAUUGAUAACGCAUUUGGCtc
Gpm6a	glycoprotein m6a	234267	UUAAUGAAACACCAAUGCCtt UCAGUAGAUUCACACAUCCtc GAGAAGCAUAGGGAAUACCtc
Gprc5a	G protein-coupled receptor, family C, group 5, member A	232431	CCAACACUUAGCUGUCGCCtt UUUCCUCUUGGGAGUAGGCtc GAAAAUGGGUGGAAUAAGGtg
Gpsn2	glycoprotein, synaptic 2	106529	UGUCUUGGUGAAAAGGGUCtt GAUUUCAGAAAUGGUGGCCtg AUCUUCAUCUUUCAGGGACtt
Hd	Huntington disease gene homolog	15194	GAUUAGAAUCCAUCAAAGCtt CAAAGUCAGUUCAUAAACCtg UUCACACGGUCUUUCUUGGtg
Hpxn	hemopexin	15458	GAACAACUUUGGAUACCCGtt CACCCAGACUUUGUCUUCCtt GACAUACACUUGAGUGCCCtg
Hrc	histidine rich calcium binding protein	15464	UUUCUCAUCUUUUUCUUCCtc AAACUCAGUUGAUAGGUCCtc UUCUCUGUGGCCUCUGUCCtt
Hsd11b1	hydroxysteroid 11-beta dehydrogenase 1	15483	GACAAUCACUUUCUUUCCCtg AAUUAUCCCAGAGAUUUCCtt CCAUUUCUCUUCCAAUCCCtt
Hyou1	hypoxia up-regulated 1	12282	GUACAAUUUGAUUCAAACCtg AGUUUUCCUCCGAGAUUCCtt AUGACUUUCUCUAAUGUCGtc
Icam1	intercellular adhesion molecule	15894	UUCUGUAACUUGUAUAUCCtg CAUAACUUAUACAUUCACCtc UGAGGAAGAACAGUUCACCtg
Igsf8	immunoglobulin superfamily, member 8	140559	GUACCGAUCAGUCCCUUCCtt UAUACCUUCCGUGUCCAGCtg UUCGGUACCGAUCAGUCCCtt
Ilvbl	ilvB (bacterial acetolactate synthase)-like	216136	UAAUACAGGCAUUAAAGCCtt GAUGCUUGUCUUGUCCACCtt UACCUUGACCACUUGAUCCtt
Ints1	integrator complex subunit 1	68510	UCUGUGAGUUCAUCGUACCtt AUCGUACCUUGGCAUGAGCtg GGGUAUGAGUAGUUAUUGGtc
Iqgap1	IQ motif containing GTPase activating protein 1	29875	UUUGUAUUCAGUAAGAUGGtc UGACUUUGUUUACAUUCCCtt UUCUUCUGUGAAAUCAACCtt
Iqgap2	IQ motif containing GTPase activating protein 2	544963	GUAAUCUGAUGUGACCUCCtc GUCCAUUAGGUUCAAGUCCtt UUUAACAGCUCUUCUUCCGtg
Iqgap3	IQ motif containing GTPase activating protein 3	404710	CCUUUCAUUAAUAGGGAGGtg CAAAAGUUGAUGUUGUCCGtg GGUUAAUCAGAACCACGGCtg
Itga1	integrin alpha 1	109700	UUGUCGAUGUCAAUUGUGGtt AUUUUCUGGAUCAGUGAGGtt CGUAUGGUAAGAUUUAAGCtg
Itga2	integrin alpha 2	16398	GCCCGGAAAAUAUUUUCGCtc AUGACUGAAAAUGUUAACCtc GUUAAAUAUAAUUCUCGGCtc
Itga6	integrin alpha 6	16403	AUUCAAUCCGUGUACAAGGtc UCUCUAUGAGUAACUUUCGtt UUCAAUAACCACUUUUGCCtt

Itgb1	integrin beta 1 (fibronectin receptor beta)	16412	CUUCUAAAUCAUCACAUCGtg GGAUAAUCAUAGUAAUGGCtc UCAAUUCCUUGUAAACAGGtt
Jph2	junctophilin 2	59091	AGAGUUCUCCAGGAUCUCCtg UGCCGUUGGUGAAUUGGCCtt GUGAAUUGGCCUUGAUAGGtt
Ktn1	kinectin 1	16709	AGGUUUUUGUUUCUUCUCCtt UUCCUUCAACAUGAUCAGGtt AUUCUUCUUCUUUUCUGCCtt
Lama1	laminin, alpha 1	16772	AUUUAUCUCCAGCAUAACCtt CGUAGCAAAUGCACAUGCCtc GUAUGCAACUUGAAAGACCtg
Lass2	longevity assurance homolog 2 (S. cerevisiae)	76893	UUAAGUCAUAGAACCAGGGtt CCGUGACAAAAGGUCUACCtc UUUUUGAGAAGACUGGGCCtg
Lbr	lamin B receptor	98386	AGGCUUGAUAUCACUCUCCtt UGAAUAUUUUGCAUCUAGCtc UGGGAUUUGUUGUCGUGGCtc
Lemd2	LEM domain containing 2	224640	CACAUUAGCUAUGUACUCCtg ACAUUCAAAAUUACCUGCCtg UGCCACAUUCAAAAUUACCtg
Lemd3	LEM domain containing 3	380664	GAGUCAAACUAUUUGGUGGtg AACAACAAUAACCUAUGGGtc GGCAAUAUGAACGAUGCCGtc
Letm1	leucine zipper-EF-hand containing transmembrane protein 1	56384	AAUCAGCUUAUCAUCAGCCtt CCUCAGCUCAUCCAGUACCtt ACAACAUACAGAGAUUCCCtt
Limk1	LIM-domain containing, protein kinase	16885	UCAGAUCCCUGUCAAUACCtg AUCAAACCGGAUAAGUUCCtt AAAUCUGGUGAGGGUAUCGtc
Limk2	LIM motif-containing protein kinase 2	16886	AUCAGGAUCCGCAUAUACCtg CUUAGAUGACAAACCUUGGtg CAAUUUGUUAAACAUGGCGtg
Lman1	lectin, mannose-binding, 1	70361	GGUUUAUUACGAAAGUCCCtc CUGAUAUCCCAAAAUGACCtt GCACCUGUAAAAUACUUGCtg
Lpgat1	lysophosphatidylglycerol acyltransferase 1	226856	ACACACAUCUCCAGUUGCCtg AUUUUUCUUGGCAAAUGCCtg CUAUUAUCCACUGGAGGCCtc
Lrp1	low density lipoprotein receptor-related protein 1	16971	UACUGGCUCAUUCUUGGCCtt GUAGUCAGUGAAGAACACCtt UUUUUGCACACAAACUGGCtt
Lrrc59	leucine rich repeat containing 59	98238	ACUGUUAUGAAAGAUUCGCtt AUUACGUCACCUUCCCAGCtt AGAAACGUAUUACGUCACCtt
Mag	myelin-associated glycoprotein	17136	GACAUUUAUUUCAUGUCCCtt UGGACUCAUACUUAUCAGGtg UCCCUUUUUGUACAGGUCCtg
Mbc2	membrane bound C2 domain containing protein	23943	GUGAAUAAUGCUGAUCAGCtt GUUGGUGCUGUAGGUAGCCtt AACCUCGUGGACUAUCACCtc
Mcam	melanoma cell adhesion molecule	84004	AUUUUCAUCGGUGCUCUCCtc CGGAAAAUCAGUAUCUGCCtc UGUCUUCCUUAACUAGGCGtg
Mettl7a	methyltransferase like 7A	70152	AAAAAGGAACCAGACAGGAtc GUACAUCACGGAGAAUCGCtt GUACUCAAGGAUAUCUACCtg
Mme	membrane metallo endopeptidase	17380	AUAGUCACACAACAGAACCtt AGAAUAGGCUUAAGUUUGGtt UUUCAAAAUGACUUCUAGCtc
Mospd3	motile sperm domain containing 3	68929	CUGAGGCUUCACAUAUCCCtc GAGGCUUCACAUAUCCCUCtg CUCAAUGCGGAAUCUGUCCtg
Msn	moesin	17698	UCUAUUCUAGAGAGCUAGGtt UCAUUGAAAGAGAUAUUCCtg CCAAAGAACCAAACUUCCCtc
Mtdh	Metadherin	67154	AAAAAAUUCACGUUUCCCGtc CAUUUAGAUGAGAAUCACCtt GUUCUUCUUCUUUUGCUCCtc
Mtm1	X-linked myotubular myopathy gene 1	17772	UUCUGAGUUUUGAUAUGCGtc AAAACUUAUCCUCCAAUGGtg GACAGUCUCACUCACAUCCtg
Mtmr14	myotubularin related protein 14	97287	UGAUUAGUGUGAAAUUGCCtc UUGCCCAGGUAUCAUCUGCtc UAGACAACUGUUAGGGAGCtc

Mybbp1a	MYB binding protein (P160) 1a	18432	ACUAGGUCUCAUCAUUGCCtt GAUCACUUUCAUGUUACCCtt UUGUUCAUGGCUUGUAGGCtg
Myh10	myosin, heavy polypeptide 10, non-muscle	77579	UCCUGAAUAGUAGCGGUCCtt AUGUACGCUCAUCUUUAGCtt GCUCUUCUUUAAUACUAGCtg
Myh14	myosin, heavy polypeptide 14	71960	GGAUUGAUCCUCACGAUCCtg AUGGAAGCUGCAUUCAUCCtt GUACAUUUCAACAAUGGCCtc
Myh9	myosin, heavy polypeptide 9, non-muscle	17886	GUACAUCUCCACGAUCUCCtc GUCCUUGUUCACCUUCACCtt UACCAGCUCUACAAUGGCCtc
Myl9	myosin, light polypeptide 9, regulatory	98932	AUGGCGAAGACAUUGGACGta AUCAUGUUGAAGGCCUCCUta CUUCUUAUCAAUGGGUGCCtc
Mylc2b	myosin light chain, regulatory B	67938	CGGAUAUAUUGUCCUGGGCtt AAAUCCGGAUAUAUUGUCCtg CUAAGUGACAGAAAGGGCCtg
Myo10	myosin X	17909	AUUGUACUCUGCUUGUAGGtg AAUAAUCUACAAUUCUCCCtc CUCUUUAAAUAUCUUCUCGtc
Myo1b	myosin IB	17912	CCUGAUUGACUUCUGCUCCtt UGUUCUUGUCAACAAAUCCtt UUUGUUUGUGCCUUAAUGCtt
Nat10	N-acetyltransferase 10	98956	ACUACAACAAAAAGAGACCtc UGUUUUGUUUCCAGUUUCCtt AAUACAAAUUCAAACAGCGtg
Ncln	nicalin homolog (zebrafish)	103425	AACGAAGGCUACGUUGUCCtg GUAAGCAUUCAUCACUUGCtt UGAGUCUAUCUGCUCCUCCtg
Nde1	nuclear distribution gene E homolog 1 (A nidulans)	67203	AGAUACAAUUUGAUCAUGCtg AAUAAAGCCUUUUUUUGCCtc UGGCAUCAUACGUUAGAGCtg
Ndel1	nuclear distribution gene E-like homolog 1 (A. nidulans)	83431	UAACUCUCUGCUUCCUUCCtg CUUCUAACUCUCUGCUUCCtt CAUAAUUCAGAGAUGUUCCtg
Ndufa13	NADH dehydrogenase (ubiquinone) 1 alpha subcomplex, 13	67184	CUUCCAGUUGGGCACAUCCtt CAUGAUGAUGGCUUCCUCCtc CUUUAUUAUGUGCGUUGGCtc
Ndufa4	NADH dehydrogenase (ubiquinone) 1 alpha subcomplex, 4	17992	UCAACAUGAUUUCAUGCAUtc UUGUUCUUUCUGUCCCAGCtg UUCAUUGGGACCCAGUUUGtt
Ndufb4	NADH dehydrogenase (ubiquinone) 1 beta subcomplex 4	68194	AGUCUUUCCUUUCUGUCCCtg AUUUUCUGUCCAGUUUUCCtt ACUGAAGCAGAUACUCCCGtt
Ndufb5	NADH dehydrogenase (ubiquinone) 1 beta subcomplex, 5	66046	AGAAUGAUCAAUGAACUCCtt AGUGUUCAGGGAUGUAGCCtt CUUUAACCGUAACUCAGCCtt
Ndufc2	NADH dehydrogenase (ubiquinone) 1, subcomplex unknown, 2	68197	UCAAGAAUUUCAGCAUAGGtt GGACGUAACGAACAGAAGCtg AGAGGAACAGGAACAAGCCtt
Nnt	nicotinamide nucleotide transhydrogenase	18115	CAUCAAAUUAUAUACGACCtc UAUUGUCACUCUUGGAACCtg GGAUUUACACCACAGUGCCtg
Noc2l	nucleolar complex associated 2 homolog	57741	UUCUUUAUCUUCUUCUUCCtg ACAACUUCAUGGAACAGCCtg CAGGUAUUCCAGAAUAAGGtc
Noc4l	nucleolar complex associated 4 homolog	100608	GUAUUUGUAUGUGGCUCCCtg CAAGAUGUCGAACACCGCGtt CAAGUGUCUGUAAUUCUCGtt
Nppa	natriuretic peptide precursor type A	230899	CUACAUUUAACAUCGAUCGtg AGGAUCUUUUGCGAUCUGCtc GAUUUGCUCCAAUAUGGCCtg
Nptn	neuroplastin	20320	UACAUAAGGGUGUGAGAGCtg GCAUUGUUUAAAAUGUACCtg AAAGUUAUACGGUAAGCCCtt
Nrm	nurim (nuclear envelope membrane protein)	106582	UAAACUUUCAGAUAGGCCCtg AGGGCUUAGAACUAGCUCCtc UUAGGAGACCACACAGAGCtg
Nrp1	neuropilin 1	18186	CAUAGCGACAGAACAUUCCtc AGAUGUGAGGUACCCUGGGtt CAAAUCGAGUUAUCAGUGGtt
Nup210	nucleoporin 210	54563	AACAUUCUUAUAGACAGCCtc AGAGACAAUCUGAAUGCCGtg UAGAUGAUGUAGAAACAGCtt

Pak1	p21 (CDKN1A)-activated kinase 1	18479	UAAUUUCUCUAAGAUCUCCtc GUCCUUCUUUUUCUUCUCCtc GUGGUUCAAUCACAGAUCGtg
Pard3	par-3 (partitioning defective 3) homolog (C. elegans)	93742	UAAAUCUACUCCAUUGACCtc ACUUCCAGCGGUGUUCUGCtt GGCGGAACAUAUGUUGUGCtt
Pard6a	par-6 (partitioning defective 6,) homolog alpha (C. elegans)	56513	AUCUAUAACUGAAGACACCtg AUUACGCUGGUUGGCAGGCtt GAACCAUGUUUGUGCAGCCtc
Pbxip1	pre-B-cell leukemia transcription factor interacting protein 1	229534	AUCUUUCCUAGGGUGUACCtt UAAUUCUUUGCCAUCUGCCtt AAGUUCUUCUUUCUGAGCCtg
Pcyox1	prenylcysteine oxidase 1	66881	UUUAUUCCUUGAGAUAGGGtg AAACACGUCAAUCUUCACGtc CAGCUCUUUGACAAAUCGCtt
Pde3a	phosphodiesterase 3A, cGMP inhibited	54611	UAGCUUUUACAUGGUUAGCtg ACAUGAAGAGAUUCCAGGCtg UUAUGAUAAGGAAUGUCCCtg
Pdia6	protein disulfide isomerase associated 6	71853	GACACUAUGUCAGAUCUCGtc CUAGAAGAAUACAGACCGCtg UCCAAUUCACUGCUACAAUtc
Pecam1	platelet/endothelial cell adhesion molecule 1	18613	GAUAAUUUCUGUAAACUCCtg CUCAAUCGUGGUUUUUUCCtt CUUAUAGAACAGCACCCGGtg
Pex14	peroxisomal biogenesis factor 14	56273	UCCGAUUCAAAAGAAGUCCtt GAUGACGUAGACUCGUUGCtg UUCUUAAGAAAUGCUCUCCtg
Pgrmc1	progesterone receptor membrane component 1	53328	UUUGGUCACGUCGAACACCtt AUUACAAGAGUUUGAAACCtc GAAAUACCCAAGUUUUCCCtc
Pgrmc2	progesterone receptor membrane component 2	70804	GUUCAAAUCUGAGAGGUCGtc CAGGGUGCUUAGCUUUACGtc UUCAUCUCUAAGUGCAUCCtt
Plec1	plectin 1	18810	CUUCAACUGCACAAUAGCCtt AGUGAGAUGGUCUGUUCCGtg CUGGUGGUCAAUGAGACCCtt
Plp1	proteolipid protein (myelin) 1	18823	AUGAAACUAAUCAAGAUCGtc UUCUUUCUUUCUUUCACCCtt GAAAUAGGUCUCAAUUAGCtt
Plvap	plasmalemma vesicle associated protein	84094	UUGCUGCAUGACUGUUUCCtt GAUCCUUUUCUUGAAUUCCtc CUGUUUGCUCAGGUUAGCCtg
Podxl	podocalyxin-like	27205	AAAAGGAAAAUUAAGGCCCtg UGUUUUAGUCUUGUCCACCtc GGCAUAGAUGGAGAUUGGGtt
Pom121	nuclear pore membrane protein 121	107939	CAUACAAUUCAAUUCUUCCtc UGUUCUUUUCUUCUUCUCCtt GCGCCUUCUCUUGUUUUCCtg
Por	P450 (cytochrome) oxidoreductase	18984	UGAUCUCCAGAUUCAUACCtg CAGCCAAUCAUAGAAGUCCtg GAAAACAGAACAAUGUCCGtt
Ppapdc3	phosphatidic acid phosphatase type 2 domain containing 3	227721	CUUGUUCUUGUCUGUUGCCtt CCCAGAUUCAAUAGGUUCCtg AGAUUCAAUAGGUUCCUGGtg
Ppib	peptidylprolyl isomerase B	19035	UGUUUUUGUAGCCAAAUCCtt GACUGUGACUUUAGGUCCCtt UUGUGACUGGCUACCUUCGtc
Ppp1r12a	protein phosphatase 1, regulatory (inhibitor) subunit 12A	17931	UUCUAUGGUAAGUGGAUCCtt UUCUUUCUAGAGCUCUUCGtt CAUCUGCUACAUCAAAGGCtg
Ppp1r12b	protein phosphatase 1, regulatory (inhibitor) subunit 12B	329251	ACAUCUUCUAUUCUUCCGCtg UCACAAUACCCACACUGGCtc GUAACACCUUGAGUAGACCtt
Prkcz	protein kinase C, zeta	18762	CACUUCCUCACAGAGGUCCtt AUUACACGCUAACUUUUCCtg UUUUAAGACGUGUGAGGCCtt
Ptk7	PTK7 protein tyrosine kinase 7	71461	UGAUAAAGACGAUAGCGGCtt UCAUAUAAGUGUCAAAAGCtc CUGGAAAGCACCAGAAUCCtg
Ptplad1	protein tyrosine phosphatase-like A domain containing 1	57874	ACUGUGAUGUUCACCUGCCtc UGUGAUGCUGAUAGCAGGGtt UUCCCAGGUUCUGAUUUCGtt
Ptpru	protein tyrosine phosphatase, receptor type, U	19273	GUCUAAGCCUAUGUAGCCCtt GAAAUAGAUGAGAUAGGCCtt GAUGAAGAUAUAUUGUUCCtc

Ptrh2	peptidyl-tRNA hydrolase 2	217057	ACUUACGGUCUUACUUUCCtt CUUACAGUCAGUCCCAAGGtt GUUUAUGAAUUAGAACAGCtg
Ramp2	receptor (calcitonin) activity modifying protein 2	54409	CGUAGUCUUCCAUCUUCCCtt UUUUGACACAAGGCUGUCCtc AAAGUGUAUCAGGUGAGCCtc
Rdx	radixin	19684	AACUGUUUUUACAACCUGGtc CUAUCUCAUAUUAUACACCtc CUUCAGGAAAGAAUUUAGCtc
Reep5	receptor accessory protein 5	13476	GUUAUUGGAAGCUCAGACCtc AACUUUGGUAGACAACUCCtt UAUAUAAUCAUACACUGCGtg
Rilp	Rab interacting lysosomal protein	280408	AUAGCUAGUACAGGCGAGGtt CUCCUUGAGCAAGAACACGtt AGCAGAGCUCAGAGAUCCCtt
Rock1	Rho-associated coiled-coil containing protein kinase 1	19877	ACAUCGUACCAUACCUUCCtt ACAAAUGAGAUUUUUUGCCtc UUGGAAUGCAUAAAAAAGCtg
Rock2	Rho-associated coiled-coil containing protein kinase 2	19878	AUUUCUUCCAAGUCGUACCtc AUAAACCUUCUGUGAUGCCtt AAGCUUCAUUGCAUAAACCtt
Rpn1	ribophorin I	103963	AAAAUCUCCCACUUUUCCCtt UUCUAGGUUGUUGUCUUCCtc GGGAGAGUAGAAAUAAUGGtt
Rpn2	ribophorin II	20014	GAGUCAAAUUCAAUCUUCCtt GUAAACAUGUAAGCACAGCtc UUUCUUGACAUCUGGCACCtg
Rrbp1	ribosome binding protein 1	81910	CCUUCUUUUUCUUCUCUCCtt GUGAGUUUUCGCCAUCUCCtt UCCUUCUAUUUUUUUUGUCCtg
Rtn2	reticulon 2 (Z-band associated protein)	20167	GUCCUUCCAGUACAACAGGtc CCUCUCAUUCGGCUUUGGCtt AUACUGGUCAAUCUGGGCCtg
Rtn4	reticulon 4	68585	AUAUUUCUGAACCAAUUCCtc GAUAGCUUGGAUCACACCCtt UCAGAUUCCAAAUAUGCCCtg
Ryr2	ryanodine receptor 2, cardiac	20191	UUUCCACAUCCACCUGCCCtt AAAGUCUGUUGCCAAAUCCtt CUUUGAUUUUCUUAGCACCtt
Scara5	scavenger receptor class A, member 5 (putative)	71145	AUUAAGGGUUUCUACUUGCtg UUUGUGACAUGGACCAUCCtc UUGGCAAGGGUGAUGUUCCtc
Sccpdh	saccharopine dehydrogenase (putative)	109232	AUAUCAAAUACAGACGCGGtt UUCAGCUCUCUACAAUAGCtg CCAUUUCAUCAAGUGAGGCtg
Scn10a	sodium channel, voltage-gated, type X, alpha	20264	UUCAAGUCCAACUGAGGCCtg CAGUAAAGCGAUAAAAAGGtt AUUCAUUAAGACAAAACCCtc
Sec22b	SEC22 vesicle trafficking protein homolog B (S. cerevisiae)	20333	AAUCCAAUGCUGAGAGUGCtt UCGAAAGAGUUGCUUAGCCtg AGUGAAAAGUCAUGGCUCCtg
Sec61b	Sec61 beta subunit	66212	AGCCCAAUCUAUGAUCGCGtg UGGGUUUUUUUCCUUCUUCtt CCACAGCUGGCAUUUUUUCtc
Sec63	SEC63-like (S. cerevisiae)	140740	UGUACGUAUUAGAAUCUGGtc UGUAGGAAUAAAUAUUUGGCtg AAUUUGCUCCGCGUUCUGGtc
Sf3b1	splicing factor 3b, subunit 1	81898	AAUCUUUGGAGGACGAUGCtc AAUAUAGGUGUUCUUAUCGtc UUUCUUGGUCAUAAUAACCtg
Sftpc	surfactant associated protein C	20389	UGAUGUAGCAGUAGGUUCCtg GAGUUUUCUAGCGAAAGCCtc GCUUGUCUGACAAAGACCCtt
Sfxn1	sideroflexin 1	14057	UACAAAAGCAUUAAGAGGCtg UAGUCAUGCACCACUUUCCtc GGAUAUUUAGUCUUAGACCtt
Sfxn5	sideroflexin 5	94282	AAGCCAAUUCCCAAAAACCtt AGCUCACACGAAAUUGUGCtg AUGAUGUCCAAGAAGUGCCtg
Sgcb	sarcoglycan, beta (dystrophin-associated glycoprotein)	24051	CUUAUAUAUGGAAAGCUCCtt AAACACAUUUGGAAUCAGGtt UGCUCUUUGUUAACAUUCCtc
Sgcg	sarcoglycan, gamma (dystrophin-associated glycoprotein)	24053	AGUGUUCAAAAAGAGCUCCtt AUAAAAAUUCCGACUCUCCtt GUGUUUUAGCAAUGAGCCCtc

Sirpa	signal-regulatory protein alpha	19261	GUUGAUGUCAUUUGUGUCCtg UUUGGCGAGUACAUAGACCtc AUGGAGUUUAGUACCACCCtg
Slc12a1	solute carrier family 12, member 1	20495	UCCUUUGAAGAUGUUGUCCtt AAAAUUGUCAUAGCACUCCtg CCAUCUCCAUUAGCAACCCtg
Slc12a2	solute carrier family 12, member 2	20496	AGCCAAACUUUACAACUCCtt CAUCUAUAGUAUUCUUCCCtt UUAAAUAGUACGCUCCUCCtc
Slc1a2	solute carrier family 1 (glial high affinity glutamate transporter), member 2	20511	ACAUUUUUCUGACCCUUCCtt GACGAAUCUGGUCACACGCtt AACUGAUUGGUCCUUUUGGtg
Slc1a3	solute carrier family 1 (glial high affinity glutamate transporter), member 3	20512	GAACGAAAAGUACUUCACCtc UAAUUUGAUGCGAUUAAGGtc GUAACUCUUAACAUCUUCCtt
Slc25a22	solute carrier family 25 (mitochondrial carrier, glutamate), member 22	68267	GUCUGAAGAAGUCAUUAGCtg CUUCACCACAUCACAAGGGtt AAGUGUCCUCAUUAACACCtc
Slc25a3	solute carrier family 25 (mitochondrial carrier, phosphate carrier), member 3	18674	GUAUGUUGCUAUAUAAGGCtt UGUAGAACGCAUUUAAGCCtt CCACAGGUAGGUGUUUUCCtc
Slc25a4	solute carrier family 25 (mitochondrial carrier, adenine nucleotide translocator), member 4	11739	UCAUCUUUUGCAAUCUUCCtc UCUGUAGAUGAUGAUGCCCtg UCCGACUUGAAGAUCUUGGtg
Slc25a42	solute carrier family 25, member 42	73095	CAUCCUUGCUCUAACCAGGtc UCUACAUGGUGCAACCUGCtg AAUCAACACCCAGAUCACCtc
Slc25a5	solute carrier family 25 (mitochondrial carrier, adenine nucleotide translocator), member 5	11740	CACGCAGUCUAUGAUGCCCtt GUACUGACACAUUAAAGCCtt UGUACAUGAUAUCAGUUCCtt
Slc27a2	solute carrier family 27 (fatty acid transporter), member 2	26458	UCAAUGGUAUCUUGUAUCCtc AGGCGAUGAUGAUUGAUGGtt UACUUGAUCAGCUCAUACCtt
Slc38a3	solute carrier family 38, member 3	76257	ACUCUUCUGAAGGAAGCCCtt AUGGAGGUCAUCCUAAUGGtt CUAAUGGUUUCCUCCAUGCtg
Slc39a14	solute carrier family 39 (zinc transporter), member 14	213053	AGGGUUGAAGCCAAAAGCCtc CUCUGUCUGUUCAUUCUCCtc UGACAUCCAAUCUAGUACCtt
Slc4a1	solute carrier family 4 (anion exchanger), member 1	20533	CCAGAAAAUCCAGUGUACCtt CUGGUCCAUCAUCAGUUCCtg UGAUCAUCUUCCGUUCUGGtt
Smpd4	sphingomyelin phosphodiesterase 4	77626	UUCCUUGGCUGGAAAAUCCtc AUUCUCUUGAAUGGAUGCCtt CCACAUUUCCACAAAAACCtg
Spag4	sperm associated antigen 4	245865	AACUAUUCCACAGUAUGCGtg UAACACCAUGCUCAGCACCtg GAACUAUUGCUGUUCUCGCtg
Spag4l	sperm associated antigen 4-like	76407	GCCAUUCUGCUGAUAUAGCtt UGUCGUGGUUAUACGUGGCtg GAUUGUCUUAGGAAUGUGCtg
Ssr1	signal sequence receptor, alpha	107513	CUAGUGAUUCCAAAAUUCCtt UACUGAAAUUACCACUUCCtt GAUGUAAAACUGGUAGUCCtg
Stx1b2	syntaxin 1B2	56216	GUGCUGUUUCUUCACUUGCtc CUUCACUUGCUCCACAUCCtc ACUCAUCCAUAAAGUGGUCtc
Stx5a	syntaxin 5A	56389	GUUGAGGCUAUUGAUAUCCtg UUUGAUGAUGUAUGUUAGCtc GCUUAUAAAAAUCUCAAGGtg
Sunc1	Sad1 and UNC84 domain containing 1	194974	CAAAUGUUUGAAUGGUUGCtt CAGCUUCAAUGACAGAGGCtc AACUUUCUGAGGUCCCAGCtt
Syne1	synaptic nuclear envelope 1 NM_153399	64009	CAGUUAGCUCAUCACAGGCtt ACUCAUGAAUUUCAUCACGtt GAUUUUCUUCAAACAUGCCtt
Syne1	synaptic nuclear envelope 1 NM_022027	64009	UUGAUAAGCUCUAGUUGGGtc GACAAAUCCUGCUGACUGCtt CUAAUGAAGUGCUUGAGCCtg
Syne2	synaptic nuclear envelope 2	319565	GGUUUUCUUCUGAGUGUCCtc UUUCUUCUGAGUGUCCUCCtg UACAGUAGGUCUCACUUGCtg
Syt1	synaptotagmin I	20979	GAGAACAUUUAAAAACUCCtc AUACUGGUAUAUACAACGGtg CUUGGAAAAGGCAUCUUCCtt

Tapbp	TAP binding protein	21356	AAAUGCCGUAGCCUUUUCCtg CAACCUUUCUAGAACUUCCtc AUAGUGAACUCCAUGCUGCtt
Thbd	thrombomodulin	21824	AUGUACAAAUAUGCUGAGCtt GCACUGUCAUCAAAUGUCCtt ACAUACAGGAGUAAGAGCCtg
Tm7sf2	transmembrane 7 superfamily member 2	73166	GAAGCCAUUAAUCAGAUGGtt AGUCAUACAUGGAAUUUCCtg AUAAAGCUGGUGAGAGUGGtc
Tm9sf1	transmembrane 9 superfamily member 1	74140	CUCAAAGUAAUACAAUUCCtc UAUUCUUUGUGCGACAAGGtg AUAGUAGUGGUAAGUUUCCtg
Tm9sf2	transmembrane 9 superfamily member 2	68059	CUUUUGUUUGUCUUCAGCCtt AUCCACAAUCCAGUGAUGCtg UAAACGUAAACUUAUACGGtg
Tmc8	transmembrane channel-like 8	217356	AUCCAGGACAGAAGGAUCGtg UUCAUUGCUGAUUUCGUGCtt AAUCUCGUAGAGAGCUCCCtc
Tmed10	transmembrane emp24-like trafficking protein 10 (yeast)	68581	AAUGGACUCGGAAAGGUCCtc GUCUAGAAUCACGAGUUGGtc UACUGUUAGUAGAAUGGCCtt
Tmem14c	transmembrane protein 14C	66154	CAACCAUCAGCAAACUGGCtc CAUAAUUUCAUAGCAGACCtg AGGAAAACCCACACAUUCCtg
Tmem173	transmembrane protein 173	72512	AGCUGAUUGAACAUUCGGAtc GGCUGAUCCAUACCACUGAtg AGGAUGUACAGUCUUCGGCtc
Tmem20	transmembrane protein 20	240660	UCAUUAUCGCUACGAGUCCtg GUAAUCAUCUCUAAGAUCCtt AACCAAAUAUAAAUGGUGGtc
Tmem35	transmembrane protein 35	67564	AUACAAGGAUGGUUGCUCCtc UUAGUUCAAGAUCAGAGCCtc GACUGUGUCUAGUAAAAGGtt
Tmem43	transmembrane protein 43	74122	UUAUGUGUACCAGUCUUCCtt CUUUGUCUCCUUCUUCACCtg GGAAUAUGGGAUUAGUUGGtc
Tmem48	transmembrane protein 48	72787	AAAAGAUUCAAACACUCCCtc UUUGAACUCCAAGAAUUGCtg UGCUUAAGACUAUAAAGGCtg
Tmem53	transmembrane protein 53	68777	UAUAGUAAGUAGGAUAGUCtc CAAGAGAAUCACCACAGGCtg ACCAUACGUUCCACAUCCCtg
Tmem74	transmembrane protein 74	239408	AUGAGACCAUUCAUUAGGGtt AAAAGAAGUUUCUAGUUCCtg GCGAUCAGCCAUUACUUGGtt
Tmpo	thymopoietin	21917	UGUGUUCUUUCUUCUUUCCtt UCAUCUUUAUCUUCUAGCCtg UGGUUUGUACUUUCUUAGCtg
Tmtc3	transmembrane and tetratricopeptide repeat containing 3	237500	ACAUCGGCAAGGUGUACCCtt UCUUCAGAGCUUCAUUUGGtt GAUUGAAAAACGAUAGUGCtc
Tnk2	tyrosine kinase, non-receptor, 2	51789	CUCAAAGUCAUCCUCAUCCtg UUGGUGUUUACGUAGGCGGtc GGUACAAAGGCGUAAUUGGtc
Tor1aip1	torsin A interacting protein 1	208263	UUCAUUCAUCACUGAAGCCtc CACUUUCUCUUCAAUUUCCtt GCAUAAGUUGCUUAUAGGGtc
Tor1aip2	torsin A interacting protein 2	240832	UUUAAGAUCAGAUGUGGGCtg GACUUUCUGACCUGUCACCtg AGUCUUUCUCAAUGUAUCCtg
Tpm2	tropomyosin 2, beta	22004	GGUAACAAUUUUCAGCUCCtc UUAUCAGAAAGUGACAGGCtg AUACUUUUCCACCUCGUCCtc
Trip10	thyroid hormone receptor interactor 10	106628	ACAAAUAUGUACAACCACGtg UGCGAAGUCAUUGACCUCCtg GUGUAAUUCGAUGAGGACCtg
Trpm1	transient receptor potential cation channel, subfamily M, member 1	17364	UUUUCCAAUCAGGUCUUCCtt UGGCAGCCUUGAUCAGACCtt CAGACCUUUCCCAAACACCtg
Tsnax	translin-associated factor X	53424	CAAAGUGAACUAAAGUAGGtg UGGAGAAGAAAAAUUGUCCtc GAGUCUCUCAUAUUUGUCGtg
Txndc10	thioredoxin domain containing 10	67988	AUUGAUACAAUGAUCUGGCtt AAAAUCUCUAUGGAAGUGGtc AACUGCUAUGGCCACAAGCtt

Tyro3	TYRO3 protein tyrosine kinase 3	22174	ACCAGUAAAUGGUUACGGGtt CAUGAGAUCAUACACUUCCtc CUGAGAAAUCUUGGUUUCCtc
Ugt1a2	UDP glucuronosyltransferase 1 family, polypeptide A2	22236	AAGGCAUAGGUUUUGAGGGtg AAAACUGGAAUUCAGUUGCtg ACAAGAAUUUGAGUAGAGGtc
Ugt1a6a	UDP glucuronosyltransferase 1 family, polypeptide A6A	94284	UCCACGACAAUCAUGUUGUtc ACGACAAUCAUGUUGUUCCtg AAGUGGUUGUUUCCAAAGGtg
Ugt2b5	UDP glucuronosyltransferase 2 family, polypeptide B5	22238	GAGGCUGAAAGUUUGUUCAtg ACACUAAGGACUAUAGUGGtt AAGUCAAGUGUUUAGAAGGtg
Ugt3a2	UDP glycosyltransferases 3 family, polypeptide A2	223337	AUCAGCAAAUUUCUUUUCCtg AAAUGCUCCUGGAUAGUGCtg UACUGAGAAAGGAUUUCCCtt
Unc50	unc-50 homolog (C. elegans)	67387	UGCCGAAAUCGAAAGAGCCtt GACAGUUUCUCUAGGAUGCtc AUUUACAAGAACUCAUCCCtt
Unc84a	unc-84 homolog A (C. elegans)	77053	GUUGAUACUAAAAGCUGGCtt AAGCUCUGGAUUCAUAGCCtt CUUCUCUGUUUGACUGUCCtg
Unc84b	unc-84 homolog B (C. elegans)	223697	GGACUGUCUUUAAACACGGtg UUCCGAGUCUUGGUGAUGCtc GCCGUUGAAUCUAAAAGCCtc
Vamp2	vesicle-associated membrane protein 2	22318	GAAAGUUUUCAGUCGAACCtc AAGAUAAGGGAAAGAUCGGtt AAAAAGAUUAGAUCCUUCCtc
Vapa	vesicle-associated membrane protein, associated protein A	30960	AGGUUCCAUAUCAUUCAGCtt GUGGAACAGCUUUGCUAGGtt UUUAUCCGAAUGUGCUACCtt
Vapb	vesicle-associated membrane protein, associated protein B and C	56491	CCGAAGUCCGUCUUCUUCCtt UGGGUUGCCAAGCUUUAGGtt UUUAAAACACACAUUUCGGtc
Vil2	villin 2	22350	CAGUGACAAUGAAUCUUGCtt GCCAAUCGUCUUUACCACCtg UACAGAACAAAACUUUCCCtt
Wasl	Wiskott-Aldrich syndrome-like (human)	73178	UACUCAGAGUGGAUUAGCCtt AGGUUAUGUGAUAAACUGGtt UCUUUGCUAAAAAAUAGCCtg
Ywhae	tyrosine 3-monooxygenase/tryptophan 5-monooxygenase activation protein, epsilon polypeptide	22627	UCUUUAAUUUGUCCUCUCCtc UAAUUUGUCCUCUCCUCCCtt ACAACAGAUUAACUUGAGCtc
Zcd1	zinc finger, CDGSH-type domain 1	52637	GCACGAGGUUGGUUUAGCCtt AGGUGACAUCACAACACGCtg CUUCUUCUUUCAACAAACGtg
Zcd2	zinc finger, CDGSH-type domain 2	67006	CUUCUUUAUUUAGCCUACCtt AAGAUUGAUCAAGCUAUCCtt CUUCAAACCAAUCAUAACCtc

2.1.6 Antibodies

Primary antibodies used for immunofluorescent stainings or Western Blot analysis are listed in Table 2.9. Alexa fluorophore-conjugated secondary antibodies and streptavidin were bought from Life Technologies and 4',6-diamidino-2-phenylindole dihydrochloride (DAPI) from Molecular Probes (#D1306). Alexa fluorophore-conjugated secondary antibodies were diluted 1:200-1:500 in IF blocking buffer for immunofluorescent stainings (section 2.3.8). Prior to usage, diluted secondary antibodies were pre-cleared by centrifugation at 12000 × g for 3 min. Horse radish peroxidase-conjugated secondary antibodies (Santa Cruz) were diluted 1:10,000 in WB blocking buffer and used for Western Blot analysis (section 2.4.2).

Table 2.9: Primary antibodies.

Antigen	Host	Source	Cat.No/ Clone	IF	WB
Akap9	rabbit	Sigma-Aldrich	#HPA026109	1:100	
Cep152	rabbit	Sigma-Aldrich	#HPA039408	1:100	-
Cdk5rap2	rabbit	Bethyl Laboratories	#IHC-00063	1:500	-
c-Myc	mouse	Clontech	9E10	1:500	-
c-Myc	mouse	Thermo Fisher Scientific	#13-2500	-	1:2000
GAPDH	mouse	GeneTex	#GTX627408	-	1:2000
GM130	mouse	BD Transduction Laboratories™	#610823	1:500	-
Histone H3	rabbit	Sigma-Aldrich	#H0164	-	1:3000
MHC	mouse	DSHB	MF20	1:200	1:500
Myogenin	mouse	DSHB	F5D	1:200	-
Nesprin-1	mouse	A gift from Glenn E. Morris	MANNES1E	1:200	1:500
Nesprin-1	mouse	A gift from Brian Burke		SN	- 1:500
PCM1	rabbit	Bethyl Laboratories	#A301-149A	1:500	-
Pericentrin	mouse	BD Transduction Laboratories™	#611814	1:500	1:500
Pericentrin	rabbit	Covance	#PRB432C	1:500	-
Pericentrin	rabbit	A gift from Kunsoo Rhee		1:2000	-
Sun1	rabbit	Sigma-Aldrich	#AV49929	-	1:500
Sun1	mouse	A gift from Brian Burke	12F10	1:500	1:500
Sun2	rabbit	ImmuQuest	#IQ444	-	1:1000
Sun2	mouse	A gift from Brian Burke		1:500	1:500
γ-tubulin	mouse	Sigma-Aldrich	#T6557	1:100	1:500
Tubulin	rat	European Collection of Animal Cell Culture	#92092402, YL1/2	1:200	1:1000

DSHB - Developmental Studies Hybridoma Bank ; ECACC = European Collection of Animal Cell Cultures; MHC - myosin heavy chain; SN - undiluted hybridoma supernatant

2.2 Molecular biological methods

2.2.1 Transformation of chemically competent *E. coli*

Transformation of chemically competent *E. coli* (TOP10 strain) was performed using a heat shock protocol. Therefore, 50 μL of competent bacteria were thawed on ice and incubated with 1 μL of purified plasmid DNA for 30 min on ice. Heat shock was performed at 42°C for 40s. Bacteria were immediately placed on ice for 2 min and 250 μL of S.O.C. medium was subsequently added. After incubation for 1 hour at 37°C with agitation, 20-80 μL of bacteria solution were plated on LB-Agar plates containing antibiotics as a selection marker. LB-Agar plates were incubated overnight at 37°C. The next day, bacteria clones were picked and used to inoculate 3 mL of LB medium. Following incubation under constant shaking for 4-6 hours at 37°C, bacteria solution was diluted 1:1000 in 200 mL of fresh LB medium containing antibiotics for overnight propagation. For longterm storage, bacteria were mixed with 50% glycerol/ddH_2O in a 1:1 ratio and kept at -80°C.

2.2.2 Plasmid DNA isolation from *E. coli* cultures

To isolate ultrapure plasmid DNA from overnight cultures, the NucleoBond® Xtra Midi or Maxi kit from Machery-Nagel (Cat.No #740412, #740414) was used according to manufacturer's instructions. DNA concentration was measured using a spectrophotometer (DeNovix DS-11). Purified plasmid DNA was sequenced by GATC Biotech using commercial available company primers.

2.3 Cell biological methods

2.3.1 Mammalian cell lines

C2C12 cells: Mouse C2C12 myogenic precursor cells were purchased from ATCC (American Type Culture Collection, Manassas, Virginia). Originally, Yaffe and Saxel (1977) obtained C2 myoblasts from the thigh muscle of adult C3H donor mice after crush injury. Thereby, C2 lines were obtained after several and selective passaging of these isolated myoblasts. The C2C12 cell line is a subclone of the C2 myoblasts (Blau et al., 1983) that can be induced to differentiate into multinucleated myotubes upon serum withdrawal. Therefore, the C2C12 cell line is generally used to study myogenic differentiation processes.

Human immortalized myoblasts: Human myoblasts were obtained from a

healthy control or from a congenital muscular dystrophy patient carrying a homozygous nonsense mutation within the *SYNE1 gene (nucleotide 23560 G>T)*. Human myoblasts were immortalized by Kamel Mamchaoui and Vincent Mouly (Center for Research in Myology, Paris, France) by transduction with both telomerase-expressing and cyclin-dependent kinase 4-expressing vectors as described previously (Holt et al., 2016; Mamchaoui et al., 2011).

2.3.2 Cell Cultivation

C2C12 myogenic precursor cells or human immortalized myoblasts were cultivated in a humidified incubator at 37°C/5% CO_2 in their respective Growth Medium (Table 2.2). C2C12 cells and human immortalized myoblasts were only grown up to 70% confluency and passaged every two to three days to avoid induction of differentiation. For passaging, cells were washed twice in PBS and incubated with 0.05% Trypsin/EDTA at 37°C until cells started to detach. Trypsinization was stopped by adding Growth Medium and cells were seeded on new plastic dishes at dilutions of 1:10 to 1:20. To induce myogenic differentiation, cells were washed twice with their respective Differentiation Medium and incubated at 37°C/5% CO_2 for the indicated time points.

2.3.3 Transfection of DNA

Transfection using jetPrime®

For co-transfection of dsRed-PACT and GFP-Nesprin-1α or GFP, respectively, 8-well μ-slides (ibidi, #80826) were coated with sterile-filtered 0.1% gelatin/ddH_2O for 20 min at room temperature. One day prior to transfection, 9.000 C2C12 cells were seeded per well in 200 μL Growth Medium. When cells reached approximately 80% confluency, cell transfection was carried out using jetPrime® (Polyplus-transfection, #114-07) according to manufacturer's instructions. In brief, a total amount of 1 μg DNA was diluted in 50 μL jetPrime® buffer and mixed by vortexing vigorously for 10 s. 2 μL jetPrime® reagent were added, the mixture was vortexed again for 10 s and shortly spun down. After incubation for 10 min at room temperature, the transfection mix was added drop wise onto the cells which were kept in 200 μL freshly added Growth medium containing serum and antibiotics. The following day, the Growth Medium was replaced to circumvent toxic side effects of the transfection reagent.

For co-transfection of myc-PACT and GFP-Nesprin-1α or GFP, respectively, C2C12 cells were seeded on 10 cm dishes one day prior to transfection. When cells reached

approximately 80% confluency, transfection was performed using jetPrime® as described above. In total, 10 μg of DNA (5 μg GFP-Nesprin-1α or GFP + 5 μg myc-PACT) were diluted in 500 μL jetPrime® buffer and then mixed with 20 μL jetPrime® reagent.

Transfection using Lipofectamine® 2000

For live-cell imaging experiments, C2C12 cells were seeded in 2 mL Growth Medium on gelatinated FluoroDish cell culture dishes (World Precision Instruments, #FD35-100) at a density of approximately 80% confluency. 8 hours later, transfection of dsRed-PACT or EB1-GFP was performed using Lipofectamine® 2000 (Invitrogen, #11668-019) according to manufacturer's instructions. Therefore, 5 μL Lipofectamine® reagent were diluted in 100 μL Opti-MEM® (Gibco, # 31985062) and incubated for 5 min at room temperature. In parallel, 2.5 μg DNA were diluted in 100 μL Opti-MEM® and gently mixed by inverting the tube. The diluted transfection reagent was added to the diluted DNA, gently mixed by inverting the tube and incubated at room temperature for 20 min. 200 μL of the transfection mix were drop wise added onto the cells in 2 mL freshly replaced Growth Medium containing serum and antibiotics.

2.3.4 Transfection of siRNA

C2C12 cells were seeded just before transfection on gelatinated 96-well ibiTreat μ-plates (ibidi, #89626) (9.000 cells per well) in 200 μL Growth Medium without antibiotics. Transfection of siRNA was performed using Lipofectamine® RNAiMAX (Invitrogen, #13778-150). Therefore, 0.6 μL of Lipofectamine® RNAiMAX reagent were diluted in 20 μL Opti-MEM®, gently mixed by inverting the tube and incubated for 5 min at room temperature. In parallel, 1 μL siRNA of a stock concentration of 10 μM (10 pmol siRNA) were diluted in 20 μL Opti-MEM® and gently mixed by inverting the tube. The diluted Lipofectamine® RNAiMAX solution was added to the diluted siRNA, gently mixed by inverting the tube and incubated for 20 min at room temperature. Subsequently, the transfection mix was added to the cells (final concentration of siRNA: 42 nM) and incubated for 5 hours at 37°C/5% CO_2. After the incubation time, the medium was replaced by Growth Medium containing antibiotics.

For the siRNA screen, reverse transfection using Lipofectamine® RNAiMAX was performed. In contrast to the procedure described beforehand, gelatinated Falcon® 96-well Imaging plates (Corning, #353219) were used. Additionally, the transfection complex was prepared directly inside the plate by placing firstly 10 μL Opti-MEM®

and 1 μL siRNA mix of a stock concentration of 10 μM (10 pmol siRNA) into each well. Secondly, a master mix of Lipofectamine® RNAiMAX reagent and Opti-MEM® (0.3 μL reagent and 10 μL Opti-MEM® per well) was prepared, incubated for 5 min at room temperature and then added to each well using a multi-step pipette. The transfection mix was incubated inside the plate for 20 min at room temperature while C2C12 cells were trypsinized. 100 μL of cells diluted in Growth Medium without antibiotics (final concentration of siRNA: 83 nM), yielding a confluency of about 30%, were added to each well. After incubation for 5 hours at 37°C/5% CO_2, the medium was replaced by 200 μL fresh Growth Medium containing antibiotics.

2.3.5 Genereation of Nesprin-1-depleted C2C12 cells using CRISPR/ Cas9

Nesprin-1-depleted C2C12 cell lines were generated by Dr. Yin Loon Lee (Institute of Medical Biology, A*STAR, Singapore) using the CRISPR/Cas9 system. In brief, C2C12 cells were transfected overnight using Lipofectamine 3000 according to manufacturer's instructions with pX330 encoding Nesprin-1 N- and C-termini-directed sgRNAs (N-terminus: ACATCACCAATGTGATGCAG, C-terminus: CCGTTGGTATATCTGAGCAT) and pEGFP-N1 in a 9:9:2 ratio. Cells with high levels of EGFP expression, representing high levels of pX330 transfection, were sorted as single cells into 96-well plates at the Singapore Immunology Network FACS facility. Loss of Nesprin-1 NE localization in clonal lines was assessed by immunofluorescence microscopy.

2.3.6 Generation of pTripZ-mycBirA*-Nesprin-1α stable C2C12 cell lines

Dr. Alessandra Calvi (Institute of Medical Biology, A*STAR, Singapore) designed and created the pTripZ-mycBirA*-Nesprin-1α vector and generated C2C12 cells lines stably expressing mycBirA*-Nesprin-1α. In brief, mouse cDNA was obtained from mouse hindlimb skeletal muscle RNA using ThermoScript™ RT-PCR System for First-Strand cDNA Synthesis (Invitrogen, Carlsbad, CA, #11146-024) according to manufacturer's instructions. Nesprin-1α cDNA was obtained by PCR from mouse skeletal muscle cDNA and ligated into pcDNA3.1 with an EGFP tag using the following primers 5'-GCGCCTCGAGATGGTGGTGGCAGAGGACTTGC-3' and 5'-GCGCCTTAAGTCA-GAGTGGAGGAGGACCGTT-3'. pTripZ-mycBirA*-Nesprin-1α was obtained by PCR amplification of Nesprin-1α from pcDNA3.1 containing Nesprin-1α followed by restriction digestion and ligation (Chojnowski

et al., 2015). Subsequently, C2C12 cells were transduced with lentivirus expressing myc-BirA*-Nesprin-1α and stable integration of the transgene was selected for using 0.67 μg/mL puromycin.

2.3.7 Mouse strains and primary myoblasts

The Sun1$^{-/-}$ and Sun2$^{-/-}$ mice that were previously described by Chi et al. (2009) were maintained by our collaborators Dr. Yin Loon Lee and Prof. Dr. Brian Burke at the A*STAR Biological Resource Centre facility in accordance with the guidelines of the Institutional Animal Care and Use Committee. Primary myoblasts were obtained essentially as previously described (Solovei et al., 2013) from E18.5 mouse embryos, and maintained in Ham's F10 (Gibco) containing 20% fetal bovine serum and 10 μg/ml bFGF (Invitrogen, Carlsbad, CA, #13256029).

2.3.8 Immunofluorescence (IF)

For immunofluorescent stainings, C2C12 cells were seeded on gelatinated 96-well ibiTreat μ-plates (ibidi, #89626) and human immortalized myoblasts on cover slips coated with Matrigel (Corning Life Sciences, #354230) diluted 1:100 in DMEM. After differentiation for the indicated time points, cells were fixed in 4% paraformaldehyde (PFA) for 15 min at room temperature or in icecold methanol for 20 min at -20°C. Cells were then washed three times in PBS. PFA-fixed cells were permeabilized with 0.5% Triton X-100/PBS for 5 min at room temperature and then washed again three times with PBS. Subsequently, cells were incubated in 10% goat serum for 30 min at room temperature and incubated with primary antibodies (Table 2.9) diluted in blocking buffer over night at 4°C. The next day, cells were washed three times in PBS and then incubated with fluorophore-conjugated secondary antibodies and DAPI (1:10,000) in blocking buffer for 1 hour at room temperature. After three washes in PBS, cells were mounted in Fluoromount-G (Southern Biotech, #0100-01) or Vectashield (Vector Laboratories, #H-1000).

2.3.9 Microtubule regrowth assay

C2C12 cells or human immortalized myoblasts were differentiated in their respective Differentiation Medium (Table 2.2) for 48 hours. Subsequently, cells were treated with 5 μg/mL nocodazole (Sigma-Aldrich, #M1404) in Differentiation Medium for 2 hours. After a quick wash with Differentiation medium, cells were incubated in fresh, pre-heated Differentiation Medium for 4 to 6 min (human immortalized cells) or 5 min (C2C12 cells) at 37°C/5% CO_2. Cells were immediately incubated with

pre-extraction buffer for 30 s, fixed with 4% PFA and stained as indicated following the IF protocol (2.3.8). MT regrowth was quantified by counting the number of Myogenin-positive nuclei that showed at least 50% of MT seeds at the NE.

2.4 Biochemical methods

2.4.1 Preparation of cell lysates

To prepare total protein extracts from C2C12 cells grown on 6-well plastic dishes, cells were washed once with PBS to remove dead cells and debris. Subsequently, cells were lysed in 200 μL 1% SDS/PBS per well and plates were rotated until cells started to detach. Plates were quickly frozen at -20°C and then thawed again under gentle rotation. Cells were harvested using a cell scraper and lysates were loaded onto a QIAshredder-homogenizer (Qiagen, #79656). After centrifugation at full speed for 1 min, the homogenized lysate was collected into a tube and total protein concentration was measured as described in section 2.4.1.
For preparation of cell lysates used in immunoprecipitation assays see section 2.4.3.

Bicinchoninic acid (BCA) assay

For measuring the total protein concentration of cell lysates, the Pierce BCA Protein Assay Kit (Thermo Fisher Scientific, #23225) was used according to manufacturer's instructions. In brief, 10 μL of each sample were diluted with 40 μL ddH_2O (1:5 dilution) and 1 mL BCA reagent (50:1 ratio of Reagent A and Reagent B) was added. The mixtures were incubated for 30 min at 37°C and the absorbance of 2 μL was measured at 562 nm using a spectrophotometer (DeNovix DS-11). BCA reagent mixed with 50 μL ddH_2O was used as a Blank standard to correct the 562 nm measurements of all samples. Finally, the protein concentration was determined using a Blank-corrected Bovine Serum Albumin (BSA) standard curve ranging from 0, 25, 125, 250, 500, 750, 1000, to 1500 μg/mL.

2.4.2 SDS-PAGE and Western Blot

To separate total protein extracts from cell lysates (section 2.4.1), 30 to 50 μg of each sample were mixed with 4x Laemmli sample buffer (Bio-Rad, #1610747) containing 10% freshly added β-mercaptoethanol and heated for 5 min at 95°C.
For analysis of proteins with molecular weights up to approximately 120 kDa, samples were loaded onto 4-15% Mini-PROTEAN TGX protein gels (Bio-Rad, #4561084) together with the Novex sharp pre-stained protein standard. Sodium dodecysulfate

polyacrylamide gel electrophoresis (SDS-PAGE) was run in 1x TGS buffer at 120 V to 140 V using the Bio-Rad Mini Protean Tetra Cell electrophoresis chamber. Subsequently, proteins were transferred onto a nitrocellulose membrane (TransBlot® Turbo™ Mini Nitrocellulose Transfer Packs (BioRad, #1704158) using the protocol for mixed molecular weight proteins of the Bio-Rad TransBlot®Turbo™ blotting system.

For analysis of proteins with high molecular weight (e.g. centrosomal proteins such as Pericentrin), samples were loaded on 4-12% NuPAGE™ Bis-Tris protein gels (Invitrogen, #NP0335) together with the HiMark pre-stained protein standard. SDS-PAGE was run in 1x NuPAGE®MOPS SDS running buffer at 140 V using the XCell SureLock™ Mini-Cell electrophoresis system (Novex, Life Technologies). Proteins were transferred at 4°C overnight (approximately 16 hours) at 30 V in WB Transfer buffer using the Bio-Rad Wet/Tank Blotting system.

After protein transfer, membranes were placed in ddH_2O and then stained with Ponceau S to confirm equal protein loading and successful transfer. Membranes were then destained using TBS-Tween, blocked in blocking solution for 1 h at room temperature under constant shaking and incubated with primary antibodies overnight at 4°C. The following day, membranes were washed three times with TBS-Tween for 5 min under constant shaking and incubated for 1 h at room temperature with horseradish peroxidase-(HRP)-conjugated secondary antibodies diluted 1:10,000 in blocking solution. Membranes were again washed three times with TBS-Tween for 5 min under constant shaking and incubated for 5 min at room temperature with SuperSignal™ West Pico PLUS Chemiluminescence substrate (Thermo Fisher Scientific, #34080) or Luminata Classico Western HRP Substrate (Millipore, #WBLUC0100), respectively, to detect highly abundant proteins (e.g. GAPDH). To detect low abundant proteins (e.g. Pericentrin), membranes were incubated for 5 min at room temperature with Luminata Forte Western HRP Substrate (Millipore, #WBLUF0100). Chemiluminescence signals were detected using films (GE Healthcare, #10094984) or the VWR®Imager CHEMI Premium. Images were processed using Fiji and arranged using Adobe Illustrator CS5.

Western Blot stripping was rarely performed when proteins of similar sizes needed to be detected. To this end, membranes were incubated with Roti®-Free Stripping Buffer (Carl Roth, #0083) for 30 min at 56°C under agitation. Membranes were subsequently washed three times with TBS-Tween, re-blocked and incubated with primary and secondary antibodies prior to Western Blot detection as decribed above.

2.4.3 Immunoprecipitation (IP) using GFP-Trap® beads

C2C12 cells expressing myc-PACT and GFP-Nesprin-1α or myc-PACT and GFP, respectively, were differentiated for two days in Differentiation Medium. Cells were then washed once with PBS, trypsinized and collected into tubes. After centrifugation for 5 min at 400× g at 4°C, the cell pellet was washed twice with 10 mL of icecold PBS and subsequently resuspended in IP Lysis Buffer. Following incubation for 30 min on ice, cell lysates were centrifuged for 15 min at 15.000× g at 4°C. The supernatant was transferred to a new tube and the protein concentration was determined (section 2.4.1). For each sample, 25 μL of GFP-Trap®_A beads (ChromoTek, #gta-20) were transferred into icecold IP Wash Buffer. Beads were washed twice with IP Wash Buffer after centrifugation for 2 min at 2.500× g at 4°C. 1500 μg of cell lysate were diluted 1:1 in IP WASH buffer and some lysate was saved for Western Blot analysis (input). Diluted cell lysates were added to the equilibrated beads and incubated under rotation for 2 hours at 4°C. Beads were then centrifuged for 2 min at 2.500× g at 4°C and resuspended in icecold IP Wash Buffer. This washing step was repeated twice before beads were resuspended in 50 μL 2x Laemmli buffer. Subsequently, samples were heated for 10 min at 95°C. Beads were removed from all samples by centrifugation for 2 min at 2.500× g at room temperature. All supernatants and input samples were then analyzed by SDS-PAGE and Western Blot analysis (section 2.4.2).

2.4.4 Proximity-dependent biotin identification method (BioID)

This experiment was carried out in collaboration with Dr. Yin Loon Lee of Prof. Dr. Brian Burke's laboratory at the Institute of Medical Biology, A*STAR in Singapore. Thereby, I performed the first experiment with Dr. Yin Loon Lee together, while the experiment was additionally repeated two times by Dr. Yin Loon Lee alone.

Stably transduced cells were expanded in 5-layer flasks and directly harvested after cells reached 90-100% confluency (myoblast samples) or switched to Differentiation Medium for 4 days (myotube samples). Before harvesting, both myoblast and myotubes samples were incubated with 50 μM biotin and 1 μg/mL doxycycline for 1-2 days. In parallel, control myoblast and myotube samples were incubated without biotin and doxycycline, or solely with 50 μM biotin.
For harvesting, cells were washed twice with PBS and then incubated at 37°C with 10 mL 0.05% Trypsin/EDTA per multi-layer flask. Trypsinization was stopped by adding Growth Medium or Differentiation Medium, respectively, and multi-layer

flasks were washed with PBS to collect all cells for each condition in one Falcon tube. Cells were spun down at room temperature at 1200 rpm for 5 min and the supernatant was removed. Cell pellets were resuspended in 20 mL PBS and the centrifugation step was repeated twice. After the final centrifugation, cells were resuspended in 1 mL PBS and transferred to a new Eppendorf tube. Cells were again spun down at room temperature at 1200 rpm for 5 min and the remaining PBS was completely removed. Cells were shock frozen in liquid nitrogen and kept at -80°C until all conditions were collected.
For cell lysis, cell pellets were thawed and 1-2 mL Kyle lysis buffer were added. Samples were sonicated (1 min, 10 s PULSE on, 20 s PULSE off) and then centrifuged for 20 min at 16.000× g at 4°C. Subsequently, the supernatant was transferred to a clean Eppendorf tube and some lysate was saved as 'input' for Western Blot analysis.
For affinity capture of biotinylated proteins, each supernatant was incubated with 100 μL Dynabeads (MyOne Steptavadin C1; Invitrogen, # 65001) for 2 hours at room temperature under rotation. Beads were washed twice with 1 mL of Buffer A and then with 1 mL of Buffer B under rotation for 5 to 10 min. 100 μL of each sample was transferred into a new tube and saved for Western Blot analysis. Beads were then collected on a magnet and the remaining Buffer B was thoroughly removed. After further centrifugation at 6000× g for 2 min, dried beads were frozen until in-solution digestion was performed (see section 2.4.5).

2.4.5 Mass spectrometry and data processing

All samples of the BioID experiment were analyzed by mass spectrometry and further processed with the help of Dr. Radoslaw M. Sobota at the Institute of Molecular and Cell Biology, A*STAR in Singapore.

Mass spectrometry samples were in-solution digested. After streptavidin affinity purification, beads were denatured using 50% TFE in 100 mM TEAB. Proteins were reduced in 25 mM TCEP and alkylated with 55 mM CAA. Prior digestion, samples were further diluted with 100 mM TEAB to achieve TFE final concentration below 5%. Digestion with LysC (Wako) for 4 hours (1:100 enzyme/protein ratio) and Trypsin (Promega) for 18 hours (1:100) was performed. Following acidification with 1% TFA, samples were desalted with Sep-Pak C-18 cartridges (Waters). Samples were labelled with TMT 6plex isobaric labelling (Thermo) according to manufacturer's instructions. Samples were desalted on C18 Basic Resins 10 μm (Dr. Maisch) and eluted using a step gradient (4 fractions) containing 17.5%; 25%; 30%; 50%

acetonitrile further optimised to (3 fractions) 15%, 22%, 50% acetonitrile in 7.5% ammonium hydroxide. Each fraction was vacuum centrifuged and submitted for analysis. An Orbitrap Fusion (Thermo) mass spectrometer coupled to nanoUPLC Easy LC 1000 system (Thermo) was used for analysis. Samples were injected and separated in EasySpray column 50 cm x 75 μm (C18, 1.8 μm) in a 120 min gradient (Solvent A: 0.1% Formic Acid; Solvent B: 0.1% Formic acid / 99.9% Acetonitrile) in data dependent mode using Orbitrap analyzer (speed mode -3 sec cycle) with ion targets and resolution (OT-MS 4xE5, resolution 60K, OT-MS/MS 1E5, resolution 15k). Peak lists were generated with Proteome Discoverer 2.1 software (Thermo) and searches were done with Mascot 2.5.1 (Matrix Science) against concatenated forward/decoy Mouse Uniprot with BirA sequences database (109799 entries) with the following parameters: precursor mass tolerance (MS) 30 ppm, OT-MS/MS 0.06 Da, 3 missed cleavages; static modifications: Carboamidomethyl (C); variable modifications: Oxidation (M), Deamidated (NQ), Acetyl N-terminal protein Phospho (STY), Biotin(K). Forward/decoy searches were used for false discovery rate estimation for PSM and peptides matching high confidence (FDR 1%) and medium confidence (FDR 5%).
Following protein identification, extracted TMT reporter abundances were used for protein quantitation. For protein normalization, the bait (BirA-Nesprin-1α) expression was assessed in both myoblasts and myotubes. Using BirA* specific peptides, correcting factors were derived and used for normalization of specific Nesprin-1α-interacting proteins. Proteins identified in at least 2 biological replicates were used for further analysis and illustration (Figure 3.18) by Dr. Bruno Cadot at the Center for Research in Myology in Paris, France.

2.5 Computer simulations

Computer simulations were carried out by Dr. Bruno Cadot at the Center for Research in Myology, Paris, France.
Computer simulations were performed using Cytosim (Nedelec and Foethke, 2007). In brief, overdamped Langevin equations are used to describe the motion of elastic fibers and nuclei in a viscous fluid in the presence of Brownian motion. All stochastic events (motor binding, MT catastrophes, and MT nucleation) are generated as first-order random events. The simulation parameters are summarized in Table S1 (Appendix, Chapter 6). Myotubes have elliptical shapes, 95 $\times$ 14 μm for five nuclei, 114 $\times$ 14 μm for six nuclei, 133 $\times$ 14 μm for seven nuclei, 152 $\times$ 14 μm for eight nuclei and 171 $\times$ 14 μm for nine nuclei, with the cytoplasm having homogenous

constant viscosity, as shown experimentally (Figure 3.27 A). The elliptical boundary confines MTs, centrosomes, and nuclei. A soft excluded volume interaction applies to centrosomes, MTs, and nuclei, preventing these objects from overlapping, but MTs only interact with each other via molecular motors (MT-MT steric interactions are not considered). Nuclei nucleate MTs, which undergo dynamic instability with no rescues. Moreover, the growth rate is reduced by force with a sensitivity of 1.5 pN and depends on the availability of tubulin monomers, for which a fixed pool is prescribed. The catastrophe rate depends on the growth rate as observed *in vitro* (Janson et al., 2003). MTs are nucleated horizontally, leading to their organization parallel to the long axis of the myotube, as shown by the EB1 comets angle analysis (Figure 3.27 B, C). MTs interact with nuclei via the dynein and kinesin motor proteins located at the NE. A given density of motor proteins is evenly distributed on nuclear surfaces. All motor proteins exert Hookean forces and move along bound MTs with a linear force-velocity relationship. The maximum number of MTs nucleated by one nucleus has been estimated by counting the number of EB1 comets near myotube nuclei.

2.6 Imaging

2.6.1 Epi-fluorescence and confocal microscopy

Wide-field epi-fluorescence imaging was performed on an inverted Nikon Ti microscope equipped with a XY-motorized stage (Nikon) using 20x 0.45 NA S Plan Fluor air or 40x 1.3 NA Plan Fluor oil objectives with a 1.5x magnifier (Nikon). Digital images were acquired with a CoolSNAP HQ2 camera (Roper Scientific) using Metamorph Software (Molecular Devices) and processed in Fiji. For analyses of C2C12 cells after MT regrowth assay, a maximum projection of four 0.25 μm z-sections was directly created during imaging using Metamorph. Wide-field epi-fluorescence images were also acquired on a DeltaVision CORE (Applied Precision) equipped with a xenon light source and bandpass filters with a Plan Apochromat 40x/1.35 NA (Olympus) oil-immersion objective lens (Olympus) and a CCD camera (no binning; CoolSNAP HQ, Photometrics). For deconvolved images, z-spacing was fixed at 0.2 μm on the DeltaVision CORE and deconvolution then completed using the SoftWorX program (Applied Precision). Confocal images of human immortalized cells after MT regrowth assay and staining were acquired on a Leica SPE confocal microscope using the 63x 1.3 NA Apo objective or on a Nikon Spinning disk confocal with EMCCD camera using a 60x (oil) 1.4 NA objective.

2.6.2 Live-cell imaging

For live-cell imaging of human immortalized myoblasts, 200.000 cells per well were plated on a 6-well plate in Growth Medium. Two days after seeding the cells, cells were washed twice with Differentiation Medium and then kept in an environmental chamber at 37°C/5% CO_2 (Okolab, Pozzuoli, Italy). Bright-field images were acquired every 15 min over a time frame of 63 hours using a 10x 0.3 NA PL Fluo objective on an inverted Nikon Ti microscope and Metamorph Software (section 2.6.1).

For live-cell imaging of dsRed-PACT-transfected C2C12 cells (section 2.3.3), cells were washed twice with Differentiation Medium and then kept at 37°C/5% CO_2 for 24 hours. The next day, the Differentiation Medium was renewed and cells were placed in an environmental chamber at 37°C/5% CO_2. Images were acquired every 10 min over a time frame of 70 hours using a 40x 1.3 NA Plan Fluor oil objective on an inverted Nikon Ti microscope and Metamorph Software (section 2.6.1). During imaging, a maximum projection of four 0.25 μm z-sections was automatically created for each position and time point by Metamorph. Metamorph was also used to create and export movies which were further processed and compiled into montages using Fiji.

For live-cell imaging of EB1-GFP comets, C2C12 cells transfected with EB1-GFP were differentiated in Differentiation Medium for five days. Subsequently, EB1-GFP-expressing-C2C12 myotubes were imaged with stream acquisition (250 ms/frame) in an environmental chamber at 37°C/5% CO_2.

2.6.3 Structured-illumination microscopy (SIM)

Wild type C2C12 cells were grown on gelatinated cover slips and induced to differentiation upon confluency. 48 hours later, cells were subjected to MT regrowth assay as described in (section 2.3.9) and stained as indicated. Cover slips were mounted using Vectashield and sealed with nail polish. Using the 488 nm, 568 nm, and 643 nm laser lines and standard filter sets, 3D-SIM images were obtained on the OMX V4 Blaze (GE Healthcare). Thereby, we used multicolour beads mounted on coverslips (TetraSpec, Invitrogen) to control exact registration (within 40 nm) of the three-colour channels.

2.6.4 SD-*d*STORM

Wild type C2C12 cells were grown on gelatinated cover slips and induced to differentiation upon confluency. After 48 hours of differentiation, cells were fixed and stained for Nesprin-1 (MANNES1E) and Pericentrin (Covance) following the IF protocol (section 2.3.8). Cells were incubated with Alexa Fluor 647 (Invitrogen) and CF 680 (Biotium, Fremont, California) labelled secondary antibodies diluted 1:200 in blocking buffer for 1 hour at room temperature. Lehmann et al. (2016) have been previously proven that this dye pair is applicable for spectral demixing SD-*d*STORM. Shortly before SD-*d*STORM imaging, cover slips were mounted in imaging buffer on slides with moulds (Carl Roth, Karlsruhe, Germany). Images were acquired on a custom-build SD-*d*STORM system using a 700-DCXXR dichroic mirror and a F76-635 emission bandpass filter (AHF Ana-lysentechnik, Tubingen, Germany) and reconstructed as described previously (Lampe et al., 2012; Lehmann et al., 2016).

2.7 Image Analysis

2.7.1 Manual quantification of Pericentrin/Akap450 at the NE

We counted the number of nuclei with more than 50% of Pericentrin or Akap450, respectively, at the NE in Myogenin-(MYOG)- or myosin heavy chain-(MHC)-positive cells.

2.7.2 CellProfiler analysis

C2C12 cells transfected with different siRNAs (see section 2.1.5) were stained for Pericentrin, myosin heavy chain (MHC) and DAPI. Subsequently, cells were automatically imaged using a customer developed journal (created by Dr. Bruno Cadot) for 96-well imaging plates in Metamorph. For each well, 30 images were thereby acquired and stitched together using the scan slide plugin of Metamorph. All images were analyzed for fusion index and Pericentrin levels at the nucleus in myotubes using CellProfiler (Carpenter et al., 2006) (CellProfiler pipeline by Dr. Bruno Cadot). In brief, CellProfiler was first optimized to identify Pericentrin rings (Figure 2.1 A) as well as myotube (Figure 2.1 B) and nuclei areas (Figure 2.1 C) as primary objects. Subsequently, nuclei (Figure 2.1 D) or Pericentrin rings (Figure 2.1 E) were masked on the identified myotubes, respectively. The fusion index was obtained by calculating the ratio of the nuclei area within myotubes over the total nuclei area within one image. Finally, Pericentrin levels at the nucleus in myotubes

were determined by normalizing the area of masked Pericentrin rings in myotubes to the area of masked nuclei in myotubes. The data for all 30 images per well were averaged and further processed in Microsoft Excel.

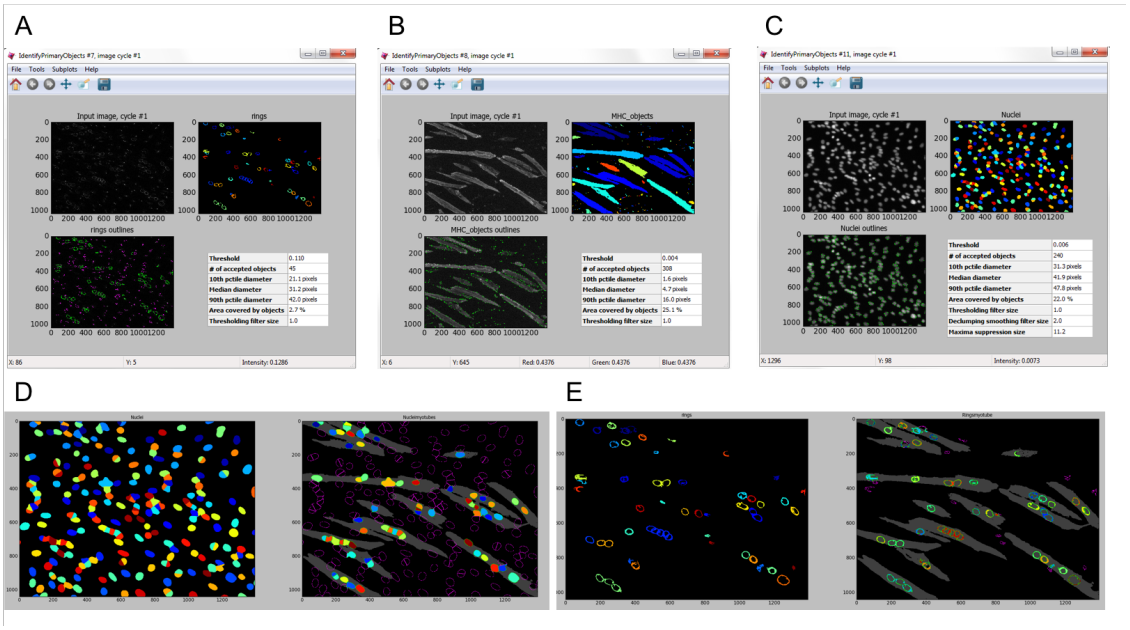

Figure 2.1: Workflow of the CellProfiler analysis. Pericentrin rings **(A)**, myotubes **(B)** and nuclei **(C)** were defined as primary objects using CellProfiler. **(D)** Nuclei or **(E)** Pericentrin rings were masked on myotubes. The fusion index and the levels of Pericentrin at the nucleus were then determined as follows:
fusion index = (area of nuclei in myotubes) / (total area of nuclei);
Pericentrin at the NE = (area of Pericentrin rings in myotubes) / (area of nuclei in myotubes)

2.7.3 Spreading factor analysis

For determining the spreading factor, we used differentiated muscle cells stained for myosin heavy chain (MHC) and DAPI to visualize myotubes and nuclei, respectively. We tracked the position of both myotube ends and all nuclei within each myotube using Metamorph. Subsequently, we calculated the maximal theoretical distance between all nuclei within one myotube (d_{ideal}) and the experimentally observed distances (d1, d2, d3 etc.) according to the myotube length (Figure 2.2) (Excel macro by Dr. Bruno Cadot, Center for Research in Myology, Paris). The spreading factor was then determined as the median of all observed distances normalized to the maximal theoretical distance.

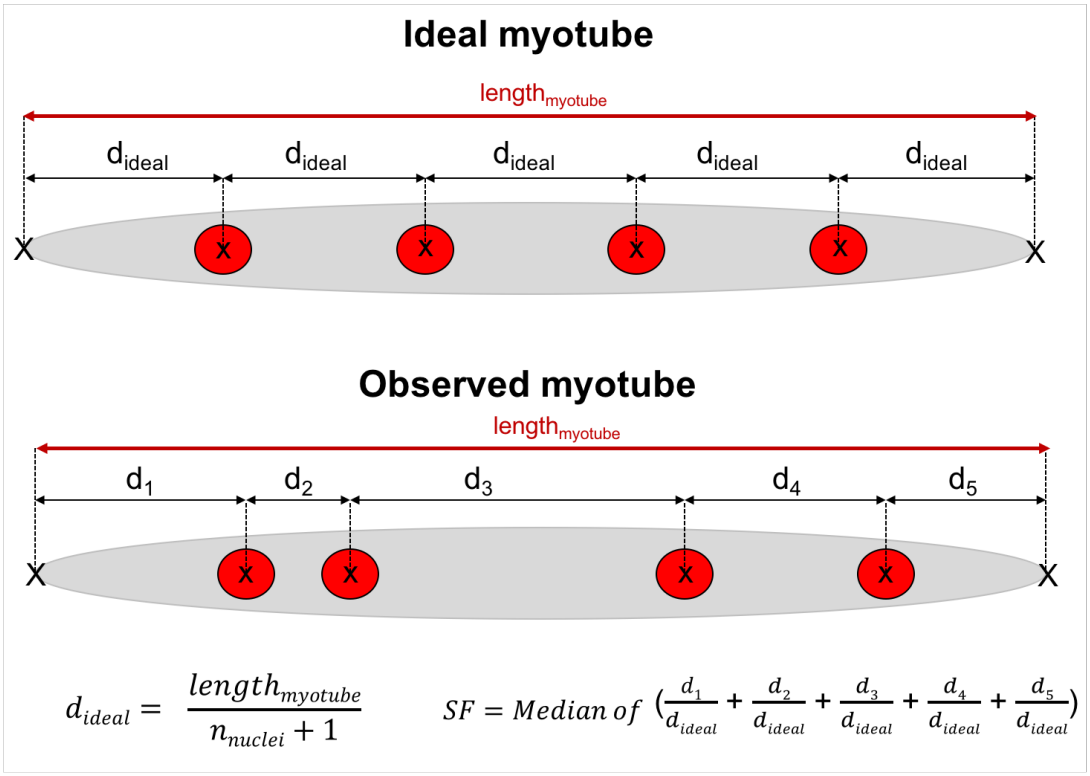

Figure 2.2: Model of the spreading factor analysis. Myotubes in an ideal set up as well as one exemplified myotube observed in cell culture experiments are depicted in grey, while nuclei are shown in red. The maximal theoretical distance between nuclei (d_{ideal}) is determined as the myotube length divided by the number of nuclei + 1. The spreading factor (SF) is defined as the median of all observed interdistances normalized to the maximal theoretical distance. *d, distance; n, number; SF, spreading factor*

2.7.4 Western Blot quantification

Western Blots were quantified for individual protein bands based on densitometry using Fiji. Therefore, each protein band was measured using a rectangle to define a single region of interest (ROI). In order to compare the density of one individual protein band with others, the same ROI was used for all measurements. All values were corrected using a background measurement and were then normalized to the respective loading control.

2.8 Statistical analysis

Statistical tests were performed using GraphPad Prism (GraphPad Prism Software Inc. version 6) and are further described in each figure legend. Statistical significance is represented as follows: *** $p<0.001$; ** $p<0.01$, *$p<0.05$; n.s., not statistically

significant.

3 Results

3.1 Recruitment of centrosomal proteins to the NE

During skeletal muscle formation, the recruitment of several centrosomal proteins, including Pericentrin, Akap450, and γ-tubulin, to the nucleus is now well established. However, additional information about the recruitment dynamics and if centrosomal proteins are directly recruited from the centrosome are still missing.
To address this, we took advantage of the C-terminal PACT (Pericentrin-Akap450 centrosomal targeting) domain of Pericentrin fused to dsRed. The PACT domain was initially shown by Gillingham and Munro to be sufficient for bringing GFP or RFP to the centrosome and was thus ideal to follow its localization during the process of myogenic differentiation by live-cell imaging (Figure 3.1).
In dsRed-PACT-overexpressing C2C12 myoblasts, dsRed-PACT localized to two closely spaced perinuclear spots, resembling the two centrioles of the centrosome (frame 13:30 hh:min, arrows). These two centriole-like dots were highly motile and their distance seemed to increase during time progression (frame 15:10 to 18:30 hh:min). Within approximately 2 hours, starting from time frame 18:30 hh:min, we additionally observed faint dsRed fluorescence at the perinuclear rim (frame 20:10 hh:min). The fluorescence at the perinuclear rim but also at the perinuclear spots continuously increased over time (frame 21:50 to 35:10 hh:min). The two perinuclear spots seemed to push against the nucleus and often followed invaginations of the NE.

Overall, we confirmed that the PACT domain is sufficient to target dsRed to the centrosome in myoblasts and additionally to the nucleus in differentiating C2C12 cells. However, during the process of dsRed-PACT localization to the NE, we could not observe if dsRed-PACT was first released from the centrosome and then directly moved to the NE or if newly synthesized dsRed-PACT molecules within the cytoplasm localized to the NE independently of the centrosome.

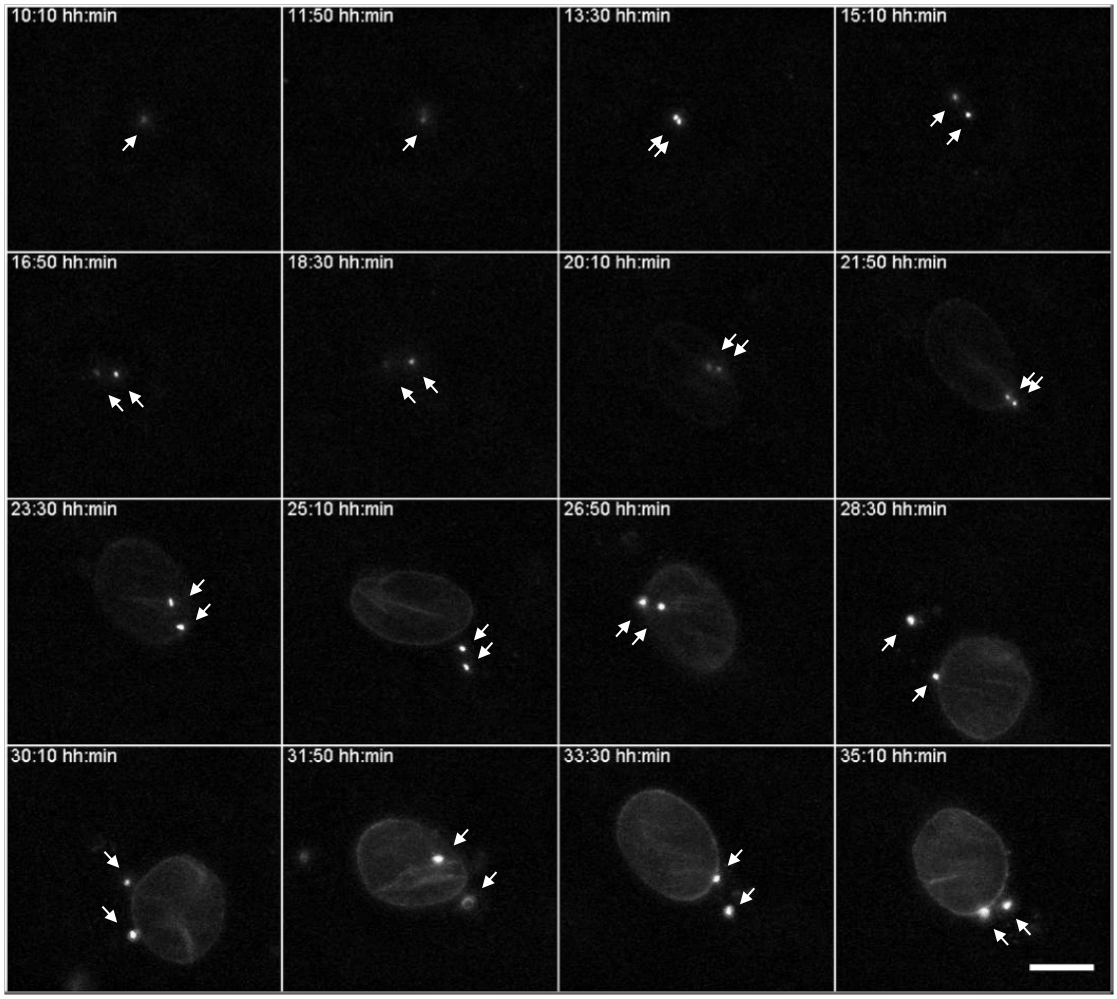

Figure 3.1: Time-lapse video microscopy of dsRed-PACT during myogenic differentiation. Depicted is a montage of frames from live-cell imaging of C2C12 cells overexpressing dsRed-PACT during differentiation. Arrows point to the centrosome or centriole-like structures, respectively. Scale bar, 10 μm.

3.2 Identifying the nuclear receptor for NE localization of centrosomal proteins

Several studies have reported the reorganization of various centrosomal proteins to the nucleus throughout myogenic differentiation (Bugnard et al., 2005; Fant et al., 2009; Srsen et al., 2009; Tassin et al., 1985a). Yet, how centrosomal proteins or the dsRed-PACT domain are recruited and anchored to the NE remained unanswered. We therefore aimed to identify nuclear receptors that build a so far unknown link between the nucleus and centrosomal proteins.

3.2.1 Nesprin-1 - a potential receptor for Pericentrin?

In order to determine potential receptor and NE-associated protein complexes that are implicated in the recruitment of centrosomal proteins to the nucleus, we performed small interfering RNA (siRNA) screens using the myogenic precursor C2C12 cell line and automated immunofluorescence microscopy (Figure 3.2). Based on previous published mass spectrometry studies of NE fractions, we chose 238 potential nuclear transmembrane proteins or NE-associated proteins, respectively, and conceived a pool of three siRNAs for each gene (Kislinger et al., 2006; Schirmer et al., 2003; Wilkie et al., 2011). After transfection and subsequent differentiation of C2C12 myogenic precursor cells, myotubes were stained and automatically imaged. To analyze the effects of each gene on myogenic differentiation capacity and Pericentrin recruitment to the nucleus, we developed an analysis pipeline within CellProfiler for measuring the fusion index and Pericentrin levels at the NE in mytoubes (section 2.7.2). All results were compared to C2C12 cells transfected with a non-targeting control siRNA or to C2C12 cells silenced for *Pericentrin*. Note that the siRNAs used to target *Pericentrin* mRNAs in C2C12 cells as well as the antibodies used to identify Pericentrin levels at the NE, recognize all Pericentrin isoforms (see section 1.4.1), so that we refer here to 'Pericentrin' throughout the text.

Among the 238 tested genes, the majority of 200 genes did not increase or decrease Pericentrin levels at the NE more than 20%, respectively, and were therefore considered to have no substantial effects on Pericentrin recruitment to the nucleus (Figure 3.3; see Appendix chapter 6, Table 6.1 for a complete list of all results). Pericentrin recruitment to the NE was increased upon knockdown of seven genes (*Sec61b, Ugt1a2, Bcam, Podxl, Rpn1, Mospd3, Tmem74,* see Appendix chapter 6, Table 6.1), while Pericentrin levels at the NE were decreased after knockdown of 31 genes (Figure 3.3).

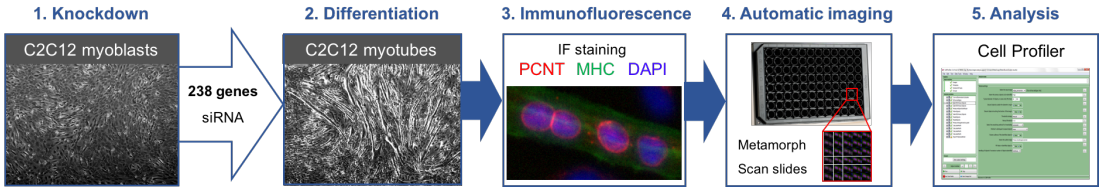

Figure 3.2: Workflow of the siRNA screen. C2C12 myoblasts were transfected in 96-well imaging plates with siRNA pools against 238 genes encoding for proteins with potential transmembrane domains. After three to four days of myogenic differentiation, C2C12 myotubes were fixed and stained for Pericentrin (PCNT, red), myosin heavy chain (MHC, green) and nuclei (DAPI, blue). Immunofluorescence images were acquired using a Metamorph-based automatic imaging system. Consequently, immunofluorescence images were analyzed for fusion index and the levels of Pericentrin at the NE within myotubes by using CellProfiler.

Among the genes showing decreased Pericentrin relocalization after silencing, *low density lipoprotein receptor-related protein 1 (Lrp1)* and *MYB binding protein (P160) 1a (Mybbp1a)* displayed the strongest effect. Lrp1 is a large transmembrane protein that belongs to the LDL receptor family and functions in endocytosis and in various signaling cascades (Boucher and Herz, 2011; Herz and Strickland, 2001), whereas Mybbp1a binds to a variety of transcription factors, including c-Myb, PGC-1α, Prep1, NF-κB, and Aire, and inhibits their transactivation activity (Abramson et al., 2010; Díaz et al., 2007; Fan et al., 2004; Owen et al., 2007; Tavner et al., 1998). However, knockdown of *Lrp1* or *Mybbp1a* also resulted in a strong decrease of the fusion index, suggesting that Lrp1 and Mybbp1a might play crucial roles during myogenic differentiation.

As Pericentrin depletion itself did not have an impact on the fusion index, we were rather interested in these candidate genes which upon silencing showed reduced Pericentrin levels at the NE but at the same time had no or only mild effects on the early differentiation process. Candidates that fulfilled these criteria were components of the LINC complex, the KASH domain proteins Syne1 and Syne2 (also known as Nesprin-1 and Nesprin-2), as well as the SUN domain protein Unc84a (also known as Sun1). Strikingly, knockdown of *Syne1* (referred hereafter as Nesprin-1) resulted not only in decreased Pericentrin intensity levels at the NE as assessed by CellProfiler analysis but also visually in abnormal Pericentrin localization within the cytoplasm (see section 3.2.2, Figure 3.5). In contrast, Pericentrin levels seemed to be slightly decreased but not mislocalized upon *Syne2* (referred hereafter as Nesprin-2) silencing. However, further validation of Nesprin-2 as a potential receptor candidate for Pericentrin failed, when C2C12 cells were silenced for *Nesprin-2* using different sets of siRNAs (data not shown). This result was in agreement with other

studies showing that the expression of Nesprin-2 decreases from the myoblast to the myotube state, thus making Nesprin-2 an unlikely candidate for Pericentrin recruitment during myogenic differentiation (Espigat-Georger et al., 2016; Randles et al., 2010).
The SUN domain protein Spag4l (also known as Sun5) was previously reported to be exclusively expressed in testis and was not taken into further consideration as C2C12 cells silenced for *Spag4l* additionally demonstrated a reduced fusion index (Frohnert et al., 2011; Jiang et al., 2011).
Taken together, among the 31 genes from the siRNA screen showing decreased Pericentrin relocalization after silencing, only Nesprin-1-depleted cells displayed mislocalized clusters of Pericentrin within the cytoplasm. Thus, we hypothesized that Nesprin-1 might be potentially important for recruiting Pericentrin and other centrosomal proteins to the NE during myogenic differentiation and decided to explore this candidate and the underlying mechanism in more detail.

3.2.2 Validating the LINC complex as nuclear receptor

To validate if Nesprin-1 could be the nuclear receptor for Pericentrin and other centrosomal proteins, we firstly analyzed if Pericentrin is colocalizing with Nesprin-1 at the nucleus of differentiated C2C12 cells by applying spectral demixing direct stochastic optical reconstruction microscopy (SD-*d*STORM was performed together with Dr. Jan Schmoranzer, Charité Universitätsmedizin Berlin, Campus Mitte, CharitéCrossOver, Berlin, Germany). SD-*d*STORM is a super-resolution technique with a lateral resolution of 20-35 nm (Lampe et al., 2012; Lehmann et al., 2016). Nesprin-1 and Pericentrin appeared in close proximity at the nucleus (Figure 3.4, SD-*d*STORM, insets) at the spatial resolution of SD-*d*STORM and completely overlapped when the same SD-*d*STORM data was rendered at the approximate resolution of a conventional wide-field microscope (Figure 3.4, wide-field, insets). Thus, this result confirms the spatial co-organization of Nesprin-1 and Pericentrin at the nucleus of differentiated muscle cells.
By way of further confirming the results from the siRNA screen, we depleted C2C12 myoblasts for Nesprin-1 using two different siRNAs and determined Pericentrin localization upon myogenic differentiation (Figure 3.5). Note that the siRNAs used to target *Nesprin-1* mRNAs in C2C12 cells as well as the antibody (MANNES1E) used to identify Nesprin-1 levels at the NE target a region nearby the KASH domain encoding sequence and therefore potentially recognize Nesprin-1 giant but also other smaller isoforms such as Nesprin-1α due to the high sequence similarity of these isoforms. We confirmed that both siRNAs efficiently knocked down the

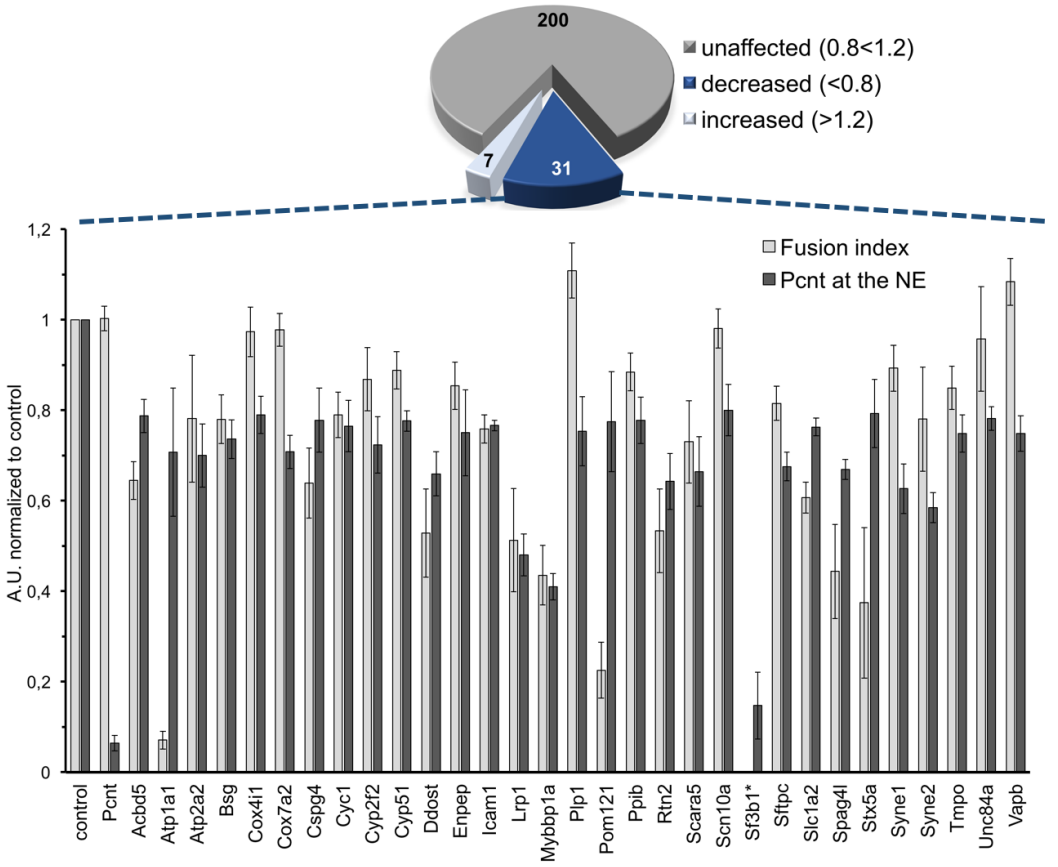

Figure 3.3: Hits of the siRNA screen showing decreased Pericentrin levels at the NE. The pie chart indicates the number of genes (total = 238) that resulted in increased (more than 1.2, while control = 1) or decreased (lower than 0.8, control = 1) Pericentrin (Pcnt) levels at the NE in myotubes, respectively. The majority of genes had no effect (between 0.8 and 1.2) on Pcnt levels at the NE. The bottom graph shows the result (fusion index and Pcnt levels at the NE) for 31 genes that displayed decreased Pericentrin recruitment to the NE upon silencing. Results were normalized to control sample and are depicted as the average of three to four independent experiments. Error bars represent the standard error of the mean (S.E.M.). Note that silencing of *Sf3b1* resulted in induced cell death and is therefore marked by an asterisk (*).

smaller muscle-specific Nesprin-1 isoform, Nesprin-1α, as assessed by Western Blot analysis (Figure 3.5 D). In myotubes transfected with non-targeting control siRNA, Pericentrin typically localized to the nuclear rim in about 80% of myotube nuclei (Figure 3.5 A, B). When cells were effectively depleted for Pericentrin itself (Figure 3.5 C), Pericentrin was expectably absent from the nucleus (Figure 3.5 A, B). Similarly, Pericentrin was absent at myotube nuclei in Nesprin-1-depleted cells and instead mislocalized within perinuclear regions or generally within the cytoplasm. Note, that the decreased levels of Pericentrin at the NE upon Nesprin-1 silencing

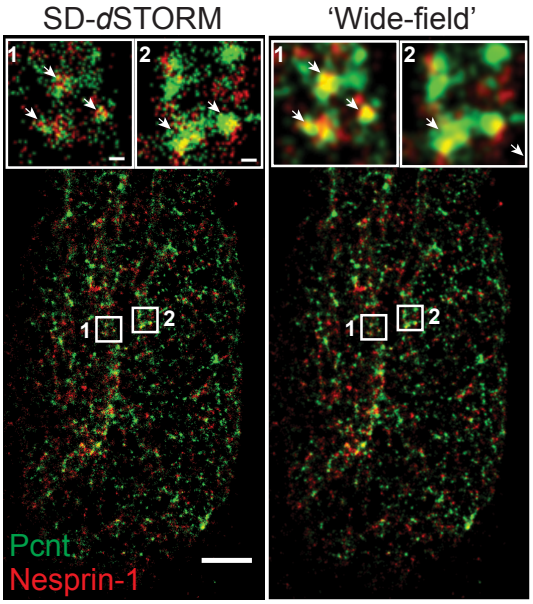

Figure 3.4: SD-*d*STORM reveals Pericentrin and Nesprin-1 colocalization at the NE. Dual colour SD-*d*STORM image of Pericentrin (Pcnt, green) and Nesprin-1α/Nesprin-1 (red, MANNES1E mAb) at the nuclear surface of a differentiated C2C12 myoblast (left) and the same SD-*d*STORM image rendered to the resolution of a conventional wide-field microscope (right). Insets show higher magnifications of colocalization regions (arrows). Scale bar, 1 μm. Scale bar of insets, 100 nm.
Cell preparation, staining and imaging was performed by Petra Gimpel. Image reconstruction and analysis was done by Dr. Jan Schmoranzer, Charité Universitätsmedizin Berlin, Campus Mitte, CharitéCrossOver, Berlin.

were not due to altered gene expression since protein levels of Pericentrin were unaffected and constant throughout differentiation (Figure 3.6).
Considering that Nesprin-1 is retained at the outer nuclear membrane through its interaction with Sun1/2 and that Sun1 (also termed Unc84a) was one of the major candidates of the siRNA screen showing decreased Pericentrin levels at the nucleus (Figure 3.3), we further elucidated the effects of Sun1 and Sun2 on Pericentrin recruitment.
First, we depleted C2C12 cells for Sun1, Sun2 or both Sun1 and Sun2 (Sun1/2), verified efficient knockdown by Western Blot analysis (Figure 3.5 E, F) and analyzed the number of Pericentrin-positive myotube nuclei (Figure 3.5 A, B). While Pericentrin NE localization was not affected in Sun2-depleted myotubes, Sun1 depletion slightly but significantly decreased the number of Pericentrin-positive myotube nuclei. Strikingly, Sun1-depleted myotubes also visually displayed changed Pericentrin localization to the nuclear poles rather than an equal distribution around the nuclear rim (Figure 3.5 A, Sun1). However, Pericentrin mislocalization within the cytoplasm, as demonstrated in Nesprin-1-silenced myotubes, was only observed upon double depletion of Sun1 and Sun2.
To validate these data and to exclude eventual off-target effects of the siRNAs, we analyzed Pericentrin localization in differentiated myoblasts isolated from *Sun1*$^{-/-}$, *Sun2*$^{-/-}$ *or Sun1*$^{-/-}$*;Sun2*$^{-/-}$ knockout mice (in collaboration with Dr. Yin Loon Lee, Institute of Medical Biology, A*STAR, Singapore). In line with our previous findings, only *Sun1*$^{-/-}$*;Sun2*$^{-/-}$ myotubes lacked Pericentrin at the NE but instead showed

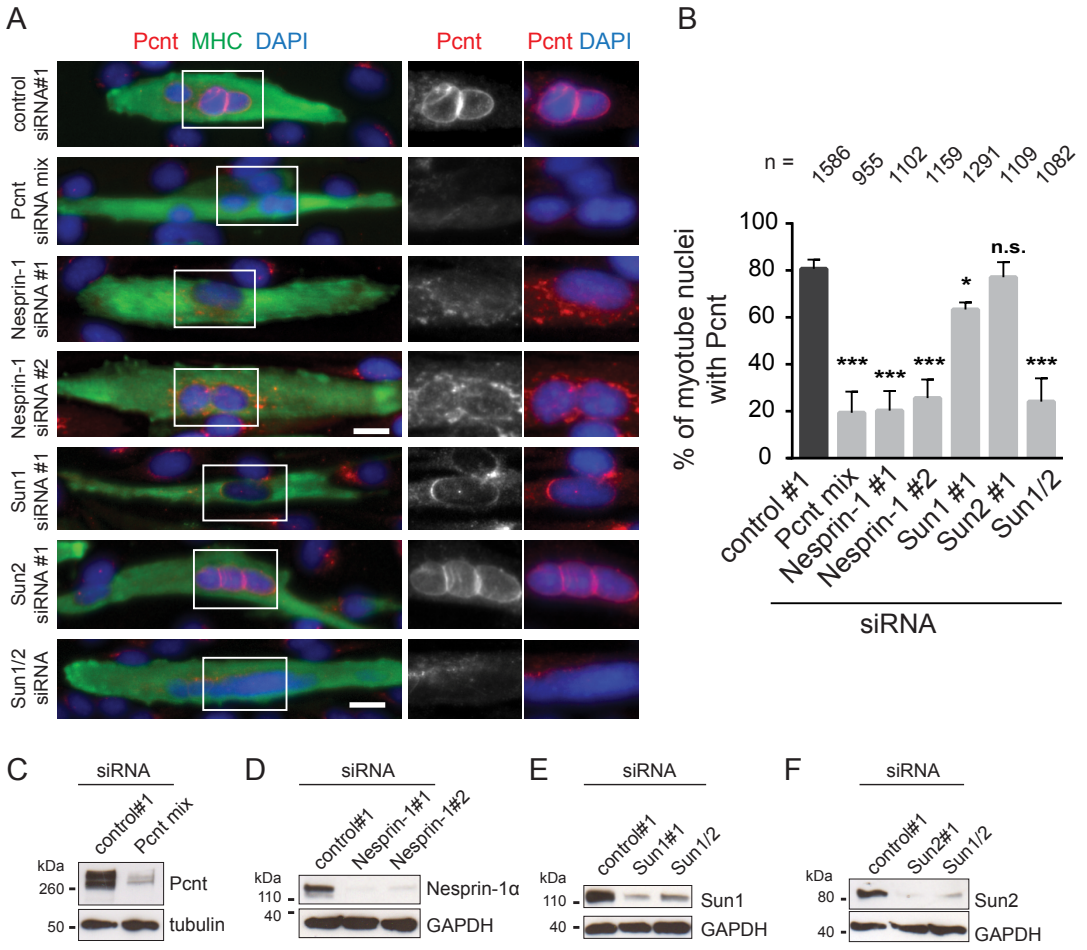

Figure 3.5: The LINC complex is required for recruiting centrosomal proteins during myogenic differentiation. **(A)** Representative epi-fluorescence images of 48 h differentiated C2C12 myotubes, transfected with control siRNA#1, Pcnt siRNAmix, two different siRNAs for Nesprin-1 (Nesprin-1 siRNA#1 or Nesprin-1 siRNA#2), Sun1, Sun2 or both Sun1 and Sun2 (Sun1/2). Cells were stained for Pericentrin (Pcnt, red), nuclei (DAPI, blue) and myosin heavy chain (MHC, green) to identify differentiated myotubes. White squares indicate selected regions for higher magnifications of Pericentrin staining alone (Pcnt, red) or together with nuclei (DAPI, blue) shown on the right. Scale bar, 20 μm. **(B)** Quantification of Pericentrin recruitment to the NE in myotube nuclei after treatment with the indicated siRNAs. Error bars ± SD. n represents total number of nuclei from at least three independent experiments. *** $p<0.001$; *$p<0.05$; n.s., not statistically significant, t-test. **(C)** Immunoblot of anti-Pericentrin (Pcnt) and anti-tubulin (anti-tyrosinated α-tubulin, YL 1/2) as loading control in C2C12 cells treated with non-targeting control siRNA#1 or a mix of two Pericentrin siRNAs (Pcnt mix). **(D)** Western Blot of 48 h differentiated C2C12 cells transfected with non-targeting control siRNA#1 or two different siRNAs to Nesprin-1 (Nesprin-1 #1 or Nesprin-1 #2) stained for Nesprin-1α/Nesprin-1 (MANNES1E) or GAPDH as a loading control. **(E)** C2C12 were transfected with non-targeting control siRNA#1, Sun1 or Sun1 and Sun2 siRNA (Sun1/2), respectively, differentiated for 48 h and subjected to SDS-PAGE and Western Blot analysis using anti-Sun1 and anti-GAPDH antibodies. **(F)** C2C12 were transfected with non-targeting control siRNA#1, Sun2 or Sun1 and Sun2 siRNA (Sun1/2), respectively, differentiated for 48 h and subjected to SDS-PAGE and Western Blot analysis using anti-Sun2 and anti-GAPDH antibodies.

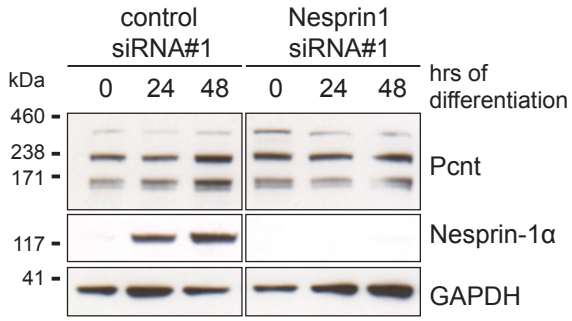

Figure 3.6: Pericentrin protein levels remain unchanged upon Nesprin-1 depletion. C2C12 cells were treated with non-targeting control siRNA#1 or Nesprin-1 siRNA#1, differentiated for the indicated time points (hours of differentiation), subjected to SDS-PAGE and Western Blot analysis using anti-Pericentrin (Pcnt), anti-Nesprin-1α/Nesprin-1 (MANNES1E) and anti-GAPDH antibodies.

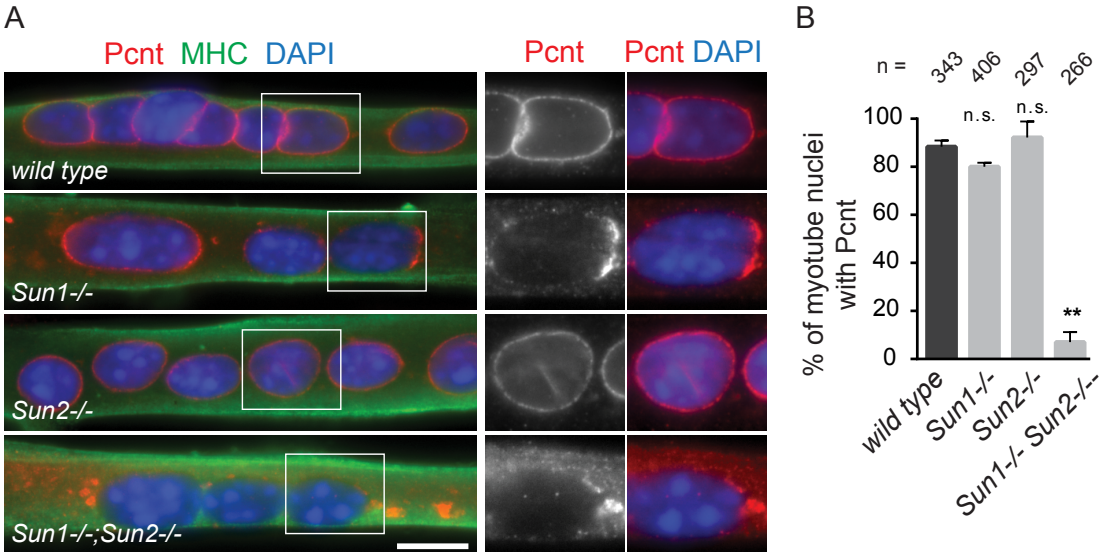

Figure 3.7: Sun1/2 are required for Pericentrin recruitment to the nucleus. (A) Representative epi-fluorescence images of 72 h *in vitro* differentiated primary myotubes from wild type, *Sun1*$^{-/-}$, *Sun2*$^{-/-}$ or *Sun1*$^{-/-}$;*Sun2*$^{-/-}$ knockout mice, stained for Pericentrin (Pcnt red), MHC (green), and nuclei (DAPI, blue). White squares indicate selected regions for higher magnifications of Pericentrin staining alone (Pcnt, red) or together with nuclei (DAPI, blue) shown on the right. Scale bar, 20 μm. **(B)** Quantification of Pericentrin recruitment to the NE in primary myotubes of *wild type, Sun1-/-, Sun2/- or Sun1/-;Sun2-/-* knockout mice. Error bars ± SD. n represents total number of nuclei from two independent experiments. ** p<0.01; n.s., not statistically significant, t-test.
Primary myoblasts were isolated by Dr. Yin Loon Lee at the IMB in Singapore and were differentiated in vitro by Petra Gimpel and Dr. Yin Loon Lee at the Center for Research in Myology in Paris. Image acquisition and preparation as well as quantification was performed by Petra Gimpel.

Pericentrin mislocalization within the cytoplasm (Figure 3.7 A, B). *Sun1*$^{-/-}$ myotubes displayed again a prominent redistribution of Pericentrin to the nuclear poles, however, the total number of Pericentrin-positive myotube nuclei was not significantly decreased. According to the RNAi data (Figure 3.5 A, B) as well as to the siRNA screen (Figure 3.3), where Sun2 was not part of the candidates showing decreased Pericentrin levels at the NE, *Sun2*$^{-/-}$ myotubes demonstrated no obvious effect on Pericentrin localization. Collectively, these data suggested that Sun1 might have a more pronounced role in localizing Pericentrin to the nucleus during myogenic differentiation but that Sun1 and Sun2 potentially function redundantly.

To test this hypothesis, we determined endogenous protein levels of Sun1 and Sun2 over 96 hours of myotube formation using C2C12 cells. While Sun1 protein levels increased over time together with myosin heavy chain as a marker for differentiation, Sun2 protein levels remained unchanged throughout the differentiation process (Figure 3.8 A). To elucidate if Sun1 and Sun2 could compensate for each other's function, we analyzed the relative protein expression levels of both SUN domain proteins upon depletion of Sun1, Sun2 or both Sun1/2 in C2C12 cells (Figure 3.8 B). Quantification of protein levels after 0 and 48 hours of differentiation revealed a similar increase of Sun1 and constant protein levels of Sun2 in C2C12 cells transfected with non-targeting control siRNA (Figure 3.8 C). Contrarily, relative protein levels of Sun2 were increased upon silencing of Sun1 when compared to control cells both after 0 and 48 hours of differentiation. C2C12 cells silenced for Sun2 showed slightly reduced protein levels of Sun1 when compared to the respective control, although the tendency of increased Sun1 protein levels from 0 to 48 hours of differentiation was still detectable. Taking into account that Sun1-depletion showed stronger effects on Pericentrin localization at the NE and that Sun1 was additionally increased during myogenic differentiation, we believe that Sun1 is the dominant SUN domain protein involved in binding Nesprin-1α/Nesprin-1 and thus localizing Pericentrin to the NE. However, in conditions were Sun1 is absent, increased Sun2 protein levels might functionally compensate for the loss of Sun1.

3.2.3 Pericentrin, Akap450, and PCM1 are mislocalized in *SYNE1 (23560 G>T)* patient myotubes

Several mutations within genes encoding proteins of the LINC complex have been connected with striated muscle diseases, including Emery-Dreifuss muscular dystrophy (EDMD) (Meinke et al., 2014; Wheeler et al., 2007; Zhang et al., 2007b). In a patient with an EDMD-like phenotype, compound heterozygous mutations

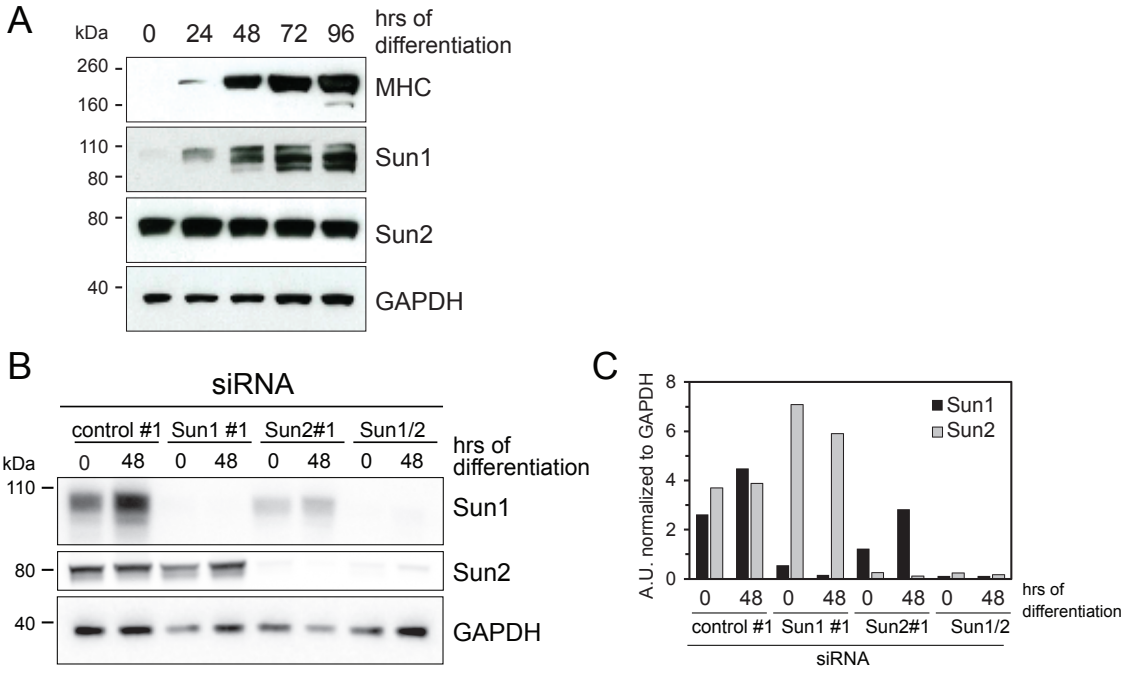

Figure 3.8: Sun1 and Sun2 during myogenic differentiation. (A) C2C12 cells were differentiated for the indicated time points (hours of differentiation) in Differentiation Medium. Cell lysates were analyzed by SDS-PAGE and Western Blot using antibodies against myosin heavy chain (MHC) as a marker for differentiation, Sun1, Sun2 or GAPDH as loading control. **(B)** C2C12 cells transfected with control siRNA#1 or Sun1#1, Sun2#1 or both Sun1 and Sun2 (Sun1/2) siRNAs, respectively, were differentiated for 0 or 48 hours (hrs) in Differentiation Medium. Cell lysates were subjected to SDS-PAGE and Western Blot analysis using specific antibodies against Sun1, Sun2 or GAPDH as loading control. **(C)** Quantification of Western Blots shown in (B). Band intensities for Sun1 or Sun2 were measured using Fiji and normalized to total GAPDH protein levels. A.U., arbitrary units.

within *SUN1* (p.G68D p.G338S) were previously demonstrated to affect Pericentrin localization to the nucleus (Meinke et al., 2014). Therefore, we hypothesized that a recently identified mutation within the *SYNE1 gene (23560 G>T)* that encodes Nesprin-1 would also lead to defects in NE localization of centrosomal proteins. This homozygous nonsense mutation was found in a congenital muscular dystrophy patient and was reported to result in decreased mRNA expression of both Nesprin-1 giant and Nesprin-1α (Holt et al., 2016; Mamchaoui et al., 2011).

First, we confirmed by immunofluorescence that Nesprin-1 isoforms were present at the NE in wild type healthy control myotubes but were absent in *SYNE1 (23560 G>T)* patient myotubes (Figure 3.9 A). Next, we examined NE localization of Pericentrin and two additional centrosomal proteins, Akap450 and PCM1, that are known to be recruited to the NE during skeletal muscle formation (Oddoux

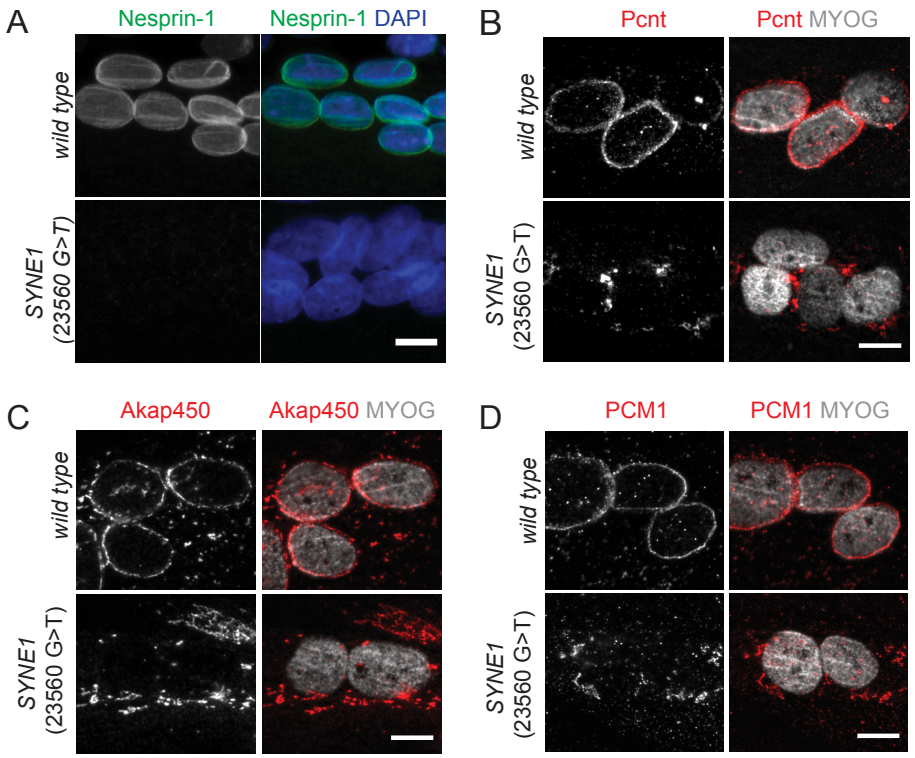

Figure 3.9: *SYNE1 (23560 G>T)* patient myotubes fail to recruit centrosomal proteins to the NE. (A) Representative epi-fluorescence images of differentiated human immortalized myotubes from a healthy control (wild type) or from a patient carrying a nonsense mutation within the *SYNE1 (23560 G>T)* gene immunostained for Nesprin-1 (MANNES1E, green) and nuclei (DAPI, blue). Scale bar, 10 μm. **(B)** Representative epi-fluorescence image of differentiated human immortalized myotubes from a healthy control (wild type) or from a patient carrying a nonsense mutation within the *SYNE1 (23560 G>T)* gene immunostained for **(B)** Pericentrin (Pcnt, Ab gift from Kunsoo Rhee, red), **(C)** Akap450 (red) or **(D)** PCM1 together with Myogenin (MYOG, grey) as differentiation marker. Scale bar, 10 μm.

et al., 2013; Srsen et al., 2009). We were particularly interested to analyze Akap450 localization in comparison to Pericentrin, as both Pericentrin and Akap450 were demonstrated to possess a C-terminal PACT domain and to interact with each other (Gillingham and Munro, 2000; Takahashi et al., 2002). Moreover, we chose to analyze PCM1 localization in comparison to Pericentrin, as PCM1 was shown to be important for Pericentrin localization to the centrosome (Dammermann and Merdes, 2002).

In line with our previous results using C2C12 cells, we observed nuclear rim stainings for Pericentrin, Akap450, and PCM1 in wild type human myotubes (Figure 3.9 B-D). Conversely, Pericentrin, Akap450, and PCM1 did not localize to the NE but were often found within the cytoplasm at perinuclear regions in *SYNE1 (23560 G>T)*

patient myotubes.
These data confirm the importance of Nesprin-1 in recruiting Pericentrin, Akap450 and PCM1 to the NE during myogenic differentiation. As all three centrosomal proteins were mislocalized in *SYNE1 (23560 G>T)* patient myotubes, this suggests that Pericentrin, Akap450 and PCM1 might localize to the NE through a similar mechanism.

In differentiated C2C12 depleted for Nesprin-1 as well as in *SYNE1 (23560 G>T)* patient myotubes, centrosomal proteins that were mislocalized to the cytoplasm appeared to be restricted at perinuclear regions. However, which cellular structure was implicated in retaining centrosomal proteins near the nucleus or how these aggregates were composited was not addressed yet. As the Golgi complex was shown to reorganize to the nucleus together with centrosomal proteins during myogenic differentiation (Lu et al., 2001; Zaal et al., 2011), we speculated that the Golgi complex might impact localization of centrosomal proteins in Nesprin-1-depleted cells as well. To test this hypothesis, we co-stained differentiated human wild type or *SYNE1 (23560 G>T)* patient cells for Akap450, PCM1, and Pericentrin together with the cis-Golgi marker GM130 (Figure 3.10). Akap450 completely colocalized with GM130 at the NE but also at cytoplasmic sites within wild type myotubes (Figure 3.10 A). In comparison, Akap450 also colocalized with GM130, when both proteins were mislocalized within the cytoplasm near the nucleus in *SYNE1 (23560 G>T)* patient myotubes. Also PCM1 and Pericentrin colocalized with GM130 at the NE in wild type myotubes and seemed to be concentrated at mislocalized Golgi complex fragments in *SYNE1 (23560 G>T)* patient myotubes.

Next, we wanted to test if the observed aggregates still contain centrioles and thus might reflect centrosome-like structures in the absence of Nesprin-1. In human wild type myotubes, we found the centriole marker Cep152 in close contact with Golgi complex elements within the cytoplasm but not with reorganized GM130 at the NE (Figure 3.11). Similarly, Cep152 localized to Golgi complex fragments near the nucleus in *SYNE1 gene (23560 G>T)* patient myotubes, without revealing any obvious differences when compared to wild type myotubes.

Generally, these data indicate that the aggregates observed in Nesprin-1-deficient cells contain multiple centrosomal proteins, including Akap450, PCM1 and Pericentrin, which are collectively retained at mislocalized Golgi complex fragments. Some but not all of the Golgi complex elements within the cytoplasm contain additionally

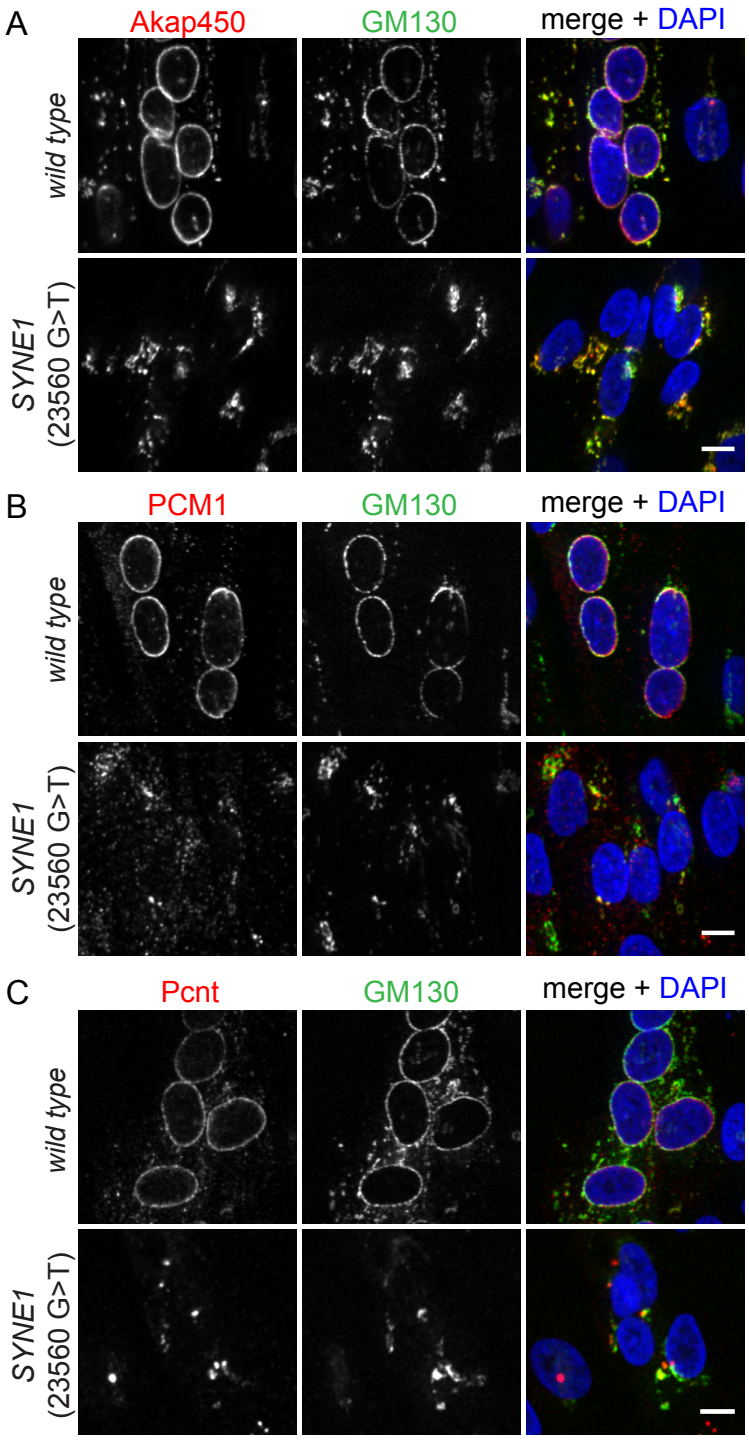

Figure 3.10: Akap450, PCM1, and Pericentrin are mislocalized together with Golgi fragments in *SYNE1 (23560 G>T)* patient myotubes. Differentiated human immortalized myotubes from a healthy control (wild type) or from a patient carrying a nonsense mutation within the *SYNE1 (23560 G>T)* gene were immunostained for **(A)** Akap450 (red), **(B)** PCM1 (red) or **(C)** Pericentrin (Pcnt; red, Ab gift from Kunsoo Rhee) together with GM130 (green) and nuclei (DAPI, blue). Scale bar, 10 μm.

the centriole marker Cep152 and might function together with mislocalized Akap450, PCM1 and Pericentrin as centrosome-like structures when Nesprin-1 is missing.

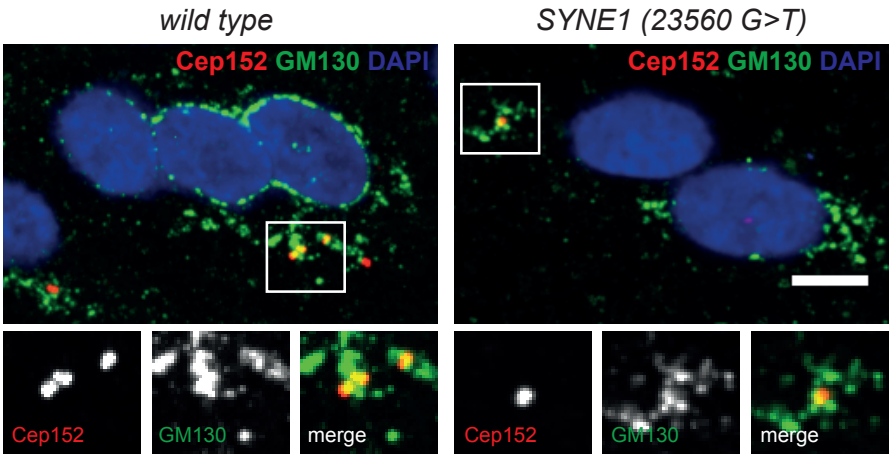

Figure 3.11: Centrioles are enclosed by Golgi fragments in human myotubes. Differentiated human immortalized myotubes from a healthy control (wild type) or from a patient carrying a nonsense mutation within the *SYNE1 (23560 G>T)* gene were immunostained for Cep152 as a centriole marker (red), GM130 (green) and nuclei (DAPI, blue). Scale bar, 10 μm.

3.3 Interdependent recruitment of centrosomal proteins

So far, we have shown that several centrosomal proteins localize to the nucleus in dependence of Nesprin-1 and Sun1/2-containing LINC complexes. Yet, if these centrosomal proteins are individually recruited by the LINC complex during myogenic differentiation or interdependently of other centrosomal proteins remained an open question.

To distinguish between these two possibilities, we analyzed C2C12 myotubes for NE localization of centrosomal proteins that are known to either interact with each other, like Akap450 and Pericentrin (Takahashi et al., 2002), and/or to depend on other centrosomal proteins for their localization to the centrosome. As described above, Pericentrin was demonstrated to localize to the centrosome in a Pcm1-dependent manner (Dammermann and Merdes, 2002). Pericentrin in turn, was shown to be required for centrosome localization of another PCM component, namely Cdk5Rap2 (Buchman et al., 2010). Cdk5Rap2 was further determined to localize to the Golgi-complex in dependence of Pericentrin and Akap450 (Wang et al., 2010). Thus, we

set out to examine the impact of Akap450, Pcm1, Pericentrin and Cdk5Rap2 on NE localization of the other centrosomal proteins. C2C12 myoblasts were individually silenced for these centrosomal proteins and upon differentiation stained for Akap450, Pcm1, Pericentrin and Cdk5Rap2.

C2C12 cells treated with non-targeting control siRNA displayed perfect nuclear rim staining for Akap450, while Akap450 was expectably absent from the nucleus in cells depleted of Akap450 itself (Figure 3.12). In comparison, neither Pcm1, Pericentrin or Cdk5Rap2 depletion affected NE localization of Akap450.

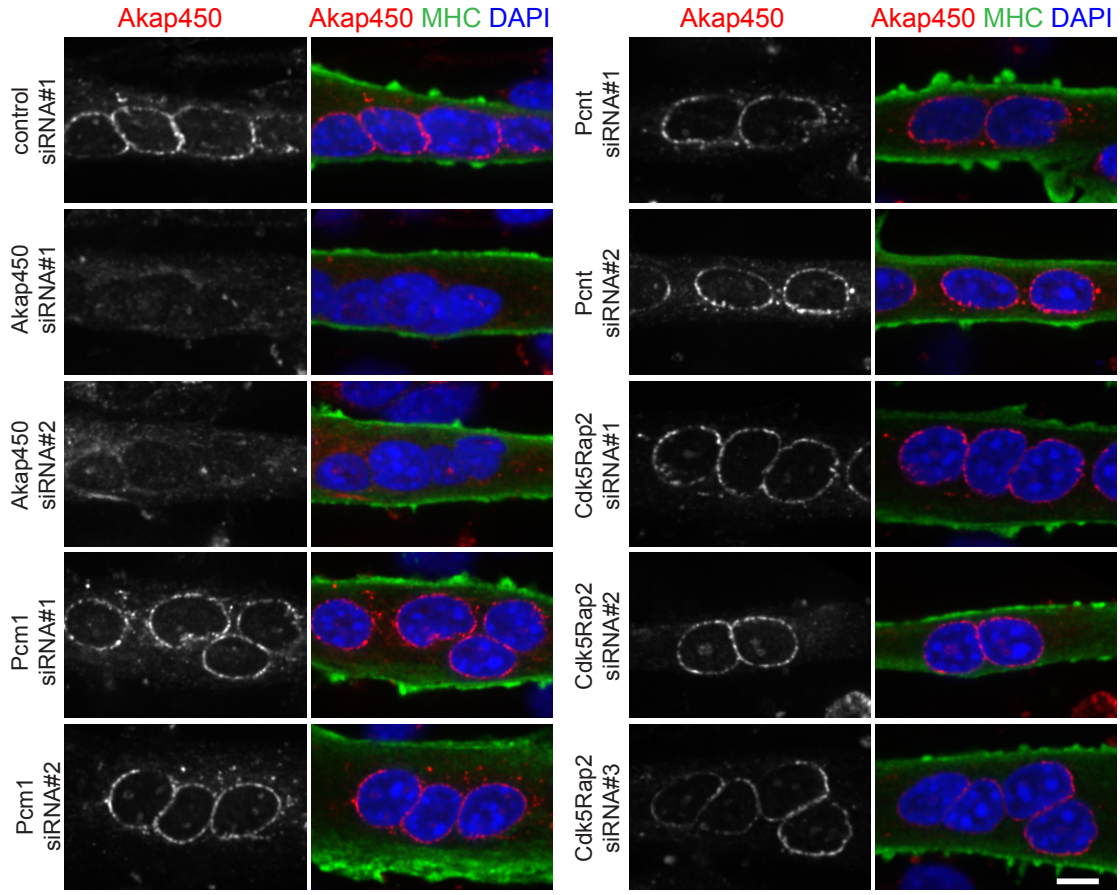

Figure 3.12: Akap450 is recruited to the NE independently of Pcm1, Pcnt or Cdk5Rap2. Representative fluorescence images of 48 h differentiated C2C12 myotubes, transfected with control siRNA#1, two different siRNAs for Akap450, two different siRNAs for Pcm1, two different siRNAs for Pericentrin (Pcnt) or three different siRNAs for Cdk5Rap2. Cells were stained for Akap450 (red), nuclei (DAPI, blue) and myosin heavy chain (MHC, green) to identify differentiated myotubes. n = 4 independent experiments. Scale bar, 10 μm.

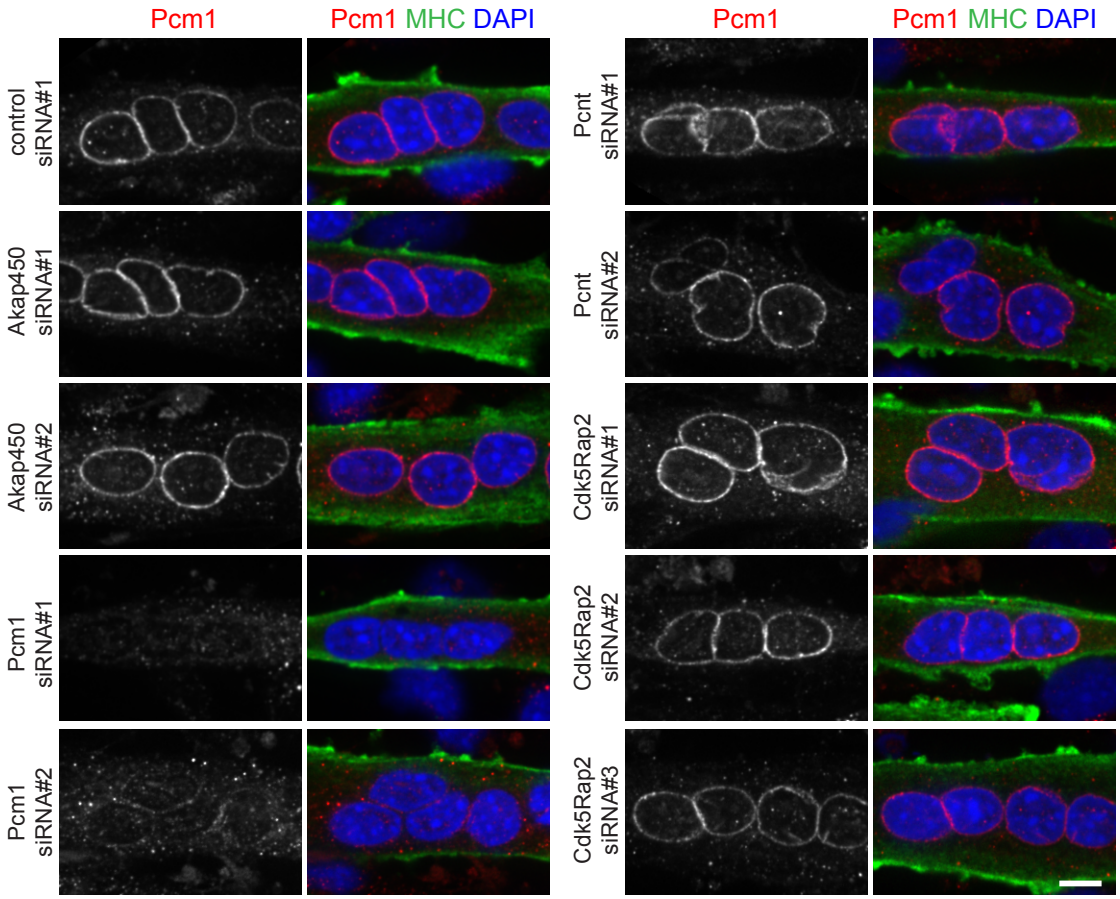

Figure 3.13: Pcm1 is recruited to the NE independently of Akap450, Pcnt or Cdk5Rap2. Representative fluorescence images of 48 h differentiated C2C12 myotubes, transfected with control siRNA#1, two different siRNAs for Akap450, two different siRNAs for Pcm1, two different siRNAs for Pcnt or three different siRNAs for Cdk5Rap2. Cells were stained for Pcm1 (red), nuclei (DAPI, blue) and myosin heavy chain (MHC, green) to identify differentiated myotubes. n = 4 independent experiments. Scale bar, 10 μm.

Similar results were obtained, when we determined NE localization of Pcm1 in comparison to control or Pcm1-depleted cells (Figure 3.13). None of the other siRNA-mediated depletions had an obvious effect on Pcm1 localization to the NE. However, knockdown of Pcm1 seemed to affect NE localization of Pericentrin as assessed by the decreased nuclear rim staining compared to control myotubes (Figure 3.14), while knockdown of Akap450 or Cdk5Rap2 had no effect on Pericentrin NE localization.

Nuclear rim staining of Cdk5Rap2 was very weak even in C2C12 myotubes treated with non-targeting control siRNA but was clearly decreased upon silencing for Cdk5Rap2 itself (Figure 3.15). While Cdk5Rap2 localization to the nucleus was unaffected in Akap450- or Pcm1-depleted myotubes and comparable to the respective

control, Cdk5Rap2 nuclear rim staining was apparently decreased in Pericentrin-depleted cells.

Collectively, these data show that Akap450 and Pcm1 are recruited to the nucleus independently of the other centrosomal proteins investigated here. Contrarily, NE localization of Pericentrin most likely depends on the presence of Pcm1, while Cdk5Rap2 in turn is dependent on Pericentrin localization to the nucleus. Thus, we assume that some centrosomal proteins might be directly recruited to the NE by the LINC complex or by other unknown adaptor proteins, while others possibly rely on mutual interactions with other centrosomal proteins.

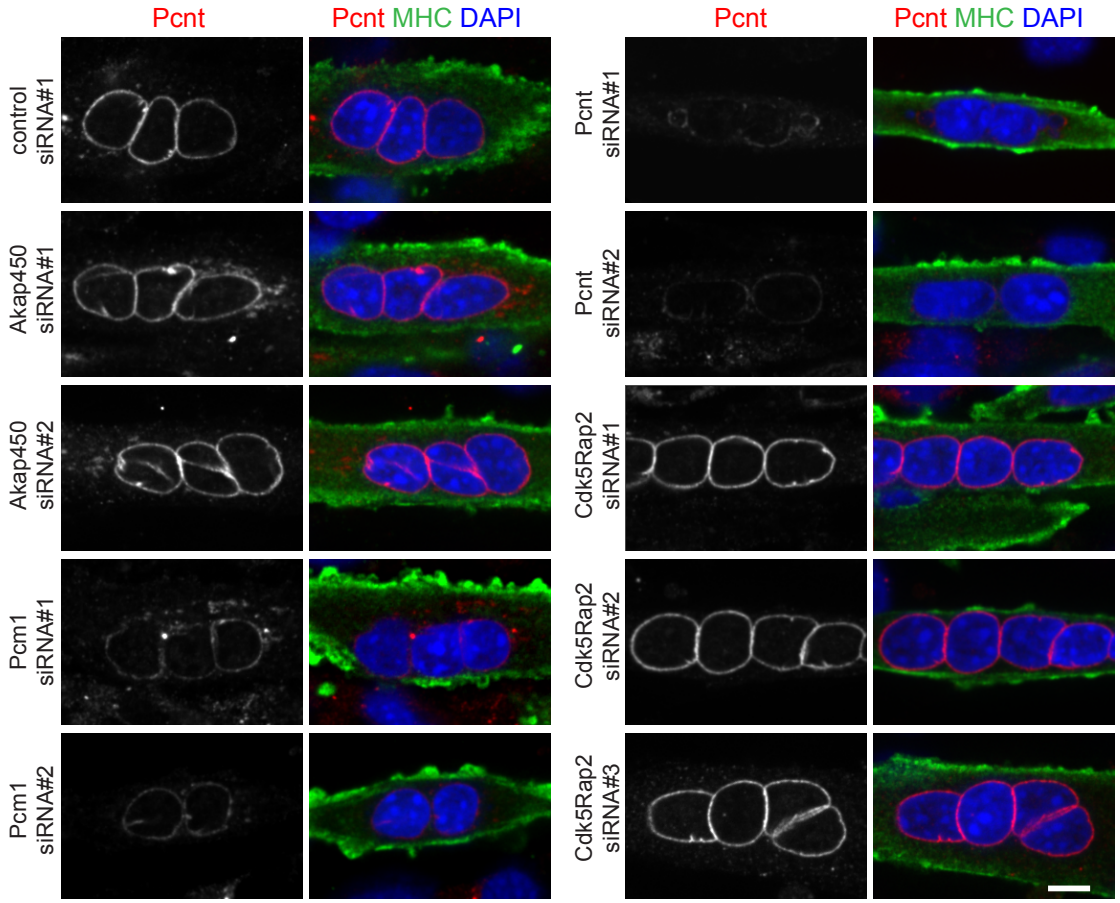

Figure 3.14: Pcnt recruitment to the NE requires Pcm1 but is independent of Akap450 or Cdk5Rap2. Representative fluorescence images of 48 h differentiated C2C12 myotubes, transfected with control siRNA#1, two different siRNAs for Akap450, two different siRNAs for Pcm1, two different siRNAs for Pcnt or three different siRNAs for Cdk5Rap2. Cells were stained for Pericentrin (Pcnt, red), nuclei (DAPI, blue) and myosin heavy chain (MHC, green) to identify differentiated myotubes. n = 4 independent experiments. Scale bar, 10 μm.

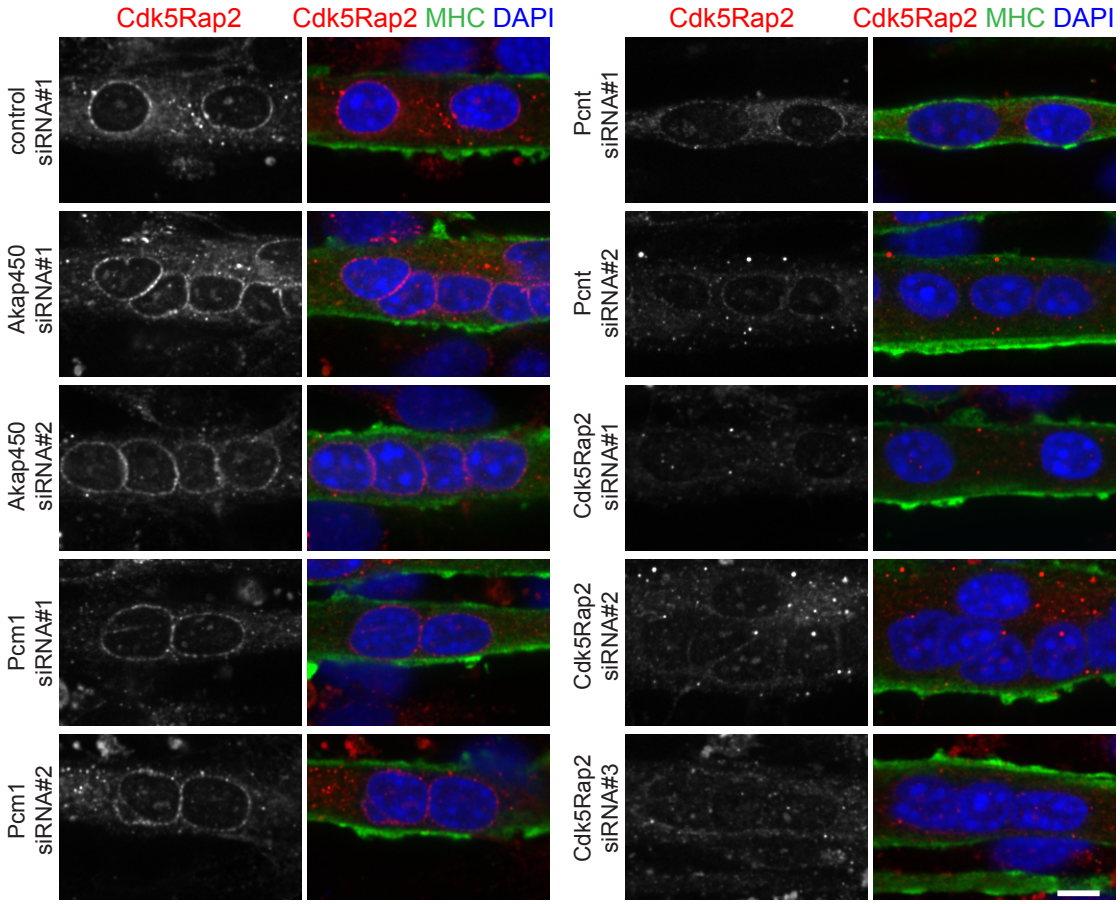

Figure 3.15: Cdk5Rap2 recruitment to the NE is dependent on Pcnt but independent of Akap450 or Pcm1. Representative fluorescence images of 48 h differentiated C2C12 myotubes, transfected with control siRNA#1, two different siRNAs for Akap450, two different siRNAs for Pcm1, two different siRNAs for Pcnt or three different siRNAs for Cdk5Rap2. Cells were stained for Cdk5Rap2 (red), nuclei (DAPI, blue) and myosin heavy chain (MHC, green) to identify differentiated myotubes. n = 4 independent experiments. Scale bar, 10 μm.

3.4 Involvement of Nesprin-1α in NE localization of centrosomal proteins

During muscle formation, Nesprin-1 giant has been reported to be mostly replaced by dominant expression of smaller isoforms (Randles et al., 2010). Thereby, Nesprin-1α has been demonstrated to be predominantly expressed in cardiac and skeletal muscle and to be highly increased, both on mRNA and protein levels, during skeletal muscle differentiation (Duong et al., 2014; Holt et al., 2016; Rajgor et al., 2012; Warren et al., 2005; Zhang et al., 2001). As the biological function for this muscle-specific isoform remained uncertain so far, we were interested if Nesprin-1α could be the dominant isoform implicated in the recruitment of Pericentrin and other centrosomal

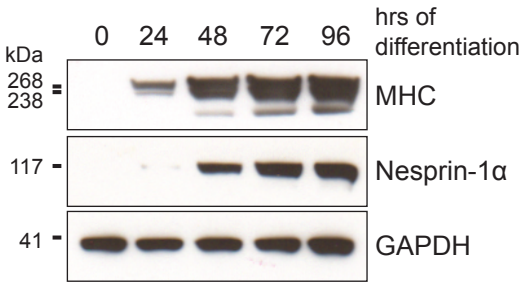

Figure 3.16: Nesprin-1α is upregulated during myogenic differentiation. C2C12 cells were differentiated for 0, 24, 48, 72, and 96 hours (hrs) in Differentiation Medium. Cell lysates were analyzed by SDS-PAGE and Western Blot using antibodies against Nesprin-1α/Nesprin-1 (MANNES1E mAb), myosin heavy chain (MHC) as a marker for differentiation and GAPDH as loading control.

proteins to the NE.

3.4.1 Nesprin-1α expression increases during myogenic differentiation

To test whether Nesprin-1α expression was also increased in C2C12 cells, we examined Nesprin-1α protein levels during myogenic differentiation. On the protein level, expression of Nesprin-1α was firstly detected after 48 hours of differentiation and further increased with time together with the differentiation marker myosin heavy chain (MHC).

Next, we wanted to uncover if centrosomal proteins were associated with Nesprin-1α during muscle formation. To this extent, we created in collaboration with Prof. Brian Burke's laboratory (Dr. Alessandra Calvi, Institute of Medical Biology, A*STAR, Singapore) a C2C12 cell line stably expressing doxycycline-inducible myc-BirA*-Nesprin-1α and took advantage of the proximity-dependent biotin identification method (BioID).

3.4.2 BioID identifies Akap450, Pcnt, and Pcm1 to be associated with Nesprin-1α in myotubes

BioID coupled to mass spectrometry is a novel and powerful approach to study protein-protein interactions in a natural cellular environment by determining biotinylated proteins in close proximity to a fusion protein (Roux et al., 2013, 2012). BioID is especially advantageous for transmembrane or highly insoluble proteins as standard biochemical approaches are often limited due to protein insolubility or weak protein interaction. This technique is based on a 35 kDa *Escherichia coli* biotin protein ligase, BirA, fused to a protein of interest (here mycBirA*-Nesprin-1α). BirA catalyzes firstly the formation of biotinoyl-5'-AMP (bioAMP) from biotin and adenosine triphosphate (ATP) and secondly the reaction of bioAMP with a

lysine residue of a target peptide. Within the BioID system, a specific BirA mutant (R118G; referred hereafter as BirA*) is used which prematurely releases bioAMP and therefore allows biotinylation of proteins based on proximity, regardless of any target sequence. When myc-BirA*-Nesprin-1α is expressed in mammalian cells, proteins that are close to or directly interacting with Nesprin-1α should be biotinylated upon addition of biotin (Figure 3.17). After cell lysis and biotin affinity capture using streptavidin-conjugated beads, all biotinylated proteins can then be identified by mass spectrometry analysis.

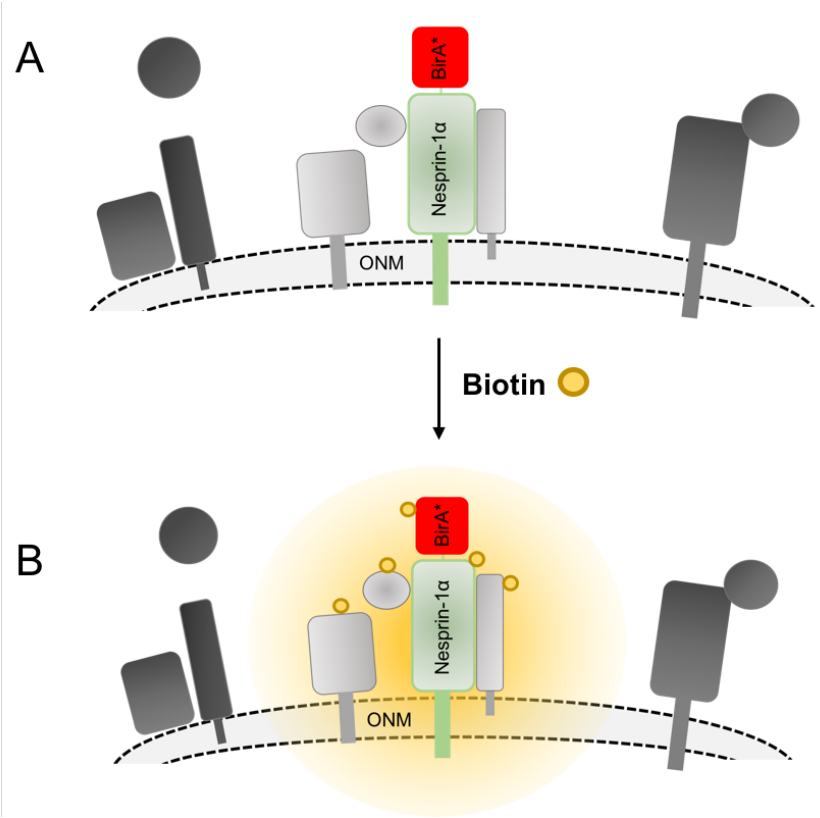

Figure 3.17: Model for BioID applied to BirA*-Nesprin-1α. (A) The promiscuous biotin-ligase fusion protein, BirA*-Nesprin-1α, is expressed in mammalian cells and ideally localizes to the outer nuclear membrane (ONM) as expected from its endogenous counterpart. **(B)** Upon addition of biotin, proteins will be biotinylated if they are directly interacting with BirA*-Nesprin-1α or if they are in close proximity (proteins depicted in light grey). In contrast, non-vicinal proteins (proteins depicted in dark grey) outside of the bioAMP diffusion radius (yellow circle) will not be biotinylated. Scheme is not drawn to scale.

We applied the BioID method to C2C12 cells stably and doxycycline-inducibly expressing mycBirA*-Nesprin-1α (Figure 3.18 A) to determine Nesprin-1α-associated or interacting proteins. Firstly, we confirmed that mycBirA*-Nesprin-1α is properly

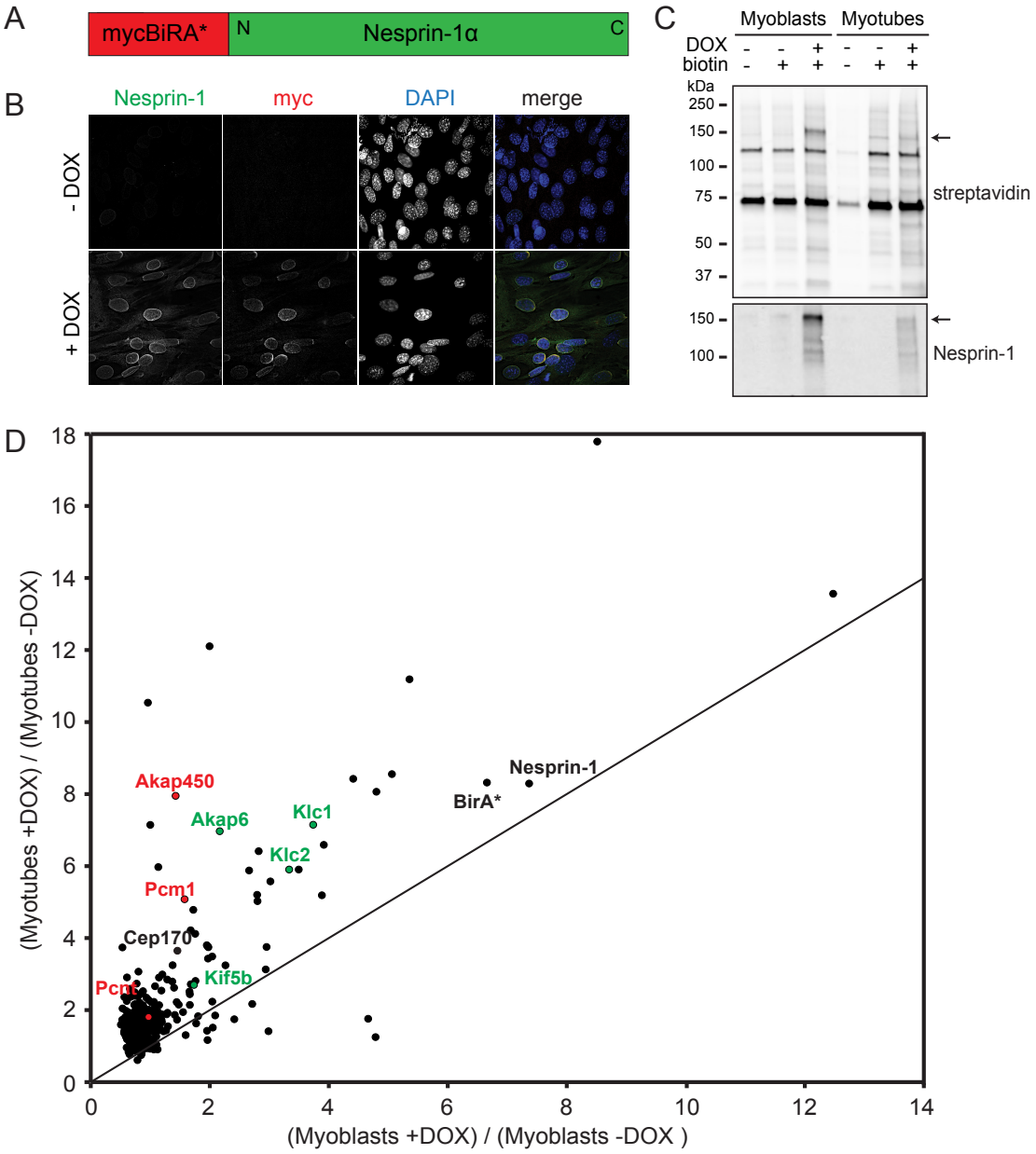
A
mycBiRA*
N
Nesprin-1α
C
B
Nesprin-1
myc
DAPI
merge
- DOX
+ DOX
C
Myoblasts
Myotubes
DOX
biotin
kDa
250
150
100
75
50
37
streptavidin
Nesprin-1
D
(Myotubes +DOX) / (Myotubes -DOX)
(Myoblasts +DOX) / (Myoblasts -DOX)
Nesprin-1
BirA*
Akap450
Akap6
Klc1
Klc2
Pcm1
Cep170
Kif5b

Figure 3.18: BioID identifies Akap450, Pcnt and Pcm1 as Nesprin-1α-vicinal proteins in myotubes. (A) Schematic representation of the construct used for the BioID experiment. Myc-BirA* was fused to the N-terminal part of Nesprin-1α (BioID-Nesprin-1α). *This construct has been designed and cloned by Dr. Alessandra Calvi, Institute of Medical Biology, A*STAR, Singapore.* **(B)** Non-differentiated C2C12 cells stably expressing doxycycline-inducible myc-BirA*-Nesprin-1α were treated with (+ DOX) or without (- DOX) doxycycline, fixed and stained for Nesprin-1 (green, clone 9F10), myc (red) or nuclei (DAPI, blue). Scale bar, 20 μm. *This experiment as well as image preparation was performed by Dr. Yin Loon Lee, Institute of Medical Biology, A*STAR, Singapore.* **(C)** C2C12 myoblasts or myotubes stably expressing myc-BirA*-Nesprin-1α were treated with or without doxycycline and biotin, harvested and subjected to immunoprecipitation using streptavidin-beads. Expression of myc-BirA*-Nesprin-1α after doxycycline addition was confirmed by Western Blot using anti-Nesprin-1 (clone 9F10) antibody. Biotinylated proteins were detected using fluorescent conjugates of streptavidin. Arrows point to BioID-Nesprin-1α. *Western Blot analysis was performed by Petra Gimpel and Dr. Yin Loon Lee.* **(D)** Depicted are normalized quantities of proteins purified on streptavidin beads in BioID-Nesprin-1α-expressing C2C12 myotubes (Y-axis) and myoblasts (X-axis) treated with biotin (+biotin). Each protein quantity is the ratio of the amount of a protein in cells treated with doxycycline (+DOX) to the amount from untreated cells (-DOX), as determined by tandem mass tag quantitative mass spectrometry following streptavidin affinity purification. Proteins in green are previously described binding partners of Nesprin-1α or Nesprin-1, while proteins shown in red are known centrosomal proteins investigated in this study.
Please see also Appendix, Chapter 6, Table S2 for a complete list of all results. *Mass spectrometry analysis and data processing was performed by Dr. Radoslaw M. Sobota at the Institute of Molecular and Cell Biology, Agency for Science, Technology and Research (A*STAR) in Singapore. Graphical illustration was done by Dr. Bruno at the Center for Research in Myology in Paris, France.*

localizing to the NE in C2C12 myoblasts after addition of doxycycline (Figure 3.18 B). Subsequently, we induced the expression of mycBirA*-Nesprin-1α in C2C12 myoblasts and myotubes in the presence of biotin to compare Nesprin-1α-associated proteins during myogenic differentiation. For control samples, both C2C12 myoblasts and myotubes were treated without doxycycline and without biotin (-DOX -biotin) or with biotin only (-DOX + biotin), respectively. Following biotin affinity capture, we verified successful biotinylation and expression of mycBirA*-Nesprin-1α in both the myoblast and myotube samples (+DOX + biotin) by Western Blot analysis (Figure 3.18 C, arrows). Note that expression of mycBirA*-Nesprin-1α was reduced in myotubes compared to myoblasts and that the results obtained by mass spectrometry analysis were therefore normalized to the respective expression levels. Additionally, biotinylation of endogenous proteins (-DOX -biotin) was analyzed for myoblast and myotube samples using streptavidin (Figure 3.18 C). Thereby, proteins seemed to be less endogenously biotinylated in myotubes than in myoblasts. To account for induced biotinylation of proteins in the absence of doxycycline, resulting from some basal level expression of mycBirA*-Nesprin-1α, we furthermore determined the biotinylation status in myoblasts and myotubes treated with biotin only (-DOX +biotin, Figure 3.18 C). While biotin-induced biotinylation (-DOX + biotin) was

comparable to the amount of endogenously biotinylated proteins (-DOX -biotin) in myoblasts, total biotinylation in the presence of biotin (-DOX +biotin) was increased compared to untreated conditions (-DOX -biotin) in myotubes. However, most importantly, Western Blot analysis revealed increased levels of biotinylated proteins in the presence of biotin when mycBirA*-Nesprin-1α was expressed in both the myoblast and myotube condition (+DOX +biotin).
To determine and quantify all selectively isolated proteins of control (-DOX -biotin; -DOX +biotin) and experimental samples (+DOX +biotin) in myoblasts and myotubes, we used tandem mass tag labelling and mass spectrometry analysis. After normalization according to different bait (mycBirA*-Nesprin-1α) expression levels, we calculated the ratio of each identified peptide in cells treated with doxycycline and biotin (+DOX +biotin) to the amount from cells treated with biotin only (-DOX -biotin). By illustrating these protein quantities from myotubes over myoblasts, we were able to identify overall 446 proteins in at least two out of three experiments, which showed increased association with mycBirA*-Nesprin-1α during myogenic differentiation (Figure 3.18 D). Among the strongest hits, were previously described interactors, including muscle A-kinase anchoring protein (mAkap, also known as Akap-6), kinesin light chains 1 and 2 (Klc1/2) and Kif5b which have been reported to localize to the nucleus in a Nesprin-1α or Nesprin-1 dependent manner, respectively (Pare et al., 2005; Wilson and Holzbaur, 2015). Remarkably, we further determined four centrosomal proteins, Akap450, Pcm1, centrosomal protein 170 (Cep170) and Pericentrin which were highly associated with myc-BirA*-Nesprin-1α in myotubes. Taken together, these data confirm that Nesprin-1α might be the relevant isoform at the NE for binding centrosomal proteins during myogenic differentiation.

3.4.3 Nesprin-1α is involved in binding of the PACT domain

To further strengthen a possible role for Nesprin-1α in recruiting centrosomal proteins to the nucleus in muscle cells, we overexpressed dsRed-PACT together with GFP-Nesprin-1α or GFP, respectively, in C2C12 myoblasts. Thereby, we identified non-differentiated cells by co-staining for Myogenin (not shown) and analyzed the percentage of cells showing dsRed-PACT at the NE. In GFP-expressing non-differentiated C2C12 myoblasts, dsRed-PACT localized exclusively to the centrosome (Figure 3.19 A, B). By contrast, in GFP-Nesprin-1α-expressing cells, dsRed-PACT localized to the centrosome and additionally to the NE in about 30% of non-differentiated C2C12 myoblasts.
This indicates that Nesprin-1α is important for NE localization of centrosomal proteins. However, the recruitment process seems to be temporarilly coordinated during

myogenic differentiation as only one-third and not the majority of non-differentiated cells displayed dsRed-PACT localization to the NE.

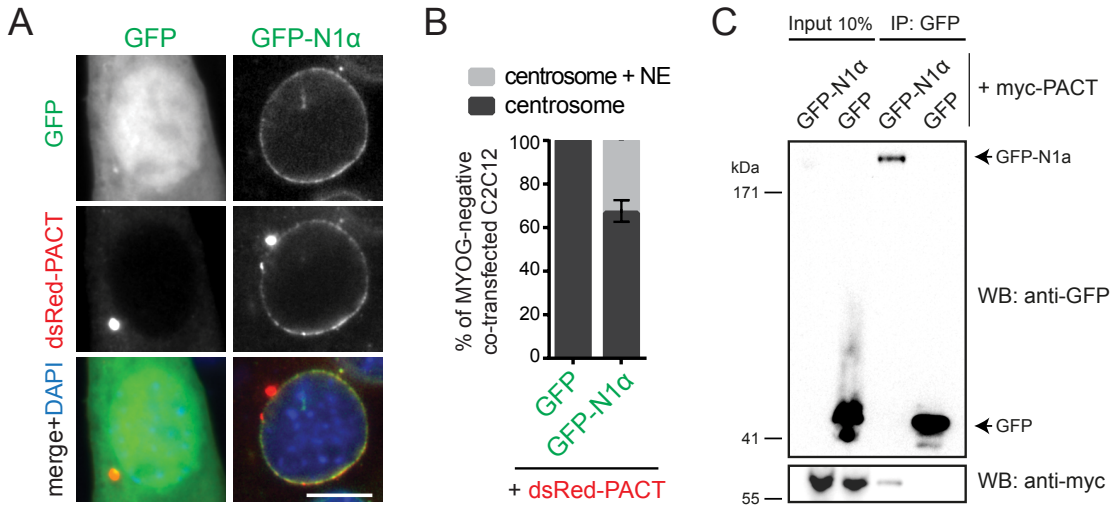

Figure 3.19: Nesprin-1α is sufficient to recruit the PACT domain to the nucleus. (A) Representative epi-fluorescence images of C2C12 myoblasts transfected with dsRed-PACT and GFP or GFP-Nesprin-1α, respectively. Cells were stained for nuclei (DAPI, blue) and Myogenin (not shown). Scale bar, 10 μm. **(B)** Quantification of dsRed-PACT recruitment to the NE in non-differentiated, Myogenin-negative C2C12 cells expressing GFP or GFP-Nesprin-1α (GFP-N1α), respectively. Error bars ± SD. n represents total number of nuclei from three independent experiments. **(C)** C2C12 cells were transfected with myc-PACT and GFP-Nesprin-1α (GFP-N1α) or GFP, respectively. After differentiation for two days, whole cell lysates were subjected to GFP immunoprecipitation (IP) and SDS-PAGE/ Western Blot (WB) analysis using anti-GFP and anti-myc antibodies.

To test if the PACT domain is sufficient to bring centrosomal proteins to the nucleus by binding to Nesprin-1α, we performed co-immunoprecipitation assays of differentiated C2C12 cells expressing myc-PACT and GFP-Nesprin-1α or GFP as a control (Figure 3.19 C). Although GFP-Nesprin-1α was hardly detectable in whole cell lysates (input), GFP-Nesprin-1α was clearly immunoprecipitated using GFP beads. Moreover, GFP-Nesprin-1α co-precipitated myc-PACT, while GFP alone did not.

This demonstrates that the PACT domain and thus most likely proteins such as Pericentrin and Akap450 harboring this domain, are found together with Nesprin-1α in one protein complex.

3.4.4 Nesprin-1α rescues Pericentrin and Akap450 mislocalization in Nesprin-1-depleted cells

To ultimately proof if the Nesprin-1α isoform is sufficient for recruiting centrosomal proteins to the NE, we used C2C12 cell lines stably depleted for NE-associated Nesprin-1 by CRISPR/Cas9 and reintroduced doxycycline-inducible mycBirA*-Nesprin-1α, the construct which we previously used for the BioID experiment (experiments were performed by Dr. Yin Loon Lee, Institute for Medical Biology, A*STAR, Singapore). In the absence of doxycycline, when Nesprin-1 was not expressed (-DOX), Pericentrin and Akap450 were not detected at the NE as in wild type cells but were mislocalized within the cytoplasm (Figure 3.20 A, C) in differentiated Myogenin-positive cells. In the presence of doxycycline (+DOX), when Nesprin-1α was expressed and present at the NE, Pericentrin and Akap450 localization to the NE was rescued (Figure 3.20 A-D, +DOX).
Taken together, these data establish a functional role for Nesprin-1α as a molecular receptor at the NE for binding centrosomal proteins during muscle formation.

3.5 Microtubule nucleation from the nucleus in differentiated muscle cells

Recruitment of centrosomal proteins to the NE has been proposed to be required for Microtubule (MT) nucleation from the nucleus in differentiated muscle cells (Tassin et al., 1985a). Therefore, we aimed to investigate if the identified molecular receptors for centrosomal proteins were also required for MT nucleation from the nucleus in differentiated myoblasts and myotubes.

3.5.1 The LINC complex is involved in MT nucleation from the NE

If MT nucleation from the nucleus depends on NE localization of centrosomal proteins, then based on our data, there should also be a requirement for Nesprin-1-containing LINC complexes. We thus set out to determine whether Nesprin-1 and Sun1/2 were involved in MT nucleation and organization from the nucleus during skeletal muscle formation.
Using 3D structured illumination microscopy (SIM), we first demonstrated that Pericentrin is localized to the ONM close to Nesprin-1α/Nesprin-1 and that MTs emanate from these complexes in differentiated C2C12 myoblasts (Figure 3.21).

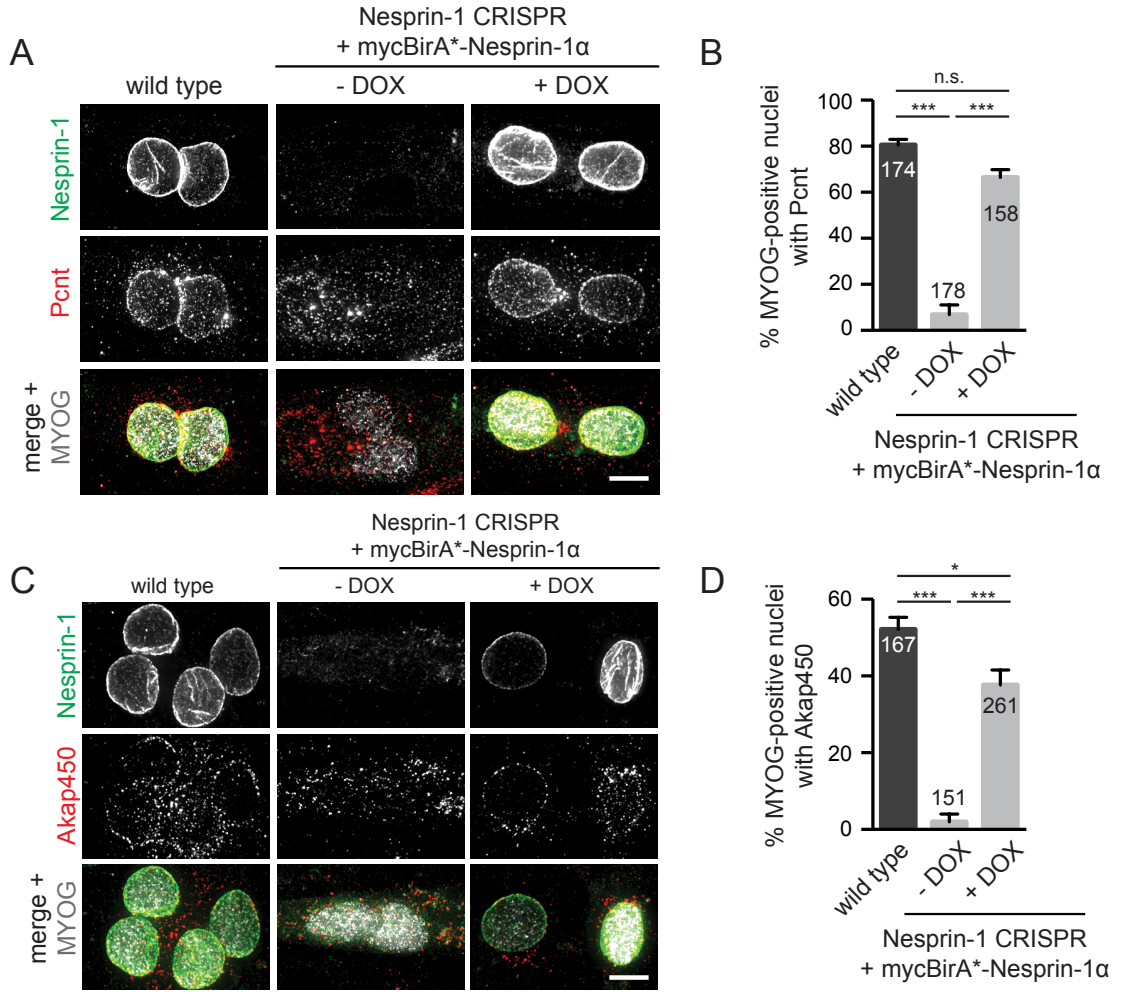

Figure 3.20: Reintroduction of Nesprin-1α in Nesprin-1-depleted cells rescues NE localization of Pericentrin and Akap450. (A) C2C12 wild type or Nesprin-1 CRISPR mutant cells transduced with mycBirA*-Nesprin-1α without and with 1 μg/ml doxycycline (±DOX) were differentiated for 48 h, fixed and stained for Nesprin-1 (green, clone 9F10), Pericentrin (Pcnt, red), and Myogenin (MYOG, grey) Scale bar, 10 μm. **(B)** Quantification of Pericentrin recruitment to the NE in Myogenin-(MYOG)-positive nuclei as described (A). Error bars ± SEM. n represents total number of nuclei from three independent experiments. ***p<0.001; n.s., not statistically significant, Tukey's multiple comparisons test following a one-way ANOVA. **(C)** C2C12 wild type or Nesprin-1 CRISPR mutant cells transduced with mycBirA*-Nesprin-1α without and with 1 μg/ml doxycycline (±DOX) were differentiated for 48 h, fixed and stained for Nesprin-1 (green, clone 9F10), Akap450 (red), and Myogenin (MYOG, grey) Scale bar, 10 μm. **(D)** Quantification of Akap450 recruitment to the NE in Myogenin (MYOG)-positive nuclei as described in (C). Error bars ± SEM. n represents total number of nuclei from three independent experiments. ***p<0.001, *p<0.05, one-way ANOVA with Tukey's multiple comparisons test.
*All experiments and quantifications shown in **(A)-(D)** were performed by Dr. Yin Loon Lee, Institute for Medical Biology, A*STAR, Singapore.*

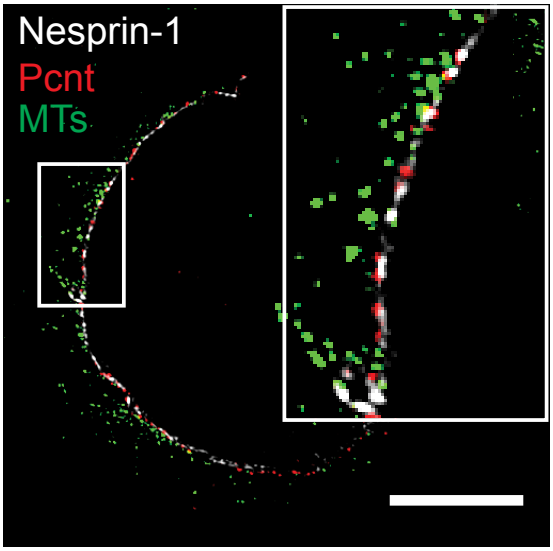

Figure 3.21: MTs emanate from foci containing Pericentrin and Nesprin-1α/ Nesprin-1. 3D-SIM fluorescent image of the nucleus of a differentiated C2C12 cell, stained for Nesprin-1α/ Nesprin-1 (white, MANNES1E mAb), Pericentrin (Pcnt, red) and microtubules (MTs, green) after nocodazole washout to allow MT regrowth. Scale bar, 5 μm.

Next, we explored how MTs are organized in C2C12 myotubes silenced for Nesprin-1, Sun1, Sun2 or both Sun1/2 by performing immunofluorescent stainings. In control myotubes, we observed a dense array of longitudinal MTs as previously described by Tassin et al. (Figure 3.22 A, untreated). Overall, this longitudinal MT array was not altered by any of these siRNA mediated depletions, while Pericentrin localization was similarly affected as described above.

However, due to the compact and highly dense network of MTs, it was impossible to determine small changes of MT organization at the level of the nucleus. Therefore, we turned to MT regrowth assays to monitor the starting points of MT nucleation after complete MT depolymerization using nocodazole. In the presence of nocodazole, MTs were depolymerized in all conditions, whereas Pericentrin localization per se was not affected (Figure 3.22 A, nocodazole). After nocodazole-washout, more than 60% of differentiated, Myogenin-positive, control cells displayed MT regrowth from the NE and additionally from seeds within the cytoplasm (Figure 3.22 B, C). In contrast, silencing for Nesprin-1 resulted in significantly decreased MT regrowth from the NE but did not impair MT nucleation from Pericentrin-positive cytoplasmic seeds. Similarly, we observed a reduction of MT regrowth from the NE in Sun1/2-depleted C2C12 cells, while depletion of Sun1 or Sun2 alone had little or no effect on overall MT regrowth. Interestingly, we noticed in cells transfected with Sun1 siRNA that MTs regrew from the NE at sites of Pericentrin displacement to the nuclear poles. This might again reflect a more pronounced role for Sun1 in localizing Pericentrin and thus MT nucleation to the NE in differentiated muscle cells.

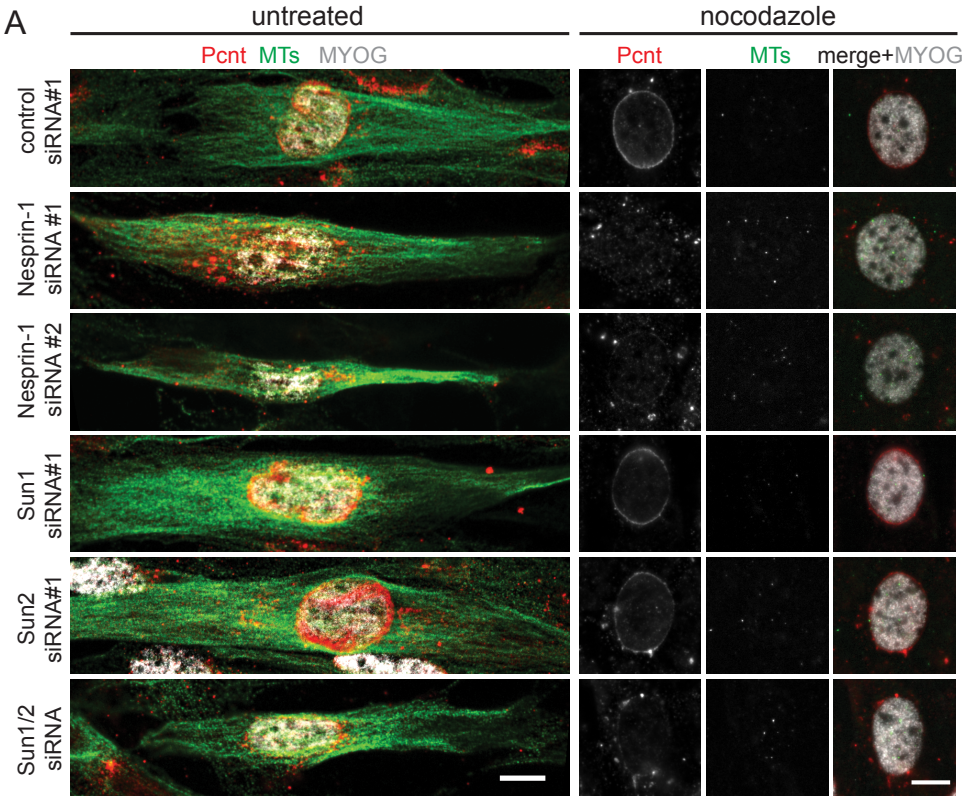
A
untreated
nocodazole
Pcnt MTs MYOG
Pcnt
MTs
merge+MYOG
control siRNA#1
Nesprin-1 siRNA #1
Nesprin-1 siRNA #2
Sun1 siRNA#1
Sun2 siRNA#1
Sun1/2 siRNA

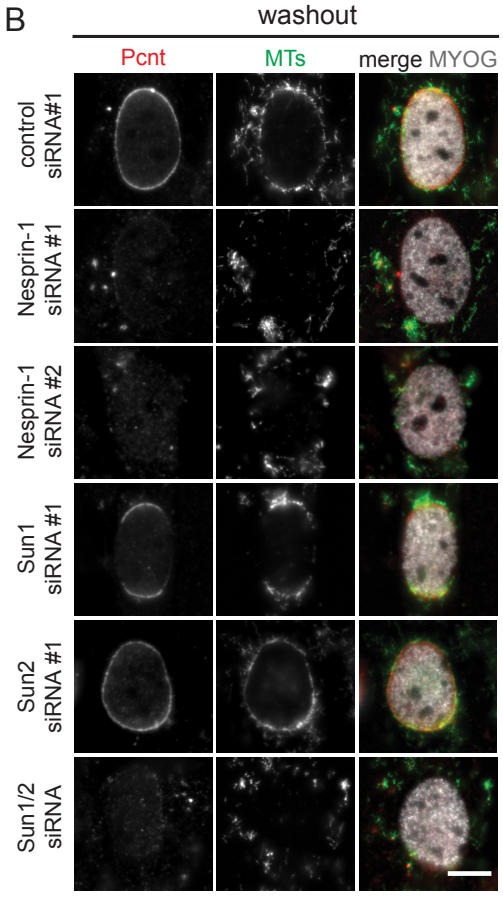
B
washout
Pcnt
MTs
merge MYOG
control siRNA#1
Nesprin-1 siRNA #1
Nesprin-1 siRNA #2
Sun1 siRNA #1
Sun2 siRNA #1
Sun1/2 siRNA

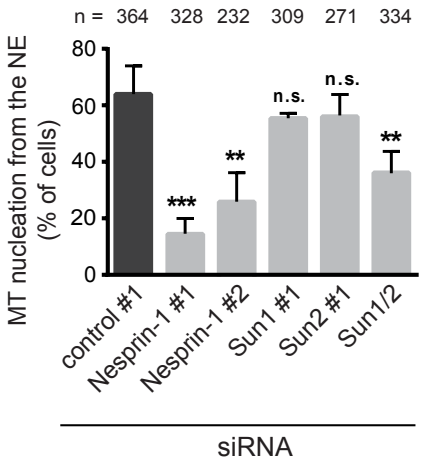
C
n = 364 328 232 309 271 334
MT nucleation from the NE (% of cells)
80
60
40
20
0
***
**
n.s.
n.s.
**
control #1
Nesprin-1 #1
Nesprin-1 #2
Sun1 #1
Sun2 #1
Sun1/2
siRNA

Figure 3.22: MT nucleation from the NE requires Nesprin-1 and Sun1/2. (A) 48 h differentiated C2C12 cells, treated with control siRNA#1, two different siRNAs to Nesprin-1 (Nesprin-1 #1 or Nesprin-1 #2), Sun1, Sun2 or both Sun1 and Sun2 (Sun1/2) siRNAs, were incubated with or without (untreated) nocodazole and immunostained for Pericentrin (Pcnt, red), microtubules (MTs, green) and Myogenin (MYOG, grey). Scale bar, 10 μm. **(B)** 48 h differentiated C2C12 cells, treated with control siRNA#1, two different siRNAs to Nesprin-1 (Nesprin-1 #1 or Nesprin-1 #2), Sun1, Sun2 or both Sun1 and Sun2 (Sun1/2) siRNAs, were immunostained for Pericentrin (Pcnt, red), microtubules (MTs, green) and Myogenin (MYOG, grey) after nocodazole washout. Scale bar, 10 μm. **(C)** Graph shows the mean percentage (%) of Myogenin-positive cells with MT nucleation from the NE as described in (B). Error bars ± SD. n represents total number of nuclei from at least three independent experiments. *** $p<0.001$; *$p<0.05$; n.s., not statistically significant, t-test.

In order to further validate the MT nucleation defects from the nucleus in Nesprin-1-depleted C2C12 cells, we performed the same MT regrowth assay in human wild type and *SYNE1 (23560 G>T)* patient cells. Thereby, we first confirmed that both wild type and *SYNE1 (23560 G>T)* patient myotubes exhibited longitudinal MT arrays (Figure 3.23 A, untreated), comparable to those observed in C2C12 myotubes. Treatment with nocodazole completely depolymerized MTs in wild type or *SYNE1 (23560 G>T)* patient cells but did not impact NE-associated or cytoplasmic localization of PCM1 (Figure 3.23 A, nocodazole). When MTs were let to recover after nocodazole-washout, more than 80% of Myogenin-positive nuclei of wild type myotubes nucleated MTs in a sun-like pattern from the nuclear surface (Figure 3.23 B, C). In comparison, in almost all *SYNE1 (23560 G>T)* patient myotubes, MT nucleation occurred from mislocalized PCM1-positive seeds within the cytoplasm but not from the NE.
Overall, these results strongly suggest a key role for the LINC complex, consisting of Nesprin-1 and Sun1/2, in MT nucleation from the NE through the recruitment of centrosomal proteins.

3.5.2 Akap450 is required for MT nucleation from the NE

Several centrosomal proteins were described in literature to be recruited to the NE during myogenic differentiation (Bugnard et al., 2005; Fant et al., 2009; Srsen et al., 2009). However, which of these centrosomal proteins are in turn required for MT nucleation from the NE remained uncertain so far.
To address this question, we focussed on centrosomal proteins known to be important for MT nucleation at the centrosome as well as on centrosomal proteins that were identified by BioID using mycBirA*-Nesprin-1α (Figure 3.18 D). Among these centrosomal proteins, Cep192 was shown to function as MT regulator through the

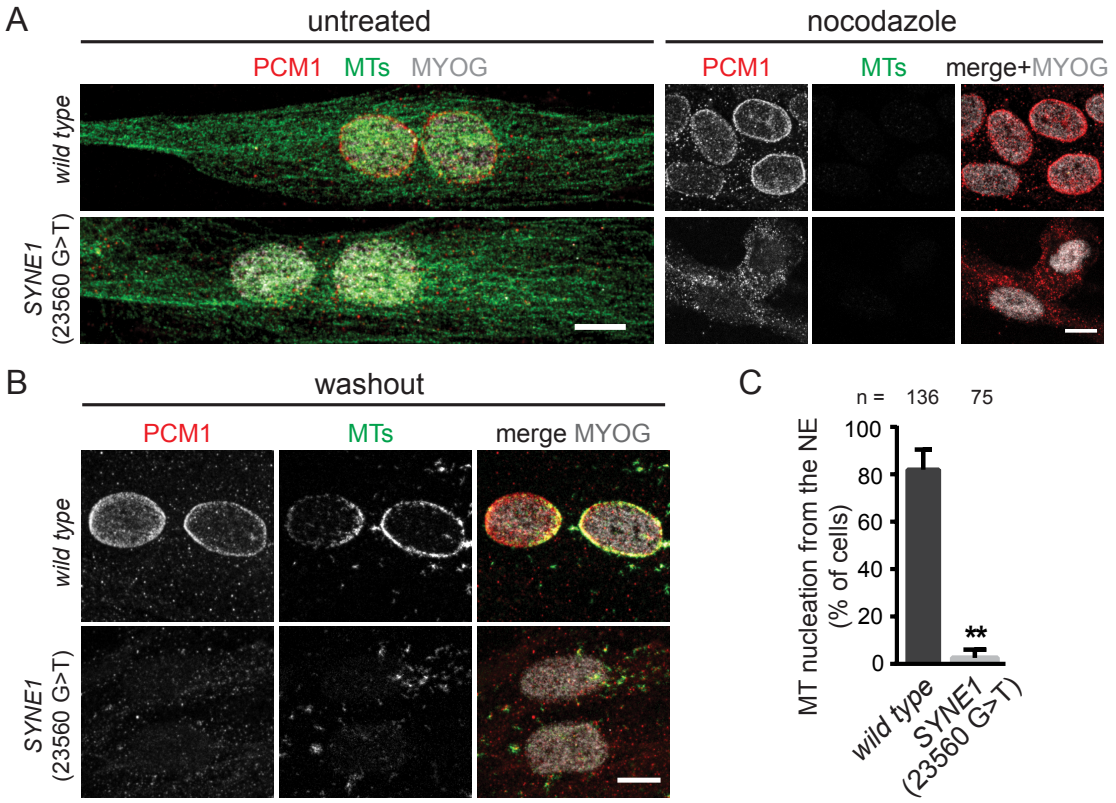

Figure 3.23: MT organization and nucleation in human wild type and *SYNE1 (23560 G>T)* patient myotubes. (A) Human immortalized myotubes from a healthy control (wild type) or from a patient carrying a nonsense mutation within the *SYNE1 (23560 G>T)* gene were treated with or without (untreated) nocodazole and immunostained for PCM1 (red), microtubules (MTs, green) and nuclei (DAPI, blue). Scale bar, 10 μm. **(B)** Differentiated human immortalized myotubes from a healthy control (wild type) or from a patient carrying a nonsense mutation within the *SYNE1 (23560 G>T)* gene were immunostained for PCM1 (red), microtubules (MTs, green) and Myogenin (MYOG, grey) after nocodazole washout. Images represent maximum projections of confocal z-sections. Scale bar, 10 μm. **(C)** Graph shows the mean percentage (%) of Myogenin-positive cells with MT nucleation from the NE as described in (B). Error bars ± SD. n represents total number of nuclei from two independent experiments. *** p<0.001; **p<0.05; n.s., not statistically significant, t-test.

recruitment of γ-tubulin at the onset of mitosis and more importantly to control centrosomal versus non-centrosomal MTs during interphase (O'Rourke et al., 2014; Yang and Feldman, 2015). Cdk5Rap2 was described to bind γ-tubulin ring complexes (γ-TuRC) and to activate γ-TuRC-mediated MT nucleation (Choi et al., 2010). Also Pericentrin and Akap450 were implicated in γ-TuRC-anchoring to centrosomes by binding to GCP2/GCP3 through their N-terminal domains (Takahashi et al., 2002). Solely Pcm1, which was identified by BioID of mycBirA*-Nesprin-1α was not described to be directly implicated in MT nucleation at the centrosome but in MT-dependent recruitment of centrosomal proteins (Dammermann and Merdes, 2002).

Before investigating if these centrosomal proteins were involved in MT nucleation from the NE, we first depleted C2C12 cells for γ-tubulin (Tubg1), Pericentrin, Cep192, or Cdk5Rap2, respectively, and analyzed their impact on Pericentrin localization or myotube formation during myogenic differentiation. While depletion of Cep192 slightly affected myogenic differentiation as assessed by the decreased fusion index, depletion of Cdk5Rap2 rather showed an opposite effect (Figure 3.24 A). However, none of these siRNA-mediated depletions had an impact on Pericentrin localization to the NE, when compared to control or Pericentrin siRNA conditions. Thereby, we confirmed efficient knockdown of γ-tubulin, Pericentrin and Cdk5Rap2 by Western Blot analysis (Figure 3.24 B, Figure 3.5 C) or immunofluorescent stainings (Figure 3.15 Cdk5Rap2 siRNA#1-3). Unfortunately, we did not further verify if Cep192 protein levels were efficiently decreased upon siRNA treatment due to the lack of commercially available antibodies.

Next, we analyzed the effect of Pericentrin, Cep192, or Cdk5Rap2 depletion on MT nucleation from the NE by performing MT regrowth assays in differentiated C2C12 cells (Figure 3.24 C, D). When we silenced C2C12 cells for γ-tubulin itself, both MT nucleation within the cytoplasm and MT regrowth from the NE were reduced. Nevertheless, the latter effect was not significant which might result from the way of quantification. As we just counted the number of Myogenin-positive cells with at least 50% of MT seeds at the NE, we would not reveal any defects regarding MT length or absolute numbers as observed upon γ-tubulin depletion. In cells treated with Pericentrin, Cep192 or Cdk5Rap2 siRNA, MT regrowth from the NE was not significantly altered and was comparable to control siRNA treated cells.

Because none of the known γ-TuRC-binding proteins at the centrosome, tested so far, displaced MT nucleation, we turned to analyze the requirement of centrosomal proteins identified by mycBirA*-Nesprin-1α BioID experiments for MT nucleation from the NE. In C2C12 cells silenced for Pericentrin or Pcm1, MTs regrew from the

NE to a similar extent as observed in control cells (Figure 3.25 A, B). Strikingly, cells treated with Akap450 siRNA showed significantly reduced MT regrowth from the NE and rather displaced MT nucleation to the cytoplasm. Note, that we confirmed efficient knockdown of Akap450, Pericentrin or Pcm1 using these sets of siRNAs by immunofluorescent stainings (Figure 3.12 Akap450 siRNA#1/2; Figure 3.14 Pcnt siRNA#1/2; Figure 3.13 Pcm1 siRNA#1/2).
Taken together, these results suggest a role for Akap450 as the dominant γ-TuRC-receptor at the NE in mediating MT nucleation from the nucleus during myogenic differentiation.

3.6 Nuclear positioning

During skeletal muscle formation, nuclear centration and nuclear spreading movements were demonstrated to depend on a functional MT network, on MT motor proteins, such as dynein and kinesin-1, as well as on MT-associated proteins (MAPs) (Cadot et al., 2015, 2012; Metzger et al., 2012; Wilson and Holzbaur, 2012, 2015). If active MT nucleation from the NE, however, is a prerequisite for proper nuclear positioning remained unanswered until now. To address this question we aimed to determine the impact of Nesprin-1-mediated MT nucleation from the NE via Akap450 on nuclear positioning.

3.6.1 Nesprin-1 is important for nuclear positioning

Nesprin-1 was already previously reported to be required for nuclear movement in skeletal muscle through the recruitment of kinesin-1 motor proteins to the nucleus (Chapman et al., 2014; Grady et al., 2005; Wilson and Holzbaur, 2015; Zhang et al., 2010, 2007c). Thereby, kinesin-1 anchored to the nucleus by Nesprin-1 was proposed to transport nuclei as a cargo along MTs in myotubes.
We confirmed that Nesprin-1 is involved in the distribution of skeletal muscle nuclei by analyzing the spreading factor in differentiated C2C12 cells transfected with non-targeting control or Nesprin-1-targeting siRNAs. The spreading factor is defined as the ratio between the observed and the maximal theoretical average distance between nuclei according to the myotube length (see section 2.7.3 for further details). In Nesprin-1-depleted myotubes, nuclei were less spread throughout the myotube and the spreading factor was significantly reduced when compared to control myotubes (Figure 3.26 A, B). Similar results were obtained when we analyzed the spreading factor in human control or *SYNE1 (23560 G>T)* patient myotubes (Figure 3.26 C-F). Nuclei of wild type myotubes were more evenly distributed throughout the

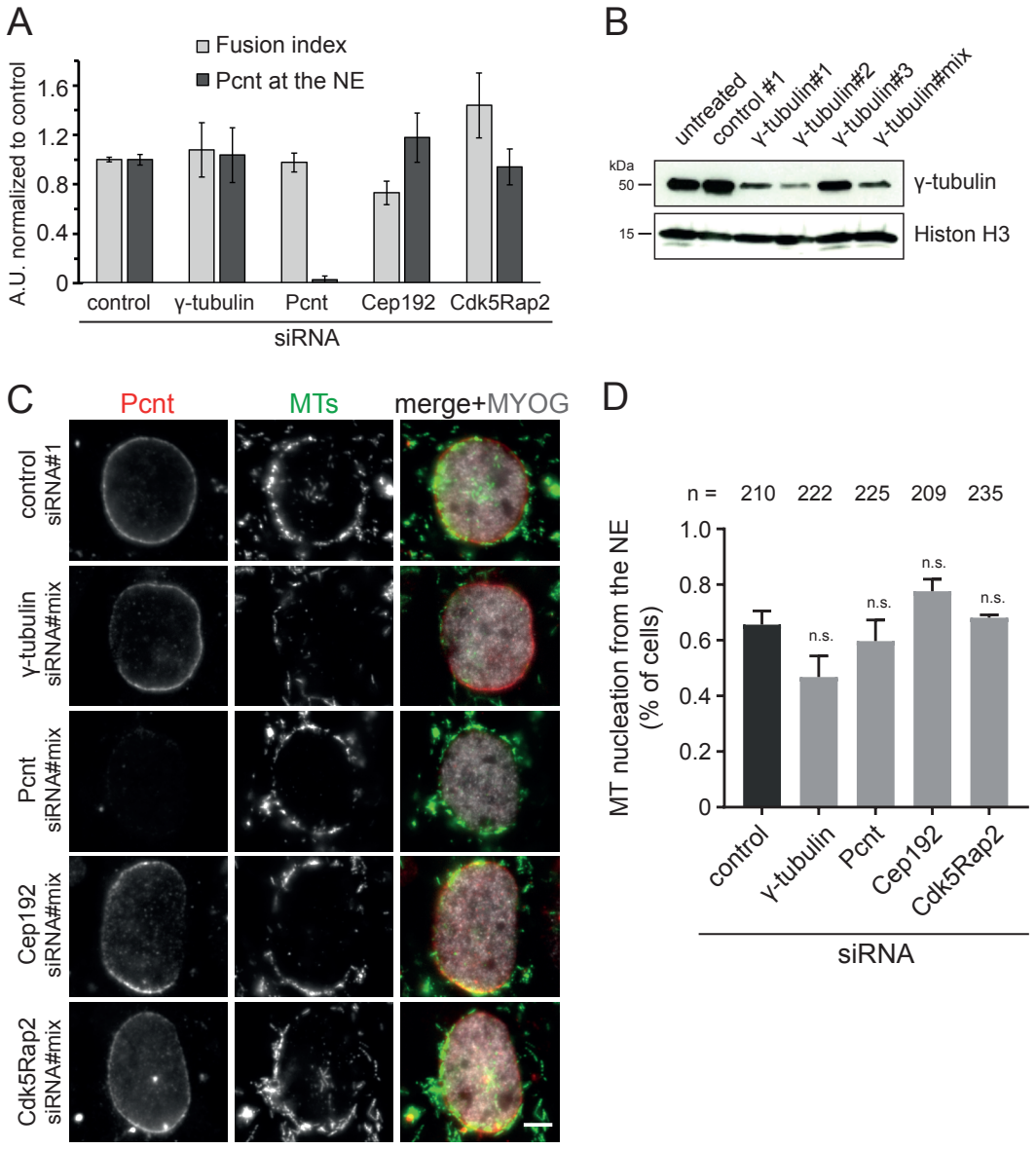

Figure 3.24: MT nucleation from the NE does not require Pcnt, Cep192, or Cdk5Rap2. **(A)** C2C12 myoblasts were transfected with non-targeting control siRNA#1, a mix of three siRNAs against γ-tubulin, a mix of two siRNAs against Pericentrin (Pcnt), a mix of three siRNAs against Cep192 or a mix of three siRNAs against Cdk5Rap2, respectively. 48 hours differentiated cells were immunostained for Pericentrin, myosin heavy chain (MHC), and nuclei (DAPI) and subsequently analyzed for fusion index and Pericentrin recruitment to the NE using CellProfiler. **(B)** C2C12 cells were treated without (untreated) or with non-targeting control siRNA #1, three single siRNAs against γ-tubulin (γ-tubulin#1, γ-tubulin#2, γ-tubulin#3) or with a mix of all three siRNAs against γ-tubulin (γ-tubulin#mix). Cells were differentiated for 48 hours and cell lysates were subjected to SDS-PAGE and Western Blot analysis using the indicated antibodies. **(C)** 48 hours differentiated C2C12 cells, treated with the indicated siRNAs, were immunostained for Pericentrin (Pcnt, red), microtubules (MTs, green) and Myogenin (MYOG, grey) after 8 min of nocodazole washout. Scale bar, 5 μm. **(D)** Graph shows the mean percentage (%) of Myogenin-positive cells with MT nucleation from the NE as described in (C). Error bars $\pm$ SD. n represents total number of nuclei from two independent experiments. n.s., not statistically significant, Mann-Whitney test.

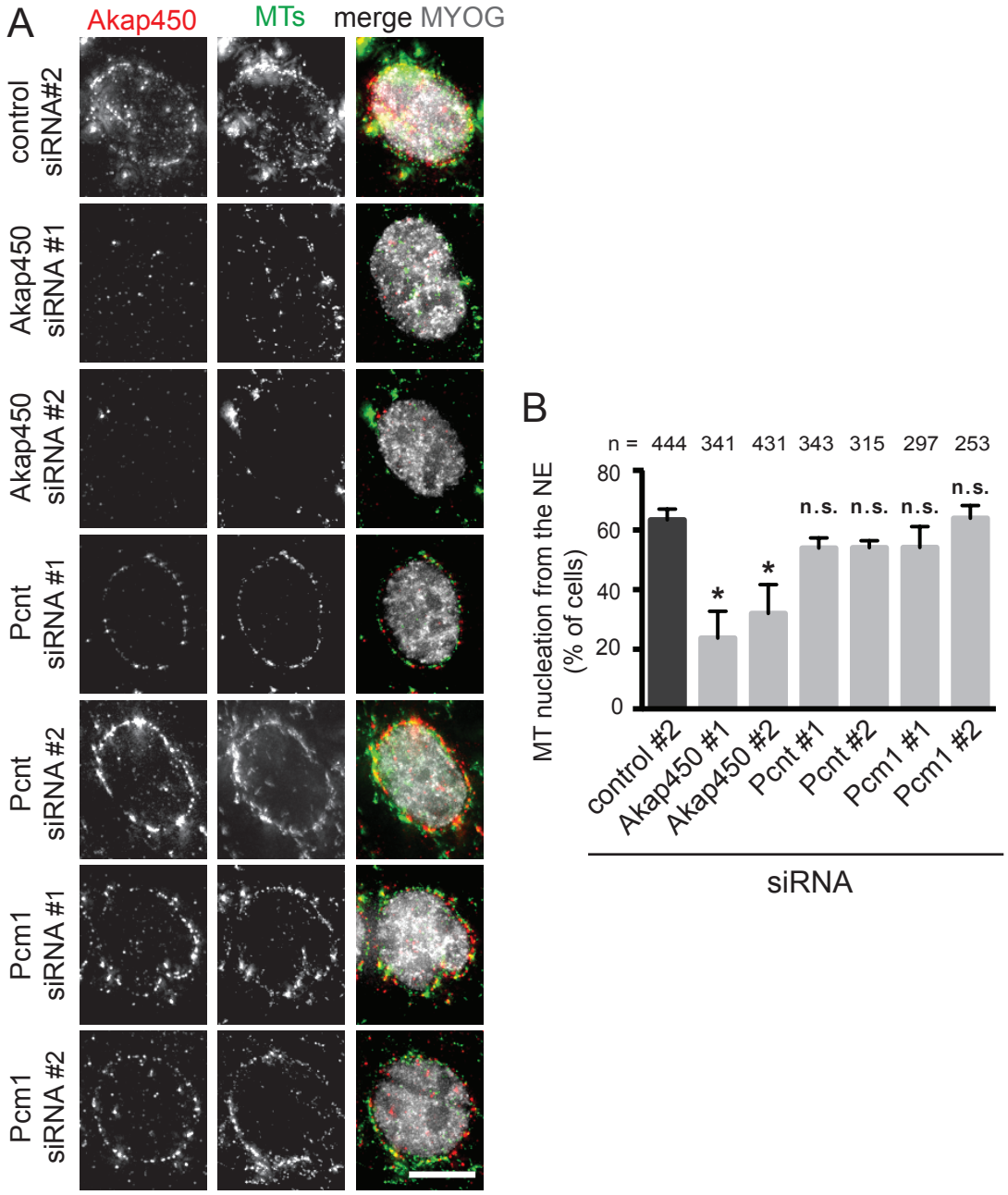

Figure 3.25: MT nucleation from the NE is mediated by Akap450. **(A)** 48 hours differentiated C2C12 cells, treated with control siRNA#2, two different siRNAs to Akap450 (Akap450 siRNA#1, Akap450 siRNA#2), Pericentrin (Pcnt #1, Pcnt#2) or Pcm1 (Pcm1#1, Pcm1#2) were immunostained for Akap450 (red), microtubules (MTs, green) and Myogenin (MYOG, grey) after nocodazole washout. Scale bar, 10 μm. **(B)** Graph shows the mean percentage (%) of Myogenin-positive cells with MT nucleation from the NE as described in (A). Error bars ± SEM. n represents total number of nuclei from two independent experiments. *p<0.05; n.s., not statistically significant, one-way ANOVA with Dunnett's multiple comparisons test.
*All experiments and quantifications shown in **(A)-(B)** were performed by Dr. Yin Loon Lee, Institute for Medical Biology, A*STAR, Singapore.*

myotube, while nuclei of *SYNE1 (23560 G>T)* patient myotubes predominantly clustered in the middle of the myotube (Figure 3.26 C, E, F). Additionally, *SYNE1 (23560 G>T)* patient myotubes showed a decreased spreading factor when compared to wild type myotubes (Figure 3.26 D).
Together, these results validate that Nesprin-1 is involved in nuclear positioning during muscle formation. However, global depletion of Nesprin-1 most likely prevents both kinesin-1 localization to the nucleus (Wilson and Holzbaur, 2015) and MT nucleation from the NE (section 3.5). Thus, it is impossible to evaluate by siRNA-mediated depletion of Nesprin-1 if the observed nuclear positioning defects arise from an absence of kinesin-1 motor proteins at the nucleus or from defective MT nucleation.

3.6.2 Cytosim as computational model for nuclear movement

To assess solely the impact of MT nucleation from the NE on nuclear positioning, we developed a computational model of nuclear movement in myotubes using the cytoskeleton simulation engine Cytosim (Nedelec and Foethke, 2007), in collaboration with Dr. François Nédélec, Cell Biology and Biophysics Unit, European Molecular Biology Laboratory, Germany, and Dr. Bruno Cadot, Center for Research in Myology, France. To set the simulation parameters, we first experimentally determined the myotube shape. Therefore, myotube areas of C2C12 cells were analyzed relatively to the number of nuclei per myotube and were then used to optimize myotubes generated by Cytosim (Figure 3.27 A). The elliptical myotube boundary was set to restrict movements of MTs, nuclei and centrosomes inside the myotube. To simulate MTs correctly, we analyzed overall MT organization using EB1-overexpressing C2C12 cells (Figure 3.27 B). EB1 is a plus-end-tracking protein that localizes to plus-ends of growing MTs and is therefore often used to track MTs in live-cell imaging experiments (Honnappa et al., 2009). Tracking and analyzing the angle of all EB1 comets relatively to the long axis of the myotube revealed that MTs were horizontally nucleated (Figure 3.27 C). In control simulations, MTs were thus set to be nucleated from the nucleus parallel to the long axis of the myotube. Additionally, nuclei harboured MT plus-end (Kif5b) and MT minus-end (dynein) directed motor proteins as described in literature (Cadot et al., 2012; Wilson and Holzbaur, 2015). MTs were furthermore allowed to interact with cytoplasmic MAP4 and Kif5b-MAP7 complexes to achieve MT sliding and anti-parallel MT organization as observed *in vitro* (Metzger et al., 2012; Mogessie et al., 2015). Using these minimal settings, we simulated nuclear movements within *in silico* myotubes (see Appendix 6, Table S1 for a complete list of simulation parameters). Nuclei moved dynamically and became

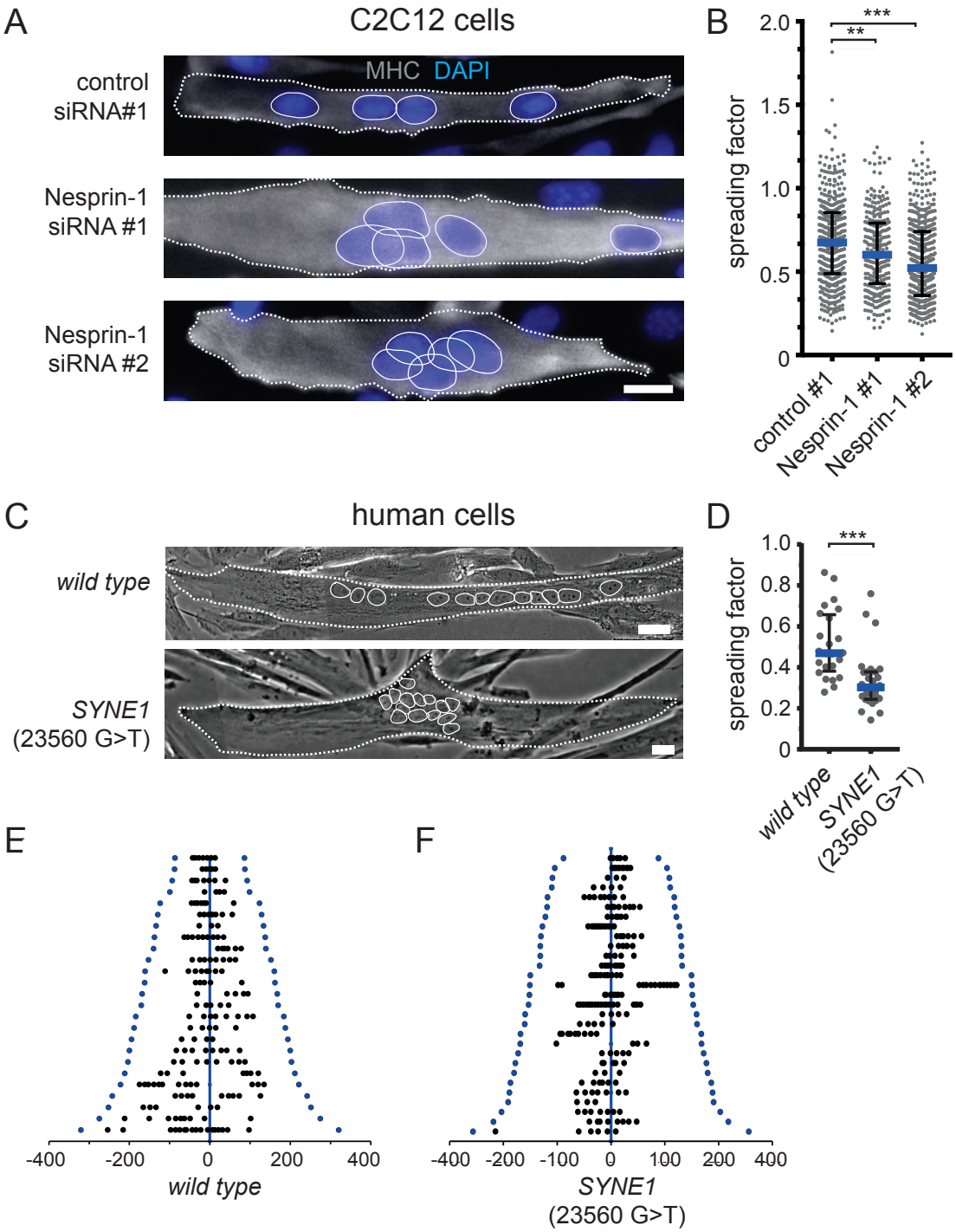
A
C2C12 cells
control siRNA#1
MHC DAPI
Nesprin-1 siRNA #1
Nesprin-1 siRNA #2
B
spreading factor
2.0
1.5
1.0
0.5
0
***
**
control #1
Nesprin-1 #1
Nesprin-1 #2
C
human cells
wild type
SYNE1 (23560 G>T)
D
spreading factor
1.0
0.8
0.6
0.4
0.2
0
***
wild type
SYNE1 (23560 G>T)
E
-400
-200
0
200
400
wild type
F
-400
-200
-100
0
100
200
400
SYNE1 (23560 G>T)

Figure 3.26: Nesprin-1 is required for nuclear positioning in muscle cells. (A) C2C12 cells were transfected with control siRNA#1 or two different siRNAs for Nesprin-1 (Nesprin-1 siRNA#1 or Nesprin-1 siRNA#2), differentiated for 48 hours and stained for nuclei (DAPI, blue) and myosin heavy chain (MHC, white). Myotube outlines are marked by dashed lines and nuclei are encircled. Scale bar, 20 μm. **(B)** Spreading factor analysis of nuclei in C2C12 myotubes as shown in (A). Results are depicted as median (blue line) with interquartile range (black bars) from three independent experiments. *** p<0.001, **p<0.05, Mann-Whitney test. **(C)** Representative images taken from live-cell imaging of differentiated human immortalized cells from a healthy control (wild type) or *SYNE1 (23560 G>T)* patient cells. Myotube outlines are marked by dashed lines and nuclei are encircled. Scale bar, 20 μm. **(D)** Spreading factor analysis of nuclei in human myotubes as shown in (C). Results are depicted as median (blue line) with interquartile range (black bars) from two independent experiments. *** p<0.001, Mann-Whitney test. **(E)** Two-dimensional representations of nuclear distributions in wild type or *SYNE1 (23560 G>T)* patient myotubes. Each myotube is represented on a single line with blue dots representing the myotube edges and black dots the nuclei. The blue line indicates the midline of the myotube. Note that all myotubes are arranged in descending order of the myotube length.

evenly dispersed along the long axis in simulated myotubes, when MT nucleation occurred from the NE and kinesin-1 motor proteins (Kif5b) were retained at the nucleus (Figure 3.27 D, F; MT from NE+, Kif5B at NE+). These computational nuclear movements strikingly resembled those observed in cultured myotubes and clearly recapitulated nuclear positioning events *in vitro*.
Next, we removed the MT nucleation activity from the NE and added it to centrosome-like structures randomly positioned in the cytoplasm, as observed in Nesprin-1-depleted myotubes *in vitro*. Under this condition, we kept Kif5b at the NE in order to analyze the impact on MT nucleation from the NE on nuclear positioning irrespectively of plus-end motor proteins. Strikingly, nuclei were found to cluster in the middle of the myotube or in small groups throughout the myotube (Figure 3.27 D, G; MT from NE-, Kif5B at NE+). Moreover, the spreading factor was significantly decreased in this situation when compared to control simulated myotubes (Figure 3.27 E). Finally, we simulated nuclear distribution in myotubes where we removed both MT nucleation activity and Kif5b from the NE. In this situation, nuclei further clustered in groups throughout the myotube and the spreading factor was decreased even more, when compared to removal of MT nucleation alone (Figure 3.27 D, E, H; MT from NE-, Kif5B at NE-).

Collectively, these simulations strongly support the hypothesis that MT nucleation from the NE is required for proper nuclear positioning in myotubes in addition to the recruitment of Kif5b/kinesin-1 to the NE.

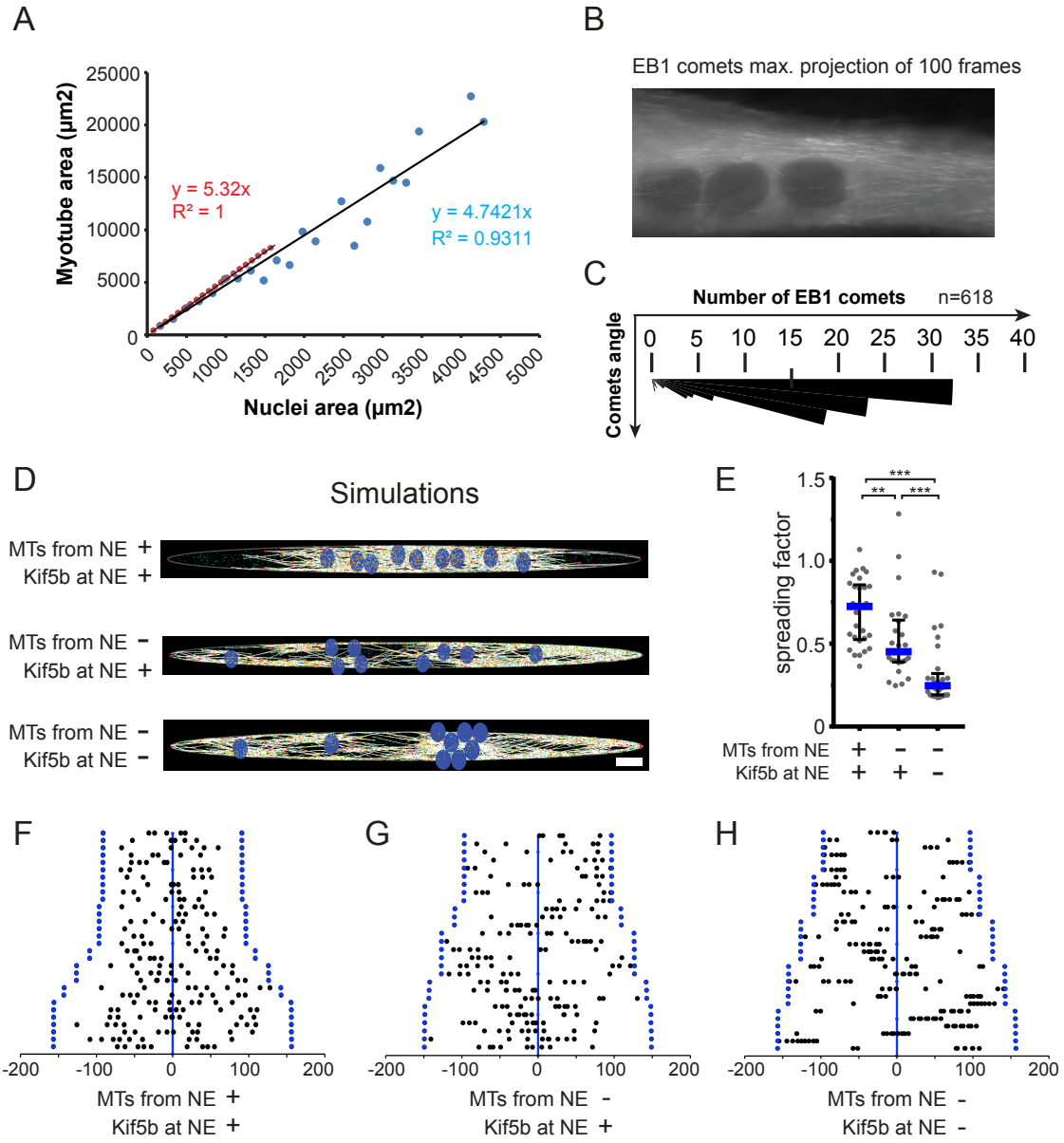
A
Myotube area (µm2)
Nuclei area (µm2)
y = 5.32x
R² = 1
y = 4.7421x
R² = 0.9311
B
EB1 comets max. projection of 100 frames
C
Number of EB1 comets
n=618
Comets angle
D
Simulations
MTs from NE +
Kif5b at NE +
MTs from NE −
Kif5b at NE +
MTs from NE −
Kif5b at NE −
E
spreading factor
MTs from NE + − −
Kif5b at NE + + −
F
MTs from NE +
Kif5b at NE +
G
MTs from NE −
Kif5b at NE +
H
MTs from NE −
Kif5b at NE −

Figure 3.27: MT nucleation from the NE is required for proper nuclear positioning. **(A)** The myotube area was plotted over the number of nuclei for C2C12 myotubes (blue dots) or for simulated myotubes generated using Cytosim (red dots). **(B)** EB1-GFP-expressing myotubes were imaged using stream acquisition (250 ms/frame). We used a maximum projection of 100 frames to measure the angle of each comet compared to the long axis of the myotube. **(C)** All comet angles were then normalized over a 90° quadrant and distributed in 5° steps, thus revealing a preferential orientation of EB1 comets towards the long axis of the myotube. **(D)** Snapshots of myotubes simulated with Cytosim. Nuclei are blue and MTs in white. Three conditions are shown from top to bottom, with and without MTs nucleated from NE, and Kif5b anchored at NE as indicated. The third condition demonstrates nuclear clustering in myotubes where both MT nucleation and Kif5b motor proteins were removed from the NE (MTs from NE-, Kif5b at NE-). Scale bar, 20 μm. **(E)** Spreading factor analysis of nuclei in simulated myotubes as shown in (D). Results are depicted as median (blue line) with interquartile range (black bars). *** $p<0.001$, **$p<0.05$, Mann-Whitney test. **(F)-(H)** Two-dimensional representations of nuclear distributions in myotubes after computer simulations. We compared nuclear positioning in myotubes (F) with MT nucleation activity and Kif5b motor proteins at the NE (control; MTs from NE+, Kif5b at NE+), (G) without MT nucleation activity but Kif5b motor proteins at the NE (MTs from NE-; Kif5b at NE+) or (H) without both MT nucleation activity and Kif5b motor proteins at the NE (MTs from NE-; Kif5b at NE-). Thereby, each myotube is represented on a single line (y-axis) with blue dots representing the myotube edges and black dots the nuclei. The blue line indicates the midline of the myotube. Note that all myotubes are arranged in descending order of the myotube length.
Computer simulations and all experiments for determining computer simulation parameters were performed by Dr. Bruno Cadot (Center for Research in Myology in Paris, France).

3.6.3 Akap450 is required for nuclear positioning

Among the centrosomal proteins known to localize to the nucleus during skeletal muscle formation, solely Akap450 seemed to be involved in MT nucleation from the NE. If this is the case, then based on our simulation data, removing Akap450 should also affect nuclear positioning in myotubes, while removing other centrosomal proteins involved in MT nucleation at the centrosome should have no effect. To test this, we depleted C2C12 cells for Akap450, Pcm1, Pericentrin or Cdk5Rap2 and analyzed the spreading factor following differentiation in myotubes. Remarkably, nuclei were found to cluster in Akap450-silenced myotubes, leading to a significantly reduced spreading factor when compared to myotubes treated with non-targeting control siRNA (Figure 3.28 A, B). In contrast, myotubes depleted for Pcm1 or Pericentrin displayed no obvious nuclear positioning defects and no significant alterations regarding the spreading factor. Spreading factor analysis of Cdk5Rap2-silenced myotubes revealed different results depending on the siRNA. While nuclei were normally distributed in C2C12 cells treated with Cdk5Rap2-targeting siRNAs #1 and #2, nuclei were more clustered in C2C12 myotubes treated with Cdk5Rap2-targeting siRNA #3, resulting in a decreased spreading factor.
However, as two different siRNAs showed no effect for Cdk5Rap2 on nuclear distribution, we assume that the decreased spreading factor observed upon treatment

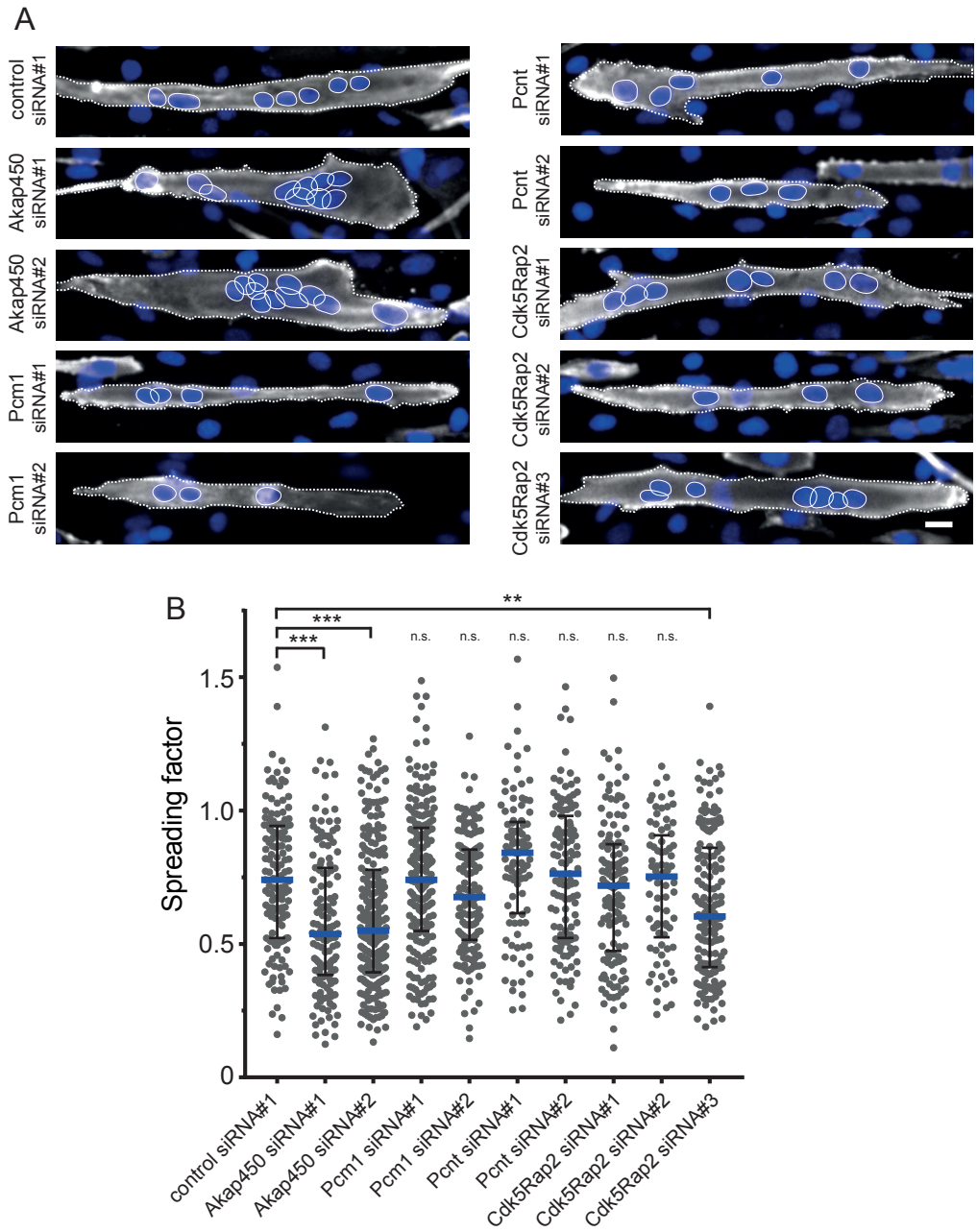

Figure 3.28: Akap450 is required for nuclear positioning. (A) C2C12 cells were transfected with control siRNA#1 or two different siRNAs for Akap450 (Akap450 siRNA#1 or Akap450 siRNA#2), Pcm1 (Pcm1 siRNA#1 or Pcm1 siRNA#2), Pericentrin (Pcnt siRNA#1 or Pcnt siRNA#2) or three different siRNAs for Cdk5Rap2 (Cdk5Rap2 siRNA #1, Cdk5Rap2 siRNA#2 or Cdk5Rap2 siRNA#3). Cells were differentiated for 48 hours and stained for nuclei (DAPI, blue) and myosin heavy chain (MHC, white). Myotube outlines are marked by dashed lines and nuclei are encircled. Scale bar, 20 μm. **(B)** Spreading factor analysis of nuclei in C2C12 myotubes as shown in (A). Results are depicted as median (blue line) with interquartile range (black bars) from four independent experiments. *** $p<0.001$, **$p<0.05$, ANOVA Dunn's multiple comparison test.

with Cdk5Rap2 siRNA#3 might result from potential siRNA off-target effects.

Taken together, these data affirm the importance of Akap450-mediated MT nucleation from the nucleus to ensure proper nuclear distribution within myotubes.

4 Discussion

During skeletal muscle formation, the centrosome-organized MT network is rearranged to the nucleus together with a plethora of centrosomal proteins, the Golgi complex and ER exit sites. In differentiated myoblasts and myotubes, the nucleus thus takes over the function as a non-centrosomal MTOC. However the underlying mechanisms driving the rearrangements during myogenic differentiation and especially how centrosomal proteins and MT nucleation capacity are displaced and anchored at the NE remained unanswered until now. In the present study, we show that the LINC complex is required for the recruitment of centrosomal proteins and MT nucleation capacity to the NE (Figure 4.1). This specific LINC complex comprises two developmentally-expressed components, the muscle-specific isoform Nesprin-1α at the ONM and Sun1 at the INM. Although the protein levels of Sun2 remain constant throughout the myogenic differentiation process, Sun2 can contribute to anchor Nesprin-1α at the ONM. Among the centrosomal proteins (Pericentrin, Akap450, Pcm1, Cdk5Rap2) that are recruited to the NE in a Nesprin-1α/Nesprin-1-dependent manner, Pcm1 is partially required to target Pericentrin to the nucleus. NE localization of Pericentrin is required to target Cdk5Rap2 to the nucleus. Moreover, the centrosomal protein Akap450 colocalizes with the *cis*-Golgi component GM130 at the NE and is required for initiating MT nucleation from the nucleus. In turn, Akap450-Nesprin-1-mediated MT nucleation from the nucleus is important for correct nuclear positioning in skeletal muscle cells; any defects within the underlying mechanism affect nuclear spreading movements.

4.1 Involvement of Nesprin-1α/Nesprin-1 in MTOC relocalization to the nucleus

Nesprin-1 is a large KASH protein of the ONM that is known to connect the nucleus to the cytoskeleton via its cytoplasmic extensions (Starr and Fridolfsson, 2010). Using a siRNA screen against 238 genes encoding potential nuclear transmembrane or NE-associated genes, we identified here Nesprin-1 as a promising candidate to localize Pericentrin, a scaffolding component of the PCM, to the NE (Figure 3.3). In

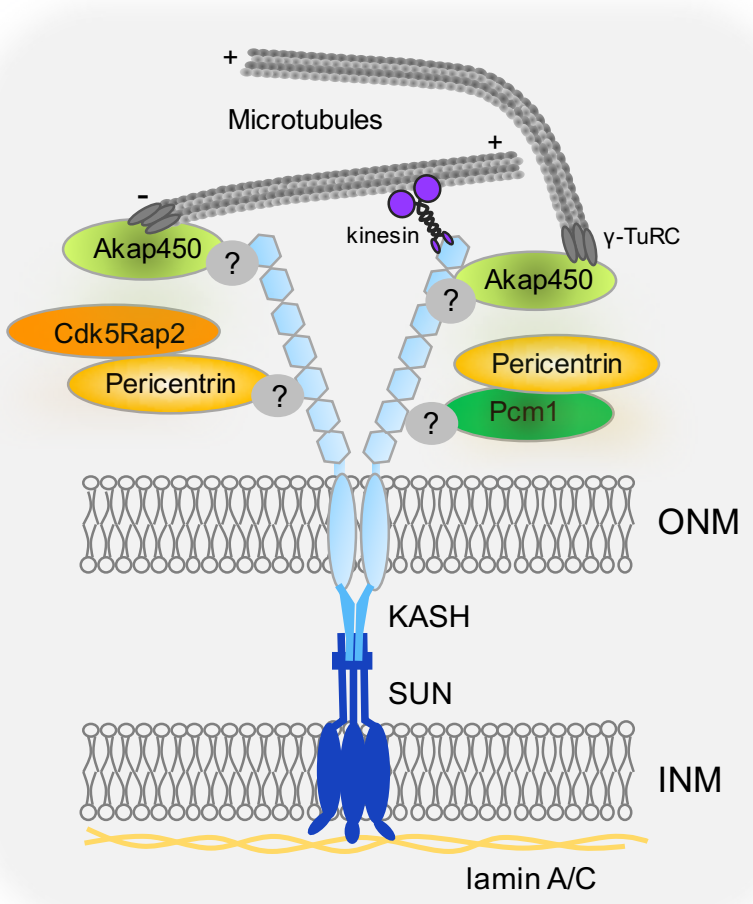

Figure 4.1: Model for MTOC formation at the nucleus in skeletal muscle cells. The KASH domain protein Nesprin-1α is up-regulated during myogenic differentiation and localized at the outer nuclear membrane (ONM) by binding to the SUN domain proteins Sun1/2 of the inner nuclear membrane (INM). During skeletal muscle formation, Nesprin-1α recruits several centrosomal proteins, including Akap450, Pcm1, Pericentrin, and Cdk5Rap2 to the nucleus. Pcm1 is at least in part involved in localizing Pericentrin to the nuclear envelope (NE) but may require itself unknown adaptor proteins to bind to Nesprin-1α. Pericentrin is important to bring Cdk5Rap2 to the nucleus but might require other factors than Pcm1 in order to interact with Nesprin-1α. Akap450 localizes to the NE either through direct interaction with Nesprin-1α or unknown adaptor proteins and drives microtubule nucleation from the nucleus, likely by binding to components of the γ-TuRC. Additionally, Nesprin-1α can interact with kinesin motor proteins, which move towards the microtubule plus-end to mediate nuclear positioning. Scheme is not drawn to scale.

differentiated C2C12 cells depleted of Nesprin-1 using two different siRNAs as well as in myotubes from a congenital muscular dystrophy patient carrying a nonsense mutation within the *SYNE1 (23560 G>T)* gene, Pericentrin, PCM1 and Akap450 were absent at the NE and instead mislocalized together with Golgi complex fragments within the cytoplasm (Figure 3.5, Figure 3.9, Figure 3.10). These findings

are consistent with a recent report that was published during the preparation of our own manuscript, showing that Pericentrin, PCM1, γ-tubulin and Cdk5Rap2 are reduced at the NE in Nesprin-1 depleted C2C12 myotubes (Espigat-Georger et al., 2016).

Although Nesprins were suggested to function together with SUN domain proteins in transcription control (Akhtar and Gasser, 2007), the reduced NE-localization of Pericentrin in Nesprin-1 depleted cells was not simply resulting from altered Pericentrin protein levels during myogenic differentiation (Figure 3.6). In cardiomyocytes, NE localization of Pericentrin was previously correlated with the increased expression of Pericentrin S (Miyoshi et al., 2006a; Zebrowski et al., 2015). Compared to cardiomyocytes, we and others did not observe an isoform switch of Pericentrin during the course of C2C12 differentiation (Figure 3.6) (Zaal et al., 2011). However, as we used anti-Pericentrin antibodies recognizing all Pericentrin isoforms, we cannot exclude the possibility that also in skeletal muscle cells Pericentrin S might be the predominant isoform localizing to the NE.

In skeletal and cardiac muscle, a shorter and tissue-specific isoform of Nesprin-1, termed Nesprin-1α, predominates but a specific function for Nesprin-1α in these differentiated tissues remained uncertain (Duong et al., 2014; Holt et al., 2016; Pare et al., 2005; Randles et al., 2010). Consistent with published data, we found Nesprin-1α to be up-regulated during myogenic differentiation of C2C12 cells and speculated that Nesprin-1α might be the relevant isoform for bringing centrosomal proteins to the NE (Holt et al., 2016; Randles et al., 2010). Indeed, using the BioID technique, we revealed Nesprin-1α to be preferentially associated with three centrosomal proteins, Akap450, Pcm1 and Pericentrin in myotubes (Figure 3.18). BioID is a novel technique to determine potential protein-protein interactions based on proximity within an estimated radius of 10-20 nm (Kim et al., 2014; Roux et al., 2013). Based on the high number of peptide counts for Akap450 in comparison to the other two centrosomal proteins, Pcm1 and Pericentrin, it is tempting to speculate that Akap450 might be more proximal to Nesprin-1α than Pcm1 and Pericentrin. However, the number of peptide counts as determined by tandem mass tag quantitative mass spectrometry is not necessarily proportional to the proximity of the bait protein (here myc-BirA*-Nesprin-1α). The number of peptide counts could also be influenced, for example, by the relative abundance of the identified protein within myoblasts and myotubes or by the number of lysine residues that are accessible for biotinylation.

Our data further suggested a key role for Nesprin-1α in bringing centrosomal proteins to the NE during skeletal muscle formation, as Nesprin-1α was sufficient to rescue

NE-localization of Pericentrin and Akap450 in differentiated C2C12 cells that had been rendered Nesprin-1-deficient using CRISPR/Cas9 (Figure 3.20). Whether Nesprin-1α fulfills this function exclusively or whether other Nesprin-1 KASH-containing isoforms comprising most of the Nesprin-1α domains (e.g. Nesprin-1 giant, Nesprin-1β) can contribute to the recruitment of centrosomal proteins is still under investigation. One could hypothesize that the muscle-specific Nesprin-1α isoform is more prone to target centrosomal proteins to the NE during myogenic differentiation when compared to other Nesprin-1 isoforms which are ubiquitously expressed and not restricted to certain tissues. This would explain why non-muscle cells (e.g. U2OS cells), which express Nesprin-1, are capable to acquire centrosomal proteins at their nuclei upon fusion with differentiated muscle cells but to a lesser extent than muscle nuclei (Fant et al., 2009). It will be interesting to investigate in future studies if certain domain structures of Nesprin-1α and/or additional Nesprin-1α-binding factors could confer specificity for centrosomal protein recruitment in skeletal muscle cells.
Recruitment of centrosomal proteins to the NE was previously suggested to be a prerequisite for MT nucleation from the NE (Tassin et al., 1985a). In line with this hypothesis, we found MTs emanating from the nucleus in close proximity to foci containing Pericentrin and Nesprin-1 (Figure 3.21). Additionally, MTs failed to regrow from the NE in differentiated C2C12 cells or in *SYNE1 (23560 G>T)* patient myotubes, when centrosomal proteins were mislocalized within the cytoplasm (Figure 3.22, Figure 3.23). Interestingly, the overall longitudinal MT organization at steady state was unaffected in the absence of Nesprin-1, suggesting that cytoplasmic nucleated MTs are sufficient to generate a dense array of parallel organized MTs and that the underlying mechanisms driving MT alignment (e.g. oMap4) are not perturbed (Mogessie et al., 2015). This raises the question if MT nucleation from the NE is biologically relevant or after all dispensable for muscle cells. Our data support an important function for NE-mediated MT nucleation in nuclear positioning (discussed in section 4.6). However, if also other biological processes, such as intracellular transport of mRNAs, require active MT nucleation from the NE in skeletal muscle cells, remains to be determined in future studies.

4.2 Involvement of Sun1 and Sun2 in MTOC relocalization to the nucleus

Nesprins are known to be anchored at the ONM by binding to SUN domain proteins of the INM, thereby forming LINC complexes (Crisp et al., 2006). In order to

examine which of the SUN domain proteins is involved in complex formation with Nesprin-1α/Nesprin-1 and thus in relocalizing MTOC function to the NE during myogenic differentiation, we assessed the impact of Sun1 and Sun2 on Pericentrin recruitment and MT nucleation. We identified *Sun1 (Unc84a)* but not *Sun2 (Unc84b)* among the 31 genes showing decreased Pericentrin levels at the NE upon siRNA-mediated silencing in C2C12 myotubes (Figure 3.3). This result was confirmed with different sets of siRNAs targeting *Sun1* or *Sun2*, respectively, and with *in vitro* cell culture systems of isolated myoblasts from *Sun1*$^{-/-}$ and *Sun2*$^{-/-}$ knockout mice (Figure 3.5 A, B; Figure 3.7). In both systems, Sun1 depletion resulted in slightly decreased Pericentrin levels at the NE and in a prominent localization of Pericentrin at the nuclear poles, whereas Sun2 depletion had no effect. Interestingly, MT nucleation from the NE was restricted to Pericentrin-positive sites at the NE and in the case of Sun1-depleted cells occurred from nuclear poles (Figure 3.22). However, only double depletion of Sun1 and Sun2 displaced Nesprin-1α/Nesprin-1 from the NE (data not shown), as previously described (Lei et al., 2009), and thus recapitulated the Pericentrin and MT mislocalization phenotype associated with Nesprin-1 deficiency (Figure 3.5 A, B; Figure 3.7, Figure 3.22). This suggested that either both Sun1 and Sun2 are required for MTOC relocalization during myogenic differentiation or that Sun1 and Sun2 could functionally compensate each other. Our data indicated, in agreement with other studies, that Sun1 protein levels increase during the course of myogenic differentiation, whereas Sun2 proteins levels remain largely constant (Figure 3.8) (Mattioli et al., 2011). Sun2 protein levels were slightly elevated upon Sun1 depletion, thus supporting the idea that Sun2 could functionally compensate for the loss of Sun1. Together with previous work showing an enrichment of Sun2 at nuclear poles (Mattioli et al., 2011), our data suggest that in the absence of Sun1, Sun2 might predominate within LINC complexes, resulting in MTOC recruitment to the nuclear poles. In line with our results, Pericentrin localization and MT nucleation at the NE was affected in myotubes from a patient with an EDMD-like phenotype, carrying compound heterozygous mutations within *SUN1* p.G68D/p.G338S (Meinke et al., 2014). Interestingly, these patient myotubes additionally displayed nuclear positioning defects, thus strengthening our hypothesis that MTOC recruitment to the NE and in turn active MT nucleation from the nucleus is important for nuclear positioning (as discussed in section 4.6).

4.3 Centrosomal proteins involved in NE-mediated MT nucleation

During skeletal muscle formation, a plethora of centrosomal proteins were reported to relocalize to the NE (Bugnard et al., 2005; Fant et al., 2009; Oddoux et al., 2013; Srsen et al., 2009). This relocalization of centrosomal proteins was proposed to be a requirement for MT nucleation from the nucleus (Tassin et al., 1985a). We identified Akap450 as the major anchoring protein for NE-localized MT nucleation in skeletal muscle cells among the centrosomal proteins studied here (Pericentrin, Pcm1, Cep192, Cdk5Rap2, Akap450), which were previously implicated in the recruitment of γ-TuRC components in proliferating cells (Figure 3.25) (Choi et al., 2010; Dammermann and Merdes, 2002; Fong et al., 2008; Gomez-Ferreria et al., 2007; Pelletier et al., 2004; Takahashi et al., 2002; Zimmerman et al., 2004). Akap450 and Pericentrin were both demonstrated to bind to the γ-TuRC components GCP2 and/or GCP3 through their N-terminal domains, thereby contributing to MT formation at the centrosome (Takahashi et al., 2002). Although it is likely that also in skeletal muscle cells Nesprin-1α-bound Akap450 recruits γ-TuRCs to the NE to induce MT nucleation, further co-stainings with γ-tubulin and/or other components of the γ-TuRC will be performed to analyze how Akap450 contributes to MT nucleation from the NE.

Interestingly, the Akap450 paralogue, Pericentrin, did not seem to play a significant role in MT nucleation from the NE nor did Pericentrin depletion affect the fusion index (Figure 3.24). This is in contrast to cardiomyocytes, where MT nucleation from the NE was recently reported to depend on Pericentrin, suggesting that MTOC formation at the nucleus is driven by a different mechanism in cardiomyocytes than in skeletal muscle cells (Zebrowski et al., 2015). In myofibers isolated from mouse skeletal muscle, Pericentrin was found at MT-nucleating Golgi elements, while Akap450 remained exclusively at the NE (Oddoux et al., 2013). One could thus hypothesize that Pericentrin might contribute at later stages during skeletal muscle formation in γ-TuRC recruitment and in turn in MT nucleation from Golgi complex elements, whereas Akap450 might exclusively control MT nucleation from the NE in myotubes and myofibers. In agreement with other studies, Pericentrin localization to the NE depended at least in part on Pcm1 (Dammermann and Merdes, 2002; Espigat-Georger et al., 2016). Although Pericentrin levels at the NE were decreased upon Pcm1 depletion (Figure 3.14), Pericentrin was not mislocalized within the cytoplasm like in the absence of Nesprin-1α/Nesprin-1, suggesting that additional factors might contribute to Pericentrin anchorage at the NE.

Similarly as in the case of Pericentrin, knockdown of Pcm1 did not affect MT nucleation from the NE in differentiated C2C12 cells (Figure 3.25). These results are in line with previous work, showing an indirect involvement of Pcm1 in MT organization but not in MT nucleation, through the recruitment of other proteins to the centrosome (e.g. Pericentrin, ninein) (Dammermann and Merdes, 2002).
In differentiated C2C12 cells, Cdk5Rap2 recruitment to the nucleus required Pericentrin and thus resembled Pericentrin-dependent localization of Cdk5Rap2 to the centrosome (Figure 3.15) (Buchman et al., 2010). Surprisingly, Pcm1 depletion did not affect NE localization of Cdk5Rap2, thus arguing against a successive recruitment process of (1) Pcm1, (2) Pericentrin and (3) Cdk5Rap2. It might be possible that a subpopulation of Pericentrin is recruited to the NE by Pcm1, while another subpopulation of Pericentrin is recruited either directly via Nesprin-1α/Nesprin-1 or other unknown adaptor proteins. If the latter subpopulation of Pericentrin would be responsible for NE localization of Cdk5Rap2, this would explain why Pcm1 depletion itself has no impact on Cdk5Rap2 recruitment. However, the diverse and multiple interactions between centrosomal proteins are even poorly characterized at the centrosome and it will be a challenging task to unravel how each centrosomal protein is anchored at the NE in dependence of Nesprin-1α/Nesprin-1.
Although Cdk5Rap2 was previously shown to anchor and activate γ-TuRC-mediated MT nucleation at the centrosome and at non-centrosomal sites (Choi et al., 2010; Fong et al., 2008), we did not observe obvious MT nucleation defects upon Cdk5Rap2 depletion (Figure 3.24). Additionally, Cdk5Rap2 was implicated in the regulation of MT dynamics and stability through interaction with the MT plus-end binding protein EB1 (Fong et al., 2009). As the MT regrowth assay that we used to determine potential MT nucleation defects upon Cdk5Rap2 depletion is exclusively based on the localization of MT seeds in fixed cells, any defects regarding MT dynamics or stability would not be revealed. To examine if Cdk5Rap2 potentially functions from the NE to control MT dynamics in skeletal muscle cells, live-cell imaging experiments of EB1-overexpressing cells in the absence or presence of Cdk5Rap2 will be helpful to address this question in future studies. Aside from the fact that Cdk5Rap2-silenced cells did not display perturbed MT nucleation from the NE, we noticed an increased fusion index upon Cdk5Rap2 depletion (Figure 3.24 A), suggesting that Cdk5Rap2 might control myogenic differentiation. Also neuronal progenitor cells were previously reported to undergo increased premature differentiation upon knockdown of Cdk5Rap2 due to reduced cell proliferation and increased cell-cycle exit (Buchman et al., 2010). It will be interesting to analyze if Cdk5Rap2 could also control cell-cycle exit of proliferating myoblasts and thus the time-wise

relocalization of centrosomal proteins to the NE in post-mitotic skeletal muscle cells. Cep192 was previously shown to regulate mitotic spindle assembly by recruiting components of the PCM, such as γ-tubulin and Pericentrin, to the centrosome (Gomez-Ferreria et al., 2007; Pelletier et al., 2004). Additionally, Cep192 was reported to regulate the generation of centrosomal versus non-centrosomal MTs by keeping the centrosome in an active MTOC state (O'Rourke et al., 2014; Yang and Feldman, 2015). We thus thought that depleting Cep192 would inactivate the centrosome and thereby enhance the MTOC potential of the nucleus during myogenic differentiation. However, knockdown of Cep192 slightly but not significantly increased MT nucleation from the NE in differentiated C2C12 cells (Figure 3.24 C, D). Furthermore, we noticed that C2C12 cells depleted of Cep192 showed a decreased fusion index upon myogenic differentiation. Although it remains questionable how Cep192 might impact myotube formation, one could speculate based on previous findings that Cep192 depletion might affect myoblast migration and thus potentially myoblast fusion (O'Rourke et al., 2014; Rochlin et al., 2010).
Overall, our data suggested that among the centrosomal proteins that are recruited to the NE, solely Akap450 was important for initiating MT nucleation from the nucleus during myogenic differentiation. If centrosomal protein recruitment is a prerequisite for MT nucleation from the NE, which is exclusively mediated by Akap450, why is there a plethora of centrosomal proteins that relocalize to the nucleus during myogenic differentiation? The biological functions of centrosomal proteins are diverse and extend far beyond the established roles in MT nucleation and MT organization. In cardiomyocytes for example, relocalization of centrosomal proteins was suggested to maintain the post-mitotic state (Zebrowski et al., 2015). Several centrosomal proteins are involved in signaling pathways by localizing certain kinases or cell-cycle regulators to the centrosome (Arquint et al., 2014), suggesting that NE-localized centrosomal proteins could form a signaling platform at the nucleus during skeletal muscle formation.

4.4 The PACT domain localizes to the NE during myogenic differentiation

Akap450 and Pericentrin contain both a C-terminal PACT domain that is required to target these proteins to the centrosome (Gillingham and Munro, 2000). By live-cell imaging of C2C12 cells overexpressing dsRed-PACT, we now showed that the PACT domain localizes dsRed to the centrosome in myoblasts but additionally to the NE upon myogenic differentiation (Figure 3.1). DsRed-PACT was found

at two perinuclear spots, resembling the centrosome or centriole-like structures which increased in size and seemed to push against the nucleus during the course of differentiation. If these two perinuclear spots are two centrosomes, each comprising a pair of centrioles and a surrounding PCM or two centrioles that disengage during the myogenic differentiation process, is difficult to evaluate. Although in studies with *Drosophila* D-PLP, the PACT domain was proposed to be linked with both centrioles and the PCM (Martinez-Campos et al., 2004), additional co-stainings with centriole and PCM markers will be needed to assess if the PACT domain of Pericentrin is localized in a similar manner in mouse C2C12 cells.

One interesting observation was that the two perinuclear spots increased in size during the differentiation process, approximately at the time when dsRed-PACT additionally localized to the NE (Figure 3.1, compare frame 21:50 and 23:30 hh:min). This raises the question, if the increase in size is simply a reflection of dsRed-PACT overexpression or resulting from a centrosome maturation process. The latter refers to a phenomenon that normally occurs in preparation for mitosis, when centrosomes accumulate additional PCM components, including γ-tubulin and other γ-TuRC recruiting proteins, in order to increase their MT organizing and nucleation potential (Bettencourt-Dias and Glover, 2007; Conduit et al., 2015). Centrosome maturation is at least in part controlled by polo-like kinase 1 (Plk1) and Aurora A kinase and Plk1-mediated phosphorylation of Pericentrin at S1235 and S1241 is required for the recruitment of PCM components to the centrosome (Lee and Rhee, 2011). It would be thus interesting to investigate if blocking Plk1 and/or Aurora A kinase activity during myogenic differentiation would prevent the increased dsRed-PACT localization at the perinuclear spots.

Because the two increased perinuclear spots seemed to push against the NE and to follow invaginations of the nucleus, it is tempting to speculate that the centrosome or centriole-like structures, respectively, are actively involved in delivering dsRed-PACT to the NE. Although material exchange between the centrosome and the nucleus was indeed observed in other systems (Bailly et al., 1989; Pockwinse et al., 1997), we did not notice an increase in dsRed fluorescence intensity at the NE and a simultaneous decrease at the perinuclear spots, when both structures were in close contact. Moreover, we did not observe a transition state with only partial dsRed-PACT localization at the nucleus (e.g. half rings). This is in contrast to fixed cells, where half nuclear rings of Pericentrin were observed to originate from the centrosome at early stages during myogenic differentiation (Zaal et al., 2011). To ultimately proof if dsRed-PACT or centrosomal proteins in general are directly delivered from the centrosome to the NE, FRAP experiments with a photoactivatable fluo-

rescent PACT construct would be helpful (Lippincott-Schwartz and Patterson, 2009). Localization of dsRed-PACT to the NE could artificially be induced in non-differentiated C2C12 myoblasts, when cells co-expressed GFP-Nesprin-1α. Under these conditions, 30% of GFP-Nesprin-1α-expressing cells showed faint dsRed-PACT fluorescence at the NE in addition to the centrosome. In comparison, dsRed-PACT localization at the NE was never observed under non-differentiating conditions in C2C12 myoblasts overexpressing GFP together with dsRed-PACT (Figure 3.19 A, B). These results suggest that Nesprin-1α is involved in bringing centrosomal proteins to the NE but that the recruitment process itself is tightly regulated according to the differentiation status. If Nesprin-1α is a key recruitment factor, one would probably naively expect more than 30% of GFP-Nesprin-1α-expressing cells showing NE localization of dsRed-PACT. However, it is possible that either adaptor proteins which themselves need to be upregulated during myogenic differentiation are required to induce the relocalization process or that centrosomal proteins need to undergo differentiation-induced post-translational modifications (e.g. phosphorylation) and/or release from the centrosome to be capable to interact with Nesprin-1α. In either case, the recruitment of dsRed-PACT would be incomplete in non-differentiated C2C12 cells, even in the presence of Nesprin-1α.
Nevertheless, we could demonstrate using co-immunoprecipitation assays that GFP-Nesprin-1α and the PACT domain of Pericentrin are found in one protein complex in C2C12 cells (Figure 3.19 C). From these co-immunoprecipitation studies, however, we cannot judge if the interaction between the PACT domain and Nesprin-1α is direct or only occurs in the presence of unknown adaptor proteins. Moreover, as centrosomal proteins usually contain large coiled-coil regions and are thus able to dimerize, we cannot exclude that the PACT domain solely dimerizes with endogenous Pericentrin or other centrosomal proteins which are recruited to the NE in a Nesprin-1α-dependent manner. To analyze if the PACT domain directly interacts with Nesprin-1α, we will need to perform *in vitro* GST pulldown assays using recombinant proteins. In turn, pulldown assays using GST-coupled fragments of Nesprin-1α could help to identify potential binding regions or motifs in Nesprin-1α that mediate binding to centrosomal proteins.

4.5 The Golgi complex as non-centrosomal MTOC in skeletal muscle cells

In some cells, such as human retinal pigment epithelium (RPE-1) cells, the Golgi complex is largely involved in generating non-centrosomal MTs during interphase

(Efimov et al., 2007). Golgi-mediated MT nucleation requires the MT-stabilizing proteins CLASPs (CLASP1 and CLASP2) as well as Akap450, which localizes to the *cis*-Golgi through GM130 (Efimov et al., 2007; Rivero et al., 2009; Zhu and Kaverina, 2013). Also in skeletal muscle fibers, Golgi complex elements, which localize together with γ-tubulin and Pericentrin to the intersections of the MT grid-like network, function in addition to the nucleus as non-centrosomal MTOCs (Oddoux et al., 2013). However, if the Golgi complex is already contributing to MT nucleation at earlier stages of myogenic differentiation is still controversially discussed.

We found here that Akap450 perfectly colocalizes with GM130 at the NE in differentiated human wild type myotubes or in the cytoplasm in *SYNE1 (23560 G>T)* patient myotubes (Figure 3.10). This suggests that Nesprin-1α/Nesprin-1 is not only involved in recruiting centrosomal proteins but also the Golgi complex to the NE during myogenic differentiation and that Akap450 localization is tightly coupled to the localization of the *cis*-Golgi. Although also Pericentrin and PCM1 colocalized with GM130 at the NE in human wild type myotubes or at cytoplasmic seeds in *SYNE1 (23560 G>T)* patient myotubes, their colocalization with GM130 was less striking when compared to Akap450. Moreover, among the centrosomal proteins tested in this study, solely Akap450 seemed to be required for MT nucleation from the NE (Figure 3.12). It is thus tempting to speculate that the Golgi complex is not only active as a non-centrosomal MTOC in skeletal muscle fibers but also in differentiated myoblasts and myotubes, when the Golgi complex is rearranged around the NE in dependence of Nesprin-1α/Nesprin-1.

Interestingly, in the absence of Nesprin-1α/Nesprin-1, Akap450, PCM1 and Pericentrin were mislocalized within the cytoplasm and particularly concentrated at Golgi complex fragments nearby the nucleus. These Golgi foci contained Cep152, suggesting that the aggregates comprising mislocalized centrosomal proteins and Golgi fragments might be partially associated with centrioles (Figure 3.11). Although Cep152 was reported to localize at the proximal end of mother centrioles (Hatch et al., 2010), recent studies additionally identified Cep152 within the PCM, forming toroidal structures that surround the mother centriole (Lawo et al., 2012). Thus, additional stainings with other centriole markers will be needed to ultimately proof if the aggregates in Nesprin-1α/Nesprin-1-depleted cells still contain centrioles. These experiments will help us to further clarify if the observed aggregates function as centrosome-like structures or if they are simply assemblies of centrosomal proteins which tend to cluster due to their coiled-coil domains.

Previous electron microscopy (EM) studies of myotubes showed that five to seven Golgi cisternae align as a perinuclear belt along the NE, with the *cis*-Golgi facing

towards the NE at a constant distance between 0.1 and 0.2 μm (Lu et al., 2001; Tassin et al., 1985b). Interestingly, in the same study MTs were shown by transmission EM to emanate from the space between the Golgi complex and the NE, suggesting that both structures could either act individually or in cooperation with each other to recruit γ-TuRCs around the nucleus and to initiate MT nucleation. To distinguish between these two possibilities, it would be helpful to perform MT regrowth assays in the presence of Golgi-altering drugs, such as Brefeldin A. However, previous reports and our own preliminary results (data not shown) showed that the Golgi complex is tightly associated with the NE in myotubes even in the presence of nocodazole, making it complicated to physically unlink the Golgi complex from the NE and thus to assess the MT nucleation capacity of both structures (Tassin et al., 1985b; Zaal et al., 2011). As the Golgi-NE distance is at the spatial resolution limit of conventional microscopy techniques, super-resolution imaging (e.g. 3D-SIM and SD-*d*STORM) could be helpful to examine if *(a)* Akap450 is exclusively localized at the *cis*-Golgi and/or the NE and if *(b)* MTs emanate in association with Akap450 from the *cis*-Golgi and/or the NE after MT regrowth assays. In order to assess if Nesprin-1α is also sufficient to relocalize the Golgi complex to the NE, it could be reasonable to overexpress the dsRed-PACT construct in C2C12 cells and subsequently analyze the percentage of non-differentiated cells that display Golgi complex reorganization.

4.6 Nuclear positioning

During skeletal muscle formation, correct nuclear positioning is achieved through distinct nuclear movements - nuclear centration, nuclear spreading, nuclear dispersion, and nuclear clustering - and involves different molecular pathways (Cadot et al., 2015). Correct nuclear positioning is thought to be important for muscle function as mislocalized nuclei are often associated with muscular diseases (Bitoun et al., 2005; Jungbluth et al., 2008; Metzger et al., 2012). Several mouse models have pointed to an involvement of Nesprin-1 in nuclear positioning and anchorage of synaptic and non-synaptic nuclei (Apel et al., 2000; Chapman et al., 2014; Grady et al., 2005; Puckelwartz et al., 2009; Zhang et al., 2007c). *In vitro*, Nesprin-1/Nesprin-2 was shown to mediate nuclear rotations and translocations by interacting with Kif5b/kinesin-1 through a conserved KLC-binding region (LEWD motif) (Wilson and Holzbaur, 2012, 2015). NE-localized kinesin and also dynein motor proteins depend on an intact and dynamic MT network to drive nuclear centration and

spreading movements (Cadot et al., 2012; Metzger et al., 2012). Although these studies already indicated an importance for Nesprin-1 and MTs in nuclear positioning, it remained uncertain if active Nesprin-1-mediated MT nucleation from the NE is required for nuclear positioning. Here, we confirmed that absence of Nesprin-1α/Nesprin-1 lead to nuclear aggregation in both C2C12 myotubes and *SYNE1 (23560 G>T)* patient myotubes (Figure 3.26). To understand if Nesprin-1α/Nesprin-1-mediated MT nucleation was involved in nuclear positioning besides Nesprin-1-mediated recruitment of Kif5b/kinesin-1, we performed computer simulations using known components involved in nuclear movement in skeletal muscle cells (Figure 3.27). Our results suggested that MT nucleation at the NE is a key factor for correct nuclear positioning, as removing MT nucleation capacity from the NE but keeping Kif5b/kinesin-1 motor proteins at the nucleus affected nuclear spreading in simulated myotubes. Nevertheless, Kif5b/kinesin-1 seemed to have an additive role in nuclear positioning since combined removal of Kif5b/kinesin-1 and MT nucleation from the NE further affected nuclear aggregation. In that manner, computer simulations allowed us to distinguish between these two Nesprin-1-mediated functions - anchoring MT nucleation capacity and recruiting Kif5b/kinesin-1 to the NE - and to decipher their contributions to nuclear positioning. Future work will address if these two different Nesprin-1 activities work within the same LINC complex containing Nesprin-1α/Nesprin-1 and Sun1/2 or if this activity is segregated.
In support of the idea that active MT nucleation from the NE is required for correct nuclear positioning, also depletion of Akap450 resulted in nuclear aggregation in C2C12 myotubes (Figure 3.28). This further confirms that Nesprin-1-Akap450-mediated MT nucleation from the NE is contributing to nuclear spreading movements during myogenic differentiation. In comparison to Akap450, neither Pcm1 nor Pericentrin depletion affected nuclear spreading in myotubes, which is in contrast to the results obtained by Espigat-Georger et al. (2016). Their data suggested that Nesprin-1-mediated recruitment of Pcm1 is required for NE-localization of motor proteins (dynactin subunit p150$^{\text{Glued}}$ and KLC1) and thus for nuclear alignment in C2C12 myotubes. As Pcm1 was already previously demonstrated to be important for Pericentrin localization to the centrosome and Pericentrin in turn was shown to interact with dynein/dynactin (Dammermann and Merdes, 2002; Purohit et al., 1999), they proposed that Pcm1-dependent recruitment of motor proteins might occur indirectly through Pericentrin. However, as we did not observe an effect on nuclear spreading movements upon either Pcm1 or Pericentrin depletion, respectively, our data is arguing against this hypothesis. The discrepancies regarding the effect of Pcm1 on nuclear positioning might result from the different methods

used to analyze nuclear positioning events in C2C12 myotubes (nuclear spreading versus nuclear alignment). As we only examined the effects of different centrosomal proteins on nuclear spreading, it is possible that Pcm1-mediated recruitment of dynein/dynactin could be important for other nuclear movements, such as nuclear centration. In comparison to Pcm1 and Pericentrin, also Cdk5Rap2 depletion using two different siRNAs did not affect nuclear spreading movements, whereas siRNA-mediated depletion of Cdk5Rap2 using a third siRNA resulted in a reduced spreading factor. Further experiments using different sets of siRNAs or CRISPR/Cas9-induced depletion of Cdk5Rap2 will be required to analyze if the observed discrepancies are truly resulting from potential siRNA off-target effects.

Overall our data contribute to the understanding how Nesprin-1α/Nesprin-1 as a component of the LINC complex can contribute to achieve proper nuclear positioning in skeletal muscle cells. Thereby, Nesprin-1α/Nesprin-1 drives nuclear movement through connecting the nucleus to MTs via motor proteins and moreover through active Akap450-mediated MT nucleation from the NE (Figure 4.1).

4.7 Outlook

Mutations within various components of the LINC complex, including Nesprin-1α/Nesprin-1, Nesprin-2, Sun1, Sun2 as well as emerin and lamin A/C, have been correlated with muscle dysfunctions in several disorders, particularly in EDMD, as well as in cardiomyopathies and ataxias (Attali et al., 2009; Ellis, 2006; Gros-Louis et al., 2007; Puckelwartz et al., 2010; Wheeler et al., 2007; Zhang et al., 2007b). Although mutations within these proteins are generally believed to affect interactions between LINC complex components and thus cytoskeleton-nucleoskeleton coupling, the precise role of the LINC complex in muscular disorders remains largely unknown. Our findings reveal a novel function for the LINC complex components Nesprin-1α/Nesprin-1 and Sun1/2 in MTOC formation at the nucleus and subsequently in nuclear positioning. Importantly, these processes were perturbed in myotubes from a congenital muscular dystrophy patient carrying a nonsense mutation within the *SYNE1 (23560 G>T)* gene. It will be important to investigate if also other EDMD-correlated point mutations within Nesprin-1 or other LINC complex-associated proteins, such as emerin or lamin A/C, affect MTOC formation at the nucleus in skeletal muscle cells (Bonne et al., 1999; Zhang et al., 2007b). Several mutations within Nesprin-1α/Nesprin-1 have been associated with severe dilated cardiomyopathy (Puckelwartz et al., 2010; Zhou et al., 2017). In cardiomyocytes, centrosomal proteins were recently demonstrated to accumulate at the NE during heart development (Zebrowski et al., 2015). Recruitment of centrosomal proteins to the nucleus was thereby suggested to be a requirement for maintaining cardiomyocytes in a post-mitotic state. Thus, it will be particularly interesting to investigate if NE localization of centrosomal proteins is also mediated by Nesprin-1α in cardiomyocytes and if the underlying mechanisms are similar to the observed processes in skeletal muscle cells.

In order to understand how MTOC formation at the nucleus could be potentially perturbed in muscle diseases, it will be important to explore the molecular pathways driving and initiating MTOC recruitment to the NE in more detail. In particular, analyzing how centrosomal proteins are released from the centrosome and which signaling cascades are involved in the spatiotemporal control of centrosomal protein recruitment could give valuable insight into the regulation of MTOC displacement during skeletal muscle formation. Investigating if Nesprin-1α-induced recruitment of centrosomal proteins is a prerequisite for the loss of centrosome integrity and centrioles during skeletal muscle formation could improve our understanding on how skeletal muscle cells maintain their post-mitotic state.

Further knowledge about non-centrosomal MTOC formation could thus not only

have an impact in the muscle field but also in other systems, such as cancer.

5 Publications

Gimpel P*, Lee YL*, Radoslaw MS, Calvi A, Koullourou V, Patel R, Mamchaoui K, Nedelec F, Shackleton S, Schmoranzer J, Burke B, Cadot B#, Gomes ER#. "Nesprin-1α-dependent microtubule nucleation from the nuclear envelope via Akap450 is necessary for nuclear positioning in muscle cells."
Submitted manuscript, in revision. *co-first authors, # co-corresponding authors

6 Appendix

Table 6.1: Results of the siRNA screen. Results for the fusion index and Pericentrin (Pcnt) levels at the nuclear envelope (NE) were normalized to the respective control sample and are depicted as the average of three to four independent experiments. S.E.M., standard error of the mean.

Gene symbol	Gene description	Fusion index ±S.E.M	Pcnt at the NE ±S.E.M.
Abhd12	abhydrolase domain containing 12	1,08 ± 0.13	0,89 ± 0.06
Acsl1	acyl-CoA synthetase long-chain family member 1	1,00 ± 0.05	0,83 ± 0.04
Acsl5	acyl-CoA synthetase long-chain family member 5	0,83 ± 0.06	1,18 ± 0.03
Acbd5	acyl-Coenzyme A binding domain containing 5	0,64 ± 0.04	0,79 ± 0.04
Aytl2	acyltransferase like 2	0,82 ± 0.07	1,04 ± 0.07
Arl6ip5	ADP-ribosylation factor-like 6 interacting protein 5	1,15 ± 0,04	0,98 ± 0,04
Ager	advanced glycosylation end product-specific receptor	1,05 ± 0,04	0,94 ± 0,07
Afg3l2	AFG3(ATPase family gene 3)-like 2 (yeast)	1,09 ± 0,04	1,09 ± 0,06
Aldh3a2	aldehyde dehydrogenase family 3, subfamily A2	1,25 ± 0,11	1,06 ± 0,02
Aldh6a1	aldehyde dehydrogenase family 6, subfamily A1	0,91 ± 0,07	1,07 ± 0,02
Ganab	alpha glucosidase 2 alpha neutral subunit	0,80 ± 0,06	0,90 ± 0,04
Aoc3	amine oxidase, copper containing 3	1,11 ± 0,07	0,97 ± 0,02
App	amyloid beta (A4) precursor protein	1,12 ± 0,08	1,15 ± 0,06
Ace	angiotensin I converting enzyme (peptidyl-dipeptidase A) 1	1,04 ± 0,10	1,09 ± 0,02
Aph1c	anterior pharynx defective 1c homolog (C. elegans)	0,92 ± 0,04	0,99 ± 0,07
Aqp1	aquaporin 1	1,23 ± 0,12	1,18 ± 0,02
Aadacl1	arylacetamide deacetylase-like 1	0,78 ± 0,09	1,02 ± 0,06
Asph	aspartate-beta-hydroxylase	0,67 ± 0,04	0,89 ± 0,04
Atp8a2	ATPase, aminophospholipid transporter-like, class I, type 8A, member 2	0,71 ± 0,04	0,91 ± 0,04
Atp2a2	ATPase, Ca++ transporting, cardiac muscle, slow twitch 2	0,78 ± 0,14	0,70 ± 0,07
Atp2b1	ATPase, Ca++ transporting, plasma membrane 1	1,04 ± 0,05	1,11 ± 0,03
Atp2b2	ATPase, Ca++ transporting, plasma membrane 2	1,17 ± 0,12	0,99 ± 0,03
Atp6v0a1	ATPase, H+ transporting, lysosomal V0 subunit A1	0,95 ± 0,08	0,80 ± 0,01
Atp4a	ATPase, H+/K+ exchanging, gastric, alpha polypeptide	1,26 ± 0,04	0,89 ± 0,04
Atp1a1	ATPase, Na+/K+ transporting, alpha 1 polypeptide	0,07 ± 0,02	0,71 ± 0,14
Atp1a2	ATPase, Na+/K+ transporting, alpha 2 polypeptide	0,64 ± 0,04	1,03 ± 0,07
Atp1a3	ATPase, Na+/K+ transporting, alpha 3 polypeptide	0,79 ± 0,06	0,85 ± 0,02
Bcap31	B-cell receptor-associated protein 31	1,02 ± 0,03	1,16 ± 0,04
Bcam	basal cell adhesion molecule	1,29 ± 0,04	1,26 ± 0,06
Bsg	basigin	0,78 ± 0,05	0,74 ± 0,04
Bcl2l13	BCL2-like 13 (apoptosis facilitator)	0,93 ± 0,14	1,01 ± 0,09
Clec14a	C-type lectin domain family 14, member a	1,13 ± 0,02	1,07 ± 0,03
Cdh2	cadherin 2	0,80 ± 0,11	0,88 ± 0,11
Cdh5	cadherin 5	0,77 ± 0,05	0,82 ± 0,15
Canx	calnexin	1,19 ± 0,03	1,00 ± 0,03
Ctsd	cathepsin D	0,87 ± 0,07	0,90 ± 0,03

Cav1	caveolin, caveolae protein 1	0,86 ± 0,04	0,95 ± 0,08
Cd34	CD34 antigen	0,80 ± 0,10	1,01 ± 0,05
Cd36	CD36 antigen	1,16 ± 0,06	0,85 ± 0,03
Cadm4	cell adhesion molecule 4	0,97 ± 0,02	1,00 ± 0,04
Cspg4	chondroitin sulfate proteoglycan 4	0,64 ± 0,08	0,78 ± 0,07
Ccdc90b	coiled-coil domain containing 90B	0,87 ± 0,03	0,87 ± 0,02
Colec12	collectin sub-family member 12	0,91 ± 0,03	1,07 ± 0,05
C3	complement component 3	1,11 ± 0,06	1,04 ± 0,07
Cyb5	cytochrome b-5	1,03 ± 0,03	1,01 ± 0,06
Cyb5b	cytochrome b5 type B	1,05 ± 0,05	0,98 ± 0,03
Cox4i1	cytochrome c oxidase subunit IV isoform 1	0,97 ± 0,06	0,79 ± 0,04
Cox6a1	cytochrome c oxidase, subunit VI a, polypeptide 1	1,01 ± 0,04	0,91 ± 0,03
Cox7a1	cytochrome c oxidase, subunit VIIa 1	1,07 ± 0,07	1,05 ± 0,07
Cox7a2	cytochrome c oxidase, subunit VIIa 2	0,98 ± 0,04	0,71 ± 0,04
Cyc1	cytochrome c-1	0,79 ± 0,05	0,76 ± 0,06
Cyp2b13	cytochrome P450, family 2, subfamily b, polypeptide 13	0,79 ± 0,06	0,88 ± 0,04
Cyp2f2	cytochrome P450, family 2, subfamily f, polypeptide 2	0,87 ± 0,07	0,72 ± 0,06
Cyp3a16	cytochrome P450, family 3, subfamily a, polypeptide 16	1,31 ± 0,04	1,13 ± 0,07
Cyp4b1	cytochrome P450, family 4, subfamily b, polypeptide 1	0,86 ± 0,04	0,91 ± 0,05
Cyp51	cytochrome P450, family 51	0,89 ± 0,04	0,78 ± 0,02
Ckap4	cytoskeleton-associated protein 4	0,90 ± 0,06	1,05 ± 0,03
Dpp4	dipeptidylpeptidase 4	1,08 ± 0,04	1,13 ± 0,03
D4Ertd429e	DNA segment, Chr 4, ERATO Doi 429, expressed	0,54 ± 0,04	0,89 ± 0,04
Dnajb11	DnaJ (Hsp40) homolog, subfamily B, member 11	0,92 ± 0,02	1,04 ± 0,05
Ddost	dolichyl-di-phosphooligosaccharide-protein glycotransferase	0,53 ± 0,10	0,66 ± 0,05
Dullard	Dullard homolog (Xenopus laevis)	0,87 ± 0,08	0,92 ± 0,06
Dag1	dystroglycan 1	1,17 ± 0,05	1,00 ± 0,06
Emd	emerin	0,97 ± 0,05	0,91 ± 0,03
Erp29	endoplasmic reticulum protein 29	0,97 ± 0,02	1,00 ± 0,05
Ergic1	endoplasmic reticulum-golgi intermediate compartment (ERGIC) 1	0,72 ± 0,08	0,99 ± 0,08
Esam1	endothelial cell-specific adhesion molecule	1,15 ± 0,04	0,94 ± 0,04
Erlin2	Erlin2 ER lipid raft associated 2	0,76 ± 0,02	0,95 ± 0,04
AI464131	expressed sequence AI464131	0,33 ± 0,07	0,95 ± 0,09
F11r	F11 receptor	1,03 ± 0,03	0,91 ± 0,05
Fads1	fatty acid desaturase 1	0,97 ± 0,01	0,99 ± 0,03
Fer1l3	fer-1-like 3, myoferlin (C. elegans)	0,64 ± 0,07	1,14 ± 0,09
Fmo1	flavin containing monooxygenase 1	1,11 ± 0,05	1,04 ± 0,04
Fmo2	flavin containing monooxygenase 2	1,04 ± 0,02	1,06 ± 0,01
Fmo3	flavin containing monooxygenase 3	0,87 ± 0,01	0,94 ± 0,05
Fmo5	flavin containing monooxygenase 5	1,09 ± 0,02	1,07 ±0,03
Gprc5a	G protein-coupled receptor, family C, group 5, member A	0,80 ± 0,04	1,07 ± 0,03
Gcs1	glucosidase 1	1,29 ± 0,03	0,92 ± 0,04
Enpep	glutamyl aminopeptidase	0,85 ± 0,05	0,75 ± 0,10
Gpd2	glycerol phosphate dehydrogenase 2, mitochondrial	0,93 ± 0,06	0,99 ± 0,03
Gpm6a	glycoprotein m6a	0,86 ± 0,05	1,03 ± 0,00
Gpsn2	glycoprotein, synaptic 2	0,87 ± 0,05	0,90 ± 0,07
Glmp	glycosylated lysosomal membrane protein	0,67 ± 0,06	0,88 ± 0,05
Glg1	golgi apparatus protein 1	0,97 ± 0,02	0,93 ± 0,04
Hpxn	hemopexin	0,90 ± 0,06	0,96 ± 0,01
Hrc	histidine rich calcium binding protein	1,27 ± 0,08	0,88 ± 0,04
Hsd11b1	hydroxysteroid 11-beta dehydrogenase 1	0,92 ± 0,01	0,89 ± 0,03
Hyou1	hypoxia up-regulated 1	0,96 ± 0,04	0,98 ± 0,04
Ilvbl	ilvB (bacterial acetolactate synthase)-like	0,66 ± 0,04	0,94 ± 0,04
Igsf8	immunoglobulin superfamily, member 8	0,87 ± 0,01	1,03 ± 0,01
Ints1	integrator complex subunit 1	0,56 ± 0,05	0,81 ± 0,06

Itga1	integrin alpha 1	0,86 ± 0,02	0,96 ± 0,04
Itga2	integrin alpha 2	0,98 ± 0,02	1,08 ± 0,03
Itga6	integrin alpha 6	1,06 ± 0,02	1,08 ± 0,04
Itgb1	integrin beta 1 (fibronectin receptor beta)	0,79 ± 0,03	0,91 ± 0,04
Icam1	intercellular adhesion molecule	0,76 ± 0,03	0,77 ± 0,01
Jph2	junctophilin 2	1,13 ± 0,04	1,14 ± 0,03
Lbr	lamin B receptor	0,81 ± 0,01	1,09 ± 0,09
Lama1	laminin, alpha 1	0,88 ± 0,07	0,86 ± 0,03
Lman1	lectin, mannose-binding, 1	1,23 ± 0,03	1,17 ± 0,04
Lemd2	LEM domain containing 2	1,09 ± 0,07	1,18 ± 0,10
Lemd3	LEM domain containing 3	0,78 ± 0,09	1,06 ± 0,03
Lrrc59	leucine rich repeat containing 59	1,14 ± 0,11	1,07 ± 0,06
Letm1	leucine zipper-EF-hand containing transmembrane protein 1	1,10 ± 0,08	1,06 ± 0,03
Lass2	longevity assurance homolog 2 (S. cerevisiae)	0,56 ± 0,04	0,89 ± 0,05
Lrp1	low density lipoprotein receptor-related protein 1	0,51 ± 0,11	0,48 ± 0,05
Lpgat1	lysophosphatidylglycerol acyltransferase 1	0,81 ± 0,09	0,81 ± 0,05
Mcam	melanoma cell adhesion molecule	0,87 ± 0,07	0,85 ± 0,07
Mbc2	membrane bound C2 domain containing protein	0,99 ± 0,03	1,12 ± 0,04
Mme	membrane metallo endopeptidase	1,18 ± 0,13	0,90 ± 0,05
Mtdh	Metadherin	1,24 ± 0,03	1,09 ± 0,02
Mettl7a	methyltransferase like 7A	0,94 ± 0,03	1,14 ± 0,04
Mospd3	motile sperm domain containing 3	0,77 ± 0,04	1,21 ± 0,03
Mybbp1a	MYB binding protein (P160) 1a	0,44 ± 0,07	0,41 ± 0,03
Mag	myelin-associated glycoprotein	0,86 ± 0,03	0,90 ± 0,03
Nat10	N-acetyltransferase 10	0,88 ± 0,12	0,99 ± 0,07
Ndufa13	NADH dehydrogenase (ubiquinone) 1 alpha subcomplex, 13	1,06 ± 0,04	1,04 ± 0,06
Ndufa4	NADH dehydrogenase (ubiquinone) 1 alpha subcomplex, 4	1,14 ± 0,05	0,84 ± 0,07
Ndufb4	NADH dehydrogenase (ubiquinone) 1 beta subcomplex 4	0,77 ± 0,04	0,90 ± 0,09
Ndufb5	NADH dehydrogenase (ubiquinone) 1 beta subcomplex, 5	1,02 ± 0,03	0,98 ± 0,02
Ndufc2	NADH dehydrogenase (ubiquinone) 1, subcomplex unknown, 2	1,12 ± 0,04	0,99 ± 0,05
Nppa	natriuretic peptide precursor type A	0,59 ± 0,05	0,95 ± 0,01
Nrp1	neuropilin 1	0,89 ± 0,05	0,97 ± 0,04
Nptn	neuroplastin	1,01 ± 0,05	1,05 ± 0,05
Ncln	nicalin homolog (zebrafish)	0,78 ± 0,12	1,19 ± 0,06
Nnt	nicotinamide nucleotide transhydrogenase	0,74 ± 0,06	0,85 ± 0,05
Pom121	nuclear pore membrane protein 121	0,23 ± 0,06	0,77 ± 0,11
Noc2l	nucleolar complex associated 2 homolog	0,62 ± 0,07	1,16 ± 0,04
Noc4l	nucleolar complex associated 4 homolog	0,93 ± 0,02	1,06 ± 0,07
Nepro	nucleolus and neural progenitor protein	0,85 ± 0,03	0,92 ± 0,06
Nup210	nucleoporin 210	0,93 ± 0,04	1,03 ± 0,02
Nrm	nurim (nuclear envelope membrane protein)	0,77 ± 0,04	0,89 ± 0,09
Ostc	oligosaccharyltransferase complex subunit (non-catalytic)	0,95 ± 0,03	1,04 ± 0,03
Por	P450 (cytochrome) oxidoreductase	1,03 ± 0,04	0,97 ± 0,05
Ptrh2	peptidyl-tRNA hydrolase 2	0,87 ± 0,05	1,02 ± 0,02
Ppib	peptidylprolyl isomerase B	0,88 ± 0,04	0,78 ± 0,05
Pex14	peroxisomal biogenesis factor 14	1,23 ± 0,01	0,99 ± 0,04
Ebp	phenylalkylamine Ca2+ antagonist (emopamil) binding protein	0,86 ± 0,05	0,89 ± 0,02
Ppapdc3	phosphatidic acid phosphatase type 2 domain containing 3	0,96 ± 0,04	1,03 ± 0,02
Pde3a	phosphodiesterase 3A, cGMP inhibited	0,84 ± 0,05	0,85 ± 0,03
Plvap	plasmalemma vesicle associated protein	0,56 ± 0,03	0,98 ± 0,06
Pecam1	platelet/endothelial cell adhesion molecule 1	0,81 ± 0,03	0,86 ± 0,03
Podxl	podocalyxin-like	0,98 ± 0,02	1,25 ± 0,03
Pbxip1	pre-B-cell leukemia transcription factor interacting protein 1	1,08 ± 0,04	0,94 ± 0,02
Pcyox1	prenylcysteine oxidase 1	0,67± 0,04	1,00 ± 0,05
Pgrmc1	progesterone receptor membrane component 1	0,93 ± 0,06	0,88 ± 0,06
Pgrmc2	progesterone receptor membrane component 2	0,93 ± 0,06	0,92 ± 0,07

Pdia6	protein disulfide isomerase associated 6	0,89 ± 0,02	0,95 ± 0,07
Ptplad1	protein tyrosine phosphatase-like A domain containing 1	0,80 ± 0,07	0,90 ± 0,02
Ptpru	protein tyrosine phosphatase, receptor type, U	1,04 ± 0,05	0,99 ± 0,06
Plp1	proteolipid protein (myelin) 1	1,11 ± 0,06	0,75 ± 0,08
Ptk7	PTK7 protein tyrosine kinase 7	0,72 ± 0,04	1,15 ± 0,05
Ramp2	receptor (calcitonin) activity modifying protein 2	1,02 ± 0,03	0,88 ± 0,02
Reep5	receptor accessory protein 5	1,01 ± 0,03	1,11 ± 0,04
Rtn2	reticulon 2 (Z-band associated protein)	0,53 ± 0,09	0,64 ± 0,06
Rpn1	ribophorin I	1,25 ± 0,10	1,25 ± 0,06
Rpn2	ribophorin II	0,77 ± 0,05	0,82 ± 0,07
Rrbp1	ribosome binding protein 1	1,01 ± 0,02	1,05 ± 0,02
0610007P14Rik	RIKEN cDNA 0610007P14 gene	0,95 ± 0,02	1,03 ± 0,03
Ryr2	ryanodine receptor 2, cardiac	0,75 ± 0,02	0,92 ± 0,03
Sccpdh	saccharopine dehydrogenase (putative)	0,35 ± 0,07	0,83 ± 0,14
Sunc1	Sad1 and UNC84 domain containing 1	0,91 ± 0,03	1,02 ± 0,06
Sgcb	sarcoglycan, beta (dystrophin-associated glycoprotein)	1,03 ± 0,03	1,16 ± 0,02
Sgcg	sarcoglycan, gamma (dystrophin-associated glycoprotein)	0,87 ± 0,02	1,05 ± 0,04
Scara5	scavenger receptor class A, member 5 (putative)	0,73 ± 0,09	0,66 ± 0,08
Sec22b	SEC22 vesicle trafficking protein homolog B (S. cerevisiae)	1,05 ± 0,02	0,98 ± 0,03
Sec61b	Sec61 beta subunit	0,97 ± 0,05	1,53 ± 0,09
Sec63	SEC63-like (S. cerevisiae)	1,00 ± 0,03	1,19 ± 0,07
Sfxn1	sideroflexin 1	0,86 ± 0,02	0,96 ± 0,02
Sfxn5	sideroflexin 5	1,07 ± 0,10	0,97 ± 0,04
Ssr1	signal sequence receptor, alpha	0,96 ± 0,03	1,09 ± 0,02
Sirpa	signal-regulatory protein alpha	0,88 ± 0,05	0,88 ± 0,06
Scn10a	sodium channel, voltage-gated, type X, alpha	0,98 ± 0,04	0,80 ± 0,06
Slc1a2	solute carrier family 1 (glial high affinity glutamate transporter), member 2	0,61 ± 0,03	0,76 ± 0,02
Slc1a3	solute carrier family 1 (glial high affinity glutamate transporter), member 3	0,93 ± 0,04	0,90 ± 0,03
Slc12a1	solute carrier family 12, member 1	1,06 ± 0,05	0,95 ± 0,04
Slc12a2	solute carrier family 12, member 2	1,14 ± 0,04	0,82 ± 0,02
Slc25a4	solute carrier family 25 (mitochondrial carrier, adenine nucleotide translocator), member 4	1,19 ± 0,06	1,05 ± 0,08
Slc25a5	solute carrier family 25 (mitochondrial carrier, adenine nucleotide translocator), member 5	1,12 ± 0,07	1,12 ± 0,07
Slc25a22	solute carrier family 25 (mitochondrial carrier, glutamate), member 22	0,84 ± 0,04	0,89 ± 0,06
Slc25a3	solute carrier family 25 (mitochondrial carrier, phosphate carrier), member 3	0,94 ± 0,05	0,90 ± 0,03
Slc25a42	solute carrier family 25, member 42	1,06 ± 0,05	1,11 ± 0,02
Slc27a2	solute carrier family 27 (fatty acid transporter), member 2	0,91 ± 0,03	1,18 ± 0,02
Slc38a3	solute carrier family 38, member 3	0,68 ± 0,05	0,87 ± 0,04
Slc39a14	solute carrier family 39 (zinc transporter), member 14	1,14 ± 0,03	1,06 ± 0,06
Slc4a1	solute carrier family 4 (anion exchanger), member 1	0,97 ± 0,05	1,05 ± 0,03
Syne1	spectrin repeat containing, nuclear envelope 1	0,89 ± 0,05	0,63 ± 0,05
Syne3	spectrin repeat containing, nuclear envelope family member 3	1,10 ± 0,01	0,95 ± 0,03
Syne4	spectrin repeat containing, nuclear envelope family member 4	1,07 ± 0,01	1,12 ± 0,04
Spag4	sperm associated antigen 4	1,08 ± 0,08	0,87 ± 0,04
Spag4l	sperm associated antigen 4-like	0,44 ± 0,10	0,67 ± 0,02
Smpd4	sphingomyelin phosphodiesterase 4	1,03 ± 0,04	1,17 ± 0,02
Sf3b1	splicing factor 3b, subunit 1	0,00 ± 0,00	0,15 ± 0,07
Scai	suppressor of cancer cell invasion	0,69 ± 0,07	0,89 ± 0,04
Sftpc	surfactant associated protein C	0,82 ± 0,04	0,68 ± 0,03
Syne1	synaptic nuclear envelope 1	0,90 ± 0,04	0,92 ± 0,06
Syne2	synaptic nuclear envelope 2	0,78 ± 0,11	0,58 ± 0,03

Syt1	synaptotagmin I	0,60 ± 0,04	0,99 ± 0,10
Stx1b2	syntaxin 1B2	1,05 ± 0,04	1,11 ± 0,02
Stx5a	syntaxin 5A	0,37 ± 0,17	0,79 ± 0,08
Tapbp	TAP binding protein	0,68 ± 0,07	0,89 ± 0,07
Txndc10	thioredoxin domain containing 10	0,88 ± 0,01	0,97 ± 0,01
Thbd	thrombomodulin	0,87 ± 0,05	0,97 ± 0,07
Tmpo	thymopoietin	0,85 ± 0,05	0,75 ± 0,04
Tor1aip1	torsin A interacting protein 1	1,14 ± 0,02	1,01 ± 0,06
Tor1aip2	torsin A interacting protein 2	0,68 ± 0,04	0,92 ± 0,05
Timm21	tranlocase of inner mitochondrial membrane 21	1,38 ± 0,05	1,01 ± 0,04
Trpm1	transient receptor potential cation channel, subfamily M, member 1	0,83 ± 0,04	0,88 ± 0,04
Timmdc1	translocase of inner mitochondrial membrane domain containing 1	0,82 ± 0,04	0,95 ± 0,06
Tm7sf2	transmembrane 7 superfamily member 2	1,00 ± 0,03	1,07 ± 0,04
Tm9sf1	transmembrane 9 superfamily member 1	1,11 ± 0,04	1,06 ± 0,04
Tm9sf2	transmembrane 9 superfamily member 2	0,86 ± 0,03	0,99 ± 0,04
Tmtc3	transmembrane and tetratricopeptide repeat containing 3	0,70 ± 0,05	0,90 ± 0,07
Tmc8	transmembrane channel-like 8	0,95 ± 0,02	1,09 ± 0,02
Tmed10	transmembrane emp24-like trafficking protein 10 (yeast)	0,81 ± 0,02	0,93 ± 0,05
Tmem120a	transmembrane protein 120A	1,16 ± 0,08	0,91 ± 0,06
Tmem14c	transmembrane protein 14C	1,16 ± 0,05	1,12 ± 0,06
Tmem173	transmembrane protein 173	0,93 ± 0,03	0,98 ± 0,07
Tmem20	transmembrane protein 20	0,95 ± 0,08	1,15 ± 0,10
Tmem209	transmembrane protein 209	1,01 ± 0,02	0,96 ± 0,07
Tmem35	transmembrane protein 35	1,06 ± 0,03	0,99 ± 0,02
Tmem43	transmembrane protein 43	0,20 ± 0,05	0,89 ± 0,09
Tmem48	transmembrane protein 48	0,80 ± 0,02	0,82 ± 0,04
Tmem53	transmembrane protein 53	1,11 ± 0,03	1,09 ± 0,02
Tmem74	transmembrane protein 74	0,85 ± 0,05	1,21 ± 0,03
Tyro3	TYRO3 protein tyrosine kinase 3	1,05 ± 0,03	1,16 ± 0,06
Ugt1a2	UDP glucuronosyltransferase 1 family, polypeptide A2	0,87 ± 0,05	1,28 ± 0,04
Ugt1a6a	UDP glucuronosyltransferase 1 family, polypeptide A6A	1,32 ± 0,11	1,05 ± 0,04
Ugt2b5	UDP glucuronosyltransferase 2 family, polypeptide B5	0,83 ± 0,03	1,13 ± 0,06
Ugt3a2	UDP glycosyltransferases 3 family, polypeptide A2	0,62 ± 0,07	1,09 ± 0,05
Unc84a	unc-84 homolog A (C. elegans)	0,96 ± 0,12	0,78 ± 0,03
Unc84b	unc-84 homolog B (C. elegans)	0,64 ± 0,01	1,06 ± 0,04
Urb2	URB2 ribosome biogenesis 2 homolog (S. cerevisiae)	0,80 ± 0,13	1,16 ± 0,03
Vamp2	vesicle-associated membrane protein 2	0,97 ± 0,01	1,16 ± 0,04
Vapa	vesicle-associated membrane protein, associated protein A	0,76 ± 0,02	1,17 ± 0,05
Vapb	vesicle-associated membrane protein, associated protein B and C	1,08 ± 0,05	0,75 ± 0,04
Zcd1	zinc finger, CDGSH-type domain 1	1,05 ± 0,03	1,05 ± 0,03
Zcd2	zinc finger, CDGSH-type domain 2	1,13 ± 0,04	1,03 ± 0,02

Table S1

Name	Value	Note
Global		
Time step	0.05s	Computational parameter
Viscosity	0.1pN s/μm²	Estimate viscosity of the cytoplasm, Daniels et al, 2006
kT	0.0042 pN μm	Thermal energy at 25°C
Cell geometry	R=7um L=190 μm / 5 nuclei	Ellipse
	L=228 μm / 6 nuclei	
	L=266μm / 7 nuclei	
	L=304μm / 8 nucleis	
	L=342μm / 9 nuclei	
Microtubules		
Rigidity	20 pN μm²	Flexural rigidity (Dogterom and Yurke, 1997; Kimura and Onami, 2005; Kozlowski etal., 2007)
Segmentation	4 μm	computational parameter
Dynamics	growing speed= 0.4 μm/s	measures (growing speed only)
	Shrinking speed= 0.8 μm/s	Brun et al, 2009
	hydrolysis rate= 0.5 μm/s	Brun et al, 2009
Growing forces	fg=1.5pN	growing velocity is slowed down by antagonostic force on plus end.
	Stiffness = 500 pN/ μm	
Total polymer	7000 per nucleus	to limit the length of MTs
Kinesin (Kif5b)		
Binding	Range= 0.05 μm	Maximal distance to which a binder can bind a filament
	Rate = 5 s^{-1}	Rate at which possible binding can occur
Unbinding	Force= 5 pN	Unbinding increases with load exponentially
	Rate= 0.1 s^{-1}	Andreasson JOL et al, eLife 2015
Stiffness	200pN/μm	
Motility	Max speed vm= 0.8 μm/s	Andreasson JOL et al, eLife 2015
	stall force fs=5 pN	
Crossslider kif5b/Map7 like		
Diffusion	20 μm²/s	
Stiffness	500pN	
Activity	Slide	Map7 moves in the direction of the applied force, with the specified mobility
Binding	Range= 0.1μm	Maximal distance to which a binder can bind a filament
	Rate = 10 s^{-1}	Rate at which possible binding can occur
Unbinding	Force = 1 pN	Load force needed to unbind
	Rate = 10 s^{-1}	Rate at which possible unbinding can occur
Motility	0.1 μm.s^{-1}.pN^{-1}	
Quantity	200 per nucleus	
Map4		
Binding	Range= 0.1 μm	Maximal distance to which a binder can bind a filament
	Rate = 2 s^{-1}	Rate at which possible binding can occur
Unbinding	Force= 3 pN	Load force needed to unbind
	Rate= 1 s^{-1}	Rate at which possible unbinding can occur
Crosslinker Map4/Map4		
Diffusion	20 μm²/s	
Stiffness	k=200pN	
Activity	Bridge	as described in Mogessie et al Elife 2015
Specificity	Antiparallel	as described in Mogessie et al Elife 2015
Quantity	400 per nucleus	
Dynein		
Binding	Range= 0.05 μm	De simone et al, Cell Reports 2016, reviewed in Reck-Peterson et al., 2012
	Rate = 5 s^{-1}	
Unbinding	Force= 3 pN	Rupp and Nedelec 2012
	Rate= 0.1 s^{-1}	motors unbinding rate is deduced from measurements of dynein processivity ~ 1-2 μm (reviewed in ReckPeterson et al., 2012) and dynein velocity ~ 1.5 μm s-1
Stiffness	k=200 pN/μm	
Motility	Max speed vm= 1 μm/s	Athale et al., 2014; reviewed in Howard, 2001; Kimura and Onami, 2005; reviewed in Reck-Peterson et al., 2012
	stall force fs=5 pN	Measurements ~1-7 (Athale et al., 2014; Goshima et al., 2005; reviewed in Howard, 2001; reviewed in ReckPeterson et al., 2012
Nuclei		
Quantity	5 to 9	Density is 1 nuclei/ 700um² of myotube (measured)
Radius	5 μm	
Nucleator (Gamma-tubulin)	Quantity = 58 / nucleus	The nucleators nucleate independently.
	Nucleation rate = 0.02 s^{-1}	50 possible new MTs per second and per nucleator
	Unbinding rate = 0.1s^{-1}	
	Unbinding force= 3 pN	
	Stiffness = 1000pN/μm	
Kif5b	Quantity = 30 / nucleus	Fixed at the NE, stiffness = 200pN/um
Dynein	Quantity = 18 / nucleus	Fixed at the NE, stiffness = 200pN/um
Centrioles (when no Nesprin-1)		
Quantity	5 per nucleus	
Radius	0.2 μm	
MT nucleation sites	11	

Table S2

Uniprot Accession	Protein Description	Gene ID	Average ratio MB +DOX/-DOX (2 to 3exp)	Average Ratio MT +DOX/-DOX (2 to 3Exp)	(SD) MB +DOX/-DOX (2 to 3 Exp)	(SD) MT +DOX/-DOX (2 to 3 Exp)	MT/MB	Protein Coverage	# Peptides	# PSMs	# Unique Peptides	# Protein Groups	# Razor Peptides	Score Mascot	# Peptides Mascot	# AAs	MW [kDa]	calc. pI
Q9CWE0	Mitochondrial fission regulator 1-like OS=Mus musculus GN=Mtfr1l PE=1 SV=1	;am54b; Mtfr1	8.513	17.786	6.452	14.556	2.089	20.761	5	21	5	1	0	446.5364758	5	289	31.706	6.1
Q9D845	Testis-expressed sequence 9 protein OS=Mus musculus GN=Tex9 PE=2 SV=1	Tex9	12.477	13.563	7.324	4.909	1.087	12.145	5	8	5	1	0	163.785	5	387	44.039	7.65
E9QQ25	Striated muscle-specific serine/threonine-protein kinase OS=Mus musculus GN=Speg PE=1 SV=1	Speg	1.998	12.103	0.859	10.279	6.059	0.736	2	5	2	1	0	127.73	2	3262	354.096	8.18
Q9CZH7	Matrix-remodeling-associated protein 7 OS=Mus musculus GN=Mxra7 PE=1 SV=2	Mxra7	5.358	11.186	1.681	2.411	2.087	6.180	2	3	2	1	0	54.34	2	178	19.445	4.26
A2AEH9	Protein Tmsb15a OS=Mus musculus GN=Tmsb15a PE=4 SV=1	Tmsb15a	0.961	10.537	0.719	0.693	10.959	8.861	1	4	1	1	0	38.65	1	79	8.904	9.09
Q99P72	Reticulon-4 OS=Mus musculus GN=Rtn4 PE=1 SV=2	Rtn4	5.063	8.553	2.166	5.422	1.689	14.544	12	28	12	1	0	386.5427273	12	1162	126.535	4.54
Q921C5	Protein bicaudal D homolog 2 OS=Mus musculus GN=Bicd2 PE=1 SV=1	Bicd2	4.412	8.422	1.453	1.794	1.909	41.585	39	113	33	1	7	1631.224064	39	820	93.334	5.44
BID001	BirA-1 long isoform OS=Mus Musculus GN=BIRAV1L PE=1 SV=1		6.658	8.319	0.488	1.912	1.249	56.627	17	129	17	1	0	1940.399868	17	332	36.49	5.64
Q6ZWR6	Nesprin-1 OS=Mus musculus GN=Syne1 PE=1 SV=2	Syne1	7.368	8.292	1.535	1.477	1.125	4.569	43	417	43	1	0	8049.642528	43	8799	1009.295	5.59
Q64010	Adapter molecule crk OS=Mus musculus GN=Crk PE=1 SV=1	Crk	4.800	8.063	4.494	7.169	1.680	6.250	2	2	2	1	0	38.95	2	304	33.794	5.55
Q70FJ1	A-kinase anchor protein 9 OS=Mus musculus GN=Akap9 PE=1 SV=2	Akap9	1.427	7.949	0.097	5.538	5.571	1.264	5	7	5	1	0	79.23333333	5	3797	435.943	5.03
Q8CD76	Kinesin light chain 1 OS=Mus musculus GN=Klc1 PE=1 SV=1	Klc1	3.739	7.146	0.731	1.294	1.911	25.162	16	39	12	1	4	709.5614286	16	616	69.452	5.96
P14069	Protein S100-A6 OS=Mus musculus GN=S100a6 PE=1 SV=3	S100a6	1.001	7.143	0.171	1.601	7.133	10.112	2	5	2	1	0	38.00947971	2	89	10.044	5.48
E9Q9K8	Protein Akap6 OS=Mus musculus GN=Akap6 PE=1 SV=1	Akap6	2.167	6.964	0.422	0.381	3.213	11.313	24	67	24	1	0	964.30073	24	2307	254.165	5.06
V9GXM1	ADP-ribosylation factor GTPase-activating protein 1 OS=Mus musculus GN=Arfgap1 PE=1 SV=1	Arfgap1	3.917	6.586	1.291	2.107	1.682	3.302	1	2	1	1	0	54.23	1	424	46.511	5.57
A2RS22	Coronin OS=Mus musculus GN=Coro1b PE=1 SV=1	Coro1b	3.315	6.517	0.712	4.565	1.966	9.711	5	14	5	1	0	120.37	5	484	53.878	5.78
E9Q616	Protein Ahnak OS=Mus musculus GN=Ahnak PE=1 SV=1	Ahnak	2.823	6.413	0.849	2.227	2.271	40.329	101	304	101	1	0	3936.383442	101	5656	603.866	6.3
P50543	Protein S100-A11 OS=Mus musculus GN=S100a11 PE=1 SV=1	S100a11	1.137	5.971	0.453	2.236	5.253	16.327	2	5	2	1	0	51.5046153	2	98	11.075	5.45
Q60598	Src substrate cortactin OS=Mus musculus GN=Cttn PE=1 SV=2	Cttn	3.495	5.903	1.579	3.314	1.689	18.681	11	18	11	1	0	262.7366667	11	546	61.212	5.4
Q91YS4	Kinesin light chain 2 OS=Mus musculus GN=Klc2 PE=1 SV=1	Klc2	3.334	5.901	1.540	4.312	1.770	21.971	12	20	9	1	0	209.17	12	619	68.378	7.06
Q80UU9	Membrane-associated progesterone receptor component 2 OS=Mus musculus GN=Pgrmc2 PE=1 SV=2	Pgrmc2	2.662	5.875	0.700	0.381	2.207	40.553	7	19	7	1	0	255.333366	7	217	23.32	5.15
Q91WL8	WW domain-containing oxidoreductase OS=Mus musculus GN=Wwox PE=1 SV=1	Wwox	3.020	5.574	0.679	2.396	1.846	20.048	8	11	8	1	0	122.89	8	414	46.483	7.02
P59325	Eukaryotic translation initiation factor 5 OS=Mus musculus GN=Eif5 PE=1 SV=1	)0047658; LOC	2.797	5.199	0.089	1.233	1.859	7.226	4	6	4	1	0	78.86858233	4	429	48.938	5.52
A0A0R4J0M9	Deubiquitinating protein VCIP135 OS=Mus musculus GN=Vcpip1 PE=1 SV=1	Vcpip1	3.886	5.186	0.579	2.214	1.335	8.770	9	23	9	1	0	474.46	9	1220	134.358	7.17
Q9R0L6	Pericentriolar material 1 protein OS=Mus musculus GN=Pcm1 PE=1 SV=2	Pcm1	1.577	5.078	0.318	3.002	3.219	9.531	18	25	18	1	0	259.4520737	18	2025	228.706	5.01
Q9ERU9	E3 SUMO-protein ligase RanBP2 OS=Mus musculus GN=Ranbp2 PE=1 SV=2	Ranbp2	2.804	5.024	1.007	1.085	1.792	13.429	39	64	39	1	0	597.6762977	39	3053	340.907	6.18
E9QA16	Protein Cald1 OS=Mus musculus GN=Cald1 PE=1 SV=1		1.725	4.782	0.260	2.001	2.772	27.239	17	29	17	1	0	381.7954765	17	536	61.799	6.93
Q9WVA4	Transgelin-2 OS=Mus musculus GN=Tagln2 PE=1 SV=4	Tagln2	1.679	4.215	0.386	1.398	2.510	15.075	3	7	3	1	0	92.37	3	199	22.381	8.24
P37804	Transgelin OS=Mus musculus GN=Tagln PE=1 SV=3	Tagln	1.757	4.119	0.787	0.064	2.344	11.443	2	2	2	1	0	35.85	2	201	22.561	8.81
Q61595	Kinectin OS=Mus musculus GN=Ktn1 PE=1 SV=1	Ktn1	1.952	3.799	0.807	2.659	1.946	24.793	37	58	3	1	33	493.3145967	37	1327	152.498	5.86
Q9D0A3	Arpin OS=Mus musculus GN=Arpin PE=1 SV=1	0034B18Rik; A	1.970	3.762	0.545	2.598	1.910	9.292	2	3	2	1	0	27.12	2	226	25.178	5.19
J3KMH5	Melanoma inhibitory activity protein 3 OS=Mus musculus GN=Mia3 PE=1 SV=1		2.956	3.750	1.040	0.787	1.268	3.457	3	4	3	1	0	101.93	3	781	87.154	8.81
Q9EP71	Ankycorbin OS=Mus musculus GN=Rai14 PE=1 SV=1	Rai14	1.978	3.743	0.855	3.006	1.893	5.107	5	5	5	1	0	35.92	5	979	108.785	6.27
P63242	Eukaryotic translation initiation factor 5A-1 OS=Mus musculus GN=Eif5a PE=1 SV=2	Eif5a	0.533	3.738	0.106	2.797	7.009	12.987	2	3	2	1	0	39.03	2	154	16.821	5.24
Q3UL22	Chaperonin subunit 8 (Theta), isoform CRA_a OS=Mus musculus GN=Cct8 PE=1 SV=1	Cct8	1.457	3.648	0.937	3.330	2.503	29.745	16	29	16	1	0	405.6334787	16	548	59.518	5.62
Q9QYJ3	DnaJ homolog subfamily B member 1 OS=Mus musculus GN=Dnajb1 PE=1 SV=3	Dnajb1	2.042	3.487	1.168	0.422	1.708	3.235	1	2	1	1	0	48.43	1	340	38.143	8.63
Q4FZC9	Nesprin-3 OS=Mus musculus GN=Syne3 PE=1 SV=1	1426I19Rik; Sy	1.972	3.429	0.572	0.355	1.739	7.077	7	10	7	1	0	95.19072199	7	975	111.966	6.33
Q6A065	Centrosomal protein of 170 kDa OS=Mus musculus GN=Cep170 PE=1 SV=2	Cep170	1.376	3.246	0.151	2.885	2.359	1.889	3	4	3	1	0	92.808854	3	1588	174.943	7.17
A0A0R4J1E2	Elongation factor 1-delta OS=Mus musculus GN=Eef1d PE=1 SV=1	Eef1d	2.266	3.241	0.217	0.353	1.430	10.000	6	10	5	1	1	116.93	6	660	72.886	6.51
F8VPM7	ELKS/Rab6-interacting/CAST family member 1 OS=Mus musculus GN=Erc1 PE=1 SV=1	Erc1	2.942	3.127	0.599	0.739	1.063	7.321	7	10	7	1	0	225.8085343	7	1120	128.252	5.91
P08121	Collagen alpha-1(III) chain OS=Mus musculus GN=Col3a1 PE=1 SV=4	Col3a1	0.802	3.065	0.022	1.934	3.820	2.117	2	4	2	1	0	67.49082117	2	1464	138.858	6.52
Q6NZJ6	Eukaryotic translation initiation factor 4 gamma 1 OS=Mus musculus GN=Eif4g1 PE=1 SV=1	Eif4g1	1.204	2.989	0.456	1.279	2.483	4.500	7	8	7	1	0	84.76	7	1600	175.967	5.4
Q9CRB2	H/ACA ribonucleoprotein complex subunit 2 OS=Mus musculus GN=Nhp2 PE=1 SV=1	Nhp2	0.610	2.907	0.271	2.143	4.768	35.948	4	10	4	1	0	245.9508772	4	153	17.236	8.41
Q99LB4	Capping protein (Actin filament), gelsolin-like OS=Mus musculus GN=Capg PE=1 SV=1	Capg	1.148	2.903	0.470	2.414	2.529	9.742	2	3	2	1	0	84.87333333	2	349	38.745	6.95
Q8BFW7	Lipoma-preferred partner homolog OS=Mus musculus GN=Lpp PE=1 SV=1	Lpp	1.287	2.846	0.322	0.244	2.212	7.993	5	13	5	1	0	170.86	5	613	65.848	7.37
Q8BH80	esicle-associated membrane protein, associated protein B and C OS=Mus musculus GN=Vapb PE=1 SV	Vapb	1.760	2.807	0.998	0.315	1.595	12.346	4	4	4	1	0	50.3396996	4	243	26.901	7.78
Q9CY58	Plasminogen activator inhibitor 1 RNA-binding protein OS=Mus musculus GN=Serbp1 PE=1 SV=2	Serbp1	1.371	2.793	0.666	1.107	2.038	11.794	4	5	4	1	0	53.17	4	407	44.687	8.54
P10107	Annexin A1 OS=Mus musculus GN=Anxa1 PE=1 SV=2	Anxa1	0.772	2.734	0.171	1.102	3.540	7.803	3	5	3	1	0	50.10162303	3	346	38.71	7.37
Q6P5H2	Nestin OS=Mus musculus GN=Nes PE=1 SV=1	Nes	1.683	2.717	1.011	1.290	1.615	13.841	21	30	21	1	0	292.4663459	21	1864	207	4.34
Q61768	Kinesin-1 heavy chain OS=Mus musculus GN=Kif5b PE=1 SV=3	Kif5b	1.733	2.696	0.573	0.413	1.556	15.265	13	21	13	1	0	395.1573043	13	963	109.484	6.44
P26039	Talin-1 OS=Mus musculus GN=Tln1 PE=1 SV=2	Tln1	1.401	2.618	0.441	0.823	1.869	7.950	19	31	19	1	0	319.6146104	19	2541	269.653	6.18
P07091	Protein S100-A4 OS=Mus musculus GN=S100a4 PE=1 SV=1	S100a4	0.660	2.589	0.359	1.051	3.921	16.832	2	5	2	1	0	53.31	2	101	11.714	5.31
Q61029	na-associated polypeptide 2, isoforms beta/delta/epsilon/gamma OS=Mus musculus GN=Tmpo PE=1	Tmpo	1.187	2.540	0.099	0.149	2.139	5.310	2	2	2	1	0	63.21	2	452	50.342	9.45
Q08093	Calponin-2 OS=Mus musculus GN=Cnn2 PE=1 SV=1	Cnn2	0.879	2.525	0.144	0.516	2.874	15.082	4	6	4	1	0	192.6633333	4	305	33.134	7.62

Uniprot Accession	Protein Description	Gene ID	Average ratio MB +DOX/-DOX (2 to 3exp)	Average Ratio MT +DOX/-DOX (2 to 3Exp)	(SD) MB +DOX/-DOX (2 to 3 Exp)	(SD) MT +DOX/-DOX (2 to 3 Exp)	MT/MB	Protein Coverage	# Peptides	# PSMs	# Unique Peptides	# Protein Groups	# Razor Peptides	Score Mascot	# Peptides Mascot	# AAs	MW [kDa]	calc. pI
Q9DCT8	Cysteine-rich protein 2 OS=Mus musculus GN=Crip2 PE=1 SV=1	Crip2	1.660	2.515	0.352	0.291	1.515	14.423	2	3	2	1	0	82.78333333	2	208	22.712	8.63
F8WID5	Tropomyosin alpha-1 chain OS=Mus musculus GN=Tpm1 PE=1 SV=1		0.740	2.494	0.476	1.759	3.371	35.890	13	23	1	1	9	212.4976952	13	326	37.39	4.72
A2AFQ2	3-hydroxyacyl-CoA dehydrogenase type-2 OS=Mus musculus GN=Hsd17b10 PE=1 SV=1	Hsd17b10	0.862	2.483	0.169	1.126	2.883	22.140	5	6	5	1	0	57.11	5	271	28.356	8.76
P14602	Heat shock protein beta-1 OS=Mus musculus GN=Hspb1 PE=1 SV=3	Hspb1	0.729	2.455	0.363	0.887	3.366	22.010	4	6	4	1	0	92.05333333	4	209	23	6.55
Q543N3	LIM and SH3 domain protein 1 OS=Mus musculus GN=Lasp1 PE=1 SV=1	Lasp1	1.667	2.438	0.804	0.622	1.463	20.152	5	7	5	1	0	91.24	5	263	29.975	7.05
Q3V3R1	lonofunctional C1-tetrahydrofolate synthase, mitochondrial OS=Mus musculus GN=Mthfd1l PE=1 SV=	Mthfd1l	0.743	2.394	0.023	1.147	3.224	10.235	10	15	9	1	1	252.107789	10	977	105.662	7.02
Q61136	Serine/threonine-protein kinase PRP4 homolog OS=Mus musculus GN=Prpf4b PE=1 SV=3	Prpf4b	0.794	2.379	0.042	1.209	2.996	18.371	18	35	18	1	0	512.4228149	18	1007	116.904	10.23
Q9ESX4	Nucleolar protein of 40 kDa OS=Mus musculus GN=Zcchc17 PE=1 SV=1	Zcchc17	0.671	2.365	0.358	0.473	3.525	21.162	6	11	6	1	0	88.02467247	6	241	27.454	9.63
P14211	Calreticulin OS=Mus musculus GN=Calr PE=1 SV=1	Calr	0.565	2.360	0.307	1.807	4.181	13.221	6	12	6	1	0	151.1245455	6	416	47.965	4.49
Q62523	Zyxin OS=Mus musculus GN=Zyx PE=1 SV=2	Zyx	0.936	2.343	0.284	0.054	2.504	15.957	7	13	7	1	0	305.71	7	564	60.507	6.4
Q9QXS1	Plectin OS=Mus musculus GN=Plec PE=1 SV=3	Plec	0.971	2.278	0.177	0.784	2.347	19.804	93	125	93	1	0	869.7809491	93	4691	533.861	5.96
B2RTM0	Histone H4 OS=Mus musculus GN=Hist2h4 PE=1 SV=1	1h4f; Hist1h4j	0.606	2.249	0.477	1.981	3.712	43.689	6	77	6	1	0	1773.280192	6	103	11.36	11.36
D3Z0X5	Pleckstrin homology-like domain family B member 1 OS=Mus musculus GN=Phldb1 PE=1 SV=1		2.043	2.235	0.876	0.283	1.094	3.796	6	7	6	1	0	77.97	6	1449	158.595	9.11
E9PWE8	Dihydropyrimidinase-related protein 3 OS=Mus musculus GN=Dpysl3 PE=1 SV=1	Dpysl3	1.061	2.227	0.332	0.492	2.099	18.887	11	22	9	1	2	296.3621053	11	683	73.838	6.46
B1AUX2	Host cell factor 1 OS=Mus musculus GN=Hcfc1 PE=1 SV=1	Hcfc1	1.446	2.221	0.127	0.293	1.536	2.344	3	6	3	1	0	55.58	3	2090	214.917	6.89
P15532	Nucleoside diphosphate kinase A OS=Mus musculus GN=Nme1 PE=1 SV=1	Nme1	1.016	2.219	0.686	0.056	2.183	13.158	2	2	2	1	0	17.27	2	152	17.197	7.37
Q9Z2I9	uccinyl-CoA ligase [ADP-forming] subunit beta, mitochondrial OS=Mus musculus GN=Sucla2 PE=1 SV=	Sucla2	0.825	2.204	0.088	0.959	2.673	21.814	11	13	11	1	0	210.9796891	11	463	50.082	7.01
D3Z722	40S ribosomal protein S19 OS=Mus musculus GN=Rps19 PE=1 SV=1		0.528	2.194	0.236	0.329	4.156	12.264	3	5	3	1	0	65.86	3	212	23.09	10.46
Q91VD9	DH-ubiquinone oxidoreductase 75 kDa subunit, mitochondrial OS=Mus musculus GN=Ndufs1 PE=1 SV	Ndufs1	0.814	2.188	0.005	0.771	2.687	5.777	4	4	4	1	0	69.75333333	4	727	79.726	5.72
P50446	Keratin, type II cytoskeletal 6A OS=Mus musculus GN=Krt6a PE=1 SV=3	Krt6a	2.714	2.169	3.379	0.549	0.799	27.667	18	75	3	1	8	710.1636752	18	553	59.299	7.94
Q9Z2I8	uccinyl-CoA ligase [GDP-forming] subunit beta, mitochondrial OS=Mus musculus GN=Suclg2 PE=1 SV=	Suclg2	0.747	2.163	0.048	0.697	2.897	13.857	6	8	6	1	0	167.84	6	433	46.811	7.02
P27546	Microtubule-associated protein 4 OS=Mus musculus GN=Map4 PE=1 SV=3	Map4; Mtap4	1.480	2.148	0.341	0.151	1.452	11.111	10	13	10	1	0	167.4701705	10	1125	117.357	4.98
Q9QYB1	Chloride intracellular channel protein 4 OS=Mus musculus GN=Clic4 PE=1 SV=3	Clic4	0.731	2.146	0.333	1.253	2.936	12.648	3	5	3	1	0	52.8	3	253	28.711	5.59
Q9QXK3	Coatomer subunit gamma-2 OS=Mus musculus GN=Copg2 PE=1 SV=1	Copg2	1.666	2.144	0.649	0.636	1.287	5.626	5	6	3	1	2	70.98	5	871	97.617	5.8
Q8BTM8	Filamin-A OS=Mus musculus GN=Flna PE=1 SV=5	Flna	0.869	2.139	0.099	0.349	2.462	20.325	45	74	41	1	4	1276.017213	45	2647	281.046	6.04
P49817	Caveolin-1 OS=Mus musculus GN=Cav1 PE=1 SV=1	Cav1	1.150	2.136	0.648	0.038	1.858	8.989	2	4	2	1	0	36.13333333	2	178	20.525	6.02
Q99LX5	Multiple myeloma tumor-associated protein 2 homolog OS=Mus musculus GN=Mmtag2 PE=2 SV=1	2310033P09Ri	0.760	2.130	0.091	0.800	2.801	20.385	4	8	4	1	0	203.8366667	4	260	29.281	9.86
Q61335	B-cell receptor-associated protein 31 OS=Mus musculus GN=Bcap31 PE=1 SV=4	Bcap31	1.094	2.128	0.088	0.826	1.946	7.755	2	3	2	1	0	61.89333333	2	245	27.939	8.7
P45952	ledium-chain specific acyl-CoA dehydrogenase, mitochondrial OS=Mus musculus GN=Acadm PE=1 SV=	Acadm	0.745	2.121	0.078	0.614	2.848	18.765	8	11	8	1	0	224.385	8	421	46.452	8.37
Q542P5	Carbonyl reductase 2, isoform CRA_b OS=Mus musculus GN=Cbr2 PE=1 SV=1	Cbr2	1.080	2.119	0.314	0.261	1.963	11.885	3	3	3	1	0	37.88	3	244	25.942	9.01
Q9WUM5	inyl-CoA ligase [ADP/GDP-forming] subunit alpha, mitochondrial OS=Mus musculus GN=Suclg1 PE=1	Suclg1	0.883	2.112	0.060	0.921	2.391	7.225	2	5	2	1	0	153.23	2	346	36.132	9.39
P50544	ery long-chain specific acyl-CoA dehydrogenase, mitochondrial OS=Mus musculus GN=Acadvl PE=1 SV	Acadvl	0.861	2.105	0.150	0.283	2.444	10.213	7	10	7	1	0	127.1046117	7	656	70.831	8.75
Q8BGT5	Alanine aminotransferase 2 OS=Mus musculus GN=Gpt2 PE=1 SV=1	Gpt2	0.818	2.099	0.034	1.081	2.564	13.218	6	6	6	1	0	65.27	6	522	57.906	8
Q52KI8	Serine/arginine repetitive matrix protein 1 OS=Mus musculus GN=Srrm1 PE=1 SV=2	Srrm1	1.075	2.064	0.344	0.727	1.921	23.362	19	42	19	1	0	862.2456757	19	946	106.798	11.87
Q8BWT1	3-ketoacyl-CoA thiolase, mitochondrial OS=Mus musculus GN=Acaa2 PE=1 SV=3	Acaa2	0.860	2.059	0.099	0.697	2.394	17.128	6	10	6	1	0	185.14	6	397	41.803	8.09
P56383	ATP synthase F(0) complex subunit C2, mitochondrial OS=Mus musculus GN=Atp5g2 PE=2 SV=2	Atp5g2	0.891	2.058	0.313	1.851	2.310	4.795	1	4	1	1	0	34.01921088	1	146	15.466	10.35
O35857	ɔchondrial import inner membrane translocase subunit TIM44 OS=Mus musculus GN=Timm44 PE=1 S	Timm44	0.887	2.051	0.039	0.031	2.313	7.743	4	4	4	1	0	51.93209426	4	452	51.059	8.13
P62983	Ubiquitin-40S ribosomal protein S27a OS=Mus musculus GN=Rps27a PE=1 SV=2	s27a-ps2; LOC	0.877	2.048	0.188	0.432	2.335	48.718	7	45	3	1	4	857.655	7	156	17.939	9.64
Q5SS40	14-3-3 protein epsilon OS=Mus musculus GN=Ywhae PE=1 SV=1	Ywhae	0.536	2.043	0.067	1.112	3.813	19.608	5	8	2	1	0	90.04568909	5	255	29.155	4.74
Q64727	Vinculin OS=Mus musculus GN=Vcl PE=1 SV=4	Vcl	0.867	2.040	0.114	0.038	2.354	6.473	6	10	6	1	0	202.2194973	6	1066	116.644	6
Q61578	NADPH:adrenodoxin oxidoreductase, mitochondrial OS=Mus musculus GN=Fdxr PE=1 SV=1	Fdxr	0.972	2.013	0.071	0.484	2.071	5.061	2	2	2	1	0	45.09	2	494	54.168	8.66
P07356	Annexin A2 OS=Mus musculus GN=Anxa2 PE=1 SV=2	Anxa2	0.816	2.002	0.113	0.852	2.451	36.578	13	34	13	1	0	532.9614286	13	339	38.652	7.69
Q99PT1	Rho GDP-dissociation inhibitor 1 OS=Mus musculus GN=Arhgdia PE=1 SV=3	Arhgdia	0.819	1.995	0.325	0.727	2.435	7.843	1	3	1	1	0	81.66666667	1	204	23.393	5.2
H3BL37	Treacle protein OS=Mus musculus GN=Tcof1 PE=1 SV=1	Tcof1	0.920	1.993	0.111	0.615	2.166	23.304	29	57	29	1	0	669.50202	29	1356	138.473	9.26
F8WGL3	Cofilin-1 OS=Mus musculus GN=Cfl1 PE=1 SV=1		0.760	1.991	0.299	0.020	2.619	30.396	6	15	6	1	0	95.83671996	6	227	24.561	8.03
Q9DCW4	Electron transfer flavoprotein subunit beta OS=Mus musculus GN=Etfb PE=1 SV=3	Etfb	0.784	1.990	0.075	0.635	2.539	23.137	5	7	5	1	0	161.15	5	255	27.606	8.1
G5E8N5	L-lactate dehydrogenase OS=Mus musculus GN=Ldha PE=1 SV=1	Ldha	0.593	1.979	0.161	1.297	3.340	18.006	6	12	6	1	0	202.8866667	6	361	39.733	8.35
H9KV00	Protein SON OS=Mus musculus GN=Son PE=1 SV=1	Son	0.810	1.971	0.041	0.102	2.434	21.276	39	106	39	1	0	2118.995883	39	2477	268.652	5.71
P97868	E3 ubiquitin-protein ligase RBBP6 OS=Mus musculus GN=Rbbp6 PE=1 SV=5	Rbbp6	0.750	1.968	0.004	0.585	2.625	11.173	20	28	20	1	0	304.2701375	20	1790	199.466	9.63
Q9Z110	Delta-1-pyrroline-5-carboxylate synthase OS=Mus musculus GN=Aldh18a1 PE=1 SV=2	Aldh18a1	0.777	1.959	0.012	0.531	2.520	10.692	10	14	10	1	0	83.63987503	10	795	87.212	7.55
A0A0R4J0G0	Phosphoenolpyruvate carboxykinase [GTP], mitochondrial OS=Mus musculus GN=Pck2 PE=1 SV=1	Pck2	0.967	1.954	0.214	0.505	2.021	14.693	8	9	8	1	0	181.0671429	8	667	73.371	7.74
Q8CI51	PDZ and LIM domain protein 5 OS=Mus musculus GN=Pdlim5 PE=1 SV=4	Pdlim5	1.129	1.953	0.325	0.100	1.730	10.998	5	7	5	1	0	125.8033333	5	591	63.259	8.25
P35486	hydrogenase E1 component subunit alpha, somatic form, mitochondrial OS=Mus musculus GN=Pdha	Pdha1	0.768	1.950	0.071	0.473	2.540	10.000	4	6	4	1	0	66.5	4	390	43.204	8.19
Q3U7R1	Extended synaptotagmin-1 OS=Mus musculus GN=Esyt1 PE=1 SV=2	Esyt1	1.553	1.945	0.443	0.783	1.253	7.326	7	9	7	1	0	103.7666667	7	1092	121.478	5.95
P16045	Galectin-1 OS=Mus musculus GN=Lgals1 PE=1 SV=3	Lgals1	0.628	1.941	0.353	1.043	3.090	37.778	6	12	6	1	0	80.295	6	135	14.856	5.49
Q922Q8	Leucine-rich repeat-containing protein 59 OS=Mus musculus GN=Lrrc59 PE=1 SV=1	Lrrc59	1.045	1.940	0.251	0.280	1.857	11.401	4	5	4	1	0	56.22	4	307	34.856	9.52
P58252	Elongation factor 2 OS=Mus musculus GN=Eef2 PE=1 SV=2	Eef2	0.872	1.936	0.227	0.811	2.222	19.347	17	45	17	1	0	657.9020602	17	858	95.253	6.83

Uniprot Accession	Protein Description	Gene ID	Average ratio MB +DOX/-DOX (2 to 3exp)	Average Ratio MT +DOX/-DOX (2 to 3Exp)	(SD) MB +DOX/-DOX (2 to 3 Exp)	(SD) MT +DOX/-DOX (2 to 3 Exp)	MT/MB	Protein Coverage	# Peptides	# PSMs	# Unique Peptides	# Protein Groups	# Razor Peptides	Score Mascot	# Peptides Mascot	# AAs	MW [kDa]	calc. pI
Q8BVQ9	26S protease regulatory subunit 7 OS=Mus musculus GN=Psmc2 PE=1 SV=1	Psmc2	1.291	1.924	0.491	0.642	1.490	18.526	8	10	8	1	0	156.9859013	8	475	52.833	6.28
Q9R112	Sulfide:quinone oxidoreductase, mitochondrial OS=Mus musculus GN=Sqrdl PE=1 SV=3	Sqrdl	0.894	1.924	0.146	0.038	2.151	14.667	5	8	5	1	0	161.1524942	5	450	50.25	9.09
Q60605	Myosin light polypeptide 6 OS=Mus musculus GN=Myl6 PE=1 SV=3	Myl6	0.849	1.923	0.375	1.100	2.265	64.901	10	56	9	1	2	1126.832442	10	151	16.919	4.65
Q61171	Peroxiredoxin-2 OS=Mus musculus GN=Prdx2 PE=1 SV=3	Prdx2	0.704	1.923	0.432	0.844	2.731	26.768	5	9	5	1	0	122.5226495	5	198	21.765	5.41
P47738	Aldehyde dehydrogenase, mitochondrial OS=Mus musculus GN=Aldh2 PE=1 SV=1	Aldh2	0.821	1.921	0.116	0.661	2.339	18.304	10	14	10	1	0	225.4107832	10	519	56.502	7.62
Q04750	DNA topoisomerase 1 OS=Mus musculus GN=Top1 PE=1 SV=2	Top1	0.872	1.919	0.135	0.420	2.200	28.162	23	47	23	1	0	435.4126455	23	767	90.819	9.33
P43275	Histone H1.1 OS=Mus musculus GN=Hist1h1a PE=1 SV=2	Hist1h1a	0.839	1.911	0.385	0.600	2.277	29.577	7	29	5	1	0	546.0106954	7	213	21.772	10.93
Q80UG5	Septin-9 OS=Mus musculus GN=Sept9 PE=1 SV=1	Sept9	0.983	1.907	0.250	0.449	1.940	11.664	6	8	6	1	0	109.4933333	6	583	65.534	8.9
A0A0R4J124	SRSF protein kinase 2 OS=Mus musculus GN=Srpk2 PE=1 SV=1	Srpk2	0.815	1.906	0.218	0.427	2.339	7.918	6	7	3	1	3	82.7	6	682	76.837	4.91
P17751	Triosephosphate isomerase OS=Mus musculus GN=Tpi1 PE=1 SV=4	Tpi1	0.651	1.887	0.416	0.672	2.900	12.709	3	7	3	1	0	196.0685714	3	299	32.171	5.74
Q8VCW8	Acyl-CoA synthetase family member 2, mitochondrial OS=Mus musculus GN=Acsf2 PE=1 SV=1	Acsf2	0.861	1.886	0.093	0.497	2.190	4.228	3	4	3	1	0	37.56	3	615	67.907	8.18
P38647	Stress-70 protein, mitochondrial OS=Mus musculus GN=Hspa9 PE=1 SV=3	Hspa9	0.692	1.885	0.091	1.244	2.722	34.904	23	71	22	1	2	1120.72228	23	679	73.416	6.07
Q3UL36	Arginine and glutamate-rich protein 1 OS=Mus musculus GN=Arglu1 PE=1 SV=2	Arglu1	1.276	1.880	1.098	0.577	1.474	35.793	18	76	18	1	0	197.5024065	18	271	32.868	10.36
Q60847	Collagen alpha-1(XII) chain OS=Mus musculus GN=Col12a1 PE=2 SV=3	Col12a1	1.203	1.878	0.556	0.843	1.561	0.673	2	2	2	1	0	17.78	2	3120	340.004	5.64
Q99L04	Dehydrogenase/reductase SDR family member 1 OS=Mus musculus GN=Dhrs1 PE=1 SV=1	Dhrs1	0.781	1.876	0.141	0.343	2.402	7.348	2	5	2	1	0	136.27	2	313	33.983	8.35
O54774	AP-3 complex subunit delta-1 OS=Mus musculus GN=Ap3d1 PE=1 SV=1	Ap3d1	0.971	1.868	0.093	0.703	1.923	26.939	34	61	34	1	0	583.3397881	34	1199	134.996	7.37
Q32P04	Keratin 5 OS=Mus musculus GN=Krt5 PE=1 SV=2	Krt5	1.413	1.865	1.207	0.445	1.320	24.483	19	88	7	1	6	492.454823	19	580	61.729	7.75
P48678	Prelamin-A/C OS=Mus musculus GN=Lmna PE=1 SV=2	Lmna	0.688	1.854	0.194	0.342	2.696	43.008	27	66	26	1	1	769.2096066	27	665	74.193	6.98
Q3SYP5	Keratin 16 OS=Mus musculus GN=Krt16 PE=1 SV=1	Krt16	2.092	1.849	2.073	0.214	0.884	13.433	7	60	3	1	0	794.8728777	7	469	51.574	5.2
E9QPD7	Pyruvate carboxylase OS=Mus musculus GN=Pcx PE=1 SV=1	Pcx	0.879	1.848	0.174	0.835	2.104	58.439	61	676	61	1	0	13091.39632	61	1179	129.749	6.71
D3YVN7	Elongation factor Tu OS=Mus musculus GN=Gm9755 PE=3 SV=1	Gm9755	0.737	1.844	0.056	0.779	2.502	28.761	12	16	12	1	0	185.4444735	12	452	49.507	7.56
Q61781	Keratin, type I cytoskeletal 14 OS=Mus musculus GN=Krt14 PE=1 SV=2	Krt14	1.093	1.834	0.562	0.616	1.679	28.719	15	84	1	1	6	949.8857691	15	484	52.834	5.17
Q80SY5	Pre-mRNA-splicing factor 38B OS=Mus musculus GN=Prpf38b PE=1 SV=1	Prpf38b	1.149	1.830	0.625	0.395	1.593	10.886	6	12	6	1	0	244.1966554	6	542	63.715	10.54
Q3U9G9	Lamin-B receptor OS=Mus musculus GN=Lbr PE=1 SV=2	Lbr	1.804	1.828	1.174	0.268	1.013	9.265	7	8	7	1	0	159.4228571	7	626	71.395	9.36
Q5SW88	Protein Rab1a OS=Mus musculus GN=Rab1a PE=1 SV=1	Rab1; Rab1a	0.891	1.818	0.129	0.379	2.041	41.584	9	20	5	1	4	410.225	9	202	22.358	6.21
P42208	Septin-2 OS=Mus musculus GN=Sept2 PE=1 SV=2	Sept2	0.907	1.810	0.236	0.685	1.995	6.648	3	4	3	1	0	33.43	3	361	41.499	6.55
Q99JY0	Trifunctional enzyme subunit beta, mitochondrial OS=Mus musculus GN=Hadhb PE=1 SV=1	Hadhb	0.814	1.809	0.067	0.370	2.222	9.474	5	7	5	1	0	63.22	5	475	51.353	9.38
F8VPV0	Pericentrin OS=Mus musculus GN=Pcnt PE=1 SV=1	Pcnt	0.965	1.807	0.362	0.104	1.873	0.754	2	2	2	1	0	48.95	2	2916	331.134	5.38
Q9CQN1	Heat shock protein 75 kDa, mitochondrial OS=Mus musculus GN=Trap1 PE=1 SV=1	Trap1	0.826	1.806	0.004	0.325	2.185	21.388	14	25	13	1	0	330.3504055	14	706	80.159	6.68
F6VW30	14-3-3 protein theta (Fragment) OS=Mus musculus GN=Ywhaq PE=1 SV=1		0.579	1.800	0.220	0.375	3.111	17.822	6	16	1	1	1	194.3007421	6	303	34.327	6.38
O88844	Isocitrate dehydrogenase [NADP] cytoplasmic OS=Mus musculus GN=Idh1 PE=1 SV=2	Idh1	0.878	1.799	0.299	0.480	2.049	5.556	3	4	3	1	0	58.73666667	3	414	46.644	7.17
A2A6A1	G patch domain-containing protein 8 OS=Mus musculus GN=Gpatch8 PE=1 SV=1	Gpatch8	1.124	1.795	0.271	0.177	1.598	3.721	4	6	4	1	0	136.58	4	1505	164.888	7.64
A0A0R4J083	Long-chain-specific acyl-CoA dehydrogenase, mitochondrial OS=Mus musculus GN=Acadl PE=1 SV=1	Acadl	0.769	1.794	0.168	0.198	2.334	10.930	4	5	4	1	0	112.63	4	430	47.866	8.15
C6AAF2	60 kDa chaperonin OS=Bartonella grahamii (strain as4aup) GN=groL PE=3 SV=1	oEL; Bgr_177	0.919	1.792	0.024	0.262	1.949	11.700	6	9	6	1	0	83.38345328	6	547	57.619	5.22
Q9DAW9	Calponin-3 OS=Mus musculus GN=Cnn3 PE=1 SV=1	Cnn3	0.883	1.786	0.421	0.169	2.023	8.182	2	4	2	1	0	127.67	2	330	36.406	5.72
Q9D051	uvate dehydrogenase E1 component subunit beta, mitochondrial OS=Mus musculus GN=Pdhb PE=1 S	Pdhb	0.863	1.781	0.255	0.477	2.063	22.563	7	13	7	1	0	193.28	7	359	38.912	6.87
O88569	Heterogeneous nuclear ribonucleoproteins A2/B1 OS=Mus musculus GN=Hnrnpa2b1 PE=1 SV=2	Hnrnpa2b1	0.620	1.780	0.032	0.813	2.872	20.113	7	14	6	1	1	186.9479009	7	353	37.38	8.95
P54071	Isocitrate dehydrogenase [NADP], mitochondrial OS=Mus musculus GN=Idh2 PE=1 SV=3	Idh2	0.605	1.780	0.172	0.852	2.940	7.080	3	4	3	1	0	116.85	3	452	50.874	8.69
P63101	14-3-3 protein zeta/delta OS=Mus musculus GN=Ywhaz PE=1 SV=1	Ywhaz	0.648	1.777	0.356	0.786	2.741	28.980	7	19	3	1	4	253.1805974	7	245	27.754	4.79
Q3UMA3	Hepatocyte growth factor-regulated tyrosine kinase substrate OS=Mus musculus GN=Hgs PE=1 SV=1	Hgs	0.770	1.772	0.107	0.187	2.301	2.191	2	2	2	1	0	33.81	2	776	86.089	6.16
Q8BMS1	Trifunctional enzyme subunit alpha, mitochondrial OS=Mus musculus GN=Hadha PE=1 SV=1	Hadha	0.748	1.770	0.092	1.033	2.367	17.038	12	16	12	1	0	198.3924471	12	763	82.617	9.14
Q9D0F4	NF-kappa-B-activating protein OS=Mus musculus GN=Nkap PE=2 SV=1	Nkap	0.880	1.769	0.231	0.273	2.011	12.289	4	10	4	1	0	170.13	4	415	47.199	10.13
Q5FW97	Alpha-enolase OS=Mus musculus GN=EG433182 PE=1 SV=1	1; Gm5506; Er	0.653	1.765	0.250	0.950	2.705	62.673	22	115	10	1	15	1654.934359	22	434	47.111	6.8
B9EHN0	Ubiquitin-activating enzyme E1, Chr X OS=Mus musculus GN=Uba1 PE=1 SV=1	Uba1	0.693	1.765	0.084	0.751	2.546	3.119	4	6	4	1	0	37.66726314	4	1058	117.734	5.66
Q9CZD3	Glycine--tRNA ligase OS=Mus musculus GN=Gars PE=1 SV=1	Gars	0.791	1.762	0.159	0.468	2.229	6.722	5	5	5	1	0	74.13	5	729	81.826	6.65
Q7TPR4	Alpha-actinin-1 OS=Mus musculus GN=Actn1 PE=1 SV=1	Actn1	0.767	1.761	0.162	0.608	2.295	3.475	3	5	3	1	0	96.83	3	892	103.004	5.38
B1AQ77	Keratin 15, isoform CRA_a OS=Mus musculus GN=Krt15 PE=1 SV=1	Krt15	1.009	1.760	0.468	0.618	1.744	12.281	8	96	3	1	0	596.9286045	8	456	49.463	4.86
Q6IME9	Keratin, type II cytoskeletal 72 OS=Mus musculus GN=Krt72 PE=3 SV=1	Krt72; Krt72-p	1.005	1.759	0.470	0.400	1.750	11.538	6	13	4	1	0	108.9614286	6	520	56.715	7.4
P97351	40S ribosomal protein S3a OS=Mus musculus GN=Rps3a PE=1 SV=3	Rps3a; Rps3a1	0.649	1.758	0.102	0.141	2.708	12.879	4	5	4	1	0	70.82604704	4	264	29.866	9.73
Q07417	Short-chain specific acyl-CoA dehydrogenase, mitochondrial OS=Mus musculus GN=Acads PE=1 SV=2	Acads	0.932	1.758	0.072	0.353	1.887	16.019	6	9	6	1	0	58.98381613	6	412	44.861	8.47
Q497I4	Keratin, type I cuticular Ha5 OS=Mus musculus GN=Krt35 PE=1 SV=1	Krt35	4.663	1.756	5.507	0.222	0.377	8.132	4	5	2	1	0	45.43	4	455	50.497	4.97
Q3ULU3	Branched-chain-amino-acid aminotransferase OS=Mus musculus GN=Bcat2 PE=1 SV=1	Bcat2	0.849	1.752	0.036	0.667	2.064	5.598	2	3	2	1	0	86.15666667	2	393	44.099	8.29
Q8BTI8	Serine/arginine repetitive matrix protein 2 OS=Mus musculus GN=Srrm2 PE=1 SV=3	Srrm2	0.559	1.745	0.003	0.668	3.120	27.858	63	172	54	1	10	2038.374563	63	2703	294.666	12.03
Q6IFX2	Keratin, type I cytoskeletal 42 OS=Mus musculus GN=Krt42 PE=1 SV=1	Krt42	2.413	1.744	2.591	0.271	0.723	29.425	15	63	6	1	0	710.3161291	15	452	50.102	5.16
Q149Z9	Histone H1.3 OS=Mus musculus GN=Hist1h1d PE=1 SV=1	Hist1h1d	0.927	1.743	0.415	0.154	1.881	44.796	13	114	2	1	12	2165.344536	13	221	22.086	11.03
P78371	T-complex protein 1 subunit beta OS=Homo sapiens GN=CCT2 PE=1 SV=4	CCT2	0.662	1.737	0.039	0.393	2.623	4.486	2	6	2	1	0	62.79	2	535	57.452	6.46
P63017	Heat shock cognate 71 kDa protein OS=Mus musculus GN=Hspa8 PE=1 SV=1	Hspa8	0.775	1.735	0.105	0.699	2.240	36.997	23	58	14	1	9	689.9231958	23	646	70.827	5.52

Uniprot Accession	Protein Description	Gene ID	Average ratio MB +DOX/-DOX (2 to 3exp)	Average Ratio MT +DOX/-DOX (2 to 3Exp)	(SD) MB +DOX/-DOX (2 to 3 Exp)	(SD) MT +DOX/-DOX (2 to 3 Exp)	MT/MB	Protein Coverage	# Peptides	# PSMs	# Unique Peptides	# Protein Groups	# Razor Peptides	Score Mascot	# Peptides Mascot	# AAs	MW [kDa]	calc. pI
Q3TTY5	Keratin, type II cytoskeletal 2 epidermal OS=Mus musculus GN=Krt2 PE=1 SV=1	Krt2	1.450	1.731	1.084	0.520	1.194	8.345	9	57	3	1	0	578.6812821	9	707	70.88	8.06
Q9D0E1	Heterogeneous nuclear ribonucleoprotein M OS=Mus musculus GN=Hnrnpm PE=1 SV=3	Hnrnpm	0.530	1.727	0.192	0.407	3.261	11.248	11	14	11	1	0	160.2907445	11	729	77.597	8.63
P17742	Peptidyl-prolyl cis-trans isomerase A OS=Mus musculus GN=Ppia PE=1 SV=2	Ppia	0.665	1.726	0.308	0.283	2.596	26.220	5	8	5	1	0	65.44906019	5	164	17.96	7.9
P31001	Desmin OS=Mus musculus GN=Des PE=1 SV=3	Des	0.755	1.725	0.116	0.226	2.287	50.746	26	123	22	1	0	1174.049973	26	469	53.465	5.27
Q3UDZ1	Ras homolog gene family, member G OS=Mus musculus GN=Rhog PE=1 SV=1	Rhog	0.933	1.725	0.053	0.026	1.850	23.560	4	4	3	1	1	78.86	4	191	21.295	8.12
Q9QWL7	Keratin, type I cytoskeletal 17 OS=Mus musculus GN=Krt17 PE=1 SV=3	Krt17	1.190	1.725	0.771	0.288	1.450	27.021	15	89	1	1	18	826.9942116	15	433	48.132	5.06
Q8CGK3	Lon protease homolog, mitochondrial OS=Mus musculus GN=Lonp1 PE=1 SV=2	Lonp1	0.636	1.720	0.111	1.023	2.703	9.168	8	12	8	1	0	162.74	8	949	105.776	6.57
Q3U186	Probable arginine--tRNA ligase, mitochondrial OS=Mus musculus GN=Rars2 PE=1 SV=1	Rars2	0.781	1.719	0.067	0.127	2.201	3.633	2	3	2	1	0	42.24	2	578	65.295	8.02
P52480	Pyruvate kinase PKM OS=Mus musculus GN=Pkm PE=1 SV=4	Pkm	0.861	1.716	0.261	0.756	1.993	35.217	15	46	15	1	0	840.8153488	15	531	57.808	7.47
Q99LC5	Electron transfer flavoprotein subunit alpha, mitochondrial OS=Mus musculus GN=Etfa PE=1 SV=2	Etfa	0.794	1.716	0.220	1.063	2.160	25.225	7	12	7	1	0	220.0890909	7	333	34.988	8.38
Q80X90	Filamin-B OS=Mus musculus GN=Flnb PE=1 SV=3	Flnb	0.836	1.713	0.014	0.399	2.050	4.842	12	13	7	1	0	164.3916317	12	2602	277.651	5.71
Q4VAG4	60S ribosomal protein L22 OS=Mus musculus GN=Rpl22 PE=1 SV=1	?2; LOC10050	0.895	1.702	0.179	0.276	1.901	18.750	2	7	2	1	0	211.1742857	2	128	14.75	9.19
P02535	Keratin, type I cytoskeletal 10 OS=Mus musculus GN=Krt10 PE=1 SV=3	Krt10	1.125	1.699	0.536	0.549	1.510	11.404	9	133	8	1	0	2314.477753	9	570	57.735	5.11
P63038	60 kDa heat shock protein, mitochondrial OS=Mus musculus GN=Hspd1 PE=1 SV=1	Hspd1	0.653	1.694	0.210	0.733	2.593	21.466	11	22	11	1	0	326.6969476	11	573	60.917	6.18
P14685	26S proteasome non-ATPase regulatory subunit 3 OS=Mus musculus GN=Psmd3 PE=1 SV=3	Psmd3	1.042	1.694	0.159	0.116	1.625	18.679	8	8	8	1	0	119.88	8	530	60.68	8.44
A2AEX6	Four and a half LIM domains protein 1 OS=Mus musculus GN=Fhl1 PE=1 SV=1	Fhl1	1.100	1.686	0.049	0.141	1.533	21.683	7	14	2	1	5	222.2233333	7	309	35.056	8.44
Q9DCL9	Multifunctional protein ADE2 OS=Mus musculus GN=Paics PE=1 SV=4	Paics	0.800	1.684	0.180	0.661	2.105	4.235	2	4	2	1	0	43.38	2	425	46.976	7.23
P13020	Gelsolin OS=Mus musculus GN=Gsn PE=1 SV=3	Gsn	0.839	1.677	0.163	1.027	1.999	8.846	7	21	7	1	0	275.1732151	7	780	85.888	6.18
P21550	Beta-enolase OS=Mus musculus GN=Eno3 PE=1 SV=3	Eno3	0.660	1.673	0.198	0.654	2.533	29.954	11	34	5	1	1	704.9713586	11	434	46.995	7.18
C6ACT4	Elongation factor Tu OS=Bartonella grahamii (strain as4aup) GN=tuf1 PE=3 SV=1	; Bgr_06850; E	0.706	1.672	0.288	0.378	2.370	6.138	3	3	3	1	0	41.04	3	391	42.811	5.38
F2Z456	NADH-cytochrome b5 reductase OS=Mus musculus GN=Cyb5r3 PE=1 SV=1		0.643	1.669	0.248	0.098	2.595	27.476	8	22	8	1	0	267.5398194	8	313	34.907	9.1
Q9Z204	Heterogeneous nuclear ribonucleoproteins C1/C2 OS=Mus musculus GN=Hnrnpc PE=1 SV=1	Hnrnpc	0.763	1.668	0.017	0.316	2.185	16.613	5	10	5	1	0	189.6164079	5	313	34.364	5.05
Q8BL97	Serine/arginine-rich splicing factor 7 OS=Mus musculus GN=Srsf7 PE=1 SV=1	Srsf7	1.187	1.668	0.805	0.600	1.405	12.360	2	6	2	1	0	211.7133333	2	267	30.799	11.9
O08528	Hexokinase-2 OS=Mus musculus GN=Hk2 PE=1 SV=1	Hk2	0.844	1.665	0.275	0.036	1.972	2.181	2	2	2	1	0	65.61	2	917	102.469	6.11
P10922	Histone H1.0 OS=Mus musculus GN=H1f0 PE=2 SV=4	H1f0	1.197	1.663	0.450	0.639	1.390	21.134	5	18	5	1	0	397.091568	5	194	20.848	10.9
E9Q1G8	Septin-7 OS=Mus musculus GN=Sept7 PE=1 SV=2	Sept7	0.863	1.659	0.124	0.438	1.923	5.263	3	5	3	1	0	31.29	3	437	50.617	8.57
P43274	Histone H1.4 OS=Mus musculus GN=Hist1h1e PE=1 SV=2	Hist1h1e	0.940	1.655	0.387	0.093	1.760	34.247	10	83	3	1	0	1621.968991	10	219	21.964	11.11
Q5SQB7	MCG68069 OS=Mus musculus GN=Npm1 PE=1 SV=1	Npm1	0.659	1.654	0.185	0.372	2.508	16.438	4	5	4	1	0	74.85837374	4	292	32.54	4.77
Q9DBJ1	Phosphoglycerate mutase 1 OS=Mus musculus GN=Pgam1 PE=1 SV=3	Pgam1	0.759	1.651	0.294	0.507	2.176	6.693	2	3	2	1	0	67.27	2	254	28.814	7.18
Q8K009	Mitochondrial 10-formyltetrahydrofolate dehydrogenase OS=Mus musculus GN=Aldh1l2 PE=1 SV=2	Aldh1l2	0.842	1.648	0.105	0.659	1.958	8.884	8	13	8	1	0	122.5144444	8	923	101.526	6.29
P68369	Tubulin alpha-1A chain OS=Mus musculus GN=Tuba1a PE=1 SV=1	Tuba1a	0.833	1.647	0.201	0.718	1.977	43.902	16	86	6	1	16	1384.626958	16	451	50.104	5.06
P43276	Histone H1.5 OS=Mus musculus GN=Hist1h1b PE=1 SV=2	Hist1h1b	1.040	1.644	0.469	0.133	1.580	38.117	11	55	9	1	0	1181.196949	11	223	22.562	10.92
Q8VDD5	Myosin-9 OS=Mus musculus GN=Myh9 PE=1 SV=4	Myh9	0.924	1.643	0.197	0.993	1.778	61.173	136	916	33	1	144	11782.01071	136	1960	226.232	5.66
E9QKR0	uanine nucleotide-binding protein G(I)/G(S)/G(T) subunit beta-2 OS=Mus musculus GN=Gnb2 PE=1 SV		0.946	1.639	0.082	0.109	1.732	8.377	3	6	1	1	2	88.39	3	382	41.382	6.6
Q99LC3	drogenase [ubiquinone] 1 alpha subcomplex subunit 10, mitochondrial OS=Mus musculus GN=Ndufa1	Ndufa10	0.763	1.638	0.096	0.339	2.146	11.268	4	5	4	1	0	59.06333333	4	355	40.578	7.78
Q8BGZ7	Keratin, type II cytoskeletal 75 OS=Mus musculus GN=Krt75 PE=1 SV=1	Krt75	1.772	1.627	1.198	0.226	0.918	17.241	11	53	1	1	0	425.9344828	11	551	59.704	8.31
A2AVJ7	Ribosome-binding protein 1 OS=Mus musculus GN=Rrbp1 PE=1 SV=1	Rrbp1	0.865	1.626	0.173	0.061	1.881	62.432	82	172	82	1	0	1977.565831	82	1464	158.301	9.19
Q8BMF4	due acetyltransferase component of pyruvate dehydrogenase complex, mitochondrial OS=Mus musc	Dlat	0.861	1.619	0.012	0.142	1.881	7.632	4	4	4	1	0	59.45	4	642	67.899	8.57
P51881	ADP/ATP translocase 2 OS=Mus musculus GN=Slc25a5 PE=1 SV=3	Slc25a5	0.733	1.615	0.141	0.964	2.204	35.906	12	22	7	1	5	386.0653679	12	298	32.91	9.73
Q9DAM7	Transmembrane protein 263 OS=Mus musculus GN=Tmem263 PE=1 SV=1	97468; Tmem	0.967	1.613	0.673	0.252	1.668	49.565	4	11	4	1	0	132.3936364	4	115	11.542	9.32
Q9QZD9	Eukaryotic translation initiation factor 3 subunit I OS=Mus musculus GN=Eif3i PE=1 SV=1	Eif3i	0.796	1.607	0.277	0.777	2.019	5.846	2	3	2	1	0	47.68666667	2	325	36.438	5.64
A8IP69	14-3-3 protein gamma OS=Mus musculus GN=Ywhag PE=1 SV=1	Ywhag	0.633	1.603	0.367	0.626	2.531	21.457	6	9	2	1	0	136.0442605	6	247	28.285	4.89
Q8BH95	Enoyl-CoA hydratase, mitochondrial OS=Mus musculus GN=Echs1 PE=1 SV=1	Echs1	0.807	1.602	0.200	0.622	1.986	10.000	3	4	3	1	0	49.8762985	3	290	31.454	8.48
P62196	26S protease regulatory subunit 8 OS=Mus musculus GN=Psmc5 PE=1 SV=1	Psmc5	0.665	1.598	0.207	0.119	2.402	17.980	7	9	6	1	1	98.02669985	7	406	45.597	7.55
P62071	Ras-related protein R-Ras2 OS=Mus musculus GN=Rras2 PE=1 SV=1	Rras2	0.914	1.598	0.281	0.284	1.748	30.882	5	7	5	1	0	125.9333333	5	204	23.385	6.01
Q5SXR6	Clathrin heavy chain OS=Mus musculus GN=Cltc PE=1 SV=1	Cltc	0.686	1.596	0.169	0.556	2.325	7.326	11	16	11	1	0	148.9133333	11	1679	191.864	5.69
P80317	T-complex protein 1 subunit zeta OS=Mus musculus GN=Cct6a PE=1 SV=3	Cct6a	0.507	1.595	0.247	0.533	3.146	16.573	9	18	9	1	0	193.569377	9	531	57.968	7.08
P15880	40S ribosomal protein S2 OS=Homo sapiens GN=RPS2 PE=1 SV=2	RPS2	0.692	1.592	0.146	0.776	2.301	28.328	8	17	8	1	0	368.0343541	8	293	31.305	10.24
Q99LF4	tRNA-splicing ligase RtcB homolog OS=Mus musculus GN=Rtcb PE=1 SV=1	10Wsu52e; Rt	0.684	1.592	0.176	0.336	2.328	7.921	4	5	4	1	0	56.41666667	4	505	55.214	7.23
Q642K5	40S ribosomal protein S30 OS=Mus musculus GN=Fau PE=1 SV=1	Fau	1.153	1.592	0.178	0.828	1.381	9.023	3	16	3	1	0	162.6453846	3	133	14.407	10.05
P20029	78 kDa glucose-regulated protein OS=Mus musculus GN=Hspa5 PE=1 SV=3	Hspa5	0.738	1.591	0.220	0.536	2.155	24.122	14	30	11	1	0	433.7889801	14	655	72.377	5.16
D3YWG1	Protein Gm7964 OS=Mus musculus GN=Gm7964 PE=4 SV=1		0.694	1.591	0.265	0.096	2.291	9.503	4	8	4	1	0	106.2857143	4	463	50.9	5.76
Q9Z2D6	Methyl-CpG-binding protein 2 OS=Mus musculus GN=Mecp2 PE=1 SV=1	Mecp2	0.899	1.589	0.541	0.086	1.767	19.215	8	10	8	1	0	232.67	8	484	52.275	9.96
Q5XJY5	Coatomer subunit delta OS=Mus musculus GN=Arcn1 PE=1 SV=2	Arcn1	0.918	1.586	0.185	0.252	1.728	18.004	9	12	9	1	0	191.89	9	511	57.193	6.21
Q4V9W2	Protein SREK1IP1 OS=Mus musculus GN=Srek1ip1 PE=1 SV=1	Srek1ip1	0.647	1.583	0.157	0.160	2.446	18.301	5	10	5	1	0	38.26620302	5	153	18.14	9.91
Q9Z1Q5	Chloride intracellular channel protein 1 OS=Mus musculus GN=Clic1 PE=1 SV=3	Clic1	0.664	1.579	0.222	0.742	2.380	19.087	3	3	3	1	0	94.81	3	241	26.996	5.17
Q03265	ATP synthase subunit alpha, mitochondrial OS=Mus musculus GN=Atp5a1 PE=1 SV=1	Atp5a1	0.719	1.579	0.225	0.877	2.197	42.676	26	76	24	1	2	1599.92349	26	553	59.716	9.19

Uniprot Accession	Protein Description	Gene ID	Average ratio MB +DOX/-DOX (2 to 3exp)	Average Ratio MT +DOX/-DOX (2 to 3Exp)	(SD) MB +DOX/-DOX (2 to 3 Exp)	(SD) MT +DOX/-DOX (2 to 3 Exp)	MT/MB	Protein Coverage	# Peptides	# PSMs	# Unique Peptides	# Protein Groups	# Razor Peptides	Score Mascot	# Peptides Mascot	# AAs	MW [kDa]	calc. pI
P26043	Radixin OS=Mus musculus GN=Rdx PE=1 SV=3	Rdx	0.884	1.579	0.033	0.336	1.785	10.806	7	9	2	1	0	73.68089669	7	583	68.5	6.2
P08238	Heat shock protein HSP 90-beta OS=Homo sapiens GN=HSP90AB1 PE=1 SV=4	HSP90AB1	0.703	1.579	0.110	0.702	2.244	36.326	27	108	16	1	13	1959.767022	27	724	83.212	5.03
P35700	Peroxiredoxin-1 OS=Mus musculus GN=Prdx1 PE=1 SV=1	Prdx1	0.808	1.577	0.286	0.517	1.951	42.211	9	24	7	1	2	296.5694737	9	199	22.162	8.12
Q9D881	Cytochrome c oxidase subunit 5B, mitochondrial OS=Mus musculus GN=Cox5b PE=1 SV=1	6079; Gm1127	0.605	1.573	0.172	0.187	2.599	15.504	2	3	2	1	0	47.9749538	2	129	13.838	8.12
Q9JKR6	Hypoxia up-regulated protein 1 OS=Mus musculus GN=Hyou1 PE=1 SV=1	Hyou1	0.727	1.568	0.177	0.162	2.156	6.406	7	9	7	1	0	66.06849522	7	999	111.112	5.19
Q9D0I9	Arginine--tRNA ligase, cytoplasmic OS=Mus musculus GN=Rars PE=1 SV=2	Rars	0.855	1.568	0.055	0.152	1.833	12.121	8	8	8	1	0	102.48	8	660	75.625	7.55
Q6P542	ATP-binding cassette sub-family F member 1 OS=Mus musculus GN=Abcf1 PE=1 SV=1	Abcf1	0.907	1.567	0.102	0.283	1.727	28.315	20	40	20	1	0	586.1850508	20	837	94.887	6.51
Q9DCY1	Peptidyl-prolyl cis-trans isomerase OS=Mus musculus GN=Ppib PE=1 SV=1	Ppib	1.015	1.561	0.225	0.446	1.538	22.685	5	15	5	1	0	212.0416161	5	216	23.699	9.55
A0A0A0MQF6	Glyceraldehyde-3-phosphate dehydrogenase OS=Mus musculus GN=Gapdh PE=1 SV=1	Gapdh	0.583	1.558	0.353	1.007	2.672	29.248	9	39	5	1	8	989.9756073	9	359	38.629	8.97
P20152	Vimentin OS=Mus musculus GN=Vim PE=1 SV=3	Vim	0.869	1.558	0.306	0.181	1.792	78.541	46	331	41	1	8	4539.089035	46	466	53.655	5.12
O55029	Coatomer subunit beta' OS=Mus musculus GN=Copb2 PE=1 SV=2	Copb2	0.732	1.555	0.087	0.067	2.124	1.878	2	3	2	1	0	25.57	2	905	102.384	5.3
P99024	Tubulin beta-5 chain OS=Mus musculus GN=Tubb5 PE=1 SV=1	Tubb5	0.735	1.554	0.265	0.458	2.114	42.342	18	85	3	1	27	1182.029599	18	444	49.639	4.89
Q8VDJ3	Vigilin OS=Mus musculus GN=Hdlbp PE=1 SV=1	Hdlbp	0.962	1.553	0.042	0.220	1.615	15.063	19	30	19	1	0	246.2630873	19	1268	141.655	6.87
P68104	Elongation factor 1-alpha 1 OS=Homo sapiens GN=EEF1A1 PE=1 SV=1	EEF1A1	0.698	1.553	0.140	0.497	2.223	22.727	13	54	13	1	0	497.1484649	13	462	50.109	9.01
P09405	Nucleolin OS=Mus musculus GN=Ncl PE=1 SV=2	Ncl	0.571	1.552	0.052	0.303	2.719	14.710	11	17	11	1	0	141.6216801	11	707	76.677	4.75
P48036	Annexin A5 OS=Mus musculus GN=Anxa5 PE=1 SV=1	Anxa5	0.602	1.551	0.001	0.817	2.577	9.404	3	5	3	1	0	55.77	3	319	35.73	4.96
P04264	Keratin, type II cytoskeletal 1 OS=Homo sapiens GN=KRT1 PE=1 SV=6	KRT1	1.159	1.549	0.695	0.422	1.336	51.398	36	356	27	1	12	5622.652238	36	644	65.999	8.12
Q4FJX4	Csrp1 protein OS=Mus musculus GN=Csrp1 PE=1 SV=1	Csrp1	0.913	1.549	0.390	0.422	1.698	35.233	6	11	6	1	0	218.8608038	6	193	20.57	8.57
P08249	Malate dehydrogenase, mitochondrial OS=Mus musculus GN=Mdh2 PE=1 SV=3	Mdh2	0.692	1.549	0.364	0.372	2.240	13.609	4	7	4	1	0	133.4657143	4	338	35.589	8.68
Q80ZM5	H1 histone family, member X OS=Mus musculus GN=H1fx PE=1 SV=1	H1fx	1.299	1.548	0.212	0.192	1.192	30.319	7	11	7	1	0	146.2233548	7	188	20.139	11.22
P26041	Moesin OS=Mus musculus GN=Msn PE=1 SV=3	Msn	0.770	1.545	0.133	0.495	2.008	21.317	15	33	10	1	5	188.790692	15	577	67.725	6.6
E9PYH2	Cytosolic acyl coenzyme A thioester hydrolase OS=Mus musculus GN=Acot7 PE=1 SV=1	Acot7	0.933	1.543	0.012	0.026	1.654	7.552	2	2	2	1	0	33.48	2	384	42.799	8.68
Q99KI0	Aconitate hydratase, mitochondrial OS=Mus musculus GN=Aco2 PE=1 SV=1	Aco2	0.847	1.539	0.122	0.634	1.817	17.179	11	28	11	1	0	365.1502677	11	780	85.41	7.93
P14873	Microtubule-associated protein 1B OS=Mus musculus GN=Map1b PE=1 SV=2	Map1b; Mtap1	0.938	1.537	0.246	0.259	1.638	13.231	30	51	29	1	1	590.0632096	30	2464	270.089	4.83
P62869	Transcription elongation factor B polypeptide 2 OS=Mus musculus GN=Tceb2 PE=1 SV=1	Tceb2	0.743	1.536	0.149	0.522	2.068	14.407	2	2	2	1	0	48.74	2	118	13.162	5.01
E9QNN1	ATP-dependent RNA helicase A OS=Mus musculus GN=Dhx9 PE=1 SV=1	Dhx9	0.727	1.534	0.035	0.482	2.109	6.720	9	10	9	1	0	138.0246442	9	1384	149.596	6.83
G5E924	Heterogeneous nuclear ribonucleoprotein L (Fragment) OS=Mus musculus GN=Hnrnpl PE=1 SV=1		0.735	1.533	0.170	0.619	2.087	4.715	3	3	3	1	0	64.19800347	3	615	66.89	8.18
Q8C2Q7	Heterogeneous nuclear ribonucleoprotein H OS=Mus musculus GN=Hnrnph1 PE=1 SV=1	Hnrnph1	0.728	1.526	0.000	0.317	2.097	15.890	6	14	2	1	3	230.0457143	6	472	51.185	6.8
Q8VED5	Keratin, type II cytoskeletal 79 OS=Mus musculus GN=Krt79 PE=1 SV=2	Krt79	2.052	1.512	2.117	0.596	0.737	10.546	8	38	2	1	0	215.9828571	8	531	57.517	7.69
F6YVP7	Protein Gm10260 OS=Mus musculus GN=Gm10260 PE=3 SV=2		0.599	1.509	0.008	0.338	2.517	13.816	3	5	3	1	0	63.54	3	152	17.661	10.74
Q3UAD6	Endoplasmin OS=Mus musculus GN=Hsp90b1 PE=1 SV=1	Hsp90b1	0.606	1.508	0.211	0.695	2.487	30.673	25	48	24	1	0	575.7786553	25	802	92.418	4.82
Q91YN9	BAG family molecular chaperone regulator 2 OS=Mus musculus GN=Bag2 PE=1 SV=1	Bag2	0.785	1.508	0.230	0.227	1.922	21.905	5	9	5	1	0	88.00410672	5	210	23.459	6.42
G3UY93	Valine--tRNA ligase (Fragment) OS=Mus musculus GN=Vars PE=1 SV=1		0.842	1.508	0.167	0.371	1.791	7.199	8	12	8	1	0	256.6388377	8	1278	141.317	7.75
P03930	ATP synthase protein 8 OS=Mus musculus GN=Mtatp8 PE=1 SV=1	ATP8	0.932	1.507	0.223	0.303	1.616	34.328	2	4	2	1	0	69.3	2	67	7.761	9.88
A6ZI44	Fructose-bisphosphate aldolase OS=Mus musculus GN=Aldoa PE=1 SV=1	Aldoa	0.643	1.504	0.243	0.139	2.338	10.766	4	11	4	1	0	170.5043125	4	418	45.092	7.91
P50580	Proliferation-associated protein 2G4 OS=Mus musculus GN=Pa2g4 PE=1 SV=3	Pa2g4	0.677	1.503	0.229	0.600	2.220	2.792	1	2	1	1	0	86.38	1	394	43.671	6.86
Q60932	Voltage-dependent anion-selective channel protein 1 OS=Mus musculus GN=Vdac1 PE=1 SV=3	Vdac1	0.892	1.501	0.146	0.038	1.682	10.473	3	3	3	1	0	49.91	3	296	32.331	8.43
Q78PY7	Staphylococcal nuclease domain-containing protein 1 OS=Mus musculus GN=Snd1 PE=1 SV=1	Snd1	0.810	1.495	0.035	0.740	1.845	1.978	2	3	2	1	0	57.37	2	910	102.025	7.43
P60335	Poly(rC)-binding protein 1 OS=Mus musculus GN=Pcbp1 PE=1 SV=1	Pcbp1	0.753	1.495	0.102	0.360	1.986	32.584	9	26	5	1	5	369.8529096	9	356	37.474	7.09
Q922B2	Aspartate--tRNA ligase, cytoplasmic OS=Mus musculus GN=Dars PE=1 SV=2	Dars	1.027	1.494	0.366	0.426	1.455	29.940	15	23	15	1	0	225.2964002	15	501	57.111	6.49
Q8VEK3	Heterogeneous nuclear ribonucleoprotein U OS=Mus musculus GN=Hnrnpu PE=1 SV=1	Hnrnpu	0.717	1.494	0.081	0.419	2.085	12.250	10	17	10	1	0	191.2288812	10	800	87.863	6.24
Q9ERG0	LIM domain and actin-binding protein 1 OS=Mus musculus GN=Lima1 PE=1 SV=3	Lima1	1.079	1.492	0.010	0.121	1.383	11.023	8	13	8	1	0	179.0866667	8	753	84.008	6.6
Q3TF14	Adenosylhomocysteinase OS=Mus musculus GN=Ahcy PE=1 SV=1	Ahcy; Gm4737	0.738	1.490	0.193	0.369	2.020	2.778	1	2	1	1	0	101.62	1	432	47.657	6.54
P56480	ATP synthase subunit beta, mitochondrial OS=Mus musculus GN=Atp5b PE=1 SV=2	Atp5b	0.666	1.485	0.233	0.721	2.228	30.246	12	25	12	1	0	472.1897327	12	529	56.265	5.34
P17095	High mobility group protein HMG-I/HMG-Y OS=Mus musculus GN=Hmga1 PE=1 SV=4	nga1; Hmga1-	0.571	1.484	0.091	0.003	2.597	30.841	4	8	4	1	0	152.9871429	4	107	11.607	10.32
Q8BMJ2	Leucine--tRNA ligase, cytoplasmic OS=Mus musculus GN=Lars PE=1 SV=2	Lars	0.786	1.482	0.019	0.179	1.886	8.744	9	13	9	1	0	136.245	9	1178	134.106	7.05
P09411	Phosphoglycerate kinase 1 OS=Mus musculus GN=Pgk1 PE=1 SV=4	Pgk1	0.636	1.480	0.215	0.870	2.326	11.511	5	9	5	1	0	64.38766473	5	417	44.522	7.9
P60766	Cell division control protein 42 homolog OS=Mus musculus GN=Cdc42 PE=1 SV=2	Cdc42	0.831	1.479	0.457	0.765	1.780	19.895	3	3	2	1	0	77.41333333	3	191	21.245	6.55
H3BKH6	S-formylglutathione hydrolase OS=Mus musculus GN=Esd PE=1 SV=1	Esd	0.809	1.478	0.326	0.334	1.827	7.458	2	2	2	1	0	27.11	2	295	32.808	7.83
P62858	40S ribosomal protein S28 OS=Mus musculus GN=Rps28 PE=1 SV=1	Rps28	0.669	1.477	0.139	0.526	2.208	46.377	3	4	3	1	0	83.05	3	69	7.836	10.7
P29341	Polyadenylate-binding protein 1 OS=Mus musculus GN=Pabpc1 PE=1 SV=2	Pabpc1	0.636	1.473	0.035	0.596	2.316	8.333	6	9	5	1	1	72.67639858	6	636	70.626	9.5
Q61553	Fascin OS=Mus musculus GN=Fscn1 PE=1 SV=4	Fscn1	0.798	1.472	0.240	0.277	1.846	17.444	8	10	8	1	0	152.7777778	8	493	54.474	6.89
P14923	Junction plakoglobin OS=Homo sapiens GN=JUP PE=1 SV=3	JUP	1.075	1.472	0.619	0.062	1.369	9.933	6	12	6	1	0	257.63	6	745	81.693	6.14
Q9JHU4	Cytoplasmic dynein 1 heavy chain 1 OS=Mus musculus GN=Dync1h1 PE=1 SV=2	Dync1h1	0.790	1.469	0.261	0.300	1.859	8.527	39	45	39	1	0	564.8759294	39	4644	531.71	6.42
A0A087WRX8	Serine/arginine repetitive matrix protein 2 (Fragment) OS=Mus musculus GN=Srrm2 PE=1 SV=1		0.772	1.468	0.120	0.293	1.902	68.421	10	25	1	1	0	257.64	10	171	19.684	6.38
E9Q557	Desmoplakin OS=Mus musculus GN=Dsp PE=1 SV=1	Dsp	0.959	1.466	0.294	0.167	1.529	2.775	8	12	8	1	0	115.326336	8	2883	332.706	6.8
P61222	ATP-binding cassette sub-family E member 1 OS=Mus musculus GN=Abce1 PE=1 SV=1	Abce1	0.774	1.461	0.198	0.340	1.888	18.698	10	15	10	1	0	244.9427273	10	599	67.271	8.34

Uniprot Accession	Protein Description	Gene ID	Average ratio MB +DOX/-DOX (2 to 3exp)	Average Ratio MT +DOX/-DOX (2 to 3Exp)	(SD) MB +DOX/-DOX (2 to 3 Exp)	(SD) MT +DOX/-DOX (2 to 3 Exp)	MT/MB	Protein Coverage	# Peptides	# PSMs	# Unique Peptides	# Protein Groups	# Razor Peptides	Score Mascot	# Peptides Mascot	# AAs	MW [kDa]	calc. pI
Q99MN9	Propionyl-CoA carboxylase beta chain, mitochondrial OS=Mus musculus GN=Pccb PE=1 SV=2	Pccb	0.966	1.448	0.254	0.308	1.499	56.747	25	152	25	1	0	3150.372622	25	541	58.372	7.66
E9Q6E5	Protein Srsf11 OS=Mus musculus GN=Srsf11 PE=1 SV=1	Srsf11	0.873	1.447	0.285	0.248	1.658	16.438	8	17	8	1	0	83.08	8	511	56.664	10.7
Q02248	Catenin beta-1 OS=Mus musculus GN=Ctnnb1 PE=1 SV=1	Ctnnb1	0.751	1.447	0.306	0.448	1.927	2.689	2	4	2	1	0	26.24	2	781	85.416	5.86
Q05D44	Eukaryotic translation initiation factor 5B OS=Mus musculus GN=Eif5b PE=1 SV=2	Eif5b	0.982	1.446	0.054	0.200	1.473	30.181	34	68	34	1	0	1015.438979	34	1216	137.532	5.59
Q3TML0	Protein disulfide-isomerase A6 OS=Mus musculus GN=Pdia6 PE=1 SV=1	Pdia6	0.797	1.445	0.427	0.722	1.813	3.820	1	2	1	1	0	33.79	1	445	48.659	5.19
Q8BTS0	DEAD (Asp-Glu-Ala-Asp) box polypeptide 5 OS=Mus musculus GN=Ddx5 PE=1 SV=1	Ddx5	0.743	1.445	0.097	0.548	1.946	16.260	10	15	9	1	0	138.7427273	10	615	69.223	8.92
G5E896	Enhancer of mRNA decapping 4, isoform CRA_b OS=Mus musculus GN=Edc4 PE=1 SV=1	Edc4	1.146	1.443	0.388	0.320	1.260	1.849	3	3	3	1	0	44.77	3	1406	152.389	5.82
P62996	Transformer-2 protein homolog beta OS=Mus musculus GN=Tra2b PE=1 SV=1	Tra2b	0.577	1.441	0.178	0.899	2.497	11.111	5	8	4	1	3	77.13333333	5	288	33.646	11.25
Q7TMM9	Tubulin beta-2A chain OS=Mus musculus GN=Tubb2a PE=1 SV=1	Tubb2a	1.025	1.439	0.572	0.271	1.403	38.427	17	77	1	1	5	1016.192846	17	445	49.875	4.89
Q9D6Z1	Nucleolar protein 56 OS=Mus musculus GN=Nop56 PE=1 SV=2	Nop56	0.763	1.436	0.141	0.139	1.883	40.862	19	61	19	1	0	622.7754376	19	580	64.424	9.14
P11679	Keratin, type II cytoskeletal 8 OS=Mus musculus GN=Krt8 PE=1 SV=4	Krt8	1.269	1.435	0.939	0.277	1.131	9.388	8	50	1	1	0	186.0712449	8	490	54.531	5.82
Q9CXT8	Mitochondrial-processing peptidase subunit beta OS=Mus musculus GN=Pmpcb PE=1 SV=1	Pmpcb	0.726	1.431	0.253	0.297	1.972	4.499	2	2	2	1	0	30.53	2	489	54.58	6.99
Q9JM93	ADP-ribosylation factor-like protein 6-interacting protein 4 OS=Mus musculus GN=Arl6ip4 PE=1 SV=1	Arl6ip4	1.956	1.426	1.502	0.059	0.729	24.017	5	12	5	1	0	228.7201855	5	229	25.51	11.19
P68372	Tubulin beta-4B chain OS=Mus musculus GN=Tubb4b PE=1 SV=1	Tubb4b	0.879	1.425	0.318	0.342	1.622	38.427	17	75	2	1	1	877.3541451	17	445	49.799	4.89
Q80SW1	Putative adenosylhomocysteinase 2 OS=Mus musculus GN=Ahcyl1 PE=1 SV=1	Ahcyl1	0.780	1.423	0.255	0.476	1.823	8.679	5	5	5	1	0	43	5	530	58.913	6.89
Q9FJW6	ricopeptide repeat-containing protein At5g67570, chloroplastic OS=Arabidopsis thaliana GN=DG1 PE=G1; AT5G6757		1.126	1.422	0.373	0.519	1.263	0.877	1	5	1	1	0	97.42070222	1	798	92	5.57
Q61584	Fragile X mental retardation syndrome-related protein 1 OS=Mus musculus GN=Fxr1 PE=1 SV=2	Fxr1	0.882	1.420	0.009	0.433	1.610	2.363	2	2	1	1	1	32.98718781	2	677	76.175	6.98
Q8BZX4	Splicing regulatory glutamine/lysine-rich protein 1 OS=Mus musculus GN=Srek1 PE=2 SV=1	Srek1	0.901	1.417	0.225	0.082	1.574	14.777	6	12	6	1	0	140.2733333	6	494	56.73	10.48
Q8CAQ8	MICOS complex subunit Mic60 OS=Mus musculus GN=Immt PE=1 SV=1	Immt	0.823	1.416	0.043	0.404	1.721	13.210	11	15	11	1	0	137.78	11	757	83.848	6.61
Q3TS38	UDP-glucose 6-dehydrogenase OS=Mus musculus GN=Ugdh PE=1 SV=1	Ugdh	0.791	1.415	0.347	0.371	1.788	18.256	8	9	8	1	0	194.32	8	493	54.797	7.56
Q3UGC8	Propionyl-CoA carboxylase alpha chain, mitochondrial OS=Mus musculus GN=Pcca PE=1 SV=1	Pcca	0.904	1.413	0.190	0.260	1.563	75.967	50	916	47	1	6	19058.99209	50	724	79.871	7.25
Q9Z2T6	Keratin, type II cuticular Hb5 OS=Mus musculus GN=Krt85 PE=1 SV=2	Krt85	2.987	1.411	4.081	0.491	0.472	20.118	12	32	2	1	7	229.5332398	12	507	55.723	6.42
Q1HFZ0	tRNA (cytosine(34)-C(5))-methyltransferase OS=Mus musculus GN=Nsun2 PE=1 SV=2	Nsun2	0.653	1.410	0.099	0.221	2.159	2.378	2	3	2	1	0	52.51333333	2	757	85.397	6.58
Q05CL8	La-related protein 7 OS=Mus musculus GN=Larp7 PE=1 SV=2	Larp7	1.223	1.409	0.406	0.279	1.151	28.421	14	25	14	1	0	324.5233333	14	570	64.762	9.54
Q6ZWX6	Eukaryotic translation initiation factor 2 subunit 1 OS=Mus musculus GN=Eif2s1 PE=1 SV=3	Eif2s1	0.723	1.405	0.194	0.353	1.943	37.460	11	14	11	1	0	146.1178958	11	315	36.085	5.08
O54724	Polymerase I and transcript release factor OS=Mus musculus GN=Ptrf PE=1 SV=1	Ptrf	0.830	1.405	0.010	0.103	1.692	17.602	5	5	5	1	0	77.8	5	392	43.927	5.52
O70318	Band 4.1-like protein 2 OS=Mus musculus GN=Epb41l2 PE=1 SV=2	)b4.1l2; Epb41	0.915	1.403	0.158	0.371	1.533	18.016	17	19	15	1	2	156.5091415	17	988	109.873	5.43
Q9R1C7	Pre-mRNA-processing factor 40 homolog A OS=Mus musculus GN=Prpf40a PE=1 SV=1	Prpf40a	0.830	1.401	0.027	0.292	1.688	24.029	24	43	24	1	0	522.5628571	24	953	108.412	7.69
Q5SUF2	Luc7-like protein 3 OS=Mus musculus GN=Luc7l3 PE=1 SV=1	Luc7l3	1.047	1.400	0.652	0.456	1.337	27.083	11	36	11	1	0	477.1372458	11	432	51.419	9.77
P11440	Cyclin-dependent kinase 1 OS=Mus musculus GN=Cdk1 PE=1 SV=3	Cdk1	0.724	1.398	0.083	0.342	1.932	12.458	4	5	3	1	1	60.57548245	4	297	34.085	8.43
Q8BKZ9	Pyruvate dehydrogenase protein X component, mitochondrial OS=Mus musculus GN=Pdhx PE=1 SV=1	Pdhx	0.561	1.397	0.307	0.092	2.492	4.591	2	2	2	1	0	54.91709735	2	501	53.965	7.75
P11276	Fibronectin OS=Mus musculus GN=Fn1 PE=1 SV=4	Fn1	0.753	1.397	0.297	0.248	1.854	3.956	9	11	9	1	0	80.09	9	2477	272.368	5.59
P61620	Protein transport protein Sec61 subunit alpha isoform 1 OS=Mus musculus GN=Sec61a1 PE=1 SV=2	Sec61a1	0.756	1.396	0.081	0.300	1.845	5.672	3	6	3	1	0	94.87	3	476	52.231	8.06
Q62267	Cornifin-B OS=Mus musculus GN=Sprr1b PE=2 SV=1	Sprr1b	0.660	1.392	0.038	0.580	2.110	5.229	1	3	1	1	0	18.9	1	153	16.625	7.71
Q80Y52	leat shock protein 90, alpha (Cytosolic), class A member 1 OS=Mus musculus GN=Hsp90aa1 PE=1 SV=	Hsp90aa1	0.590	1.389	0.207	0.663	2.355	21.965	18	61	8	1	0	1199.183803	18	733	84.735	5.01
P02301	Histone H3.3C OS=Mus musculus GN=H3f3c PE=3 SV=3	H3f3c; Gm742	0.573	1.389	0.326	0.609	2.426	28.676	5	21	1	1	4	73.82250351	5	136	15.305	11.14
Q8BU30	Isoleucine--tRNA ligase, cytoplasmic OS=Mus musculus GN=Iars PE=1 SV=2	Iars	0.773	1.389	0.149	0.345	1.797	6.894	9	10	9	1	0	87.21912234	9	1262	144.179	6.55
E9Q070	60S acidic ribosomal protein P0 OS=Mus musculus GN=Gm8730 PE=1 SV=1		0.648	1.385	0.280	0.453	2.139	17.035	4	8	4	1	0	99.59	4	317	34.195	6.25
Q8BML9	Glutaminyl-tRNA synthetase OS=Mus musculus GN=Qars PE=1 SV=1	Qars	0.826	1.385	0.080	0.379	1.677	4.516	4	4	3	1	0	54.82	4	775	87.621	7.31
Q9EPF5	Olfactory receptor 703 OS=Mus musculus GN=Olfr703 PE=4 SV=1	Olfr703	0.941	1.381	0.284	0.505	1.468	2.194	1	2	1	1	0	28.36	1	319	35.47	7.9
Q99LH1	Nucleolar GTP-binding protein 2 OS=Mus musculus GN=Gnl2 PE=1 SV=2	Gnl2	0.859	1.381	0.562	0.679	1.607	3.846	3	3	3	1	0	54.01	3	728	83.294	9.2
Q99N87	28S ribosomal protein S5, mitochondrial OS=Mus musculus GN=Mrps5 PE=1 SV=1	Mrps5	0.742	1.381	0.034	0.373	1.861	11.806	6	7	6	1	0	127.86	6	432	48.176	10.14
P84078	ADP-ribosylation factor 1 OS=Mus musculus GN=Arf1 PE=1 SV=2	Arf1	0.862	1.380	0.154	0.503	1.602	39.227	5	13	3	1	0	279.7122222	5	181	20.684	6.8
Q3V235	Prohibitin 2 OS=Mus musculus GN=Phb2 PE=1 SV=1	Phb2	0.747	1.379	0.126	0.606	1.845	39.130	12	16	12	1	0	146.964264	12	299	33.276	9.83
Q8CGC7	Bifunctional glutamate/proline--tRNA ligase OS=Mus musculus GN=Eprs PE=1 SV=4	Eprs	0.811	1.379	0.019	0.412	1.699	11.905	16	20	15	1	1	277.36	16	1512	169.972	7.66
P05132	cAMP-dependent protein kinase catalytic subunit alpha OS=Mus musculus GN=Prkaca PE=1 SV=3	Prkaca	0.819	1.378	0.247	0.555	1.683	20.798	8	11	3	1	5	69.53	8	351	40.545	8.79
Q60930	Voltage-dependent anion-selective channel protein 2 OS=Mus musculus GN=Vdac2 PE=1 SV=2	Vdac2	0.847	1.375	0.223	0.241	1.623	21.356	5	7	5	1	0	100.6744583	5	295	31.713	7.49
Q9R0P5	Destrin OS=Mus musculus GN=Dstn PE=1 SV=3	Dstn	0.753	1.371	0.352	0.703	1.822	19.394	3	7	3	1	0	130.9071429	3	165	18.509	7.97
Q8JZQ9	Eukaryotic translation initiation factor 3 subunit B OS=Mus musculus GN=Eif3b PE=1 SV=1	Eif3b	0.696	1.368	0.091	0.611	1.965	8.219	5	7	5	1	0	65.72333333	5	803	91.313	5.02
Q8CBB6	Histone H2B OS=Mus musculus GN=Hist1h2br PE=2 SV=1	:1h2bq; Hist1h	0.684	1.368	0.360	0.440	2.000	50.000	8	68	1	1	13	967.1025023	8	134	14.879	10.37
P19096	Fatty acid synthase OS=Mus musculus GN=Fasn PE=1 SV=2	Fasn	0.783	1.367	0.048	0.425	1.745	6.110	15	18	15	1	0	231.3435449	15	2504	272.257	6.58
P55072	Transitional endoplasmic reticulum ATPase OS=Homo sapiens GN=VCP PE=1 SV=4	VCP	0.721	1.366	0.268	0.639	1.895	13.151	10	15	10	1	0	147.9520684	10	806	89.266	5.26
Q543K5	Phosphoserine aminotransferase OS=Mus musculus GN=Psat1 PE=1 SV=1	Psat1	0.562	1.365	0.057	0.377	2.430	5.676	2	2	2	1	0	54.25	2	370	40.447	8.03
O00571	ATP-dependent RNA helicase DDX3X OS=Homo sapiens GN=DDX3X PE=1 SV=3	DDX3X	0.733	1.364	0.067	0.374	1.860	16.012	10	16	9	1	1	229.68	10	662	73.198	7.18
P06733	Alpha-enolase OS=Homo sapiens GN=ENO1 PE=1 SV=2	ENO1	0.746	1.363	0.298	0.304	1.827	38.710	14	69	2	1	1	1248.011143	14	434	47.139	7.39
Q9Z0N1	Eukaryotic translation initiation factor 2 subunit 3, X-linked OS=Mus musculus GN=Eif2s3x PE=1 SV=2	Eif2s3x	0.774	1.361	0.043	0.604	1.759	16.949	6	14	6	1	0	192.84	6	472	51.033	8.4
Q31125	Zinc transporter SLC39A7 OS=Mus musculus GN=Slc39a7 PE=1 SV=2	Slc39a7	0.942	1.360	0.202	0.305	1.444	3.571	2	4	2	1	0	42.76423798	2	476	50.625	6.87

Uniprot Accession	Protein Description	Gene ID	Average ratio MB +DOX/-DOX (2 to 3exp)	Average Ratio MT +DOX/-DOX (2 to 3Exp)	(SD) MB +DOX/-DOX (2 to 3 Exp)	(SD) MT +DOX/-DOX (2 to 3 Exp)	MT/MB	Protein Coverage	# Peptides	# PSMs	# Unique Peptides	# Protein Groups	# Razor Peptides	Score Mascot	# Peptides Mascot	# AAs	MW [kDa]	calc. pI
A2AKU9	ATP synthase subunit gamma OS=Mus musculus GN=Atp5c1 PE=1 SV=1	Atp5c1	0.636	1.359	0.354	0.354	2.137	21.212	6	19	1	1	7	329.5251347	6	297	32.75	9.13
Q5BLK2	40S ribosomal protein S20 OS=Mus musculus GN=Rps20 PE=1 SV=1	Rps20	0.725	1.352	0.022	0.126	1.864	27.731	5	9	5	1	0	160.87	5	119	13.364	9.94
Q9JKF1	Ras GTPase-activating-like protein IQGAP1 OS=Mus musculus GN=Iqgap1 PE=1 SV=2	Iqgap1	0.754	1.348	0.288	0.406	1.787	5.432	9	9	9	1	0	123.8033333	9	1657	188.624	6.48
P62852	40S ribosomal protein S25 OS=Mus musculus GN=Rps25 PE=1 SV=1	Rps25	0.591	1.347	0.272	0.714	2.281	15.200	2	3	2	1	0	63.10314037	2	125	13.734	10.11
Q5SWU9	Acetyl-CoA carboxylase 1 OS=Mus musculus GN=Acaca PE=1 SV=1	Acaca	0.570	1.345	0.331	0.329	2.360	40.853	86	344	73	1	17	4870.738967	86	2345	265.088	6.39
Q5SUC3	Calnexin OS=Mus musculus GN=Canx PE=1 SV=1	Canx	0.592	1.343	0.184	0.202	2.268	16.582	9	12	9	1	0	54.42	9	591	67.236	4.64
P09103	Protein disulfide-isomerase OS=Mus musculus GN=P4hb PE=1 SV=2	P4hb	0.702	1.342	0.456	0.684	1.911	3.143	2	2	2	1	0	29.44	2	509	57.023	4.88
Q8VHX6	Filamin-C OS=Mus musculus GN=Flnc PE=1 SV=3	Flnc	0.828	1.341	0.234	0.289	1.619	7.814	18	21	14	1	1	361.5055556	18	2726	290.937	5.95
O55143	Sarcoplasmic/endoplasmic reticulum calcium ATPase 2 OS=Mus musculus GN=Atp2a2 PE=1 SV=2	Atp2a2	0.762	1.330	0.045	0.054	1.747	16.667	17	29	11	1	6	421.5054042	17	1044	114.784	5.34
Q91YQ5	yl-diphosphooligosaccharide--protein glycosyltransferase subunit 1 OS=Mus musculus GN=Rpn1 PE=	Rpn1	0.734	1.330	0.146	0.508	1.812	8.882	5	10	5	1	0	124.95	5	608	68.486	6.46
Q7TNC4	Putative RNA-binding protein Luc7-like 2 OS=Mus musculus GN=Luc7l2 PE=1 SV=1	Luc7l2	0.855	1.320	0.394	0.523	1.544	35.969	17	30	13	1	5	239.456046	17	392	46.555	10.1
P16460	Argininosuccinate synthase OS=Mus musculus GN=Ass1 PE=1 SV=1	Ass1	0.753	1.320	0.090	0.285	1.753	19.417	9	13	9	1	0	107.3318214	9	412	46.555	8.22
Q5M9M0	60S ribosomal protein L13a OS=Mus musculus GN=Rpl13a PE=1 SV=1	Rpl13a	0.670	1.317	0.291	0.261	1.966	23.645	5	9	5	1	0	156.1134719	5	203	23.449	11.02
Q5EBQ6	60S ribosomal protein L9 OS=Mus musculus GN=Rpl9 PE=1 SV=1	Rpl9	0.923	1.317	0.018	0.417	1.428	27.083	4	6	4	1	0	170.5866667	4	192	21.868	9.95
Q9WUA2	Phenylalanine--tRNA ligase beta subunit OS=Mus musculus GN=Farsb PE=1 SV=2	Farsb	0.742	1.314	0.205	0.428	1.772	6.791	4	4	4	1	0	65.92	4	589	65.655	7.12
P62889	60S ribosomal protein L30 OS=Mus musculus GN=Rpl30 PE=1 SV=2	Rpl30-ps8; Gr	0.742	1.314	0.291	0.540	1.772	39.130	4	10	4	1	0	143.8888889	4	115	12.776	9.63
P80316	T-complex protein 1 subunit epsilon OS=Mus musculus GN=Cct5 PE=1 SV=1	Cct5	0.794	1.313	0.107	0.654	1.653	21.257	12	17	12	1	0	156.7584615	12	541	59.586	6.02
P35279	Ras-related protein Rab-6A OS=Mus musculus GN=Rab6a PE=1 SV=4	Rab6a	0.780	1.313	0.378	0.291	1.684	15.865	3	10	2	1	0	206.2	3	208	23.575	5.54
Q3TDA7	kinase C and casein kinase substrate in neurons 2, isoform CRA_a OS=Mus musculus GN=Pacsin2 PE=	Pacsin2	0.794	1.311	0.190	0.375	1.651	3.498	2	4	2	1	0	42.72649515	2	486	55.798	5.2
P46978	diphosphooligosaccharide--protein glycosyltransferase subunit STT3A OS=Mus musculus GN=Stt3a PI	Stt3a	0.871	1.305	0.136	0.584	1.499	8.794	7	10	6	1	1	115.63	7	705	80.545	8.1
Q91VM5	RNA binding motif protein, X-linked-like-1 OS=Mus musculus GN=Rbmxl1 PE=2 SV=1	Rbmxl1	1.596	1.305	0.981	0.672	0.818	10.567	5	6	3	1	2	54.86	5	388	42.136	9.99
Q9JJI8	60S ribosomal protein L38 OS=Mus musculus GN=Rpl38 PE=1 SV=3	Rpl38-ps1; Rp	0.723	1.304	0.090	0.536	1.803	14.286	1	3	1	1	0	75.09666667	1	70	8.199	10.1
Q9D0F3	Protein ERGIC-53 OS=Mus musculus GN=Lman1 PE=1 SV=1	Lman1	0.842	1.302	0.050	0.461	1.547	14.700	6	11	6	1	0	110.455	6	517	57.753	6.34
Q9D8N0	Elongation factor 1-gamma OS=Mus musculus GN=Eef1g PE=1 SV=3	Eef1g	0.702	1.302	0.198	0.673	1.856	18.307	8	13	8	1	0	169.1045571	8	437	50.029	6.74
Q69ZA1	Cyclin-dependent kinase 13 OS=Mus musculus GN=Cdk13 PE=1 SV=3	Cdk13	0.701	1.302	0.040	1.016	1.858	1.588	3	3	2	1	0	36.1759844	3	1511	164.452	9.69
Q5I0W0	ATP synthase F(0) complex subunit B1, mitochondrial OS=Mus musculus GN=Atp5f1 PE=1 SV=1	Atp5f1	0.640	1.300	0.260	0.329	2.033	6.250	2	5	2	1	0	73.26514522	2	256	28.93	9.06
P68040	Guanine nucleotide-binding protein subunit beta-2-like 1 OS=Mus musculus GN=Gnb2l1 PE=1 SV=3	Gnb2l1; Rack1	0.753	1.300	0.155	0.332	1.726	33.754	12	40	12	1	0	374.5393583	12	317	35.055	7.69
Q4FZE6	40S ribosomal protein S7 OS=Mus musculus GN=Rps7 PE=1 SV=1	Rps7	0.635	1.300	0.094	0.308	2.047	34.021	8	19	8	1	0	184.5585422	8	194	22.113	10.1
P84091	AP-2 complex subunit mu OS=Mus musculus GN=Ap2m1 PE=1 SV=1	Ap2m1	0.813	1.297	0.195	0.365	1.596	19.080	7	12	7	1	0	106.8517	7	435	49.623	9.54
P17710	Hexokinase-1 OS=Mus musculus GN=Hk1 PE=1 SV=3	Hk1	0.805	1.290	0.168	0.644	1.602	3.080	3	3	3	1	0	55.34666667	3	974	108.234	6.8
P80315	T-complex protein 1 subunit delta OS=Mus musculus GN=Cct4 PE=1 SV=3	Cct4	0.695	1.290	0.102	0.433	1.855	19.481	10	15	10	1	0	249.7551255	10	539	58.03	8.02
Q8VHM5	Heterogeneous nuclear ribonucleoprotein R OS=Mus musculus GN=Hnrnpr PE=1 SV=1	Hnrnpr	0.854	1.285	0.023	0.307	1.504	4.114	3	4	3	1	0	38.62	3	632	70.844	8.13
Q9QZ88	Vacuolar protein sorting-associated protein 29 OS=Mus musculus GN=Vps29 PE=1 SV=1	Vps29	0.796	1.283	0.310	0.460	1.612	9.890	2	2	2	1	0	54.67	2	182	20.483	6.79
Q8VDN2	Sodium/potassium-transporting ATPase subunit alpha-1 OS=Mus musculus GN=Atp1a1 PE=1 SV=1	Atp1a1	0.610	1.283	0.163	0.396	2.102	14.663	13	17	13	1	0	210.6542857	13	1023	112.91	5.45
Q3TLP8	RAS-related C3 botulinum substrate 1, isoform CRA_a OS=Mus musculus GN=Rac1 PE=1 SV=1	Rac1	0.707	1.283	0.425	0.422	1.814	13.270	3	4	2	1	0	77.61809815	3	211	23.417	8.69
P62281	40S ribosomal protein S11 OS=Mus musculus GN=Rps11 PE=1 SV=3	Rps11	0.772	1.282	0.089	0.233	1.661	44.937	9	22	9	1	0	194.8422857	9	158	18.419	10.3
Q5YLW3	40S ribosomal protein S3 OS=Mus musculus GN=Rps3 PE=1 SV=1	Rps3	0.767	1.277	0.199	0.403	1.666	60.494	15	52	15	1	0	580.2589057	15	243	26.657	9.66
P11983	T-complex protein 1 subunit alpha OS=Mus musculus GN=Tcp1 PE=1 SV=3	Tcp1	0.711	1.275	0.229	0.398	1.793	24.460	12	28	12	1	0	481.229082	12	556	60.411	6.16
Q6ZWU9	40S ribosomal protein S27 OS=Mus musculus GN=Rps27 PE=1 SV=3	7; Gm9846; Rp	0.794	1.271	0.273	0.655	1.601	38.095	3	7	1	1	4	80.25847628	3	84	9.455	9.45
Q8BHC4	Dephospho-CoA kinase domain-containing protein OS=Mus musculus GN=Dcakd PE=1 SV=1	Dcakd	0.794	1.270	0.177	0.478	1.599	3.463	1	2	1	1	0	42.29375214	1	231	26.459	9.58
P47962	60S ribosomal protein L5 OS=Mus musculus GN=Rpl5 PE=1 SV=3	Rpl5	0.685	1.268	0.175	0.330	1.851	24.916	8	20	8	1	0	128.6966667	8	297	34.379	9.77
Q62376	U1 small nuclear ribonucleoprotein 70 kDa OS=Mus musculus GN=Snrnp70 PE=1 SV=2	Snrnp70	0.590	1.268	0.138	0.651	2.149	14.063	7	10	7	1	0	55.71397766	7	448	51.961	9.94
Q5M9M4	40S ribosomal protein S15a OS=Mus musculus GN=Rps15a PE=1 SV=1	Rps15a	0.711	1.267	0.272	0.439	1.782	40.769	6	16	6	1	0	232.1654545	6	130	14.83	10.13
Q91ZW3	trix-associated actin-dependent regulator of chromatin subfamily A member 5 OS=Mus musculus GN	Smarca5	1.101	1.266	0.428	0.432	1.150	13.225	14	19	14	1	0	133.2795439	14	1051	121.55	8.15
Q542V3	Serine/arginine-rich-splicing factor 4 OS=Mus musculus GN=Srsf4 PE=1 SV=1	Srsf4	0.923	1.259	0.010	0.551	1.364	5.092	3	10	3	1	0	183.2711111	3	491	56.216	11.37
Q14C24	MCG14259, isoform CRA_a OS=Mus musculus GN=U2af1 PE=1 SV=1	U2af1	0.695	1.258	0.079	0.470	1.810	12.134	3	4	3	1	0	64.67774917	3	239	27.797	8.81
P24527	Leukotriene A-4 hydrolase OS=Mus musculus GN=Lta4h PE=1 SV=4	Lta4h	0.791	1.257	0.297	0.579	1.590	9.984	6	6	6	1	0	93.02116726	6	611	69.007	6.42
P48962	ADP/ATP translocase 1 OS=Mus musculus GN=Slc25a4 PE=1 SV=4	Slc25a4	0.728	1.255	0.145	0.483	1.722	27.181	9	20	4	1	0	387.5755477	9	298	32.883	9.72
Q922I7	MCG13402, isoform CRA_c OS=Mus musculus GN=Ptbp1 PE=1 SV=1	Ptbp1	0.647	1.254	0.087	0.288	1.938	5.405	3	8	2	1	1	140.265	3	555	59.285	9.16
P47836	40S ribosomal protein S4 OS=Gallus gallus GN=RPS4 PE=2 SV=2	RPS4X	0.695	1.251	0.153	0.500	1.800	30.038	8	20	8	1	0	247.5216454	8	263	29.576	10.15
A2AR02	Peptidyl-prolyl cis-trans isomerase G OS=Mus musculus GN=Ppig PE=1 SV=1	Ppig	0.756	1.250	0.025	0.720	1.653	7.846	7	12	7	1	0	61.04333333	7	752	88.272	10.27
P62827	GTP-binding nuclear protein Ran OS=Mus musculus GN=Ran PE=1 SV=3	999; Ran; LOC	0.712	1.250	0.242	0.446	1.757	29.167	5	32	5	1	0	596.2116041	5	216	24.408	7.49
B2RTB6	Keratin 86 OS=Mus musculus GN=Krt86 PE=1 SV=1	Krt86	4.787	1.248	6.139	0.011	0.261	16.872	10	28	1	1	0	172.4807857	10	486	53.217	5.76
Q60737	Casein kinase II subunit alpha OS=Mus musculus GN=Csnk2a1 PE=1 SV=2	Csnk2a1	0.971	1.234	0.091	0.366	1.271	27.621	8	15	8	1	0	194.8428571	8	391	45.105	7.74
Q8VDM4	26S proteasome non-ATPase regulatory subunit 2 OS=Mus musculus GN=Psmd2 PE=1 SV=1	Psmd2	0.604	1.233	0.266	0.393	2.040	4.626	3	3	3	1	0	31.58	3	908	100.139	5.17
P19324	Serpin H1 OS=Mus musculus GN=Serpinh1 PE=1 SV=3	Serpinh1	0.803	1.232	0.405	0.621	1.534	38.849	13	53	13	1	0	703.5832081	13	417	46.504	8.82
P61750	ADP-ribosylation factor 4 OS=Mus musculus GN=Arf4 PE=1 SV=2	Arf4	0.840	1.226	0.400	0.535	1.459	35.556	5	11	3	1	3	203.245	5	180	20.384	7.14

Uniprot Accession	Protein Description	Gene ID	Average ratio MB +DOX/-DOX (2 to 3exp)	Average Ratio MT +DOX/-DOX (2 to 3Exp)	(SD) MB +DOX/-DOX (2 to 3 Exp)	(SD) MT +DOX/-DOX (2 to 3 Exp)	MT/MB	Protein Coverage	# Peptides	# PSMs	# Unique Peptides	# Protein Groups	# Razor Peptides	Score Mascot	# Peptides Mascot	# AAs	MW [kDa]	calc. pI
Q61753	D-3-phosphoglycerate dehydrogenase OS=Mus musculus GN=Phgdh PE=1 SV=3	Phgdh	0.622	1.219	0.148	0.480	1.961	9.568	4	5	4	1	0	159.04	4	533	56.549	6.54
Q8BVY0	Ribosomal L1 domain-containing protein 1 OS=Mus musculus GN=Rsl1d1 PE=1 SV=1	Rsl1d1	0.918	1.217	0.254	0.352	1.326	26.327	11	31	11	1	0	735.68	11	452	50.39	9.98
P80313	T-complex protein 1 subunit eta OS=Mus musculus GN=Cct7 PE=1 SV=1	Cct7	0.686	1.217	0.196	0.445	1.773	11.029	6	9	6	1	0	144.7	6	544	59.614	7.84
Q99K48	Non-POU domain-containing octamer-binding protein OS=Mus musculus GN=Nono PE=1 SV=3	Nono	0.744	1.214	0.129	0.413	1.633	28.330	12	23	11	1	1	150.6697523	12	473	54.506	8.95
P60843	Eukaryotic initiation factor 4A-I OS=Mus musculus GN=Eif4a1 PE=1 SV=1	Eif4a1	0.727	1.208	0.208	0.414	1.662	24.877	11	29	9	1	2	456.9073203	11	406	46.125	5.48
P84104	Serine/arginine-rich splicing factor 3 OS=Mus musculus GN=Srsf3 PE=1 SV=1	Srsf3	0.721	1.199	0.192	0.370	1.664	18.293	3	6	3	1	0	120.95	3	164	19.318	11.65
Q91Z25	Actin-related protein 2/3 complex subunit 1B OS=Mus musculus GN=Arpc1b PE=1 SV=1	Arpc1b	0.767	1.194	0.232	0.286	1.557	10.106	3	5	3	1	0	99.01	3	376	41.472	8.35
Q3U4U6	T-complex protein 1 subunit gamma OS=Mus musculus GN=Cct3 PE=1 SV=1	Cct3	0.677	1.194	0.219	0.452	1.764	21.651	10	16	10	1	0	138.8267675	10	545	60.591	6.7
Q6ZWZ6	40S ribosomal protein S12 OS=Mus musculus GN=Rps12 PE=1 SV=1	Rps12	0.609	1.191	0.280	0.354	1.955	39.394	5	9	5	1	0	85.98	5	132	14.505	7.21
Q9D823	60S ribosomal protein L37 OS=Mus musculus GN=Rpl37 PE=3 SV=3	8826; Rpl37rt;	1.033	1.190	0.478	1.099	1.152	18.557	4	10	4	1	0	121.7499448	4	97	11.071	11.74
Q99MR8	lethylcrotonoyl-CoA carboxylase subunit alpha, mitochondrial OS=Mus musculus GN=Mccc1 PE=1 SV=	Mccc1	0.839	1.188	0.302	0.339	1.417	55.649	35	276	35	1	0	4686.684238	35	717	79.293	7.83
P62835	Ras-related protein Rap-1A OS=Mus musculus GN=Rap1a PE=1 SV=1	Rap1a	0.788	1.186	0.357	0.502	1.506	10.326	2	6	2	1	0	157.3456222	2	184	20.974	6.67
G5E902	MCG10343, isoform CRA_b OS=Mus musculus GN=Slc25a3 PE=1 SV=1	Slc25a3	0.686	1.184	0.102	0.381	1.726	15.084	6	13	6	1	0	157.0550436	6	358	39.711	9.29
Q9Z0X1	Apoptosis-inducing factor 1, mitochondrial OS=Mus musculus GN=Aifm1 PE=1 SV=1	Aifm1	0.752	1.171	0.094	0.690	1.558	3.105	2	2	2	1	0	49.03	2	612	66.724	9.17
Q3ULF7	Actin-related protein 3 OS=Mus musculus GN=Actr3 PE=1 SV=1	Actr3	0.801	1.169	0.295	0.117	1.459	11.244	4	4	4	1	0	95.12	4	418	47.327	5.88
P04406	Glyceraldehyde-3-phosphate dehydrogenase OS=Homo sapiens GN=GAPDH PE=1 SV=3	GAPDH	1.964	1.168	1.381	0.376	0.595	15.821	4	10	1	1	0	202.97	4	335	36.03	8.46
Q3TQ70	Beta1 subnuit of GTP-binding protein OS=Mus musculus GN=Gnb1 PE=1 SV=1	Gnb1	0.879	1.151	0.312	0.576	1.309	9.412	3	7	1	1	0	119.0471429	3	340	37.353	6
Q545V8	Casein kinase II subunit alpha' OS=Mus musculus GN=Csnk2a2 PE=1 SV=1	Csnk2a2	1.050	1.142	0.044	0.618	1.087	23.714	7	13	7	1	0	161.045922	7	350	41.189	8.56
P62849	40S ribosomal protein S24 OS=Mus musculus GN=Rps24 PE=1 SV=1	C677113; LOC	0.776	1.138	0.223	0.468	1.465	30.075	4	15	4	1	0	142.3344444	4	133	15.413	10.78
Q3ULD5	Methylcrotonoyl-CoA carboxylase beta chain, mitochondrial OS=Mus musculus GN=Mccc2 PE=1 SV=1	Mccc2	0.970	1.132	0.132	0.485	1.167	41.385	20	85	20	1	0	1895.643656	20	563	61.34	8
Q8R429	Sarcoplasmic/endoplasmic reticulum calcium ATPase 1 OS=Mus musculus GN=Atp2a1 PE=1 SV=1	Atp2a1	0.705	1.132	0.209	0.126	1.606	15.292	14	21	8	1	0	294.7892193	14	994	109.355	5.22
P26443	Glutamate dehydrogenase 1, mitochondrial OS=Mus musculus GN=Glud1 PE=1 SV=1	Glud1	0.650	1.126	0.113	0.506	1.733	8.961	4	7	4	1	0	128.6666667	4	558	61.298	8
P62918	60S ribosomal protein L8 OS=Mus musculus GN=Rpl8 PE=1 SV=2	Rpl8	0.893	1.125	0.035	0.778	1.261	22.568	6	8	6	1	0	136.4695733	6	257	28.007	11.03
Q3U2W2	MYB binding protein (P160) 1a, isoform CRA_b OS=Mus musculus GN=Mybbp1a PE=1 SV=1	Mybbp1a	0.888	1.120	0.156	0.562	1.261	27.307	33	93	33	1	0	1410.469384	33	1344	151.942	8.95
P35979	60S ribosomal protein L12 OS=Mus musculus GN=Rpl12 PE=1 SV=2	Rpl12	0.582	1.119	0.170	0.625	1.924	49.091	6	11	6	1	0	235.2029202	6	165	17.794	9.42
P12970	60S ribosomal protein L7a OS=Mus musculus GN=Rpl7a PE=1 SV=2	Rpl7a	0.849	1.111	0.195	0.541	1.309	33.083	11	45	11	1	0	911.8113154	11	266	29.958	10.56
P61255	60S ribosomal protein L26 OS=Mus musculus GN=Rpl26 PE=1 SV=1	pl26; Gm1577	0.764	1.106	0.190	0.677	1.447	23.448	6	18	6	1	0	195.6427797	6	145	17.248	10.55
Q9DCJ7	Aurora kinase A-interacting protein OS=Mus musculus GN=Aurkaip1 PE=2 SV=2	Aurkaip1	0.834	1.103	0.085	1.140	1.323	5.000	1	5	1	1	0	75.45	1	200	23.286	10.73
P62264	40S ribosomal protein S14 OS=Mus musculus GN=Rps14 PE=1 SV=3	Rps14	0.703	1.098	0.253	0.564	1.562	39.073	6	25	6	1	0	274.8728571	6	151	16.263	10.05
P62717	60S ribosomal protein L18a OS=Mus musculus GN=Rpl18a PE=1 SV=1	Rpl18a	0.898	1.094	0.224	1.077	1.219	30.114	5	8	5	1	0	184.045	5	176	20.719	10.71
P62892	60S ribosomal protein L39 OS=Mus musculus GN=Rpl39 PE=1 SV=2	Rpl39	0.977	1.092	0.470	0.783	1.118	19.608	1	6	1	1	0	57.5	1	51	6.403	12.56
E9Q7G0	Protein Numa1 OS=Mus musculus GN=Numa1 PE=1 SV=1	Numa1	1.026	1.074	0.168	0.967	1.046	7.402	15	16	15	1	0	218.1919642	15	2094	235.487	5.87
Q5SX40	Myosin-1 OS=Mus musculus GN=Myh1 PE=1 SV=1	Myh1	0.794	1.070	0.079	0.095	1.348	17.559	33	65	8	1	0	490.1461955	33	1942	223.203	5.76
P14131	40S ribosomal protein S16 OS=Mus musculus GN=Rps16 PE=1 SV=4	ps16-ps2; Rps	0.745	1.070	0.131	0.625	1.435	49.315	8	19	8	1	0	224.1647637	8	146	16.435	10.21
P47963	60S ribosomal protein L13 OS=Mus musculus GN=Rpl13 PE=1 SV=3	Rpl13	0.694	1.062	0.221	0.575	1.530	31.754	8	23	8	1	0	231.0975	8	211	24.291	11.55
P0C0S8	Histone H2A type 1 OS=Homo sapiens GN=HIST1H2AG PE=1 SV=2	M; HIST1H2AI;	0.854	1.060	0.752	0.415	1.241	32.308	5	79	1	1	0	410.1514115	5	130	14.083	10.9
Q5I0T8	Ribosomal protein L19 OS=Mus musculus GN=Rpl19 PE=1 SV=1	pl19; Rpl19-ps	0.717	1.060	0.236	1.012	1.478	4.592	1	2	1	1	0	79.38	1	196	23.451	11.47
P27659	60S ribosomal protein L3 OS=Mus musculus GN=Rpl3 PE=1 SV=3	Rpl3	0.819	1.056	0.115	0.582	1.290	22.333	11	25	11	1	0	276.36014	11	403	46.081	10.21
P14148	60S ribosomal protein L7 OS=Mus musculus GN=Rpl7 PE=1 SV=2	Rpl7	0.720	1.046	0.174	0.606	1.453	39.630	14	39	14	1	0	520.7105605	14	270	31.4	10.89
Q564D0	derived from t(12;16) malignant liposarcoma (Human), isoform CRA_a OS=Mus musculus GN=Fus PE	Fus	1.103	1.042	0.229	0.305	0.945	7.529	3	4	3	1	0	31.95	3	518	52.642	9.36
Q99020	Heterogeneous nuclear ribonucleoprotein A/B OS=Mus musculus GN=Hnrnpab PE=1 SV=1	Hnrnpab	0.890	1.038	0.131	1.010	1.166	14.035	3	3	3	1	0	56.77666667	3	285	30.812	7.91
Q9CX86	Heterogeneous nuclear ribonucleoprotein A0 OS=Mus musculus GN=Hnrnpa0 PE=1 SV=1	Hnrnpa0	0.774	1.034	0.129	1.008	1.337	14.098	4	11	3	1	0	190.372402	4	305	30.512	9.31
P41105	60S ribosomal protein L28 OS=Mus musculus GN=Rpl28 PE=1 SV=2	Rpl28	0.743	1.022	0.182	0.933	1.376	27.007	4	9	4	1	0	210.4222222	4	137	15.724	12.02
A0A0A6YX26	60S ribosomal protein L31 OS=Mus musculus GN=Rpl31 PE=1 SV=1		0.738	1.016	0.072	0.785	1.376	20.155	3	10	3	1	0	90.69965279	3	129	14.987	10.61
Q6ZWZ7	60S ribosomal protein L17 OS=Mus musculus GN=Rpl17 PE=1 SV=1	pl17; Rpl17-ps	0.768	1.003	0.021	0.646	1.306	25.543	5	14	5	1	0	89.21346087	5	184	21.383	10.18
Q8VH51	RNA-binding protein 39 OS=Mus musculus GN=Rbm39 PE=1 SV=2	Rbm39	1.009	1.003	0.095	0.897	0.994	12.453	7	10	7	1	0	117.9478581	7	530	59.37	10.1
Q91Z83	Myosin-7 OS=Mus musculus GN=Myh7 PE=1 SV=1	Myh7	0.875	1.003	0.027	0.192	1.146	19.070	35	58	19	1	1	507.8787686	35	1935	222.741	5.76
Q6ZWZ4	60S ribosomal protein L36 OS=Mus musculus GN=Rpl36 PE=1 SV=1	Rpl36	1.024	1.002	0.340	0.998	0.978	29.524	3	5	3	1	0	111.67	3	105	12.246	11.59
Q8CI11	Guanine nucleotide-binding protein-like 3 OS=Mus musculus GN=Gnl3 PE=1 SV=2	Gnl3	0.977	0.999	0.197	1.107	1.022	39.219	25	45	24	1	1	549.8448073	25	538	60.749	9.11
Q6ZWN5	40S ribosomal protein S9 OS=Mus musculus GN=Rps9 PE=1 SV=3	Rps9	0.689	0.990	0.192	0.624	1.437	41.753	10	18	10	1	0	145.2663239	10	194	22.578	10.65
E9QAZ2	Ribosomal protein L15 OS=Mus musculus GN=Gm10020 PE=3 SV=1		0.834	0.973	0.225	0.863	1.166	20.588	4	8	4	1	0	105.2524007	4	204	24.062	11.58
P47911	60S ribosomal protein L6 OS=Mus musculus GN=Rpl6 PE=1 SV=3	Rpl6	0.778	0.973	0.067	0.485	1.250	29.392	9	30	9	1	0	307.3284779	9	296	33.489	10.7
Q6IFZ8	MCG1050941 OS=Mus musculus GN=Gm5414 PE=1 SV=1	Gm5414	0.813	0.969	0.322	0.058	1.193	11.594	7	18	1	1	0	164.8845874	7	552	60.191	7.3
Q80XI4	Phosphatidylinositol 5-phosphate 4-kinase type-2 beta OS=Mus musculus GN=Pip4k2b PE=1 SV=1	Pip4k2b	1.052	0.964	0.047	0.858	0.916	19.952	9	33	6	1	4	446.1775755	9	416	47.289	7.33
P27661	Histone H2AX OS=Mus musculus GN=H2afx PE=1 SV=2	H2afx	0.603	0.957	0.386	0.387	1.588	27.273	6	76	2	1	6	298.8869847	6	143	15.133	10.74
Q9D1R9	60S ribosomal protein L34 OS=Mus musculus GN=Rpl34 PE=1 SV=2	ps1; Rpl34; G	0.843	0.957	0.204	0.629	1.135	41.880	6	14	6	1	0	154.0836364	6	117	13.284	11.47
Q99ME9	Nucleolar GTP-binding protein 1 OS=Mus musculus GN=Gtpbp4 PE=1 SV=3	Gtpbp4	0.895	0.955	0.275	0.897	1.067	9.937	8	21	8	1	0	133.7543642	8	634	74.066	9.52

Uniprot Accession	Protein Description	Gene ID	Average ratio MB +DOX/-DOX (2 to 3exp)	Average Ratio MT +DOX/-DOX (2 to 3Exp)	(SD) MB +DOX/-DOX (2 to 3 Exp)	(SD) MT +DOX/-DOX (2 to 3 Exp)	MT/MB	Protein Coverage	# Peptides	# PSMs	# Unique Peptides	# Protein Groups	# Razor Peptides	Score Mascot	# Peptides Mascot	# AAs	MW [kDa]	calc. pI
Q544E3	Phosphatidylinositol 5-phosphate 4-kinase type-2 alpha OS=Mus musculus GN=Pip4k2a PE=1 SV=1	Pip4k2a	0.989	0.953	0.299	0.732	0.963	20.494	8	28	5	1	0	300.7666667	8	405	46.122	6.99
Q9CR57	60S ribosomal protein L14 OS=Mus musculus GN=Rpl14 PE=1 SV=3	Rpl14	0.822	0.950	0.203	0.573	1.157	25.806	5	8	5	1	0	330.082014	5	217	23.549	11.02
P61486	60S ribosomal protein L36a OS=Takifugu rubripes GN=rpl36a PE=3 SV=2	LOC10106128	0.924	0.943	0.072	1.089	1.021	24.528	4	16	4	1	0	171.32	4	106	12.52	10.54
P62267	40S ribosomal protein S23 OS=Mus musculus GN=Rps23 PE=1 SV=3	Rps23	0.946	0.941	0.032	0.880	0.995	28.671	4	9	4	1	0	214.2588889	4	143	15.798	10.49
Q564E8	60S ribosomal protein L4 OS=Mus musculus GN=Rpl4 PE=1 SV=1	Rpl4	1.000	0.926	0.093	0.746	0.926	29.833	13	41	13	1	0	801.9678788	13	419	47.124	11
P24788	Cyclin-dependent kinase 11B OS=Mus musculus GN=Cdk11b PE=1 SV=2	Cdk11b	1.060	0.906	0.525	0.799	0.855	3.189	3	4	3	1	0	32.05	3	784	91.458	5.39
P14115	60S ribosomal protein L27a OS=Mus musculus GN=Rpl27a PE=1 SV=5	Rpl27a	1.124	0.906	0.528	0.801	0.806	28.378	5	21	5	1	0	287.9766546	5	148	16.595	11.12
P62737	Actin, aortic smooth muscle OS=Mus musculus GN=Acta2 PE=1 SV=1	Acta2	0.772	0.881	0.437	0.287	1.141	46.154	17	229	1	1	8	4040.417678	17	377	41.982	5.39
Q5BLJ9	60S ribosomal protein L27 OS=Mus musculus GN=Rpl27 PE=1 SV=1	Rpl27	0.735	0.868	0.159	0.646	1.181	32.353	5	16	5	1	0	134.2861507	5	136	15.788	10.56
Q497E9	40S ribosomal protein S8 OS=Mus musculus GN=Rps8 PE=1 SV=1	Rps8; Gm1550	0.854	0.858	0.145	0.684	1.005	58.173	11	27	11	1	0	445.05	11	208	24.19	10.32
O09167	60S ribosomal protein L21 OS=Mus musculus GN=Rpl21 PE=1 SV=3	Rpl21	0.782	0.851	0.045	0.899	1.088	18.750	3	4	3	1	0	44.24333333	3	160	18.55	10.49
P32067	Lupus La protein homolog OS=Mus musculus GN=Ssb PE=1 SV=1	Ssb	0.635	0.839	0.137	0.673	1.322	16.867	8	13	8	1	0	75.96739881	8	415	47.727	9.77
Q8BP67	60S ribosomal protein L24 OS=Mus musculus GN=Rpl24 PE=1 SV=2	Rpl24	0.852	0.824	0.171	0.547	0.967	45.860	10	34	10	1	0	750.7067519	10	157	17.768	11.25
P13541	Myosin-3 OS=Mus musculus GN=Myh3 PE=2 SV=2	Myh3	0.853	0.800	0.226	0.048	0.938	34.330	60	114	37	1	19	1054.620618	60	1940	223.652	5.81
Q8BG05	Heterogeneous nuclear ribonucleoprotein A3 OS=Mus musculus GN=Hnrnpa3 PE=1 SV=1	Hnrnpa3	0.851	0.782	0.163	0.888	0.918	10.290	3	9	2	1	0	157.4689383	3	379	39.628	9.01
Q5BLK1	40S ribosomal protein S6 OS=Mus musculus GN=Rps6 PE=1 SV=1	; Rps6; LOC10	0.652	0.772	0.221	0.645	1.184	33.735	10	30	6	1	4	248.5782091	10	249	28.663	10.84
Q5M9M5	60S ribosomal protein L23a OS=Mus musculus GN=Rpl23a PE=1 SV=1	Rpl23a	0.849	0.748	0.349	0.791	0.880	32.051	5	29	5	1	0	354.1114286	5	156	17.684	10.45
P47915	60S ribosomal protein L29 OS=Mus musculus GN=Rpl29 PE=2 SV=2	Rpl29; Gm821	0.787	0.608	0.203	0.661	0.772	27.500	5	23	5	1	0	361.3257143	5	160	17.576	11.84

7 Bibliography

Abmayr, S. M. and Pavlath, G. K. (2012). Myoblast fusion: Lessons from flies and mice. *Development (Cambridge, England)*, 139(4):641–656.

Abramson, J., Giraud, M., Benoist, C., and Mathis, D. (2010). Aire's Partners in the Molecular Control of Immunological Tolerance. *Cell*, 140(1):123–135.

Agarkova, I. and Perriard, J.-C. (2005). The M-band: An elastic web that crosslinks thick filaments in the center of the sarcomere. *Trends in Cell Biology*, 15(9):477–485.

Akhmanova, A. and Steinmetz, M. O. (2010). Microtubule +TIPs at a glance. *J Cell Sci*, 123(20):3415–3419.

Akhmanova, A. and Steinmetz, M. O. (2015). Control of microtubule organization and dynamics: Two ends in the limelight. *Nature Reviews Molecular Cell Biology*, 16(12):711–726.

Akhtar, A. and Gasser, S. M. (2007). The nuclear envelope and transcriptional control. *Nature Reviews Genetics*, 8(7):507–517.

Al-Bassam, J., Kim, H., Brouhard, G., van Oijen, A., Harrison, S. C., and Chang, F. (2010). CLASP promotes microtubule rescue by recruiting tubulin dimers to the microtubule. *Developmental Cell*, 19(2):245–258.

Al-Bassam, J., Kim, H., Flor-Parra, I., Lal, N., Velji, H., and Chang, F. (2012). Fission yeast Alp14 is a dose-dependent plus end-tracking microtubule polymerase. *Molecular Biology of the Cell*, 23(15):2878–2890.

Aldaz, H., Rice, L. M., Stearns, T., and Agard, D. A. (2005). Insights into microtubule nucleation from the crystal structure of human gamma-tubulin. *Nature*, 435(7041):523–527.

Alushin, G. M., Lander, G. C., Kellogg, E. H., Zhang, R., Baker, D., and Nogales, E. (2014). High-resolution microtubule structures reveal the structural transitions in $a\beta$-tubulin upon GTP hydrolysis. *Cell*, 157(5):1117–1129.

Andersen, J. S., Wilkinson, C. J., Mayor, T., Mortensen, P., Nigg, E. A., and Mann, M. (2003). Proteomic characterization of the human centrosome by protein correlation profiling. *Nature*, 426(6966):570–574.

Antin, P. B., Forry-Schaudies, S., Friedman, T. M., Tapscott, S. J., and Holtzer, H. (1981). Taxol induces postmitotic myoblasts to assemble interdigitating microtubule-myosin arrays that exclude actin filaments. *The Journal of Cell Biology*, 90(2):300–308.

Antonczak, A. K., Mullee, L. I., Wang, Y., Comartin, D., Inoue, T., Pelletier, L., and Morrison, C. G. (2016). Opposing effects of pericentrin and microcephalin on the pericentriolar material regulate CHK1 activation in the DNA damage response. *Oncogene*, 35(15):2003–2010.

Apel, E. D., Lewis, R. M., Grady, R. M., and Sanes, J. R. (2000). Syne-1, a dystrophin- and Klarsicht-related protein associated with synaptic nuclei at the neuromuscular junction. *The Journal of Biological Chemistry*, 275(41):31986–31995.

Arquint, C., Gabryjonczyk, A.-M., and Nigg, E. A. (2014). Centrosomes as signalling centres. *Philosophical Transactions of the Royal Society of London. Series B, Biological Sciences*, 369(1650).

Askham, J. M., Vaughan, K. T., Goodson, H. V., and Morrison, E. E. (2002). Evidence that an interaction between EB1 and p150(Glued) is required for the formation and maintenance of a radial microtubule array anchored at the centrosome. *Molecular Biology of the Cell*, 13(10):3627–3645.

Attali, R., Warwar, N., Israel, A., Gurt, I., McNally, E., Puckelwartz, M., Glick, B., Nevo, Y., Ben-Neriah, Z., and Melki, J. (2009). Mutation of SYNE-1, encoding an essential component of the nuclear lamina, is responsible for autosomal recessive arthrogryposis. *Human Molecular Genetics*, 18(18):3462–3469.

Au, Y. (2004). The muscle ultrastructure: A structural perspective of the sarcomere. *Cellular and molecular life sciences: CMLS*, 61(24):3016–3033.

Azimzadeh, J. and Bornens, M. (2007). Structure and duplication of the centrosome. *Journal of Cell Science*, 120(Pt 13):2139–2142.

Baas, P. W., Deitch, J. S., Black, M. M., and Banker, G. A. (1988). Polarity orientation of microtubules in hippocampal neurons: Uniformity in the axon and nonuniformity in the dendrite. *Proceedings of the National Academy of Sciences of the United States of America*, 85(21):8335–8339.

Baas, P. W. and Joshi, H. C. (1992). Gamma-tubulin distribution in the neuron: Implications for the origins of neuritic microtubules. *The Journal of Cell Biology*, 119(1):171–178.

Baas, P. W. and Lin, S. (2011). Hooks and comets: The story of microtubule polarity orientation in the neuron. *Developmental Neurobiology*, 71(6):403–418.

Bacallao, R., Antony, C., Dotti, C., Karsenti, E., Stelzer, E. H., and Simons, K. (1989). The subcellular organization of Madin-Darby canine kidney cells during the formation of a polarized epithelium. *The Journal of Cell Biology*, 109(6):2817–2832.

Bailly, E., Dorée, M., Nurse, P., and Bornens, M. (1989). P34cdc2 is located in both nucleus and cytoplasm; part is centrosomally associated at G2/M and enters vesicles at anaphase. *The EMBO Journal*, 8(13):3985–3995.

Balczon, R., Bao, L., and Zimmer, W. E. (1994). PCM-1, A 228-kD centrosome autoantigen with a distinct cell cycle distribution. *The Journal of Cell Biology*, 124(5):783–793.

Bärenz, F., Mayilo, D., and Gruss, O. J. (2011). Centriolar satellites: Busy orbits around the centrosome. *European Journal of Cell Biology*, 90(12):983–989.

Baron, A. T., Suman, V. J., Nemeth, E., and Salisbury, J. L. (1994). The pericentriolar lattice of PtK2 cells exhibits temperature and calcium-modulated behavior. *Journal of Cell Science*, 107(11):2993–3003.

Beck, M. and Hurt, E. (2017). The nuclear pore complex: Understanding its function through structural insight. *Nature Reviews Molecular Cell Biology*, 18(2):73–89.

Bentzinger, C. F., Wang, Y. X., and Rudnicki, M. A. (2012). Building Muscle: Molecular Regulation of Myogenesis. *Cold Spring Harbor Perspectives in Biology*, 4(2).

Berbari, N. F., Bishop, G. A., Askwith, C. C., Lewis, J. S., and Mykytyn, K. (2007). Hippocampal neurons possess primary cilia in culture. *Journal of Neuroscience Research*, 85(5):1095–1100.

Berkes, C. A. and Tapscott, S. J. (2005). MyoD and the transcriptional control of myogenesis. *Seminars in Cell & Developmental Biology*, 16(4):585–595.

Bettencourt-Dias, M. and Glover, D. M. (2007). Centrosome biogenesis and function: Centrosomics brings new understanding. *Nature Reviews. Molecular Cell Biology*, 8(6):451–463.

Bieling, P., Kandels-Lewis, S., Telley, I. A., van Dijk, J., Janke, C., and Surrey, T. (2008). CLIP-170 tracks growing microtubule ends by dynamically recognizing composite EB1/tubulin-binding sites. *The Journal of Cell Biology*, 183(7):1223–1233.

Bione, S., Maestrini, E., Rivella, S., Mancini, M., Regis, S., Romeo, G., and Toniolo, D. (1994). Identification of a novel X-linked gene responsible for Emery-Dreifuss muscular dystrophy. *Nature Genetics*, 8(4):323–327.

Bitoun, M., Maugenre, S., Jeannet, P.-Y., Lacène, E., Ferrer, X., Laforêt, P., Martin, J.-J., Laporte, J., Lochmüller, H., Beggs, A. H., Fardeau, M., Eymard, B., Romero, N. B., and Guicheney, P. (2005). Mutations in dynamin 2 cause dominant centronuclear myopathy. *Nature Genetics*, 37(11):1207–1209.

Blagden, S. P. and Glover, D. M. (2003). Polar expeditions–provisioning the centrosome for mitosis. *Nature Cell Biology*, 5(6):505–511.

Blau, H. M., Chiu, C. P., and Webster, C. (1983). Cytoplasmic activation of human nuclear genes in stable heterocaryons. *Cell*, 32(4):1171–1180.

Bond, J., Roberts, E., Springell, K., Lizarraga, S. B., Lizarraga, S., Scott, S., Higgins, J., Hampshire, D. J., Morrison, E. E., Leal, G. F., Silva, E. O., Costa, S. M. R., Baralle, D., Raponi, M., Karbani, G., Rashid, Y., Jafri, H., Bennett, C., Corry, P., Walsh, C. A., and Woods, C. G. (2005). A centrosomal mechanism involving CDK5RAP2 and CENPJ controls brain size. *Nature Genetics*, 37(4):353–355.

Bonne, G., Di Barletta, M. R., Varnous, S., Bécane, H. M., Hammouda, E. H., Merlini, L., Muntoni, F., Greenberg, C. R., Gary, F., Urtizberea, J. A., Duboc, D., Fardeau, M., Toniolo, D., and Schwartz, K. (1999). Mutations in the gene encoding lamin A/C cause autosomal dominant Emery-Dreifuss muscular dystrophy. *Nature Genetics*, 21(3):285–288.

Bornens, M. (2002). Centrosome composition and microtubule anchoring mechanisms. *Current Opinion in Cell Biology*, 14(1):25–34.

Boucher, P. and Herz, J. (2011). Signaling through LRP1: Protection from atherosclerosis and beyond. *Biochemical pharmacology*, 81(1):1–5.

Bray, D. and Bunge, M. B. (1981). Serial analysis of microtubules in cultured rat sensory axons. *Journal of Neurocytology*, 10(4):589–605.

Bré, M. H., Kreis, T. E., and Karsenti, E. (1987). Control of microtubule nucleation and stability in Madin-Darby canine kidney cells: The occurrence of noncentrosomal, stable detyrosinated microtubules. *The Journal of Cell Biology*, 105(3):1283–1296.

Bré, M. H., Pepperkok, R., Hill, A. M., Levilliers, N., Ansorge, W., Stelzer, E. H., and Karsenti, E. (1990). Regulation of microtubule dynamics and nucleation during polarization in MDCK II cells. *The Journal of Cell Biology*, 111(6):3013–3021.

Brouhard, G. J., Stear, J. H., Noetzel, T. L., Al-Bassam, J., Kinoshita, K., Harrison, S. C., Howard, J., and Hyman, A. A. (2008). XMAP215 is a processive microtubule polymerase. *Cell*, 132(1):79–88.

Bruusgaard, J. C., Liestøl, K., Ekmark, M., Kollstad, K., and Gundersen, K. (2003). Number and spatial distribution of nuclei in the muscle fibres of normal mice studied in vivo. *The Journal of Physiology*, 551(Pt 2):467–478.

Buchman, J. J., Tseng, H.-C., Zhou, Y., Frank, C. L., Xie, Z., and Tsai, L.-H. (2010). Cdk5rap2 interacts with pericentrin to maintain the neural progenitor pool in the developing neocortex. *Neuron*, 66(3):386–402.

Buckingham, M., Bajard, L., Chang, T., Daubas, P., Hadchouel, J., Meilhac, S., Montarras, D., Rocancourt, D., and Relaix, F. (2003). The formation of skeletal muscle: From somite to limb. *Journal of Anatomy*, 202(1):59–68.

Buckingham, M. and Relaix, F. (2015). PAX3 and PAX7 as upstream regulators of myogenesis. *Seminars in Cell & Developmental Biology*, 44:115–125.

Bugnard, E., Zaal, K. J. M., and Ralston, E. (2005). Reorganization of microtubule nucleation during muscle differentiation. *Cell Motility and the Cytoskeleton*, 60(1):1–13.

Burke, B. and Stewart, C. L. (2013). The nuclear lamins: Flexibility in function. *Nature Reviews Molecular Cell Biology*, 14(1):13–24.

Burton, P. R. (1988). Dendrites of mitral cell neurons contain microtubules of opposite polarity. *Brain Research*, 473(1):107–115.

Busch, K. E. and Brunner, D. (2004). The Microtubule Plus End-Tracking Proteins mal3p and tip1p Cooperate for Cell-End Targeting of Interphase Microtubules. *Current Biology*, 14(7):548–559.

Cadot, B., Gache, V., and Gomes, E. R. (2015). Moving and positioning the nucleus in skeletal muscle - one step at a time. *Nucleus (Austin, Tex.)*, 6(5):373–381.

Cadot, B., Gache, V., Vasyutina, E., Falcone, S., Birchmeier, C., and Gomes, E. R. (2012). Nuclear movement during myotube formation is microtubule and dynein dependent and is regulated by Cdc42, Par6 and Par3. *EMBO Reports*, 13(8):741–749.

Capers, C. R. (1960). Multinucleation of skeletal muscle in vitro. *The Journal of Biophysical and Biochemical Cytology*, 7:559–566.

Caplow, M. and Shanks, J. (1996). Evidence that a single monolayer tubulin-GTP cap is both necessary and sufficient to stabilize microtubules. *Molecular Biology of the Cell*, 7(4):663–675.

Carpenter, A. E., Jones, T. R., Lamprecht, M. R., Clarke, C., Kang, I. H., Friman, O., Guertin, D. A., Chang, J. H., Lindquist, R. A., Moffat, J., Golland, P., and Sabatini, D. M. (2006). CellProfiler: Image analysis software for identifying and quantifying cell phenotypes. *Genome Biology*, 7:R100.

Cartwright, S. and Karakesisoglou, I. (2014). Nesprins in health and disease. *Seminars in Cell & Developmental Biology*, 29:169–179.

Chabin-Brion, K., Marceiller, J., Perez, F., Settegrana, C., Drechou, A., Durand, G., and Poüs, C. (2001). The Golgi Complex Is a Microtubule-organizing Organelle. *Molecular Biology of the Cell*, 12(7):2047–2060.

Chalfie, M. and Thomson, J. N. (1979). Organization of neuronal microtubules in the nematode Caenorhabditis elegans. *The Journal of Cell Biology*, 82(1):278–289.

Chang, W., Worman, H. J., and Gundersen, G. G. (2015). Accessorizing and anchoring the LINC complex for multifunctionality. *The Journal of Cell Biology*, 208(1):11–22.

Chapman, M. A., Zhang, J., Banerjee, I., Guo, L. T., Zhang, Z., Shelton, G. D., Ouyang, K., Lieber, R. L., and Chen, J. (2014). Disruption of both nesprin 1 and desmin results in nuclear anchorage defects and fibrosis in skeletal muscle. *Human Molecular Genetics*, 23(22):5879–5892.

Chen, C.-T., Hehnly, H., Yu, Q., Farkas, D., Zheng, G., Redick, S. D., Hung, H.-F., Samtani, R., Jurczyk, A., Akbarian, S., Wise, C., Jackson, A., Bober, M., Guo, Y., Lo, C., and Doxsey, S. (2014). A unique set of centrosome proteins requires Pericentrin for spindle-pole localization and spindle orientation. *Current biology : CB*, 24(19):2327–2334.

Chen, D., Purohit, A., Halilovic, E., Doxsey, S. J., and Newton, A. C. (2004). Centrosomal anchoring of protein kinase C betaII by pericentrin controls microtubule organization, spindle function, and cytokinesis. *The Journal of Biological Chemistry*, 279(6):4829–4839.

Chen, I.-H. B., Huber, M., Guan, T., Bubeck, A., and Gerace, L. (2006). Nuclear envelope transmembrane proteins (NETs) that are up-regulated during myogenesis. *BMC cell biology*, 7:38.

Chi, Y.-H., Cheng, L. I., Myers, T., Ward, J. M., Williams, E., Su, Q., Faucette, L., Wang, J.-Y., and Jeang, K.-T. (2009). Requirement for Sun1 in the expression of meiotic reproductive genes and piRNA. *Development (Cambridge, England)*, 136(6):965–973.

Chi, Y.-H., Haller, K., Peloponese, J.-M., and Jeang, K.-T. (2007). Histone acetyltransferase hALP and nuclear membrane protein hsSUN1 function in de-condensation of mitotic chromosomes. *The Journal of Biological Chemistry*, 282(37):27447–27458.

Ching, Y. P., Qi, Z., and Wang, J. H. (2000). Cloning of three novel neuronal Cdk5 activator binding proteins. *Gene*, 242(1–2):285–294.

Choi, Y.-K., Liu, P., Sze, S. K., Dai, C., and Qi, R. Z. (2010). CDK5RAP2 stimulates microtubule nucleation by the gamma-tubulin ring complex. *The Journal of Cell Biology*, 191(6):1089–1095.

Chojnowski, A., Ong, P. F., Wong, E. S. M., Lim, J. S. Y., Mutalif, R. A., Navasankari, R., Dutta, B., Yang, H., Liow, Y. Y., Sze, S. K., Boudier, T., Wright, G. D., Colman, A., Burke, B., Stewart, C. L., and Dreesen, O. (2015). Progerin reduces LAP2α-telomere association in Hutchinson-Gilford progeria. *eLife*, 4.

Choy, R. M., Kollman, J. M., Zelter, A., Davis, T. N., and Agard, D. A. (2009). Localization and orientation of the gamma-tubulin small complex components using protein tags as labels for single particle EM. *Journal of Structural Biology*, 168(3):571–574.

Cisternas, P., Henriquez, J. P., Brandan, E., and Inestrosa, N. C. (2014). Wnt signaling in skeletal muscle dynamics: Myogenesis, neuromuscular synapse and fibrosis. *Molecular Neurobiology*, 49(1):574–589.

Cohn, R. D. and Campbell, K. P. (2000). Molecular basis of muscular dystrophies. *Muscle & Nerve*, 23(10):1456–1471.

Conduit, P. T., Wainman, A., and Raff, J. W. (2015). Centrosome function and assembly in animal cells. *Nature Reviews Molecular Cell Biology*, 16(10):611–624.

Connolly, J. A., Kiosses, B. W., and Kalnins, V. I. (1986). Centrioles are lost as embryonic myoblasts fuse into myotubes in vitro. *European Journal of Cell Biology*, 39(2):341–345.

Coombes, C. E., Yamamoto, A., Kenzie, M. R., Odde, D. J., and Gardner, M. K. (2013). Evolving tip structures can explain age-dependent microtubule catastrophe. *Current biology: CB*, 23(14):1342–1348.

Cooper, W. G. and Konigsberg, I. R. (1961). Dynamics of myogenesis in vitro. *The Anatomical Record*, 140:195–205.

Crisp, M., Liu, Q., Roux, K., Rattner, J. B., Shanahan, C., Burke, B., Stahl, P. D., and Hodzic, D. (2006). Coupling of the nucleus and cytoplasm: Role of the LINC complex. *The Journal of Cell Biology*, 172(1):41–53.

Dahl, R., Larsen, S., Dohlmann, T. L., Qvortrup, K., Helge, J. W., Dela, F., and Prats, C. (2015). Three-dimensional reconstruction of the human skeletal muscle mitochondrial network as a tool to assess mitochondrial content and structural organization. *Acta Physiologica*, 213(1):145–155.

Dammermann, A. and Merdes, A. (2002). Assembly of centrosomal proteins and microtubule organization depends on PCM-1. *The Journal of Cell Biology*, 159(2):255–266.

Datta, K., Guan, T., and Gerace, L. (2009). NET37, a nuclear envelope transmembrane protein with glycosidase homology, is involved in myoblast differentiation. *The Journal of Biological Chemistry*, 284(43):29666–29676.

De Groot, C. O., Jelesarov, I., Damberger, F. F., Bjelić, S., Schärer, M. A., Bhavesh, N. S., Grigoriev, I., Buey, R. M., Wüthrich, K., Capitani, G., Akhmanova, A., and Steinmetz, M. O. (2010). Molecular insights into mammalian end-binding protein heterodimerization. *The Journal of Biological Chemistry*, 285(8):5802–5814.

Dehmelt, L. and Halpain, S. (2005). The MAP2/Tau family of microtubule-associated proteins. *Genome Biology*, 6(1):204.

Delaval, B. and Doxsey, S. J. (2010). Pericentrin in cellular function and disease. *The Journal of Cell Biology*, 188(2):181–190.

Delgehyr, N., Sillibourne, J., and Bornens, M. (2005). Microtubule nucleation and anchoring at the centrosome are independent processes linked by ninein function. *Journal of Cell Science*, 118(Pt 8):1565–1575.

Desai, A., Verma, S., Mitchison, T. J., and Walczak, C. E. (1999). Kin I Kinesins Are Microtubule-Destabilizing Enzymes. *Cell*, 96(1):69–78.

Díaz, V. M., Mori, S., Longobardi, E., Menendez, G., Ferrai, C., Keough, R. A., Bachi, A., and Blasi, F. (2007). P160 Myb-Binding Protein Interacts with Prep1 and Inhibits Its Transcriptional Activity. *Molecular and Cellular Biology*, 27(22):7981–7990.

Dictenberg, J. B., Zimmerman, W., Sparks, C. A., Young, A., Vidair, C., Zheng, Y., Carrington, W., Fay, F. S., and Doxsey, S. J. (1998). Pericentrin and gamma-tubulin form a protein complex and are organized into a novel lattice at the centrosome. *The Journal of Cell Biology*, 141(1):163–174.

Dimitrov, A., Quesnoit, M., Moutel, S., Cantaloube, I., Poüs, C., and Perez, F. (2008). Detection of GTP-Tubulin Conformation in Vivo Reveals a Role for GTP Remnants in Microtubule Rescues. *Science*, 322(5906):1353–1356.

Diviani, D., Langeberg, L. K., Doxsey, S. J., and Scott, J. D. (2000). Pericentrin anchors protein kinase A at the centrosome through a newly identified RII-binding domain. *Current biology: CB*, 10(7):417–420.

Doxsey, S. (2001). Re-evaluating centrosome function. *Nature Reviews. Molecular Cell Biology*, 2(9):688–698.

Doxsey, S. J., Stein, P., Evans, L., Calarco, P. D., and Kirschner, M. (1994). Pericentrin, a highly conserved centrosome protein involved in microtubule organization. *Cell*, 76(4):639–650.

Drechsel, D. N., Hyman, A. A., Cobb, M. H., and Kirschner, M. W. (1992). Modulation of the dynamic instability of tubulin assembly by the microtubule-associated protein tau. *Molecular Biology of the Cell*, 3(10):1141–1154.

Drechsel, D. N. and Kirschner, M. W. (1994). The minimum GTP cap required to stabilize microtubules. *Current biology: CB*, 4(12):1053–1061.

Drewes, G., Trinczek, B., Illenberger, S., Biernat, J., Schmitt-Ulms, G., Meyer, H. E., Mandelkow, E.-M., and Mandelkow, E. (1995). Microtubule-associated Protein/Microtubule Affinity-regulating Kinase (p110mark) A NOVEL PROTEIN KINASE THAT REGULATES TAU-MICROTUBULE INTERACTIONS AND DYNAMIC INSTABILITY BY PHOSPHORYLATION AT THE ALZHEIMER-SPECIFIC SITE SERINE 262. *Journal of Biological Chemistry*, 270(13):7679–7688.

Duong, N. T., Morris, G. E., Lam, L. T., Zhang, Q., Sewry, C. A., Shanahan, C. M., and Holt, I. (2014). Nesprins: Tissue-Specific Expression of Epsilon and Other Short Isoforms. *PLoS ONE*, 9(4).

Efimov, A., Kharitonov, A., Efimova, N., Loncarek, J., Miller, P. M., Andreyeva, N., Gleeson, P., Galjart, N., Maia, A. R. R., McLeod, I. X., Yates, J. R., Maiato, H., Khodjakov, A., Akhmanova, A., and Kaverina, I. (2007). Asymmetric CLASP-dependent nucleation of noncentrosomal microtubules at the trans-Golgi network. *Developmental Cell*, 12(6):917–930.

Elhanany-Tamir, H., Yu, Y. V., Shnayder, M., Jain, A., Welte, M., and Volk, T. (2012). Organelle positioning in muscles requires cooperation between two KASH proteins and microtubules. *The Journal of Cell Biology*, 198(5):833–846.

Ellis, J. A. (2006). Emery-Dreifuss muscular dystrophy at the nuclear envelope: 10 years on. *Cellular and molecular life sciences: CMLS*, 63(23):2702–2709.

Englander, L. L. and Rubin, L. L. (1987). Acetylcholine receptor clustering and nuclear movement in muscle fibers in culture. *The Journal of Cell Biology*, 104(1):87–95.

Erickson, H. P. (2000). Gamma-tubulin nucleation: Template or protofilament? *Nature Cell Biology*, 2(6):E93–96.

Erickson, H. P. and Stoffler, D. (1996). Protofilaments and rings, two conformations of the tubulin family conserved from bacterial FtsZ to alpha/beta and gamma tubulin. *The Journal of Cell Biology*, 135(1):5–8.

Erickson, H. P., Taylor, D. W., Taylor, K. A., and Bramhill, D. (1996). Bacterial cell division protein FtsZ assembles into protofilament sheets and minirings, structural homologs of tubulin polymers. *Proceedings of the National Academy of Sciences of the United States of America*, 93(1):519–523.

Espigat-Georger, A., Dyachuk, V., Chemin, C., Emorine, L., and Merdes, A. (2016). Nuclear alignment in myotubes requires centrosome proteins recruited by nesprin-1. *Journal of Cell Science*, 129(22):4227–4237.

Evans, P. D., Vallender, E. J., and Lahn, B. T. (2006). Molecular evolution of the brain size regulator genes CDK5RAP2 and CENPJ. *Gene*, 375:75–79.

Falcone, S., Roman, W., Hnia, K., Gache, V., Didier, N., Lainé, J., Auradé, F., Marty, I., Nishino, I., Charlet-Berguerand, N., Romero, N. B., Marazzi, G., Sassoon, D., Laporte, J., and Gomes, E. R. (2014). N-WASP is required for Amphiphysin-2/BIN1-dependent nuclear positioning and triad organization in skeletal muscle and is involved in the pathophysiology of centronuclear myopathy. *EMBO molecular medicine*, 6(11):1455–1475.

Fan, M., Rhee, J., St-Pierre, J., Handschin, C., Puigserver, P., Lin, J., Jäeger, S., Erdjument-Bromage, H., Tempst, P., and Spiegelman, B. M. (2004). Suppression of mitochondrial respiration through recruitment of p160 myb binding protein to PGC-1α: Modulation by p38 MAPK. *Genes & Development*, 18(3):278–289.

Fant, X., Srsen, V., Espigat-Georger, A., and Merdes, A. (2009). Nuclei of Non-Muscle Cells Bind Centrosome Proteins upon Fusion with Differentiating Myoblasts. *PLoS ONE*, 4(12):e8303.

Farache, D., Jauneau, A., Chemin, C., Chartrain, M., Rémy, M.-H., Merdes, A., and Haren, L. (2016). Functional Analysis of γ-Tubulin Complex Proteins Indicates Specific Lateral Association via Their N-terminal Domains. *The Journal of Biological Chemistry*, 291(44):23112–23125.

Farkasovsky, M. and Küntzel, H. (2001). Cortical Num1p Interacts with the Dynein Intermediate Chain Pac11p and Cytoplasmic Microtubules in Budding Yeast. *The Journal of Cell Biology*, 152(2):251–262.

Firat-Karalar, E. N., Rauniyar, N., Yates, J. R., and Stearns, T. (2014). Proximity interactions among centrosome components identify regulators of centriole duplication. *Current biology: CB*, 24(6):664–670.

Fischer, J. A., Acosta, S., Kenny, A., Cater, C., Robinson, C., and Hook, J. (2004). Drosophila klarsicht has distinct subcellular localization domains for nuclear envelope and microtubule localization in the eye. *Genetics*, 168(3):1385–1393.

Flory, M. R. and Davis, T. N. (2003). The centrosomal proteins pericentrin and kendrin are encoded by alternatively spliced products of one gene. *Genomics*, 82(3):401–405.

Folker, E. S., Schulman, V. K., and Baylies, M. K. (2012). Muscle length and myonuclear position are independently regulated by distinct Dynein pathways. *Development (Cambridge, England)*, 139(20):3827–3837.

Folker, E. S., Schulman, V. K., and Baylies, M. K. (2014). Translocating myonuclei have distinct leading and lagging edges that require Kinesin and Dynein. *Development (Cambridge, England)*, 141(2):355–366.

Fong, K.-W., Choi, Y.-K., Rattner, J. B., and Qi, R. Z. (2008). CDK5RAP2 is a pericentriolar protein that functions in centrosomal attachment of the gamma-tubulin ring complex. *Molecular Biology of the Cell*, 19(1):115–125.

Fong, K.-W., Hau, S.-Y., Kho, Y.-S., Jia, Y., He, L., and Qi, R. Z. (2009). Interaction of CDK5RAP2 with EB1 to track growing microtubule tips and to regulate microtubule dynamics. *Molecular Biology of the Cell*, 20(16):3660–3670.

Franke, W. W., Scheer, U., Krohne, G., and Jarasch, E. D. (1981). The nuclear envelope and the architecture of the nuclear periphery. *The Journal of Cell Biology*, 91(3 Pt 2):39s–50s.

Frohnert, C., Schweizer, S., and Hoyer-Fender, S. (2011). SPAG4L/SPAG4L-2 are testis-specific SUN domain proteins restricted to the apical nuclear envelope of round spermatids facing the acrosome. *Molecular Human Reproduction*, 17(4):207–218.

Frontera, W. R. and Ochala, J. (2015). Skeletal Muscle: A Brief Review of Structure and Function. *Calcified Tissue International*, 96(3):183–195.

Fu, J. and Glover, D. M. (2012). Structured illumination of the interface between centriole and peri-centriolar material. *Open Biology*, 2(8):120104.

Gardner, M. K., Zanic, M., Gell, C., Bormuth, V., and Howard, J. (2011). Depolymerizing kinesins Kip3 and MCAK shape cellular microtubule architecture by differential control of catastrophe. *Cell*, 147(5):1092–1103.

Gigant, B., Curmi, P. A., Martin-Barbey, C., Charbaut, E., Lachkar, S., Lebeau, L., Siavoshian, S., Sobel, A., and Knossow, M. (2000). The 4 Å X-Ray Structure of a Tubulin:Stathmin-like Domain Complex. *Cell*, 102(6):809–816.

Gill, S. R., Schroer, T. A., Szilak, I., Steuer, E. R., Sheetz, M. P., and Cleveland, D. W. (1991). Dynactin, a conserved, ubiquitously expressed component of an activator of vesicle motility mediated by cytoplasmic dynein. *The Journal of Cell Biology*, 115(6):1639–1650.

Gillingham, A. K. and Munro, S. (2000). The PACT domain, a conserved centrosomal targeting motif in the coiled-coil proteins AKAP450 and pericentrin. *EMBO reports*, 1(6):524–529.

Göb, E., Schmitt, J., Benavente, R., and Alsheimer, M. (2010). Mammalian Sperm Head Formation Involves Different Polarization of Two Novel LINC Complexes. *PLoS ONE*, 5(8).

Gomes, E. R., Jani, S., and Gundersen, G. G. (2005). Nuclear movement regulated by Cdc42, MRCK, myosin, and actin flow establishes MTOC polarization in migrating cells. *Cell*, 121(3):451–463.

Gomez-Ferreria, M. A., Rath, U., Buster, D. W., Chanda, S. K., Caldwell, J. S., Rines, D. R., and Sharp, D. J. (2007). Human Cep192 Is Required for Mitotic Centrosome and Spindle Assembly. *Current Biology*, 17(22):1960–1966.

Gould, R. and Borisy, G. (1977). The pericentriolar material in Chinese hamster ovary cells nucleates microtubule formation. *The Journal of Cell Biology*, 73(3):601–615.

Grady, R. M., Starr, D. A., Ackerman, G. L., Sanes, J. R., and Han, M. (2005). Syne proteins anchor muscle nuclei at the neuromuscular junction. *Proceedings of the National Academy of Sciences of the United States of America*, 102(12):4359–4364.

Graumann, K., Runions, J., and Evans, D. E. (2010). Characterization of SUN-domain proteins at the higher plant nuclear envelope. *The Plant Journal: For Cell and Molecular Biology*, 61(1):134–144.

Griffith, E., Walker, S., Martin, C.-A., Vagnarelli, P., Stiff, T., Vernay, B., Al Sanna, N., Saggar, A., Hamel, B., Earnshaw, W. C., Jeggo, P. A., Jackson, A. P., and O'Driscoll, M. (2008). Mutations in pericentrin cause Seckel syndrome with defective ATR-dependent DNA damage signaling. *Nature Genetics*, 40(2):232–236.

Gros-Louis, F., Dupré, N., Dion, P., Fox, M. A., Laurent, S., Verreault, S., Sanes, J. R., Bouchard, J.-P., and Rouleau, G. A. (2007). Mutations in SYNE1 lead to a newly discovered form of autosomal recessive cerebellar ataxia. *Nature Genetics*, 39(1):80–85.

Guelen, L., Pagie, L., Brasset, E., Meuleman, W., Faza, M. B., Talhout, W., Eussen, B. H., de Klein, A., Wessels, L., de Laat, W., and van Steensel, B. (2008). Domain organization of human chromosomes revealed by mapping of nuclear lamina interactions. *Nature*, 453(7197):948–951.

Guillet, V., Knibiehler, M., Gregory-Pauron, L., Remy, M.-H., Chemin, C., Raynaud-Messina, B., Bon, C., Kollman, J. M., Agard, D. A., Merdes, A., and Mourey, L. (2011). Crystal structure of γ-tubulin complex protein GCP4 provides insight into microtubule nucleation. *Nature Structural & Molecular Biology*, 18(8):915–919.

Gunawardane, R. N., Martin, O. C., and Zheng, Y. (2003). Characterization of a new gammaTuRC subunit with WD repeats. *Molecular Biology of the Cell*, 14(3):1017–1026.

Gundersen, G. G., Khawaja, S., and Bulinski, J. C. (1989). Generation of a stable, posttranslationally modified microtubule array is an early event in myogenic differentiation. *The Journal of Cell Biology*, 109(5):2275–2288.

Gundersen, G. G. and Worman, H. J. (2013). Nuclear positioning. *Cell*, 152(6):1376–1389.

Hall, J. G., Flora, C., Scott, C. I., Pauli, R. M., and Tanaka, K. I. (2004). Majewski osteodysplastic primordial dwarfism type II (MOPD II): Natural history and clinical findings. *American Journal of Medical Genetics. Part A*, 130A(1):55–72.

Haque, F., Lloyd, D. J., Smallwood, D. T., Dent, C. L., Shanahan, C. M., Fry, A. M., Trembath, R. C., and Shackleton, S. (2006). SUN1 interacts with nuclear lamin A and cytoplasmic nesprins to provide a physical connection between the nuclear lamina and the cytoskeleton. *Molecular and Cellular Biology*, 26(10):3738–3751.

Haren, L., Stearns, T., and Lüders, J. (2009). Plk1-Dependent Recruitment of γ-Tubulin Complexes to Mitotic Centrosomes Involves Multiple PCM Components. *PLOS ONE*, 4(6):e5976.

Hasan, S., Güttinger, S., Mühlhäusser, P., Anderegg, F., Bürgler, S., and Kutay, U. (2006). Nuclear envelope localization of human UNC84A does not require nuclear lamins. *FEBS Letters*, 580(5):1263–1268.

Hatch, E. M., Kulukian, A., Holland, A. J., Cleveland, D. W., and Stearns, T. (2010). Cep152 interacts with Plk4 and is required for centriole duplication. *The Journal of Cell Biology*, 191(4):721–729.

Hayashi, I. and Ikura, M. (2003). Crystal structure of the amino-terminal microtubule-binding domain of end-binding protein 1 (EB1). *The Journal of Biological Chemistry*, 278(38):36430–36434.

Heald, R., Tournebize, R., Blank, T., Sandaltzopoulos, R., Becker, P., Hyman, A., and Karsenti, E. (1996). Self-organization of microtubules into bipolar spindles around artificial chromosomes in Xenopus egg extracts. *Nature*, 382(6590):420–425.

Heidemann, S. R., Landers, J. M., and Hamborg, M. A. (1981). Polarity orientation of axonal microtubules. *The Journal of Cell Biology*, 91(3 Pt 1):661–665.

Herz, J. and Strickland, D. K. (2001). LRP: A multifunctional scavenger and signaling receptor. *Journal of Clinical Investigation*, 108(6):779–784.

Herzog, W., Powers, K., Johnston, K., and Duvall, M. (2015). A new paradigm for muscle contraction. *Frontiers in Physiology*, 6.

Hinchcliffe, E. H., Miller, F. J., Cham, M., Khodjakov, A., and Sluder, G. (2001). Requirement of a centrosomal activity for cell cycle progression through G1 into S phase. *Science (New York, N.Y.)*, 291(5508):1547–1550.

Hirokawa, N. and Noda, Y. (2008). Intracellular Transport and Kinesin Superfamily Proteins, KIFs: Structure, Function, and Dynamics. *Physiological Reviews*, 88(3):1089–1118.

Hirokawa, N., Noda, Y., Tanaka, Y., and Niwa, S. (2009). Kinesin superfamily motor proteins and intracellular transport. *Nature Reviews Molecular Cell Biology*, 10(10):682–696.

Hirokawa, N. and Tanaka, Y. (2015). Kinesin superfamily proteins (KIFs): Various functions and their relevance for important phenomena in life and diseases. *Experimental Cell Research*, 334(1):16–25.

Hodzic, D. M., Yeater, D. B., Bengtsson, L., Otto, H., and Stahl, P. D. (2004). Sun2 is a novel mammalian inner nuclear membrane protein. *The Journal of Biological Chemistry*, 279(24):25805–25812.

Holmes, K. C. and Geeves, M. A. (2000). The structural basis of muscle contraction. *Philosophical Transactions of the Royal Society B: Biological Sciences*, 355(1396):419–431.

Holt, I., Duong, N. T., Zhang, Q., Lam, L. T., Sewry, C. A., Mamchaoui, K., Shanahan, C. M., and Morris, G. E. (2016). Specific localization of nesprin-1-α2, the short isoform of nesprin-1 with a KASH domain, in developing, fetal and regenerating muscle, using a new monoclonal antibody. *BMC Cell Biology*, 17:26.

Holtzer, H., Croop, J., Dienstman, S., Ishikawa, H., and Somlyo, A. P. (1975). Effects of cytochaslasin B and colcemide on myogenic cultures. *Proceedings of the National Academy of Sciences of the United States of America*, 72(2):513–517.

Honnappa, S., Gouveia, S. M., Weisbrich, A., Damberger, F. F., Bhavesh, N. S., Jawhari, H., Grigoriev, I., van Rijssel, F. J. A., Buey, R. M., Lawera, A., Jelesarov, I., Winkler, F. K., Wüthrich, K., Akhmanova, A., and Steinmetz, M. O. (2009). An EB1-Binding Motif Acts as a Microtubule Tip Localization Signal. *Cell*, 138(2):366–376.

Horn, H. F., Kim, D. I., Wright, G. D., Wong, E. S. M., Stewart, C. L., Burke, B., and Roux, K. J. (2013). A mammalian KASH domain protein coupling meiotic chromosomes to the cytoskeleton. *J Cell Biol*, 202(7):1023–1039.

Horvitz, H. R. and Sulston, J. E. (1980). Isolation and genetic characterization of cell-lineage mutants of the nematode Caenorhabditis elegans. *Genetics*, 96(2):435–454.

Hurtado, L., Caballero, C., Gavilan, M. P., Cardenas, J., Bornens, M., and Rios, R. M. (2011). Disconnecting the Golgi ribbon from the centrosome prevents directional cell migration and ciliogenesis. *The Journal of Cell Biology*, 193(5):917–933.

Hutchins, J. R. A., Toyoda, Y., Hegemann, B., Poser, I., Hériché, J.-K., Sykora, M. M., Augsburg, M., Hudecz, O., Buschhorn, B. A., Bulkescher, J., Conrad, C., Comartin, D., Schleiffer, A., Sarov, M., Pozniakovsky, A., Slabicki, M. M., Schloissnig, S., Steinmacher, I., Leuschner, M., Ssykor, A., Lawo, S., Pelletier, L., Stark, H., Nasmyth, K., Ellenberg, J., Durbin, R., Buchholz, F., Mechtler, K., Hyman, A. A., and Peters, J.-M. (2010). Systematic analysis of human protein complexes identifies chromosome segregation proteins. *Science (New York, N.Y.)*, 328(5978):593–599.

Hyman, A. A., Chrétien, D., Arnal, I., and Wade, R. H. (1995). Structural changes accompanying GTP hydrolysis in microtubules: Information from a slowly hydrolyzable analogue guanylyl-(alpha,beta)-methylene-diphosphonate. *The Journal of Cell Biology*, 128(1-2):117–125.

Ishikawa, H., Kubo, A., Tsukita, S., and Tsukita, S. (2005). Odf2-deficient mother centrioles lack distal/subdistal appendages and the ability to generate primary cilia. *Nature Cell Biology*, 7(5):517–524.

Jakobsen, L., Vanselow, K., Skogs, M., Toyoda, Y., Lundberg, E., Poser, I., Falkenby, L. G., Bennetzen, M., Westendorf, J., Nigg, E. A., Uhlen, M., Hyman, A. A., and Andersen, J. S. (2011). Novel asymmetrically localizing components of human centrosomes identified by complementary proteomics methods. *The EMBO journal*, 30(8):1520–1535.

Janson, M. E., de Dood, M. E., and Dogterom, M. (2003). Dynamic instability of microtubules is regulated by force. *The Journal of Cell Biology*, 161(6):1029–1034.

Jaspersen, S. L., Martin, A. E., Glazko, G., Giddings, T. H., Morgan, G., Mushegian, A., and Winey, M. (2006). The Sad1-UNC-84 homology domain in Mps3 interacts with Mps2 to connect the spindle pole body with the nuclear envelope. *The Journal of Cell Biology*, 174(5):665–675.

Jiang, X.-Z., Yang, M.-G., Huang, L.-H., Li, C.-Q., and Xing, X.-W. (2011). SPAG4L, a novel nuclear envelope protein involved in the meiotic stage of spermatogenesis. *DNA and cell biology*, 30(11):875–882.

Jin, W., Peng, J., and Jiang, S. (2016). The epigenetic regulation of embryonic myogenesis and adult muscle regeneration by histone methylation modification. *Biochemistry and Biophysics Reports*, 6:209–219.

Joukov, V., De Nicolo, A., Rodriguez, A., Walter, J. C., and Livingston, D. M. (2010). Centrosomal protein of 192 kDa (Cep192) promotes centrosome-driven spindle assembly by engaging in organelle-specific Aurora A activation. *Proceedings of the National Academy of Sciences of the United States of America*, 107(49):21022–21027.

Joukov, V., Walter, J., and De, N. (2014). The Cep192-Organized Aurora A-Plk1 Cascade Is Essential for Centrosome Cycle and Bipolar Spindle Assembly. *Molecular Cell*, 55(4):578–591.

Jungbluth, H., Wallgren-Pettersson, C., and Laporte, J. (2008). Centronuclear (myotubular) myopathy. *Orphanet Journal of Rare Diseases*, 3:26.

Jurczyk, A., Gromley, A., Redick, S., San Agustin, J., Witman, G., Pazour, G. J., Peters, D. J. M., and Doxsey, S. (2004). Pericentrin forms a complex with intraflagellar transport proteins and polycystin-2 and is required for primary cilia assembly. *The Journal of Cell Biology*, 166(5):637–643.

Kanai, Y., Okada, Y., Tanaka, Y., Harada, A., Terada, S., and Hirokawa, N. (2000). KIF5C, a novel neuronal kinesin enriched in motor neurons. *The Journal of Neuroscience: The Official Journal of the Society for Neuroscience*, 20(17):6374–6384.

Kano, Y., Fujimaki, N., and Ishikawa, H. (1991). The distribution and arrangement of microtubules in mammalian skeletal muscle fibers. *Cell Structure and Function*, 16(3):251–261.

Kapitein, L. C. and Hoogenraad, C. C. (2015). Building the Neuronal Microtubule Cytoskeleton. *Neuron*, 87(3):492–506.

Kardon, J. R. and Vale, R. D. (2009). Regulators of the cytoplasmic dynein motor. *Nature Reviews Molecular Cell Biology*, 10(12):854–865.

Karki, S. and Holzbaur, E. L. (1999). Cytoplasmic dynein and dynactin in cell division and intracellular transport. *Current Opinion in Cell Biology*, 11(1):45–53.

Karki, S. and Holzbaur, E. L. F. (1995). Affinity Chromatography Demonstrates a Direct Binding between Cytoplasmic Dynein and the Dynactin Complex. *Journal of Biological Chemistry*, 270(48):28806–28811.

Kawaguchi, S.-i. and Zheng, Y. (2004). Characterization of a Drosophila Centrosome Protein CP309 That Shares Homology with Kendrin and CG-NAP. *Molecular Biology of the Cell*, 15(1):37–45.

Keryer, G., Di Fiore, B., Celati, C., Lechtreck, K. F., Mogensen, M., Delouvée, A., Lavia, P., Bornens, M., and Tassin, A.-M. (2003a). Part of Ran Is Associated with AKAP450 at the Centrosome: Involvement in Microtubule-organizing Activity. *Molecular Biology of the Cell*, 14(10):4260–4271.

Keryer, G., Rios, R. M., Landmark, B. F., Skalhegg, B., Lohmann, S. M., and Bornens, M. (1993). A high-affinity binding protein for the regulatory subunit of cAMP-dependent protein kinase II in the centrosome of human cells. *Experimental Cell Research*, 204(2):230–240.

Keryer, G., Witczak, O., Delouvée, A., Kemmner, W. A., Rouillard, D., Taskén, K., and Bornens, M. (2003b). Dissociating the Centrosomal Matrix Protein AKAP450 from Centrioles Impairs Centriole Duplication and Cell Cycle Progression. *Molecular Biology of the Cell*, 14(6):2436–2446.

Khodjakov, A., Cole, R. W., Oakley, B. R., and Rieder, C. L. (2000). Centrosome-independent mitotic spindle formation in vertebrates. *Current biology: CB*, 10(2):59–67.

Khodjakov, A. and Rieder, C. L. (1999). The sudden recruitment of gamma-tubulin to the centrosome at the onset of mitosis and its dynamic exchange throughout the cell cycle, do not require microtubules. *The Journal of Cell Biology*, 146(3):585–596.

Kim, D. I., KC, B., Zhu, W., Motamedchaboki, K., Doye, V., and Roux, K. J. (2014). Probing nuclear pore complex architecture with proximity-dependent biotinylation. *Proceedings of the National Academy of Sciences of the United States of America*, 111(24):E2453–E2461.

Kim, N., Stiegler, A., Cameron, T., Hallock, P., Gomez, A., Huang, J., Hubbard, S., Dustin, M., and Burden, S. (2008). Lrp4 is a Receptor for Agrin and Forms a Complex with MuSK. *Cell*, 135(2):334–342.

Kind, J. and van Steensel, B. (2010). Genome-nuclear lamina interactions and gene regulation. *Current Opinion in Cell Biology*, 22(3):320–325.

Kislinger, T., Cox, B., Kannan, A., Chung, C., Hu, P., Ignatchenko, A., Scott, M. S., Gramolini, A. O., Morris, Q., Hallett, M. T., Rossant, J., Hughes, T. R., Frey, B., and Emili, A. (2006). Global survey of organ and organelle protein expression in mouse: Combined proteomic and transcriptomic profiling. *Cell*, 125(1):173–186.

Knight, J. D. and Kothary, R. (2011). The myogenic kinome: Protein kinases critical to mammalian skeletal myogenesis. *Skeletal Muscle*, 1:29.

Kollman, J. M., Greenberg, C. H., Li, S., Moritz, M., Zelter, A., Fong, K. K., Fernandez, J.-J., Sali, A., Kilmartin, J., Davis, T. N., and Agard, D. A. (2015). Ring closure activates yeast γTuRC for species-specific microtubule nucleation. *Nature Structural & Molecular Biology*, 22(2):132–137.

Kollman, J. M., Merdes, A., Mourey, L., and Agard, D. A. (2011). Microtubule nucleation by γ-tubulin complexes. *Nature Reviews Molecular Cell Biology*, 12(11):709–721.

Kollman, J. M., Polka, J. K., Zelter, A., Davis, T. N., and Agard, D. A. (2010). Microtubule nucleating gamma-TuSC assembles structures with 13-fold microtubule-like symmetry. *Nature*, 466(7308):879–882.

Kollman, J. M., Zelter, A., Muller, E. G. D., Fox, B., Rice, L. M., Davis, T. N., and Agard, D. A. (2008). The structure of the gamma-tubulin small complex: Implications of its architecture and flexibility for microtubule nucleation. *Molecular Biology of the Cell*, 19(1):207–215.

Komarova, Y., Groot, C. O. D., Grigoriev, I., Gouveia, S. M., Munteanu, E. L., Schober, J. M., Honnappa, S., Buey, R. M., Hoogenraad, C. C., Dogterom, M., Borisy, G. G., Steinmetz, M. O., and Akhmanova, A. (2009). Mammalian end binding proteins control persistent microtubule growth. *The Journal of Cell Biology*, 184(5):691–706.

Korfali, N., Wilkie, G. S., Swanson, S. K., Srsen, V., Batrakou, D. G., Fairley, E. A. L., Malik, P., Zuleger, N., Goncharevich, A., de las Heras, J., Kelly, D. A., Kerr, A. R. W., Florens, L., and Schirmer, E. C. (2010). The Leukocyte Nuclear Envelope Proteome Varies with Cell Activation and Contains Novel Transmembrane Proteins That Affect Genome Architecture. *Molecular & Cellular Proteomics : MCP*, 9(12):2571–2585.

Kowalski, R. J. and Williams, R. C. (1993). Microtubule-associated protein 2 alters the dynamic properties of microtubule assembly and disassembly. *Journal of Biological Chemistry*, 268(13):9847–9855.

Kracklauer, M. P., Banks, S. M. L., Xie, X., Wu, Y., and Fischer, J. A. (2007). Drosophila klaroid encodes a SUN domain protein required for Klarsicht localization to the nuclear envelope and nuclear migration in the eye. *Fly*, 1(2):75–85.

Kraemer, N., Issa, L., Hauck, S. C. R., Mani, S., Ninnemann, O., and Kaindl, A. M. (2011). What's the hype about CDK5RAP2? *Cellular and molecular life sciences: CMLS*, 68(10):1719–1736.

Kubo, A., Sasaki, H., Yuba-Kubo, A., Tsukita, S., and Shiina, N. (1999). Centriolar Satellites. *The Journal of Cell Biology*, 147(5):969–980.

Kummer, T. T., Misgeld, T., Lichtman, J. W., and Sanes, J. R. (2004). Nerve-independent formation of a topologically complex postsynaptic apparatus. *The Journal of Cell Biology*, 164(7):1077–1087.

Kutscheidt, S., Zhu, R., Antoku, S., Luxton, G. W. G., Stagljar, I., Fackler, O. T., and Gundersen, G. G. (2014). FHOD1 interaction with nesprin-2G mediates TAN line formation and nuclear movement. *Nature Cell Biology*, 16(7):708–715.

Lampe, A., Haucke, V., Sigrist, S. J., Heilemann, M., and Schmoranzer, J. (2012). Multi-colour direct STORM with red emitting carbocyanines. *Biology of the Cell*, 104(4):229–237.

Lawo, S., Hasegan, M., Gupta, G. D., and Pelletier, L. (2012). Subdiffraction imaging of centrosomes reveals higher-order organizational features of pericentriolar material. *Nature Cell Biology*, 14(11):1148–1158.

Le Grand, F. and Rudnicki, M. A. (2007). Skeletal muscle satellite cells and adult myogenesis. *Current opinion in cell biology*, 19(6):628–633.

Lechtreck, K. F. (2015). IFT–Cargo Interactions and Protein Transport in Cilia. *Trends in Biochemical Sciences*, 40(12):765–778.

Lee, K. and Rhee, K. (2011). PLK1 phosphorylation of pericentrin initiates centrosome maturation at the onset of mitosis. *J Cell Biol*, 195(7):1093–1101.

Lehmann, M., Lichtner, G., Klenz, H., and Schmoranzer, J. (2016). Novel organic dyes for multicolor localization-based super-resolution microscopy. *Journal of Biophotonics*, 9(1-2):161–170.

Lei, K., Zhang, X., Ding, X., Guo, X., Chen, M., Zhu, B., Xu, T., Zhuang, Y., Xu, R., and Han, M. (2009). SUN1 and SUN2 play critical but partially redundant roles in anchoring nuclei in skeletal muscle cells in mice. *Proceedings of the National Academy of Sciences of the United States of America*, 106(25):10207–10212.

Lewis, S. A., Ivanov, I. E., Lee, G.-H., and Cowan, N. J. (1989). Organization of microtubules in dendrites and axons is determined by a short hydrophobic zipper in microtubule-associated proteins MAP2 and tau. *Nature*, 342(6249):498–505.

Li, Q., Hansen, D., Killilea, A., Joshi, H. C., Palazzo, R. E., and Balczon, R. (2001). Kendrin/pericentrin-B, a centrosome protein with homology to pericentrin that complexes with PCM-1. *Journal of Cell Science*, 114(4):797–809.

Lin, T.-c., Neuner, A., Flemming, D., Liu, P., Chinen, T., Jäkle, U., Arkowitz, R., and Schiebel, E. (2016). MOZART1 and γ-tubulin complex receptors are both required to turn γ-TuSC into an active microtubule nucleation template. *J Cell Biol*, page jcb.201606092.

Lippincott-Schwartz, J. and Patterson, G. H. (2009). Photoactivatable fluorescent proteins for diffraction-limited and super-resolution imaging. *Trends in cell biology*, 19(11):555–565.

Liu, G.-H., Guan, T., Datta, K., Coppinger, J., Yates, J., and Gerace, L. (2009). Regulation of myoblast differentiation by the nuclear envelope protein NET39. *Molecular and Cellular Biology*, 29(21):5800–5812.

Lu, W., Schneider, M., Neumann, S., Jaeger, V.-M., Taranum, S., Munck, M., Cartwright, S., Richardson, C., Carthew, J., Noh, K., Goldberg, M., Noegel, A. A., and Karakesisoglou, I. (2012). Nesprin interchain associations control nuclear size. *Cellular and molecular life sciences: CMLS*, 69(20):3493–3509.

Lu, Z., Joseph, D., Bugnard, E., Zaal, K. J., and Ralston, E. (2001). Golgi complex reorganization during muscle differentiation: Visualization in living cells and mechanism. *Molecular Biology of the Cell*, 12(4):795–808.

Lüders, J. (2012). The amorphous pericentriolar cloud takes shape. *Nature Cell Biology*, 14(11):1126–1128.

Lüke, Y., Zaim, H., Karakesisoglou, I., Jaeger, V. M., Sellin, L., Lu, W., Schneider, M., Neumann, S., Beijer, A., Munck, M., Padmakumar, V. C., Gloy, J., Walz, G., and Noegel, A. A. (2008). Nesprin-2 Giant (NUANCE) maintains nuclear envelope architecture and composition in skin. *Journal of Cell Science*, 121(11):1887–1898.

Luther, P. K. (2009). The vertebrate muscle Z-disc: Sarcomere anchor for structure and signalling. *Journal of Muscle Research and Cell Motility*, 30(5-6):171–185.

Luxton, G. W. G., Gomes, E. R., Folker, E. S., Vintinner, E., and Gundersen, G. G. (2010). Linear Arrays of Nuclear Envelope Proteins Harness Retrograde Actin Flow for Nuclear Movement. *Science*, 329(5994):956–959.

Luxton, G. W. G., Gomes, E. R., Folker, E. S., Worman, H. J., and Gundersen, G. G. (2011). TAN lines: A novel nuclear envelope structure involved in nuclear positioning. *Nucleus (Austin, Tex.)*, 2(3):173–181.

Lyon, A. S., Morin, G., Moritz, M., Yabut, K. C. B., Vojnar, T., Zelter, A., Muller, E., Davis, T. N., and Agard, D. A. (2016). Higher-order oligomerization of Spc110p drives γ-tubulin ring complex assembly. *Molecular Biology of the Cell*, 27(14):2245–2258.

Ma, W. and Viveiros, M. M. (2014). Depletion of pericentrin in mouse oocytes disrupts microtubule organizing center function and meiotic spindle organization. *Molecular Reproduction and Development*, 81(11):1019–1029.

Maiato, H., Rieder, C. L., and Khodjakov, A. (2004). Kinetochore-driven formation of kinetochore fibers contributes to spindle assembly during animal mitosis. *The Journal of Cell Biology*, 167(5):831–840.

Malik, P., Korfali, N., Srsen, V., Lazou, V., Batrakou, D. G., Zuleger, N., Kavanagh, D. M., Wilkie, G. S., Goldberg, M. W., and Schirmer, E. C. (2010). Cell-specific and lamin-dependent targeting of novel transmembrane proteins in the nuclear envelope. *Cellular and molecular life sciences: CMLS*, 67(8):1353–1369.

Malone, C. J., Fixsen, W. D., Horvitz, H. R., and Han, M. (1999). UNC-84 localizes to the nuclear envelope and is required for nuclear migration and anchoring during C. elegans development. *Development (Cambridge, England)*, 126(14):3171–3181.

Mamchaoui, K., Trollet, C., Bigot, A., Negroni, E., Chaouch, S., Wolff, A., Kandalla, P. K., Marie, S., Di Santo, J., St Guily, J. L., Muntoni, F., Kim, J., Philippi, S., Spuler, S., Levy, N., Blumen, S. C., Voit, T., Wright, W. E., Aamiri, A., Butler-Browne, G., and Mouly, V. (2011). Immortalized pathological human myoblasts: Towards a universal tool for the study of neuromuscular disorders. *Skeletal Muscle*, 1:34.

Mandelkow, E. M., Mandelkow, E., and Milligan, R. A. (1991). Microtubule dynamics and microtubule caps: A time-resolved cryo-electron microscopy study. *The Journal of Cell Biology*, 114(5):977–991.

Manning, J. and Kumar, S. (2007). NEDD1: Function in microtubule nucleation, spindle assembly and beyond. *The International Journal of Biochemistry & Cell Biology*, 39(1):7–11.

Margolis, R. L. and Wilson, L. (1978). Opposite end assembly and disassembly of microtubules at steady state in vitro. *Cell*, 13(1):1–8.

Margolis, R. L. and Wilson, L. (1981). Microtubule treadmills–possible molecular machinery. *Nature*, 293(5835):705–711.

Martinez-Campos, M., Basto, R., Baker, J., Kernan, M., and Raff, J. W. (2004). The Drosophila pericentrin-like protein is essential for cilia/flagella function, but appears to be dispensable for mitosis. *The Journal of Cell Biology*, 165(5):673–683.

Masuda, H., Mori, R., Yukawa, M., and Toda, T. (2013). Fission yeast MOZART1/Mzt1 is an essential γ-tubulin complex component required for complex recruitment to the microtubule organizing center, but not its assembly. *Molecular Biology of the Cell*, 24(18):2894–2906.

Mattioli, E., Columbaro, M., Capanni, C., Maraldi, N. M., Cenni, V., Scotlandi, K., Marino, M. T., Merlini, L., Squarzoni, S., and Lattanzi, G. (2011). Prelamin A-mediated recruitment of SUN1 to the nuclear envelope directs nuclear positioning in human muscle. *Cell Death and Differentiation*, 18(8):1305–1315.

Maurer, S. P., Bieling, P., Cope, J., Hoenger, A., and Surrey, T. (2011). GTPgammaS microtubules mimic the growing microtubule end structure recognized by end-binding proteins (EBs). *Proceedings of the National Academy of Sciences of the United States of America*, 108(10):3988–3993.

Maurer, S. P., Cade, N. I., Bohner, G., Gustafsson, N., Boutant, E., and Surrey, T. (2014). EB1 accelerates two conformational transitions important for microtubule maturation and dynamics. *Current biology: CB*, 24(4):372–384.

Mazzarello, P., Calligaro, A., Vannini, V., and Muscatello, U. (2003). The sarcoplasmic reticulum: Its discovery and rediscovery. *Nature Reviews Molecular Cell Biology*, 4(1):69–74.

McGee, M. D., Rillo, R., Anderson, A. S., and Starr, D. A. (2006). UNC-83 IS a KASH protein required for nuclear migration and is recruited to the outer nuclear membrane by a physical interaction with the SUN protein UNC-84. *Molecular Biology of the Cell*, 17(4):1790–1801.

McIntosh, J. R., Morphew, M. K., Grissom, P. M., Gilbert, S. P., and Hoenger, A. (2009). Lattice Structure of Cytoplasmic Microtubules in a Cultured Mammalian Cell. *Journal of molecular biology*, 394(2):177–182.

Meads, T. and Schroer, T. A. (1995). Polarity and nucleation of microtubules in polarized epithelial cells. *Cell Motility and the Cytoskeleton*, 32(4):273–288.

Meinke, P., Mattioli, E., Haque, F., Antoku, S., Columbaro, M., Straatman, K. R., Worman, H. J., Gundersen, G. G., Lattanzi, G., Wehnert, M., and Shackleton, S. (2014). Muscular dystrophy-associated SUN1 and SUN2 variants disrupt nuclear-cytoskeletal connections and myonuclear organization. *PLoS genetics*, 10(9):e1004605.

Mellad, J. A., Warren, D. T., and Shanahan, C. M. (2011). Nesprins LINC the nucleus and cytoskeleton. *Current Opinion in Cell Biology*, 23(1):47–54.

Mennella, V., Keszthelyi, B., McDonald, K. L., Chhun, B., Kan, F., Rogers, G. C., Huang, B., and Agard, D. A. (2012). Subdiffraction-resolution fluorescence microscopy reveals a domain of the centrosome critical for pericentriolar material organization. *Nature Cell Biology*, 14(11):1159–1168.

Metoz, F., Arnal, I., and Wade, R. H. (1997). Tomography without Tilt: Three-Dimensional Imaging of Microtubule/Motor Complexes. *Journal of Structural Biology*, 118(2):159–168.

Metzger, T., Gache, V., Xu, M., Cadot, B., Folker, E. S., Richardson, B. E., Gomes, E. R., and Baylies, M. K. (2012). MAP and kinesin-dependent nuclear positioning is required for skeletal muscle function. *Nature*, 484(7392):120–124.

Millecamps, S. and Julien, J.-P. (2013). Axonal transport deficits and neurodegenerative diseases. *Nature Reviews Neuroscience*, 14(3):161–176.

Miller, P. M., Folkmann, A. W., Maia, A. R. R., Efimova, N., Efimov, A., and Kaverina, I. (2009). Golgi-derived CLASP-dependent microtubules control Golgi organization and polarized trafficking in motile cells. *Nature Cell Biology*, 11(9):1069–1080.

Mimori-Kiyosue, Y., Shiina, N., and Tsukita, S. (2000). The dynamic behavior of the APC-binding protein EB1 on the distal ends of microtubules. *Current Biology*, 10(14):865–868.

Mislow, J. M. K., Holaska, J. M., Kim, M. S., Lee, K. K., Segura-Totten, M., Wilson, K. L., and McNally, E. M. (2002a). Nesprin-1alpha self-associates and binds directly to emerin and lamin A in vitro. *FEBS letters*, 525(1-3):135–140.

Mislow, J. M. K., Kim, M. S., Davis, D. B., and McNally, E. M. (2002b). Myne-1, a spectrin repeat transmembrane protein of the myocyte inner nuclear membrane, interacts with lamin A/C. *Journal of Cell Science*, 115(Pt 1):61–70.

Mitchison, T. and Kirschner, M. (1984a). Dynamic instability of microtubule growth. *Nature*, 312(5991):237–242.

Mitchison, T. and Kirschner, M. (1984b). Microtubule assembly nucleated by isolated centrosomes. *Nature*, 312(5991):232–237.

Miyoshi, K., Asanuma, M., Miyazaki, I., Matsuzaki, S., Tohyama, M., and Ogawa, N. (2006a). Characterization of pericentrin isoforms in vivo. *Biochemical and Biophysical Research Communications*, 351(3):745–749.

Miyoshi, K., Onishi, K., Asanuma, M., Miyazaki, I., Diaz-Corrales, F. J., and Ogawa, N. (2006b). Embryonic expression of pericentrin suggests universal roles in ciliogenesis. *Development Genes and Evolution*, 216(9):537–542.

Mogensen, M. M. (1999). Microtubule release and capture in epithelial cells. *Biology of the Cell*, 91(4-5):331–341.

Mogensen, M. M., Malik, A., Piel, M., Bouckson-Castaing, V., and Bornens, M. (2000). Microtubule minus-end anchorage at centrosomal and non-centrosomal sites: The role of ninein. *Journal of Cell Science*, 113 (Pt 17):3013–3023.

Mogessie, B., Roth, D., Rahil, Z., and Straube, A. (2015). A novel isoform of MAP4 organises the paraxial microtubule array required for muscle cell differentiation. *eLife*, 4:e05697.

Morimoto, A., Shibuya, H., Zhu, X., Kim, J., Ishiguro, K.-i., Han, M., and Watanabe, Y. (2012). A conserved KASH domain protein associates with telomeres, SUN1, and dynactin during mammalian meiosis. *The Journal of Cell Biology*, 198(2):165–172.

Moritz, M., Braunfeld, M. B., Guénebaut, V., Heuser, J., and Agard, D. A. (2000). Structure of the gamma-tubulin ring complex: A template for microtubule nucleation. *Nature Cell Biology*, 2(6):365–370.

Moritz, M., Braunfeld, M. B., Sedat, J. W., Alberts, B., and Agard, D. A. (1995). Microtubule nucleation by gamma-tubulin-containing rings in the centrosome. *Nature*, 378(6557):638–640.

Moss, D. K., Bellett, G., Carter, J. M., Liovic, M., Keynton, J., Prescott, A. R., Lane, E. B., and Mogensen, M. M. (2007). Ninein is released from the centrosome and moves bi-directionally along microtubules. *Journal of Cell Science*, 120(17):3064–3074.

Mühlhans, J., Brandstätter, J. H., and Giessl, A. (2011). The centrosomal protein pericentrin identified at the basal body complex of the connecting cilium in mouse photoreceptors. *PloS One*, 6(10):e26496.

Müller, H., Schmidt, D., Steinbrink, S., Mirgorodskaya, E., Lehmann, V., Habermann, K., Dreher, F., Gustavsson, N., Kessler, T., Lehrach, H., Herwig, R., Gobom, J., Ploubidou, A., Boutros, M., and Lange, B. M. H. (2010). Proteomic and functional analysis of the mitotic Drosophila centrosome. *The EMBO journal*, 29(19):3344–3357.

Murata, T., Sonobe, S., Baskin, T. I., Hyodo, S., Hasezawa, S., Nagata, T., Horio, T., and Hasebe, M. (2005). Microtubule-dependent microtubule nucleation based on recruitment of γ-tubulin in higher plants. *Nature Cell Biology*, 7(10):961–968.

Murphy, S. M., Preble, A. M., Patel, U. K., O'Connell, K. L., Dias, D. P., Moritz, M., Agard, D., Stults, J. T., and Stearns, T. (2001). GCP5 and GCP6: Two new members of the human gamma-tubulin complex. *Molecular Biology of the Cell*, 12(11):3340–3352.

Nagase, T., Kikuno, R., Nakayama, M., Hirosawa, M., and Ohara, O. (2000). Prediction of the coding sequences of unidentified human genes. XVIII. The complete sequences of 100 new cDNA clones from brain which code for large proteins in vitro. *DNA research: an international journal for rapid publication of reports on genes and genomes*, 7(4):273–281.

Nazarian, J., Bouri, K., and Hoffman, E. P. (2005). Intracellular expression profiling by laser capture microdissection: Three novel components of the neuromuscular junction. *Physiological Genomics*, 21(1):70–80.

Nedelec, F. and Foethke, D. (2007). Collective Langevin dynamics of flexible cytoskeletal fibers. *New Journal of Physics*, 9(11):427.

Nguyen, M. M., McCracken, C. J., Milner, E. S., Goetschius, D. J., Weiner, A. T., Long, M. K., Michael, N. L., Munro, S., and Rolls, M. M. (2014). γ-tubulin controls neuronal microtubule polarity independently of Golgi outposts. *Molecular Biology of the Cell*, 25(13):2039–2050.

Nicot, A.-S., Toussaint, A., Tosch, V., Kretz, C., Wallgren-Pettersson, C., Iwarsson, E., Kingston, H., Garnier, J.-M., Biancalana, V., Oldfors, A., Mandel, J.-L., and Laporte, J. (2007). Mutations in amphiphysin 2 (BIN1) disrupt interaction with dynamin 2 and cause autosomal recessive centronuclear myopathy. *Nature Genetics*, 39(9):1134–1139.

Nie, S., Ke, H., Gao, F., Ren, J., Wang, M., Huo, L., Gong, W., and Feng, W. (2016). Coiled-Coil Domains of SUN Proteins as Intrinsic Dynamic Regulators. *Structure (London, England: 1993)*, 24(1):80–91.

Nishimura, T., Takahashi, M., Kim, H.-S., Mukai, H., and Ono, Y. (2005). Centrosome-targeting region of CG-NAP causes centrosome amplification by recruiting cyclin E-cdk2 complex. *Genes to Cells: Devoted to Molecular & Cellular Mechanisms*, 10(1):75–86.

Oakley, C. E. and Oakley, B. R. (1989). Identification of gamma-tubulin, a new member of the tubulin superfamily encoded by mipA gene of Aspergillus nidulans. *Nature*, 338(6217):662–664.

Odde, D. J., Cassimeris, L., and Buettner, H. M. (1995). Kinetics of microtubule catastrophe assessed by probabilistic analysis. *Biophysical Journal*, 69(3):796–802.

Oddoux, S., Zaal, K. J., Tate, V., Kenea, A., Nandkeolyar, S. A., Reid, E., Liu, W., and Ralston, E. (2013). Microtubules that form the stationary lattice of muscle fibers are dynamic and nucleated at Golgi elements. *The Journal of Cell Biology*, 203(2):205–213.

Oegema, K., Wiese, C., Martin, O. C., Milligan, R. A., Iwamatsu, A., Mitchison, T. J., and Zheng, Y. (1999). Characterization of two related Drosophila gamma-tubulin complexes that differ in their ability to nucleate microtubules. *The Journal of Cell Biology*, 144(4):721–733.

Ori-McKenney, K. M., Jan, L. Y., and Jan, Y.-N. (2012). Golgi outposts shape dendrite morphology by functioning as sites of acentrosomal microtubule nucleation in neurons. *Neuron*, 76(5):921–930.

O'Rourke, B. P., Gomez-Ferreria, M. A., Berk, R. H., Hackl, A. M. U., Nicholas, M. P., O'Rourke, S. C., Pelletier, L., and Sharp, D. J. (2014). Cep192 Controls the Balance of Centrosome and Non-Centrosomal Microtubules during Interphase. *PLoS ONE*, 9(6).

Owen, H. R., Elser, M., Cheung, E., Gersbach, M., Kraus, W. L., and Hottiger, M. O. (2007). MYBBP1a is a Novel Repressor of NF-κB. *Journal of Molecular Biology*, 366(3):725–736.

Oza, P., Jaspersen, S. L., Miele, A., Dekker, J., and Peterson, C. L. (2009). Mechanisms that regulate localization of a DNA double-strand break to the nuclear periphery. *Genes & Development*, 23(8):912–927.

Ozer, R. S. and Halpain, S. (2000). Phosphorylation-dependent localization of microtubule-associated protein MAP2c to the actin cytoskeleton. *Molecular Biology of the Cell*, 11(10):3573–3587.

Paintrand, M., Moudjou, M., Delacroix, H., and Bornens, M. (1992). Centrosome organization and centriole architecture: Their sensitivity to divalent cations. *Journal of Structural Biology*, 108(2):107–128.

Pare, G. C., Easlick, J. L., Mislow, J. M., McNally, E. M., and Kapiloff, M. S. (2005). Nesprin-1alpha contributes to the targeting of mAKAP to the cardiac myocyte nuclear envelope. *Experimental Cell Research*, 303(2):388–399.

Pasch, E., Link, J., Beck, C., Scheuerle, S., and Alsheimer, M. (2015). The LINC complex component Sun4 plays a crucial role in sperm head formation and fertility. *Biology Open*, 4(12):1792–1802.

Pavlath, G. K., Rich, K., Webster, S. G., and Blau, H. M. (1989). Localization of muscle gene products in nuclear domains. *Nature*, 337(6207):570–573.

Pelletier, L., Ozlü, N., Hannak, E., Cowan, C., Habermann, B., Ruer, M., Müller-Reichert, T., and Hyman, A. A. (2004). The Caenorhabditis elegans centrosomal protein SPD-2 is required for both pericentriolar material recruitment and centriole duplication. *Current biology: CB*, 14(10):863–873.

Petry, S., Groen, A. C., Ishihara, K., Mitchison, T. J., and Vale, R. D. (2013). Branching microtubule nucleation in Xenopus egg extracts mediated by augmin and TPX2. *Cell*, 152(4):768–777.

Piane, M., Della Monica, M., Piatelli, G., Lulli, P., Lonardo, F., Chessa, L., and Scarano, G. (2009). Majewski osteodysplastic primordial dwarfism type II (MOPD II) syndrome previously diagnosed as Seckel syndrome: Report of a novel mutation of the PCNT gene. *American Journal of Medical Genetics. Part A*, 149A(11):2452–2456.

Pickett-Heaps, J. D. (1969). The evolution of the mitotic apparatus, an attempt at comparative ultrastructural cytology in dividing cell plants. *Cytobios*, 1:257–280.

Pillers, D.-A. M. and Von Bergen, N. H. (2016). Emery–Dreifuss muscular dystrophy: A test case for precision medicine. *The Application of Clinical Genetics*, 9:27–32.

Pizon, V., Gerbal, F., Diaz, C. C., and Karsenti, E. (2005). Microtubule-dependent transport and organization of sarcomeric myosin during skeletal muscle differentiation. *The EMBO journal*, 24(21):3781–3792.

Pockwinse, S. M., Krockmalnic, G., Doxsey, S. J., Nickerson, J., Lian, J. B., van Wijnen, A. J., Stein, J. L., Stein, G. S., and Penman, S. (1997). Cell cycle independent interaction of CDC2 with the centrosome, which is associated with the nuclear matrix-intermediate filament scaffold. *Proceedings of the National Academy of Sciences of the United States of America*, 94(7):3022–3027.

Pon, J. R. and Marra, M. A. (2015). MEF2 transcription factors: Developmental regulators and emerging cancer genes. *Oncotarget*, 7(3):2297–2312.

Prosser, S. L. and Pelletier, L. (2017). Mitotic spindle assembly in animal cells: A fine balancing act. *Nature Reviews Molecular Cell Biology*, 18(3):187–201.

Przybylski, R. J. (1971). OCCURRENCE OF CENTRIOLES DURING SKELETAL AND CARDIAC MYOGENESIS. *The Journal of Cell Biology*, 49(1):214–221.

Puckelwartz, M. J., Kessler, E., Zhang, Y., Hodzic, D., Randles, K. N., Morris, G., Earley, J. U., Hadhazy, M., Holaska, J. M., Mewborn, S. K., Pytel, P., and McNally, E. M. (2009). Disruption of nesprin-1 produces an Emery Dreifuss muscular dystrophy-like phenotype in mice. *Human Molecular Genetics*, 18(4):607–620.

Puckelwartz, M. J., Kessler, E. J., Kim, G., Dewitt, M. M., Zhang, Y., Earley, J. U., Depreux, F. F. S., Holaska, J., Mewborn, S. K., Pytel, P., and McNally, E. M. (2010). Nesprin-1 mutations in human and murine cardiomyopathy. *Journal of Molecular and Cellular Cardiology*, 48(4):600–608.

Purohit, A., Tynan, S. H., Vallee, R., and Doxsey, S. J. (1999). Direct interaction of pericentrin with cytoplasmic dynein light intermediate chain contributes to mitotic spindle organization. *The Journal of Cell Biology*, 147(3):481–492.

Quintyne, N. J., Gill, S. R., Eckley, D. M., Crego, C. L., Compton, D. A., and Schroer, T. A. (1999). Dynactin is required for microtubule anchoring at centrosomes. *The Journal of Cell Biology*, 147(2):321–334.

Rajgor, D., Mellad, J. A., Autore, F., Zhang, Q., and Shanahan, C. M. (2012). Multiple novel nesprin-1 and nesprin-2 variants act as versatile tissue-specific intracellular scaffolds. *PloS One*, 7(7):e40098.

Rajgor, D., Mellad, J. A., Soong, D., Rattner, J. B., Fritzler, M. J., and Shanahan, C. M. (2014). Mammalian microtubule P-body dynamics are mediated by nesprin-1. *The Journal of Cell Biology*, 205(4):457–475.

Ralston, E. (1993). Changes in architecture of the Golgi complex and other subcellular organelles during myogenesis. *The Journal of Cell Biology*, 120(2):399–409.

Ralston, E., Lu, Z., Biscocho, N., Soumaka, E., Mavroidis, M., Prats, C., Lømo, T., Capetanaki, Y., and Ploug, T. (2006). Blood vessels and desmin control the positioning of nuclei in skeletal muscle fibers. *Journal of Cellular Physiology*, 209(3):874–882.

Ralston, E., Lu, Z., and Ploug, T. (1999). The organization of the Golgi complex and microtubules in skeletal muscle is fiber type-dependent. *The Journal of Neuroscience: The Official Journal of the Society for Neuroscience*, 19(24):10694–10705.

Ralston, E., Ploug, T., Kalhovde, J., and Lomo, T. (2001). Golgi complex, endoplasmic reticulum exit sites, and microtubules in skeletal muscle fibers are organized by patterned activity. *The Journal of Neuroscience: The Official Journal of the Society for Neuroscience*, 21(3):875–883.

Randles, K. N., Lam, L. T., Sewry, C. A., Puckelwartz, M., Furling, D., Wehnert, M., McNally, E. M., and Morris, G. E. (2010). Nesprins, but not Sun proteins, switch isoforms at the nuclear envelope during muscle development. *Developmental Dynamics*, 239(3):998–1009.

Rauch, A., Thiel, C. T., Schindler, D., Wick, U., Crow, Y. J., Ekici, A. B., van Essen, A. J., Goecke, T. O., Al-Gazali, L., Chrzanowska, K. H., Zweier, C., Brunner, H. G., Becker, K., Curry, C. J., Dallapiccola, B., Devriendt, K., Dörfler, A., Kinning, E., Megarbane, A., Meinecke, P., Semple, R. K., Spranger, S., Toutain, A., Trembath, R. C., Voss, E., Wilson, L., Hennekam, R., de Zegher, F., Dörr, H.-G., and Reis, A. (2008). Mutations in the Pericentrin (PCNT) Gene Cause Primordial Dwarfism. *Science*, 319(5864):816–819.

Razafsky, D. and Hodzic, D. (2015). A VARIANT OF NESPRIN1 GIANT DEVOID OF KASH DOMAIN UNDERLIES THE MOLECULAR ETIOLOGY OF AUTOSOMAL RECESSIVE CEREBELLAR ATAXIA TYPE I. *Neurobiology of disease*, 78:57–67.

Relaix, F. and Buckingham, M. (1999). From insect eye to vertebrate muscle: Redeployment of a regulatory network. *Genes & Development*, 13(24):3171–3178.

Relaix, F. and Zammit, P. S. (2012). Satellite cells are essential for skeletal muscle regeneration: The cell on the edge returns centre stage. *Development (Cambridge, England)*, 139(16):2845–2856.

Rice, L. M., Montabana, E. A., and Agard, D. A. (2008). The lattice as allosteric effector: Structural studies of $a\beta$- and γ-tubulin clarify the role of GTP in microtubule assembly. *Proceedings of the National Academy of Sciences of the United States of America*, 105(14):5378–5383.

Rieder, C. L., Faruki, S., and Khodjakov, A. (2001). The centrosome in vertebrates: More than a microtubule-organizing center. *Trends in Cell Biology*, 11(10):413–419.

Rios, R. M. (2014). The centrosome–Golgi apparatus nexus. *Phil. Trans. R. Soc. B*, 369(1650):20130462.

Rivero, S., Cardenas, J., Bornens, M., and Rios, R. M. (2009). Microtubule nucleation at the cis-side of the Golgi apparatus requires AKAP450 and GM130. *The EMBO journal*, 28(8):1016–1028.

Robbins, E., Jentzsch, G., and Micali, A. (1968). The centriole cycle in synchronized HeLa cells. *The Journal of Cell Biology*, 36(2):329–339.

Roberts, A. J., Kon, T., Knight, P. J., Sutoh, K., and Burgess, S. A. (2013). Functions and mechanics of dynein motor proteins. *Nature Reviews Molecular Cell Biology*, 14(11):713–726.

Rochlin, K., Yu, S., Roy, S., and Baylies, M. K. (2010). Myoblast fusion: When it takes more to make one. *Developmental biology*, 341(1):66–83.

Roll-Mecak, A. and McNally, F. J. (2010). Microtubule severing enzymes. *Current opinion in cell biology*, 22(1):96.

Rossi, A. E. and Dirksen, R. T. (2006). Sarcoplasmic reticulum: The dynamic calcium governor of muscle. *Muscle & Nerve*, 33(6):715–731.

Roubin, R., Acquaviva, C., Chevrier, V., Sedjaï, F., Zyss, D., Birnbaum, D., and Rosnet, O. (2013). Myomegalin is necessary for the formation of centrosomal and Golgi-derived microtubules. *Biology Open*, 2(2):238–250.

Roux, K. J., Crisp, M. L., Liu, Q., Kim, D., Kozlov, S., Stewart, C. L., and Burke, B. (2009). Nesprin 4 is an outer nuclear membrane protein that can induce kinesin-mediated cell polarization. *Proceedings of the National Academy of Sciences of the United States of America*, 106(7):2194–2199.

Roux, K. J., Kim, D. I., and Burke, B. (2013). BioID: A screen for protein-protein interactions. *Current Protocols in Protein Science / Editorial Board, John E. Coligan ... [et Al.]*, 74:Unit 19.23.

Roux, K. J., Kim, D. I., Raida, M., and Burke, B. (2012). A promiscuous biotin ligase fusion protein identifies proximal and interacting proteins in mammalian cells. *The Journal of Cell Biology*, 196(6):801–810.

Sabourin, L. A. and Rudnicki, M. A. (2000). The molecular regulation of myogenesis. *Clinical Genetics*, 57(1):16–25.

Saitoh, O., Arai, T., and Obinata, T. (1988). Distribution of microtubules and other cytoskeletal filaments during myotube elongation as revealed by fluorescence microscopy. *Cell and Tissue Research*, 252(2):263–273.

Sanders, A. A. W. M. and Kaverina, I. (2015). Nucleation and Dynamics of Golgi-derived Microtubules. *Frontiers in Neuroscience*, 9:431.

Sanes, J. R. and Lichtman, J. W. (2001). Induction, assembly, maturation and maintenance of a postsynaptic apparatus. *Nature Reviews. Neuroscience*, 2(11):791–805.

Schirmer, E. C., Florens, L., Guan, T., Yates, J. R., and Gerace, L. (2003). Nuclear membrane proteins with potential disease links found by subtractive proteomics. *Science (New York, N.Y.)*, 301(5638):1380–1382.

Schmidt, H. and Carter, A. P. (2016). Review: Structure and mechanism of the dynein motor ATPase. *Biopolymers*, 105(8):557–567.

Schmidt, P. H., Dransfield, D. T., Claudio, J. O., Hawley, R. G., Trotter, K. W., Milgram, S. L., and Goldenring, J. R. (1999). AKAP350, a Multiply Spliced Protein Kinase A-anchoring Protein Associated with Centrosomes. *Journal of Biological Chemistry*, 274(5):3055–3066.

Schneider, M., Lu, W., Neumann, S., Brachner, A., Gotzmann, J., Noegel, A. A., and Karakesisoglou, I. (2011). Molecular mechanisms of centrosome and cytoskeleton anchorage at the nuclear envelope. *Cellular and molecular life sciences: CMLS*, 68(9):1593–1610.

Scholey, J. M. (2008). Intraflagellar transport motors in cilia: Moving along the cell's antenna. *The Journal of Cell Biology*, 180(1):23–29.

Schroer, T. A. (2004). DYNACTIN. `http://www.annualreviews.org/doi/10.1146/annurev.cellbio.20.012103.094623`.

Schulman, V. K., Folker, E. S., Rosen, J. N., and Baylies, M. K. (2014). Syd/JIP3 and JNK Signaling Are Required for Myonuclear Positioning and Muscle Function. *PLoS Genetics*, 10(12).

Seetapun, D., Castle, B. T., McIntyre, A. J., Tran, P. T., and Odde, D. J. (2012). Estimating the Microtubule GTP Cap Size In Vivo. *Current biology : CB*, 22(18):1681–1687.

Shah, S. B., Davis, J., Weisleder, N., Kostavassili, I., McCulloch, A. D., Ralston, E., Capetanaki, Y., and Lieber, R. L. (2004). Structural and functional roles of desmin in mouse skeletal muscle during passive deformation. *Biophysical Journal*, 86(5):2993–3008.

Shao, X., Tarnasky, H. A., Lee, J. P., Oko, R., and van der Hoorn, F. A. (1999). Spag4, a novel sperm protein, binds outer dense-fiber protein Odf1 and localizes to microtubules of manchette and axoneme. *Developmental Biology*, 211(1):109–123.

Shimi, T., Pfleghaar, K., Kojima, S.-i., Pack, C.-G., Solovei, I., Goldman, A. E., Adam, S. A., Shumaker, D. K., Kinjo, M., Cremer, T., and Goldman, R. D. (2008). The A- and B-type nuclear lamin networks: Microdomains involved in chromatin organization and transcription. *Genes & Development*, 22(24):3409–3421.

Sillibourne, J. E., Milne, D. M., Takahashi, M., Ono, Y., and Meek, D. W. (2002). Centrosomal anchoring of the protein kinase CK1delta mediated by attachment to the large, coiled-coil scaffolding protein CG-NAP/AKAP450. *Journal of Molecular Biology*, 322(4):785–797.

Simpson, J. G. and Roberts, R. G. (2008). Patterns of evolutionary conservation in the nesprin genes highlight probable functionally important protein domains and isoforms. *Biochemical Society Transactions*, 36(6):1359–1367.

Solovei, I., Wang, A. S., Thanisch, K., Schmidt, C. S., Krebs, S., Zwerger, M., Cohen, T. V., Devys, D., Foisner, R., Peichl, L., Herrmann, H., Blum, H., Engelkamp, D., Stewart, C. L., Leonhardt, H., and Joffe, B. (2013). LBR and lamin A/C sequentially tether peripheral heterochromatin and inversely regulate differentiation. *Cell*, 152(3):584–598.

Sonnen, K. F., Schermelleh, L., Leonhardt, H., and Nigg, E. A. (2012). 3D-structured illumination microscopy provides novel insight into architecture of human centrosomes. *Biology Open*, 1(10):965–976.

Sosa, B. A., Kutay, U., and Schwartz, T. U. (2013). Structural insights into LINC complexes. *Current Opinion in Structural Biology*, 23(2):285–291.

Srsen, V., Fant, X., Heald, R., Rabouille, C., and Merdes, A. (2009). Centrosome proteins form an insoluble perinuclear matrix during muscle cell differentiation. *BMC cell biology*, 10:28.

Starr, D. A. and Fridolfsson, H. N. (2010). Interactions between nuclei and the cytoskeleton are mediated by SUN-KASH nuclear-envelope bridges. *Annual Review of Cell and Developmental Biology*, 26:421–444.

Starr, D. A. and Han, M. (2002). Role of ANC-1 in tethering nuclei to the actin cytoskeleton. *Science (New York, N.Y.)*, 298(5592):406–409.

Starr, D. A. and Han, M. (2003). ANChors away: An actin based mechanism of nuclear positioning. *Journal of Cell Science*, 116(2):211–216.

Steinmetz, M. O., Kammerer, R. A., Jahnke, W., Goldie, K. N., Lustig, A., and van Oostrum, J. (2000). Op18/stathmin caps a kinked protofilament-like tubulin tetramer. *The EMBO Journal*, 19(4):572–580.

Stewart, C. L., Roux, K. J., and Burke, B. (2007). Blurring the Boundary: The Nuclear Envelope Extends Its Reach. *Science*, 318(5855):1408–1412.

Stiess, M., Maghelli, N., Kapitein, L. C., Gomis-Rüth, S., Wilsch-Bräuninger, M., Hoogenraad, C. C., Tolić-Nørrelykke, I. M., and Bradke, F. (2010). Axon Extension Occurs Independently of Centrosomal Microtubule Nucleation. *Science*, 327(5966):704–707.

Straube, A. and Merdes, A. (2007). EB3 regulates microtubule dynamics at the cell cortex and is required for myoblast elongation and fusion. *Current biology: CB*, 17(15):1318–1325.

Stroud, M. J., Feng, W., Zhang, J., Veevers, J., Fang, X., Gerace, L., and Chen, J. (2017). Nesprin 1α2 is essential for mouse postnatal viability and nuclear positioning in skeletal muscle. *J Cell Biol*, page jcb.201612128.

Tai, A. W., Chuang, J.-Z., Bode, C., Wolfrum, U., and Sung, C.-H. (1999). Rhodopsin's Carboxy-Terminal Cytoplasmic Tail Acts as a Membrane Receptor for Cytoplasmic Dynein by Binding to the Dynein Light Chain Tctex-1. *Cell*, 97(7):877–887.

Tajbakhsh, S. (2009). Skeletal muscle stem cells in developmental versus regenerative myogenesis. *Journal of Internal Medicine*, 266(4):372–389.

Takahashi, M., Mukai, H., Oishi, K., Isagawa, T., and Ono, Y. (2000). Association of immature hypophosphorylated protein kinase cepsilon with an anchoring protein CG-NAP. *The Journal of Biological Chemistry*, 275(44):34592–34596.

Takahashi, M., Shibata, H., Shimakawa, M., Miyamoto, M., Mukai, H., and Ono, Y. (1999). Characterization of a Novel Giant Scaffolding Protein, CG-NAP, That Anchors Multiple Signaling Enzymes to Centrosome and the Golgi Apparatus. *Journal of Biological Chemistry*, 274(24):17267–17274.

Takahashi, M., Yamagiwa, A., Nishimura, T., Mukai, H., and Ono, Y. (2002). Centrosomal proteins CG-NAP and kendrin provide microtubule nucleation sites by anchoring gamma-tubulin ring complex. *Molecular Biology of the Cell*, 13(9):3235–3245.

Takenawa, T. and Suetsugu, S. (2007). The WASP|[ndash]|WAVE protein network: Connecting the membrane to the cytoskeleton. *Nature Reviews Molecular Cell Biology*, 8(1):37–48.

Tassin, A. M., Maro, B., and Bornens, M. (1985a). Fate of microtubule-organizing centers during myogenesis in vitro. *The Journal of Cell Biology*, 100(1):35–46.

Tassin, A. M., Paintrand, M., Berger, E. G., and Bornens, M. (1985b). The Golgi apparatus remains associated with microtubule organizing centers during myogenesis. *The Journal of Cell Biology*, 101(2):630–638.

Tavner, F. J., Simpson, R., Tashiro, S., Favier, D., Jenkins, N. A., Gilbert, D. J., Copeland, N. G., Macmillan, E. M., Lutwyche, J., Keough, R. A., Ishii, S., and Gonda, T. J. (1998). Molecular Cloning Reveals that the p160 Myb-Binding Protein Is a Novel, Predominantly Nucleolar Protein Which May Play a Role in Transactivation by Myb. *Molecular and Cellular Biology*, 18(2):989–1002.

Teixidó-Travesa, N., Villén, J., Lacasa, C., Bertran, M. T., Archinti, M., Gygi, S. P., Caelles, C., Roig, J., and Lüders, J. (2010). The gammaTuRC revisited: A comparative analysis of interphase and mitotic human gammaTuRC redefines the set of core components and identifies the novel subunit GCP8. *Molecular Biology of the Cell*, 21(22):3963–3972.

Tibelius, A., Marhold, J., Zentgraf, H., Heilig, C. E., Neitzel, H., Ducommun, B., Rauch, A., Ho, A. D., Bartek, J., and Krämer, A. (2009). Microcephalin and pericentrin regulate mitotic entry via centrosome-associated Chk1. *The Journal of Cell Biology*, 185(7):1149–1157.

Tirnauer, J. S., Grego, S., Salmon, E. D., and Mitchison, T. J. (2002). EB1–Microtubule Interactions in Xenopus Egg Extracts: Role of EB1 in Microtubule Stabilization and Mechanisms of Targeting to Microtubules. *Molecular Biology of the Cell*, 13(10):3614–3626.

Tokuyasu, K. T., Dutton, A. H., and Singer, S. J. (1983). Immunoelectron microscopic studies of desmin (skeletin) localization and intermediate filament organization in chicken cardiac muscle. *The Journal of Cell Biology*, 96(6):1736–1742.

Towbin, B. D., Gonzalez-Sandoval, A., and Gasser, S. M. (2013). Mechanisms of heterochromatin subnuclear localization. *Trends in Biochemical Sciences*, 38(7):356–363.

Tucker, J. B., Paton, C. C., Richardson, G. P., Mogensen, M. M., and Russell, I. J. (1992). A cell surface-associated centrosomal layer of microtubule-organizing material in the inner pillar cell of the mouse cochlea. *Journal of Cell Science*, 102(2):215–226.

Tzur, Y. B., Wilson, K. L., and Gruenbaum, Y. (2006). SUN-domain proteins: 'Velcro' that links the nucleoskeleton to the cytoskeleton. *Nature Reviews. Molecular Cell Biology*, 7(10):782–788.

Varga, V., Leduc, C., Bormuth, V., Diez, S., and Howard, J. (2009). Kinesin-8 motors act cooperatively to mediate length-dependent microtubule depolymerization. *Cell*, 138(6):1174–1183.

Vaughan, K. T. and Vallee, R. B. (1995). Cytoplasmic dynein binds dynactin through a direct interaction between the intermediate chains and p150Glued. *The Journal of Cell Biology*, 131(6 Pt 1):1507–1516.

Vitre, B., Coquelle, F. M., Heichette, C., Garnier, C., Chrétien, D., and Arnal, I. (2008). EB1 regulates microtubule dynamics and tubulin sheet closure in vitro. *Nature Cell Biology*, 10(4):415–421.

Voit, T., Cirak, S., Abraham, S., Karakesisoglou, I., Parano, E., Pavone, P., Falsaperla, R., Amthor, H., Schroeder, J., Muntoni, F., Guicheney, P., Nurnberg, P., Noegel, A., and Herrmann, R. (2007). C.O.4 Congenital muscular dystrophy with adducted thumbs, mental retardation, cerebellar hypoplasia and cataracts is caused by mutation of Enaptin (Nesprin-1): The third nuclear envelopathy with muscular dystrophy. *Neuromuscular Disorders*, 17(9):833–834.

Voit, T., Parano, E., Straub, V., Schröder, J. M., Schaper, J., Pavone, P., Falsaperla, R., Pavone, L., and Herrmann, R. (2002). Congenital muscular dystrophy with adducted thumbs, ptosis, external ophthalmoplegia, mental retardation and cerebellar hypoplasia: A novel form of CMD. *Neuromuscular Disorders*, 12(7–8):623–630.

Wang, Q., Du, X., Cai, Z., and Greene, M. I. (2006). Characterization of the structures involved in localization of the SUN proteins to the nuclear envelope and the centrosome. *DNA and cell biology*, 25(10):554–562.

Wang, W., Shi, Z., Jiao, S., Chen, C., Wang, H., Liu, G., Wang, Q., Zhao, Y., Greene, M. I., and Zhou, Z. (2012). Structural insights into SUN-KASH complexes across the nuclear envelope. *Cell Research*, 22(10):1440–1452.

Wang, Z., Wu, T., Shi, L., Zhang, L., Zheng, W., Qu, J. Y., Niu, R., and Qi, R. Z. (2010). Conserved Motif of CDK5RAP2 Mediates Its Localization to Centrosomes and the Golgi Complex. *The Journal of Biological Chemistry*, 285(29):22658–22665.

Wang, Z., Zhang, C., and Qi, R. Z. (2014). A newly identified myomegalin isoform functions in Golgi microtubule organization and ER–Golgi transport. *J Cell Sci*, 127(22):4904–4917.

Warren, D. T., Zhang, Q., Weissberg, P. L., and Shanahan, C. M. (2005). Nesprins: Intracellular scaffolds that maintain cell architecture and coordinate cell function? *Expert Reviews in Molecular Medicine*, 7(11):1–15.

Warren, R. H. (1974). Microtubular organization in elongating myogenic cells. *The Journal of Cell Biology*, 63(2 Pt 1):550–566.

Wheeler, M. A., Davies, J. D., Zhang, Q., Emerson, L. J., Hunt, J., Shanahan, C. M., and Ellis, J. A. (2007). Distinct functional domains in nesprin-1α and nesprin-2β bind directly to emerin and both interactions are disrupted in X-linked Emery–Dreifuss muscular dystrophy. *Experimental Cell Research*, 313(13):2845–2857.

Wiese, C. and Zheng, Y. (2000). A new function for the gamma-tubulin ring complex as a microtubule minus-end cap. *Nature Cell Biology*, 2(6):358–364.

Wilhelmsen, K., Litjens, S. H. M., Kuikman, I., Tshimbalanga, N., Janssen, H., van den Bout, I., Raymond, K., and Sonnenberg, A. (2005). Nesprin-3, a novel outer nuclear membrane protein, associates with the cytoskeletal linker protein plectin. *The Journal of Cell Biology*, 171(5):799–810.

Wilkie, G. S., Korfali, N., Swanson, S. K., Malik, P., Srsen, V., Batrakou, D. G., de las Heras, J., Zuleger, N., Kerr, A. R. W., Florens, L., and Schirmer, E. C. (2011). Several novel nuclear envelope transmembrane proteins identified in skeletal muscle have cytoskeletal associations. *Molecular & cellular proteomics: MCP*, 10(1):M110.003129.

Willems, M., Geneviève, D., Borck, G., Baumann, C., Baujat, G., Bieth, E., Edery, P., Farra, C., Gerard, M., Héron, D., Leheup, B., Le Merrer, M., Lyonnet, S., Martin-Coignard, D., Mathieu, M., Thauvin-Robinet, C., Verloes, A., Colleaux, L., Munnich, A., and Cormier-Daire, V. (2010). Molecular analysis of pericentrin gene (PCNT) in a series of 24 Seckel/microcephalic osteodysplastic primordial dwarfism type II (MOPD II) families. *Journal of Medical Genetics*, 47(12):797–802.

Wilson, M. H. and Holzbaur, E. L. F. (2012). Opposing microtubule motors drive robust nuclear dynamics in developing muscle cells. *Journal of Cell Science*, 125(Pt 17):4158–4169.

Wilson, M. H. and Holzbaur, E. L. F. (2015). Nesprins anchor kinesin-1 motors to the nucleus to drive nuclear distribution in muscle cells. *Development (Cambridge, England)*, 142(1):218–228.

Witczak, O., Skålhegg, B. S., Keryer, G., Bornens, M., Taskén, K., Jahnsen, T., and Orstavik, S. (1999). Cloning and characterization of a cDNA encoding an A-kinase anchoring protein located in the centrosome, AKAP450. *The EMBO Journal*, 18(7):1858–1868.

Worman, H. J. (2012). Nuclear lamins and laminopathies. *The Journal of Pathology*, 226(2):316–325.

Wu, J., de Heus, C., Liu, Q., Bouchet, B. P., Noordstra, I., Jiang, K., Hua, S., Martin, M., Yang, C., Grigoriev, I., Katrukha, E. A., Altelaar, A. F. M., Hoogenraad, C. C., Qi, R. Z., Klumperman, J., and Akhmanova, A. (2016). Molecular Pathway of Microtubule Organization at the Golgi Apparatus. *Developmental Cell*, 39(1):44–60.

Wu, W., Huang, R., Wu, Q., Li, P., Chen, J., Li, B., and Liu, H. (2014). The Role of Six1 in the Genesis of Muscle Cell and Skeletal Muscle Development. *International Journal of Biological Sciences*, 10(9):983–989.

Yaffe, D. and Saxel, O. (1977). Serial passaging and differentiation of myogenic cells isolated from dystrophic mouse muscle. *Nature*, 270(5639):725–727.

Yajima, H., Ogura, T., Nitta, R., Okada, Y., Sato, C., and Hirokawa, N. (2012). Conformational changes in tubulin in GMPCPP and GDP-taxol microtubules observed by cryoelectron microscopy. *The Journal of Cell Biology*, 198(3):315–322.

Yang, R. and Feldman, J. L. (2015). SPD-2/CEP192 and CDK Are Limiting for Microtubule-Organizing Center Function at the Centrosome. *Current Biology*.

Yau, K. W., van Beuningen, S. F. B., Cunha-Ferreira, I., Cloin, B. M. C., van Battum, E. Y., Will, L., Schätzle, P., Tas, R. P., van Krugten, J., Katrukha, E. A., Jiang, K., Wulf, P. S., Mikhaylova, M., Harterink, M., Pasterkamp, R. J., Akhmanova, A., Kapitein, L. C., and Hoogenraad, C. C. (2014). Microtubule minus-end binding protein CAMSAP2 controls axon specification and dendrite development. *Neuron*, 82(5):1058–1073.

Yin, H., Price, F., and Rudnicki, M. A. (2013). Satellite cells and the muscle stem cell niche. *Physiological Reviews*, 93(1):23–67.

Young, A., Dictenberg, J. B., Purohit, A., Tuft, R., and Doxsey, S. J. (2000). Cytoplasmic dynein-mediated assembly of pericentrin and gamma tubulin onto centrosomes. *Molecular Biology of the Cell*, 11(6):2047–2056.

Yu, J., Lei, K., Zhou, M., Craft, C. M., Xu, G., Xu, T., Zhuang, Y., Xu, R., and Han, M. (2011). KASH protein Syne-2/Nesprin-2 and SUN proteins SUN1/2 mediate nuclear migration during mammalian retinal development. *Human Molecular Genetics*, 20(6):1061–1073.

Zaal, K. J. M., Reid, E., Mousavi, K., Zhang, T., Mehta, A., Bugnard, E., Sartorelli, V., and Ralston, E. (2011). Who needs microtubules? Myogenic reorganization of MTOC, Golgi complex and ER exit sites persists despite lack of normal microtubule tracks. *PloS One*, 6(12):e29057.

Zebrowski, D. C., Vergarajauregui, S., Wu, C.-C., Piatkowski, T., Becker, R., Leone, M., Hirth, S., Ricciardi, F., Falk, N., Giessl, A., Just, S., Braun, T., Weidinger, G., and Engel, F. B. (2015). Developmental alterations in centrosome integrity contribute to the post-mitotic state of mammalian cardiomyocytes. *eLife*, 4.

Zhang, D., Rogers, G. C., Buster, D. W., and Sharp, D. J. (2007a). Three microtubule severing enzymes contribute to the "Pacman-flux" machinery that moves chromosomes. *The Journal of Cell Biology*, 177(2):231–242.

Zhang, J., Felder, A., Liu, Y., Guo, L. T., Lange, S., Dalton, N. D., Gu, Y., Peterson, K. L., Mizisin, A. P., Shelton, G. D., Lieber, R. L., and Chen, J. (2010). Nesprin 1 is critical for nuclear positioning and anchorage. *Human Molecular Genetics*, 19(2):329–341.

Zhang, J. and Megraw, T. L. (2007). Proper Recruitment of γ-Tubulin and D-TACC/Msps to Embryonic Drosophila Centrosomes Requires Centrosomin Motif 1. *Molecular Biology of the Cell*, 18(10):4037–4049.

Zhang, Q., Ragnauth, C., Greener, M. J., Shanahan, C. M., and Roberts, R. G. (2002). The nesprins are giant actin-binding proteins, orthologous to Drosophila melanogaster muscle protein MSP-300. *Genomics*, 80(5):473–481.

Zhang, Q., Ragnauth, C. D., Skepper, J. N., Worth, N. F., Warren, D. T., Roberts, R. G., Weissberg, P. L., Ellis, J. A., and Shanahan, C. M. (2005). Nesprin-2 is a multi-isomeric protein that binds lamin and emerin at the nuclear envelope and forms a subcellular network in skeletal muscle. *Journal of Cell Science*, 118(Pt 4):673–687.

Zhang, Q., Skepper, J. N., Yang, F., Davies, J. D., Hegyi, L., Roberts, R. G., Weissberg, P. L., Ellis, J. A., and Shanahan, C. M. (2001). Nesprins: A novel family of spectrin-repeat-containing proteins that localize to the nuclear membrane in multiple tissues. *Journal of Cell Science*, 114(Pt 24):4485–4498.

Zhang, Q., Worth, N. F., Davies, J. D., Wasner, C., Feuer, A., Ragnauth, C. D., Yi, Q., Mellad, J. A., Warren, D. T., Wheeler, M. A., Ellis, J. A., Skepper, J. N., Vorgerd, M., Schlotter-Weigel, B., Weissberg, P. L., Roberts, R. G., Wehnert, M., and Shanahan, C. M. (2007b). Nesprin-1 and -2 are involved in the pathogenesis of Emery–Dreifuss muscular dystrophy and are critical for nuclear envelope integrity. *Human Molecular Genetics*, 16(23):2816–2833.

Zhang, X., Lei, K., Yuan, X., Wu, X., Zhuang, Y., Xu, T., Xu, R., and Han, M. (2009). SUN1/2 and Syne/Nesprin-1/2 complexes connect centrosome to the nucleus during neurogenesis and neuronal migration in mice. *Neuron*, 64(2):173–187.

Zhang, X., Xu, R., Zhu, B., Yang, X., Ding, X., Duan, S., Xu, T., Zhuang, Y., and Han, M. (2007c). Syne-1 and Syne-2 play crucial roles in myonuclear anchorage and motor neuron innervation. *Development (Cambridge, England)*, 134(5):901–908.

Zhen, Y.-Y., Libotte, T., Munck, M., Noegel, A. A., and Korenbaum, E. (2002). NUANCE, a giant protein connecting the nucleus and actin cytoskeleton. *Journal of Cell Science*, 115(Pt 15):3207–3222.

Zheng, Y., Wong, M. L., Alberts, B., and Mitchison, T. (1995). Nucleation of microtubule assembly by a gamma-tubulin-containing ring complex. *Nature*, 378(6557):578–583.

Zhou, C., Li, C., Zhou, B., Sun, H., Koullourou, V., Holt, I., Puckelwartz, M. J., Warren, D. T., Hayward, R., Lin, Z., Zhang, L., Morris, G. E., McNally, E. M., Shackleton, S., Rao, L., Shanahan, C. M., and Zhang, Q. (2017). Novel nesprin-1 mutations associated with dilated cardiomyopathy cause nuclear envelope disruption and defects in myogenesis. *Human Molecular Genetics*, 26(12):2258–2276.

Zhou, Z., Du, X., Cai, Z., Song, X., Zhang, H., Mizuno, T., Suzuki, E., Yee, M. R., Berezov, A., Murali, R., Wu, S.-L., Karger, B. L., Greene, M. I., and Wang, Q. (2012). Structure of Sad1-UNC84 Homology (SUN) Domain Defines Features of Molecular Bridge in Nuclear Envelope. *Journal of Biological Chemistry*, 287(8):5317–5326.

Zhu, F., Lawo, S., Bird, A., Pinchev, D., Ralph, A., Richter, C., Müller-Reichert, T., Kittler, R., Hyman, A. A., and Pelletier, L. (2008). The Mammalian SPD-2 Ortholog Cep192 Regulates Centrosome Biogenesis. *Current Biology*, 18(2):136–141.

Zhu, X. and Kaverina, I. (2013). Golgi as an MTOC: Making microtubules for its own good. *Histochemistry and Cell Biology*, 140(3):361–367.

Zimmerman, W. C., Sillibourne, J., Rosa, J., and Doxsey, S. J. (2004). Mitosis-specific anchoring of gamma tubulin complexes by pericentrin controls spindle organization and mitotic entry. *Molecular Biology of the Cell*, 15(8):3642–3657.

Zong, Y. and Jin, R. (2013). Structural Mechanisms of the Agrin-LRP4-MuSK Signaling Pathway in Neuromuscular Junction Differentiation. *Cellular and molecular life sciences : CMLS*, 70(17):3077–3088.